CONFIDENTIAL

10 Copies

UNCLASSIFIED

MASTER

MND-3607-239-2

UNCLASSIFIED

SNAP 19 Phase III
Final Report

VOLUME II
HEAT SOURCES

DISTRIBUTION OF THIS DOCUMENT IS UNLIMITED

RESTRICTED DATA

This document contains restricted data as defined in the Atomic Energy Act of 1954. Its transmittal or the disclosure of its contents in any manner to an unauthorized person is prohibited.

MARTIN MARIETTA NUCLEAR DIVISION

UNCLASSIFIED

CONFIDENTIAL

DISCLAIMER

This report has been prepared under Contract AT(30-1)-3607 with the U.S. Atomic Energy Commission

MND-3607-239-2 C-92A, M-3679, 55th Edition AEC Research and Development Report

SNAP 19 Phase III Final Report

VOLUME II

HEAT SOURCES

MND-3607-239-2
May 1968

MARTIN MARIETTA CORPORATION NUCLEAR DIVISION
BALTIMORE, MD. 21203

LEGAL NOTICE

This report was prepared as an account of Government sponsored work. Neither the United States, nor the Commission, nor any person acting on behalf of the Commission:

A. Makes any warranty or representation, expressed or implied, with respect to the accuracy, completeness, or usefulness of the information contained in this report, or that the use of any information, apparatus, method, or process disclosed in this report may not infringe privately owned rights; or

B. Assumes any liabilities with respect to the use of, or for damages resulting from the use of any information, apparatus, method, or process disclosed in this report.

As used in the above, "person acting on behalf of the Commission" includes any employee or contractor of the Commission, or employee of such contractor, to the extent that such employee or contractor of the Commission, or employee of such contractor prepares, disseminates, or provides access to, any information pursuant to his employment or contract with the Commission, or his employment with such contractor.

FOREWORD

This three-volume report, prepared by the Martin Marietta Corporation, is an account of the SNAP 19 radioisotope thermoelectric generator program performed under United States Atomic Energy Commission Contract AT(30-1)-3607.

BLANK

ABSTRACT

A. INTRODUCTION

Summarizes phases of SNAP 19 program and describes content of Volume II.

B. OBJECTIVES AND DESIGN CRITERIA

Describes program objectives, safety philosophy and design criteria employed in developing the dispersal heat source and the intact re-entry heat source.

C. DISPERSAL HEAT SOURCE DESIGN AND DEVELOPMENT

Describes the derivation of the dispersal heat source configuration and heat source design, development and test activities.

D. IRHS DESIGN AND DEVELOPMENT

Describes intact re-entry heat source and gives its characteristics; describes assembly operations and gives information on handling and shipping. Describes development and qualification tests.

E. FLIGHT HEAT SOURCE SELECTION

Describes basis upon which selection of the intact re-entry heat source for flight was made.

BLANK

SUMMARY

A. INTRODUCTION

The most significant development effort during the SNAP 19 Phase III program was on the isotope heat source. Development effort involved fuel form and capsule configuration, culminating in use of PuO_2 microspheres in an intact re-entry heat source.

B. OBJECTIVES AND DESIGN CRITERIA

The objectives of the dispersal heat source program were to design a heat source capable of containing the required thermal inventory and meeting system and safety philosophy requirements. A further objective was assessment of the structural integrity under impact, thermal shock and creep-to-rupture conditions.

The safety philosophy was that of minimizing the probability of accident occurrence and the consequence of accidents to the population; during re-entry the fuel was to be dispersed at high altitude.

The design criteria were focused on the retention, as far as possible, of the generator configuration developed in earlier phases of the program. Other considerations were those of fuel loading capability, material compatibility and current fuel capsule technology.

The broad objectives of the intact re-entry heat source program were development of a heat source (as an alternate to the dispersal capsule) that would maintain fuel containment through re-entry and, to the degree practicable, minimize dispersion of fuel upon impact.

Principal design criteria for the intact re-entry heat source were minimum of change to generator design, venting of the capsule to prevent pressure buildup and a barrier system to prevent chemical reaction between materials.

C. DISPERSAL HEAT SOURCE DESIGN AND DEVELOPMENT

The heat source initial design point was the SNAP 9A burnup-type capsule. This metallic fueled initial design was improved to attain greater impact strength. In order to achieve greater stability, the PuO_2 microsphere fuel form was adopted. The lower specific power of the microspheres made necessary a change from the original six-capsule design to a single large capsule with an annular fuel arrangement. This latter capsule provided atmospheric dispersal of the fuel upon re-entry.

A comprehensive development and testing program was conducted to verify the design.

D. IRHS DESIGN AND DEVELOPMENT

The intact re-entry heat source (IRHS) consists principally of a fuel capsule with filter (vent) and canister, a heat shield, a chemical reaction barrier system and compliant support members. Analyses and tests were performed to ensure that the design met intact re-entry requirements.

The capsules were fueled and heat sources assembled at Mound Laboratory. Casks used for shipment were those of the dispersal capsule program modified to suit the IRHS.

Development and qualifications tests included impact and drop tests, chemical reaction barrier tests, aerodynamic tests, simulated re-entry tests and prototype qualification tests. Extensive testing was also conducted in the filter development program. These included environmental, metallographic, physical property, particle retention and impact tests.

Based on the test data, it is concluded that the IRHS will perform the mission for which it was designed.

E. FLIGHT HEAT SOURCE SELECTION

The nuclear safety assessments of the dispersion capsule and the intact re-entry heat source designs were conducted by evaluating each sequential operation of the mission profile. A probabilistic combination of potential abort events, disposition of fuel, and effect on the population was used to establish the risk.

A comprehensive review of the safety analyses for the dispersal and intact re-entry systems was conducted and the Atomic Energy Commission ultimately selected the intact re-entry heat source for the SNAP 19 Nimbus B mission.

CONTENTS

BLANK

LIST OF ILLUSTRATIONS

LIST OF ILLUSTRATIONS (continued)

LIST OF ILLUSTRATIONS (continued)

LIST OF ILLUSTRATIONS (continued)

LIST OF TABLES

BLANK

I. INTRODUCTION

The most significant development effort conducted during the SNAP 19 program involved the isotopic heat source. Under Phase II of the program, the metallic plutonium fuel form was replaced by the more stable PuO_2 microsphere fuel form. The resulting capsule redesign and qualification effort was initiated under Phase II and completed under Phase III. The safety approach for this capsule design was based upon dispersal of the isotope inventory during atmospheric re-entry. Subsequently, a heat source redesign effort was initiated in the spring of 1967. The objective of this effort was to develop and qualify an intact re-entry heat source (IRHS); i.e., a heat source which would ensure containment of the isotopic inventory until earth impact.

This volume of the final report presents the objectives, design criteria, configuration and major development aspects of both the dispersal and intact re-entry heat sources. Greater emphasis is placed on the intact re-entry heat source in view of its selection for the flight system.

BLANK

II. OBJECTIVES AND DESIGN CRITERIA

A. DISPERSAL HEAT SOURCE

1. Program Objectives

The SNAP 19 Phase II effort was extended to perform a fuel capsule redesign, which was necessitated by a change in the fuel form from plutonium metal to PuO_2 microspheres (Ref. II-1). The objective of this effort was to design a heat source that would contain the required thermal inventory (initially 625 watts) and which was consistent with system requirements and the safety philosophy. It was necessary, therefore, to design a fuel containment assembly with the same physical envelope as the initial fuel containment structure, thus enabling the previously developed thermoelectric modules and generator housing to remain unchanged.

A further objective of the effort was to assess the structural integrity of the single-capsule dispersal design relative to its capability to survive impact, susceptibility to thermal shock and the time to failure, i.e., creep-to-rupture life of the capsule.

2. Safety Philosophy

The nuclear safety philosophy selected for the dispersal-type SNAP 19/Nimbus B system was to minimize the probability of accident occurrence and the consequence of accidents to the population. A dispersion mode of re-entry for abort and for post-mission operations was selected for the fuel form. The approach to achieving the safety philosophy was predicated on the inherent integrity of the fuel form and the SNAP 19 safety design.

A dispersion re-entry mode necessitates a fuel form which, by virtue of its physical form and chemical composition, will result in a minimum of radioactive material being introduced into the ecological cycle upon release. Therefore, the fuel form must be insoluble, chemically inert and sized to be nonrespirable. In addition, the fuel form must possess a high degree of structural integrity when subjected to re-entry aerothermodynamic conditions and subsequent terrestrial environment. Consequently, a high melting point compound in a physical form possessing a high crush strength and resistance to spalling is required.

The Pu-238 dioxide plasma-fired microspheres in the size range of 50 to 250 microns was selected as the fuel form. This size range presents an exceedingly low probability for ingestion and inhalation of the microspheres.

The key elements in the safety analysis are microsphere disposition and the biological effects of the microspheres when the SNAP 19/Nimbus B system is exposed to the operational abort aspects of the mission. The SNAP 19 system design approach was formulated with respect to the various operational phases of the mission profile, namely:

(1) Transportation

(2) Launch pad operations

(3) Preorbital

(4) Orbital

(5) Post-mission.

a. Transportation

For the prelaunch phase of the operation, the fuel capsule and shipping container assemblies were designed to:

(1) Provide sufficient radiobiological shielding to comply with Federal (ICC) regulations for shipment of radioactive materials

(2) Endure prolonged storage at an ambient temperature of 120° F without exterior surface temperature exceeding 180° F

(3) Endure the standard transportation fire.

b. Launch pad operations

The principal fuel capsule design criterion was fuel containment if the SNAP 19 system is exposed to credible accident conditions. These conditions are:

(1) Shock overpressure resulting from the explosion of missile propellants on the launch pad

(2) Impact on typical media present at the Air Force Western Test Range at impact velocities characteristic of launch aborts

(3) Thermal shock resulting from immersion of the fuel capsule in the sea. Containment material for the fuel should be sufficiently resistant to seawater corrosion to provide a reasonable time (> 1 year) for intact recovery.

c. Preorbital

Fuel dispersion is permitted when the SNAP 19 generator fuel capsule structure is exposed to aerodynamic heating effects characteristic of aborts prior to orbital injection.

d. Orbital

The fuel capsule design is such that the fuel will be contained during the SNAP 19/Nimbus B mission time. If there is a low orbit abort, aerothermodynamic heating will cause fuel release, preferably above 240,000 feet altitude, thus avoiding melting and possible breakup of individual microspheres.

e. Post-mission

The nominal orbital lifetime of the SNAP 19/Nimbus B spacecraft while in a 600-nautical mile orbit is estimated to be greater than 1600 years. As the fuel decays, helium pressure builds up in the fuel capsule. The capsule was designed to contain this pressure for approximately 20 years.

3. Design Criteria

The basic generator design had been developed during Phase II and electrically heated generators had been built and tested. An electrically heated generator subsystem was environmentally tested at the Phase II requirements. It was therefore desirable, in changing the fuel form, to minimize changes to the basic design of the generator. Essentially, this required a capsule design which permitted retention of

the outer configuration of the heat distribution block. Thus, from these surfaces radially outward, the generator would not change. Other considerations were those of fuel loading capability, materials compatibility and current fuel capsule technology. Specific design criteria were:

(1) To retain the outer (side wall) periphery of the heat distribution block. Thus, the basic generator design is unchanged.

(2) To use, if possible, the Phase II capsule which had been qualified with Pu metal simulant. A seven-capsule array was permissible even at the cost of additional weight.*

(3) To use Haynes-25 capsule material because of previous successful application and fabrication experience

(4) To use a capsule liner assembly to hold the fuel so as to comply with the then existent heat source assembly techniques

(5) To use Haynes-25 liner material because of its demonstrated compatibility with oxide fuel

(6) Requirement for helium pressure containment capability for 20 years or better

(7) Locate the fuel in the capsule so as to promote a uniform heat distribution at the thermoelectrics.

B. INTACT RE-ENTRY HEAT SOURCE

1. Program Objectives

In May 1967, Atomic Energy Commission approval was received to pursue development of an intact re-entry heat source (IRHS) as an alternate to the dispersal heat sources.

The broad objectives of the IRHS program were to develop a SNAP 19 heat source that would maintain fuel containment through the atmospheric re-entry modes and, to the degree practicable, minimize dispersion of fuel on impact.

Development was to proceed on a best-effort basis under a schedule that was consistent with delivery of generators for the Nimbus B launch; i.e., all reasonable steps were to be taken to protect the schedule.

2. Safety Philosophy

The primary nuclear safety objectives for the SNAP 19 IRHS development program were to provide a heat source assembly capable of:

(1) Preventing dispersal of the fuel after a launch abort and the resulting earth impact by containment within the fuel capsule (no sensible aerodynamic heating).

*Initial work showed that a single large capsule was required (Ref. II-1). On a weight basis, a single capsule is also preferred for metal fuel. However, thermal considerations in both normal operation and re-entry heating result in a multiple capsule design. In addition, structural strength is inherently favorable in a small-diameter capsule.

(2) Preventing atmospheric dispersal of the isotopic fuel prior to earth impact after a launch abort or orbit abort involving sensible aerodynamic heating.

(3) Minimizing chemical reactions among the IRHS components which could lead to potential hazards, or which might compromise the integrity of the heat shield.

The philosophy for transportation launch pad operations was the same as for the dispersal heat sources. (See Chapter II-A)

3. Design Criteria

The program objectives and physical constraints demanded selection of design criteria which were beyond the current state of the art. Most significant was the need to reduce the fuel capsule size appreciably below the dispersal capsule dimensions and yet provide space for the nominal 570 thermal watts of fuel. This reduction was necessary to provide volume for the graphite heat shield assembly. To meet the program objectives and physical constraints, design criteria were imposed as follows:

(1) Design the IRHS to be physically and functionally interchangeable with the dispersal heat source to minimize or avoid generator changes.

(2) Vent the capsule to eliminate the need for the void volume required in the sealed capsule designs to accommodate the gaseous helium decay product of plutonium-238. This approach eliminates the uncertainties of long-term creep-to-rupture predictions.

(3) Design the capsule vent or filter assembly to allow passage of helium but retain fuel particles under all normal operating or early abort conditions.

(4) Employ a single-wall Haynes-25 capsule (without the usual liner) to make maximum use of available space with minimum development complexity. Include a dual fuel filling port closure in the single-wall capsule to facilitate surface decontamination.

(5) Use graphite as the heat shield material because of its materials compatibility with the generator and its desirable high temperature properties.

(6) Provide a barrier system inside the IRHS to preclude heat shield reaction with molten Haynes-25 or the PuO_2 during the re-entry heat pulse.

(7) Design the heat source for handling and operation in the same environment as the dispersal capsules, except for shipping and storage (IRHS assembly, shipment and storage to be in an inert atmosphere to avoid the necessity for development of an oxidization resistant coating on the graphite heat shield).

III. DISPERSAL HEAT SOURCE DESIGN AND DEVELOPMENT

The major design change that evolved in Phase III was the change from the multiple capsule design of Phase II to a single dispersion fuel capsule using PuO_2 microspheres as the fuel. The derivation of this configuration is discussed below, followed by a presentation of the capsule operational characteristics. The assembly operations conducted at the fueling facility and the ancillary equipment required for interstate transportation of the fueled units are also described. Since separate reports have been issued to document the evaluation and development tests conducted with the dispersion capsule, only summaries of these efforts have been included, giving test objectives and significant results.

A. DERIVATION OF CONFIGURATION

1. Fuel Burnup

The major criteria during Phases I and II of the SNAP 19 Program and initially in Phase III were retention of fuel upon ground impact for the case of no re-entry heating such as a launch pad abort, and fuel release and burnup (reduction to submicron size) upon atmospheric re-entry (Ref. III-1).

The burnup fuel capsule, similar to that used in SNAP 9A, contained metallic plutonium. The SNAP 19 generator contained six capsules in a segmented graphite fuel block. Segmentation allowed separation of the block by the hypersonic airstream after generator shell destruction. Separation was demonstrated in hypersonic tunnel tests during Phase II.

The SNAP 9A design was changed during Phase II to attain greater impact strength. Five configurations were tested and the selected design qualified. This capsule could survive impact on granite at greater than terminal velocity.

The Phase II capsule (Fig. III-1) weighed 1.3 pounds and contained approximately 225 grams of plutonium metal. The capsule shell was of Haynes-25 and the fuel was encased in a liner of tantalum. Six such capsules were to provide a total nominal inventory of 610 watts per generator.

It was later learned that the melting point of the as-produced metallic fuel was lower than previously indicated. This meant that the fuel, or portions of it, could be near melting or molten during certain SNAP 19 operations, such as thermal cycling in a vacuum chamber. Further, studies by Mound Laboratory (Ref. III-2) showed that containment over a long period cannot be assured where plutonium metal is at or near its melting point. Therefore, work was started on consideration of other fuel forms.

2. Fuel Dispersal

The Phase III program was started with the fuel capsule shown in Fig. III-1. Because of the problem discussed above, a study of alternate forms of plutonium was performed as part of the parallel Phase II activity. The study (Ref. III-3) considered plutonium-zirconium alloy and plutonium-dioxide (PuO_2) microspheres.

The ceramic fuel form, PuO_2, was recommended. This fuel form provided positive assurance of material compatibility during all SNAP 19 test or mission operations. The fuel configuration was microspheres of 50 to 250 microns diameter. Preliminary analysis showed that this material could, upon orbital re-entry, be dispersed in non-respirable sizes.

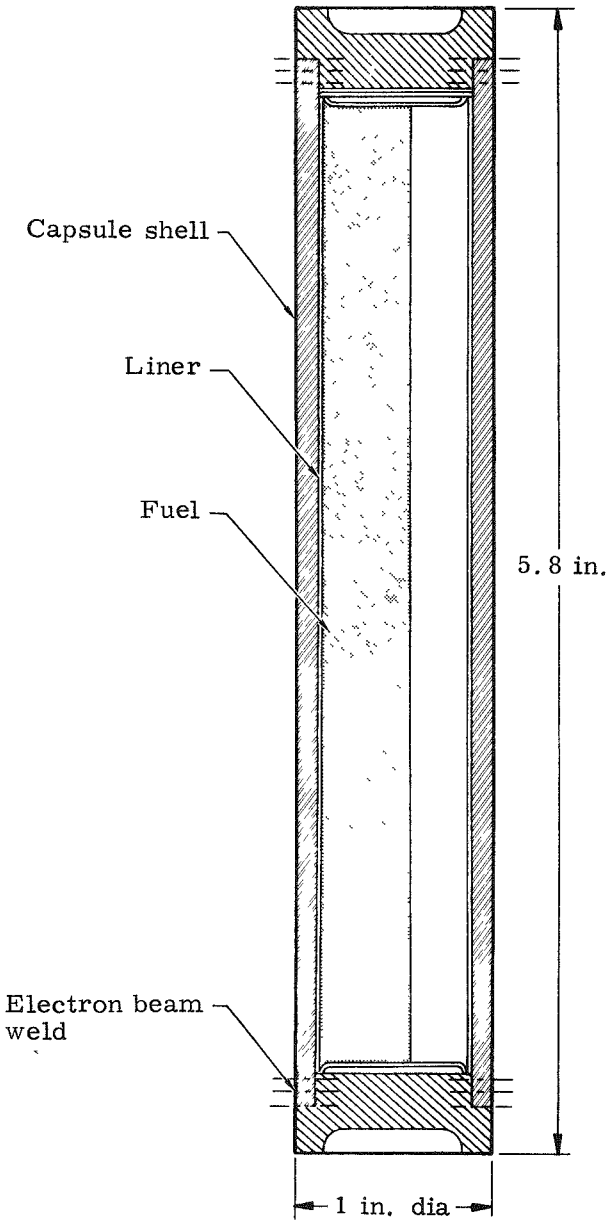

FIG. III-1. PHASE II FUEL CAPSULE

The study also considered fuel capsule configuration. Because the oxide is of lower specific power than the metallic fuel, the required generator inventory was too large in volume for six capsules of the qualified design. A seven-capsule design and variations on a single large capsule design were analyzed. A single capsule of annular fuel array was selected. Development of the new capsule was begun as part of the Phase II program, which was then being conducted in parallel with Phase III (Ref. III-4). The dispersal heat source is discussed in the succeeding sections of this chapter.

B. CONFIGURATION AND OPERATIONAL DESIGN

1. Configuration

The fuel capsule is a right circular cylinder (Fig. III-2). The fuel is encapsulated in an annular cylinder formed by two 0.020-inch liners (inner and outer) and end caps. Two porous plugs restrict movement of fuel particles into the central core and still allow the helium generated in the fuel annulus to pass to the core.

Pertinent capsule dimensions (inches) are:

(1) Outside diameter of capsule = 2.980 ± 0.002

(2) Inside diameter of capsule = 2.780 ± 0.002

(3) Length of capsule = 6.125 max

(4) Outside diameter of outer liner = $2.766 \begin{smallmatrix} + 0.000 \\ - 0.006 \end{smallmatrix}$

(5) Wall thickness of outer liner = 0.015/0.023

(6) Outside diameter of inner liner = 1.985 ± 0.005

(7) Wall thickness of inner liner = 0.015/0.023

(8) Effective fuel length (considering spacers) = 4.924/5.070

(9) Porous plug thickness = 0.125 ± 0.030.

All capsule parts (including liners and porous plugs) are made of Haynes alloy No. 25. Table III-1 is a listing of the results of the chemical analysis and mechanical tests performed on the material from which the fueled capsules were fabricated. The melting temperature range used was 2425° to 2570° F. Other physical and chemical properties are presented in Ref. III-5.

The fuel capsule weighs about 3.7 pounds unfueled and about 7.2 pounds fueled.

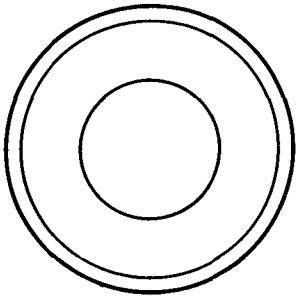

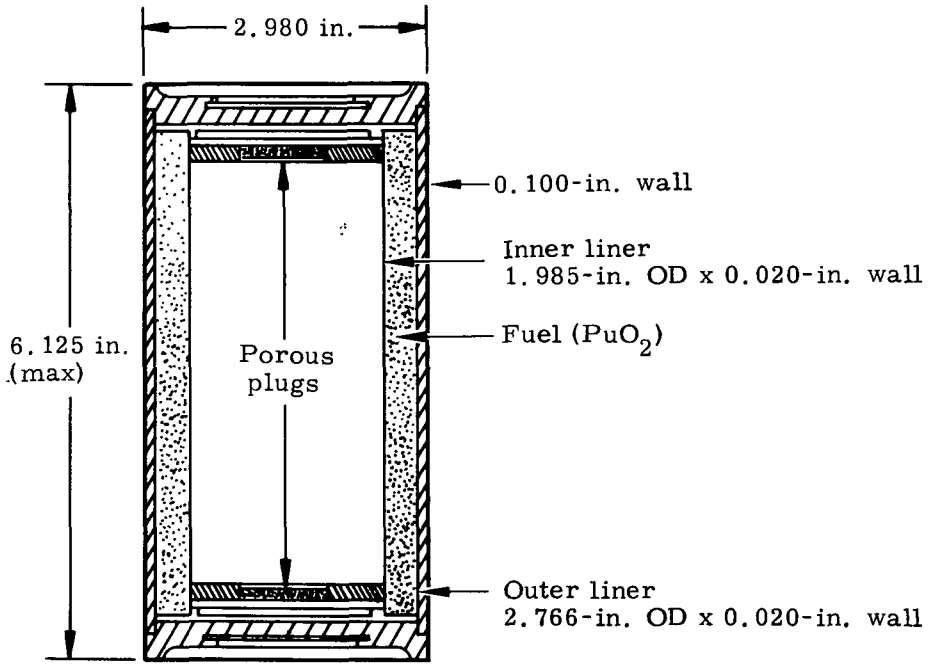

All material Haynes-25

FIG. III-2. PHASE III FUEL CAPSULE

TABLE III-1

Haynes Alloy No. 25 Chemical Analysis and Mechanical Test Summary--Fuel Capsule Material

Composition:

Element	Heat No. L4-1683 (% weight)	Check Analysis (% weight)
Cr	20.09	19.79
W	14.91	14.79
Ni	9.96	10.02
Fe	1.69	1.48
Mr	1.41	1.30
Si	0.10	0.12
C	0.07	0.07
P	0.017	0.016
S	0.011	0.013
Co	Balance	Balance

Tensile Test at Room Temperature:

Ultimate strength	= 141,350 psi
0.2% yield offset	= 67,100 psi
Percent elongation*	= 60.0

Stress Rupture:

Temperature	= 1500° F
Stress	= 24,000 psi
Time	= 88 hr
Percent elongation*	= 105.8

*In specimen length initially four times diameter.

2. Nominal Operating Temperature and Internal Pressure

Nominal generator operating conditions with a thermal fuel loading of 570 watts yields the temperature profile for the heat source that is given in Table III-2. These temperatures are effectively constant for the duration of the mission due to the long half life of the fuel.

TABLE III-2

Dispersal Heat Source Temperature Profile at Launch (°F)

	Argon, Nominal Load	Argon, Open-circuit
Heat distribution block	970	1210
Capsule surface	1040	1270
Outer liner	1100	1330
Maximum fuel temperature	1660	1890

The internal void volume for helium accumulation is 17.9 $in.^3$, which is based on a 570-watt fuel loading, fuel power density of 2.6 watts/cm^3, a packing fraction of 0.75 and capsule tolerances that minimize total internal capsule volume. The internal pressure at any time after encapsulation may be obtained directly from Fig. III-3 when the specified void volume is used. Complete release of all generated helium from the fuel particles was assumed in developing Fig. III-3.

3. Structural Characteristics

All structural calculations were performed using the capsule wall as the location of the primary mode of failure. Analytically, the stress in the capsule end caps could reach the yield point before the walls. However, internal pressure tests indicate that the capsule caps will deform before failure occurs. The deformation will result in the stress condition changing from bending stress (proportional to $\left(\frac{1}{\text{thickness}}\right)^2$) to hoop stress (proportional to $\left(\frac{1}{\text{thickness}}\right)$). Since the cap is thicker than the wall, it is expected that the wall will be exposed to a higher stress level than the cap before failure occurs.

a. Operating conditions

The Larson-Miller parameter (Ref. III-6) was used to determine the time-to-rupture for each combination of temperature and pressure throughout the shelf life plus mission life and beyond. A cumulative time-to-rupture technique (Ref. III-7) was used because the stress condition in the capsule wall changes with time and the Larson-Miller parameter was used because the stress condition in the capsule wall changes with time and the Larson-Miller parameter (Fig. III-4) is for a given stress level. For each arbitrary time increment (five years), the maximum pressure and maximum temperature were used to determine the time-to-rupture, using the Larson-Miller equation shown below:

$$Z = T_w (\log t_r + 20)$$

Knowing the time-to-rupture, the percent of rupture life (ψ) used during the ith five-year increment may be calculated as shown below:

$$\psi_i = \frac{t_r}{\Delta t_i} \times 100$$

where:

ψ_i = percent of rupture life used during the ith time interval

T_w = capsule wall absolute temperature (°R)

t_r = time to rupture (hr)

Z = Larson-Miller parameter (°R)

Δt_i = length of ith time interval (hr)

The accumulated rupture life used is defined as:

$$\bar{\psi}_n = \sum_{i=o}^{n} \psi_i$$

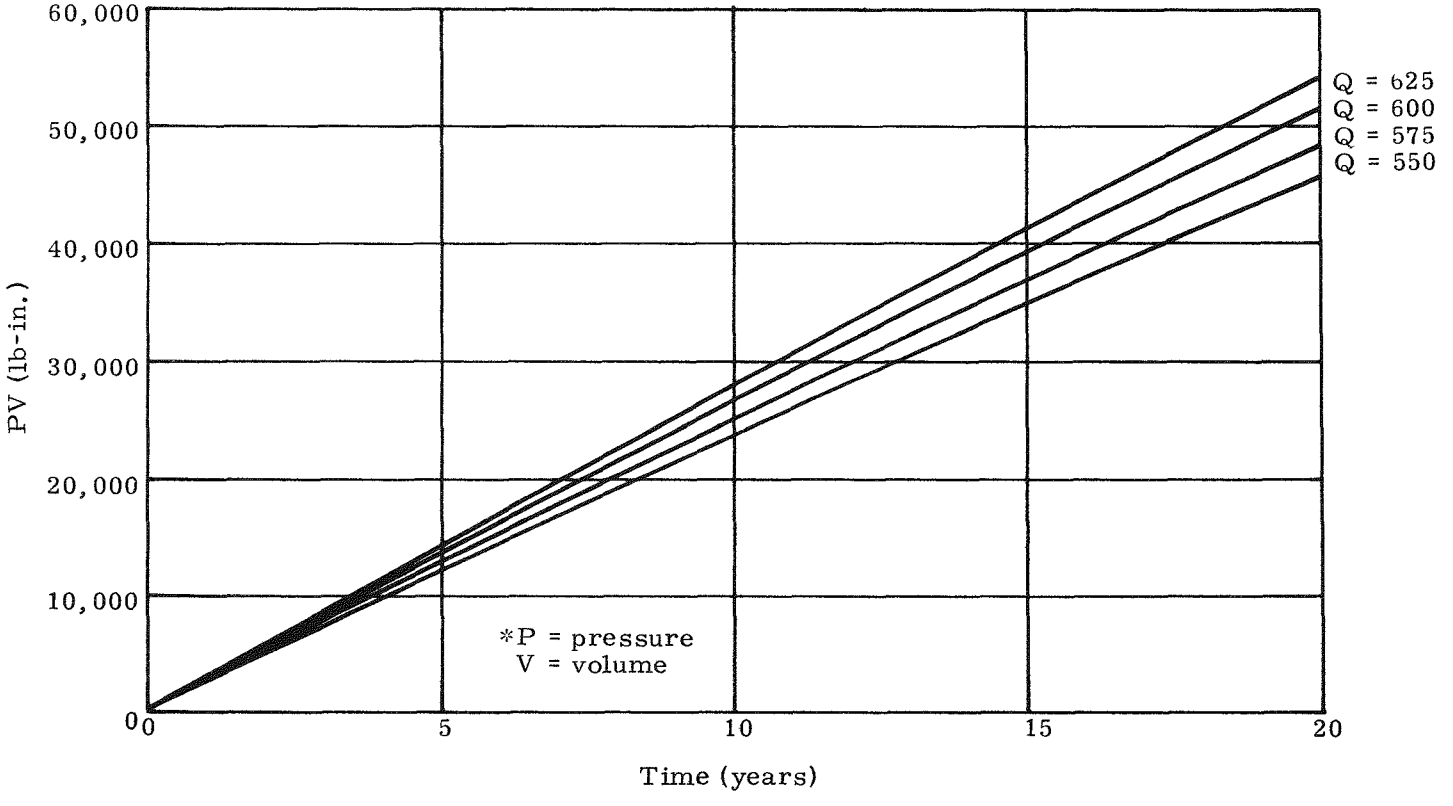

FIG. III-3. PV VERSUS TIME

CONFIDENTIAL

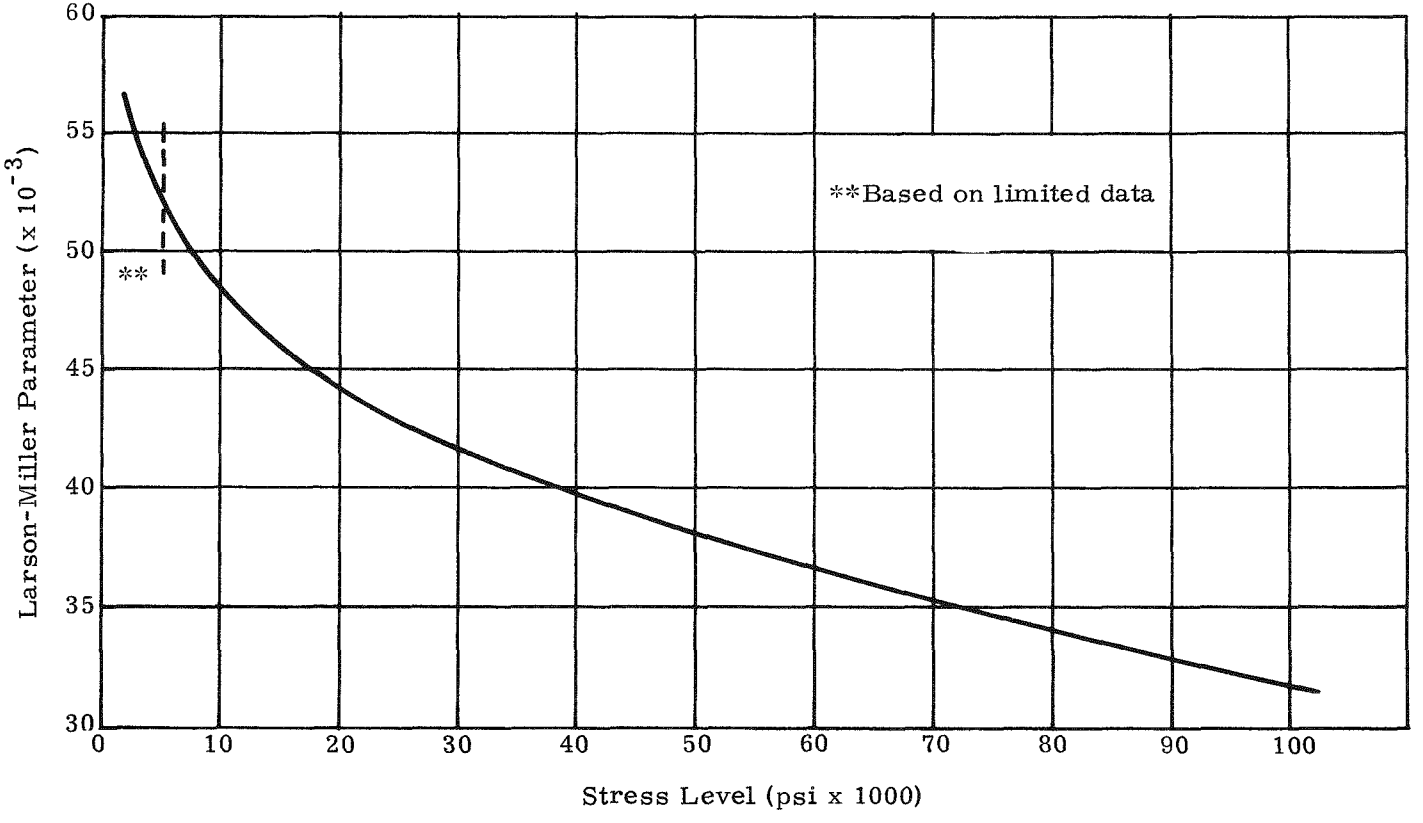

FIG. III-4. LARSON-MILLER PARAMETER--HAYNES ALLOY NO. 25

The time of failure is determined when $\bar{\Psi}$ exceeds 100%. Several possible combinations of fuel loading and power density were examined (Fig. III-5) and found to have time-to-rupture of more than 10 years. Figure III-5 calculations were made using the temperature data presented in Table III-2 (including open-circuit temperatures).

b. Accident conditions

In the event of a transportation accident fire or launch pad abort fire, the capsule temperature will be significantly higher than during operation of the generator. A sample calculation using the following fueling parameters was made:

(1) Thermal power = 570 watts

(2) Power density = 2.6 watts/cm^3 (bulk)

(3) Mass density = 9.1 gm/cm^3

(4) Time after fueling = 15 months

(5) Specific power Pu-238 = 0.570 watts/gm

The resulting times-to-rupture were:

$T_{capsule}$ (°F)	$t_{rupture}$
1700	5.7 years
1800	3.4 months
1900	9.2 days
2000	25 hours
2100	3 hours

4. Aerodynamic Characteristics

Only hypersonic aerodynamic coefficients are required for the trajectory analysis of the fuel capsule. The fuel capsule is in free molecular flow above about 390,000 feet altitude, in transitional flow from 390,000 feet to about 250,000 feet and in continuum flow below 250,000 feet. Therefore, a trajectory computation over this range of altitude must be able to adjust the aerodynamic coefficients as a function of altitude. No theoretical procedures are available to estimate the aerodynamic characteristics in transitional flow. However, this adjustment can be accomplished by providing discrete curves (independent of altitude) for the free molecular and continuum altitudes and an interpolation formula for the intermediate range. The coefficients derived for the present analysis are shown in Figs. III-6 and III-7. The free molecular values are theoretical (according to Ref. III-8) and the continuum values were obtained from tests conducted in the NASA Langley 31-inch Continuous Flow Hypersonic Facility (Ref. III-9). The interpolation formula devised by Matting and Chapman (Ref. III-10) on the basis of a kinetic theory model is:

$$C_x = C_{x_{cont}} \left[1 + \left(\frac{C_{x_{FM}} - C_{x_{cont}}}{C_{x_{cont}}} \right) e^{-(15\,\rho R)\,(1+E)} \right]$$

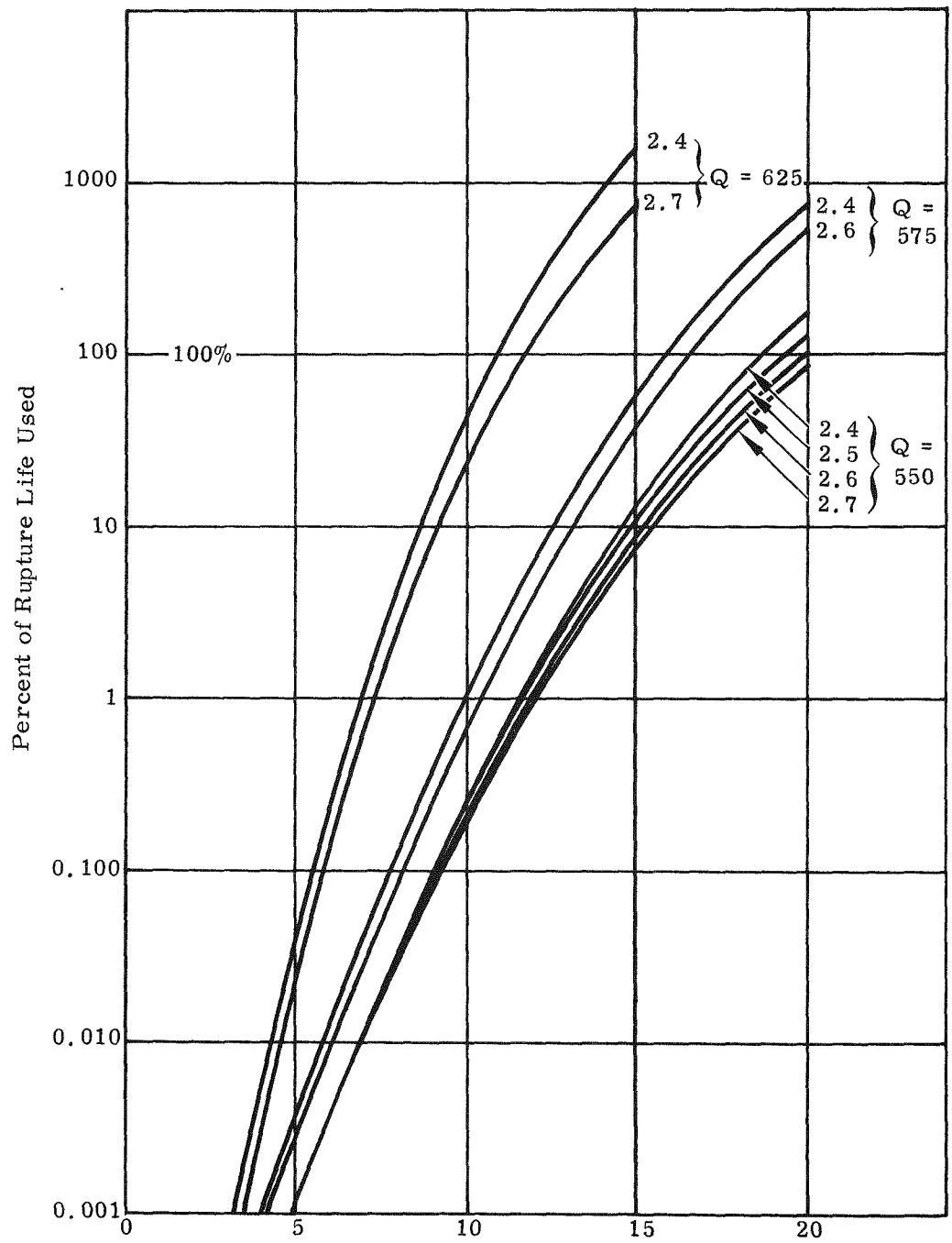

FIG. III-5. CUMULATIVE STRESS-RUPTURE TIME VERSUS FUEL LOADING

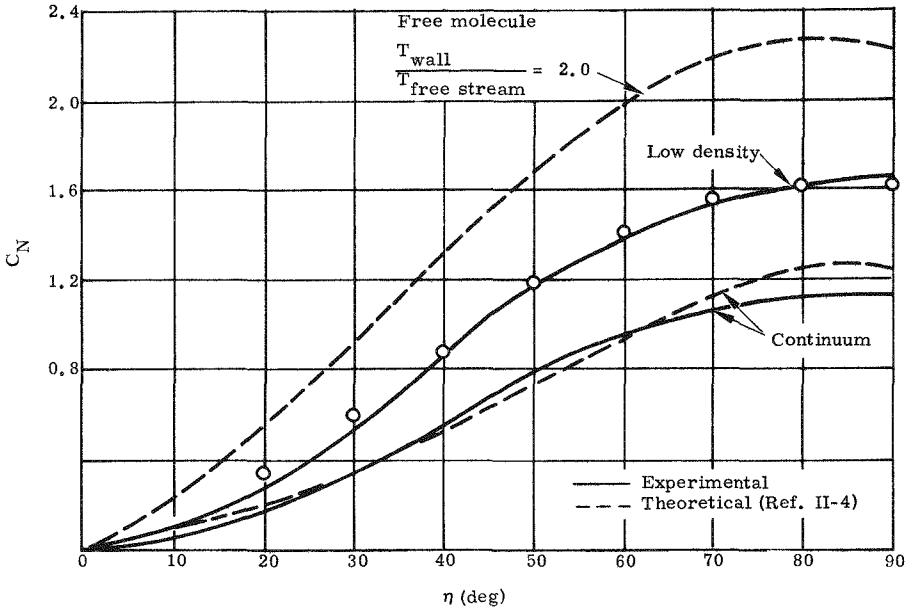

FIG. III-6. NORMAL FORCE AERODYNAMIC COEFFICIENTS FOR SNAP 19 FUEL CAPSULE

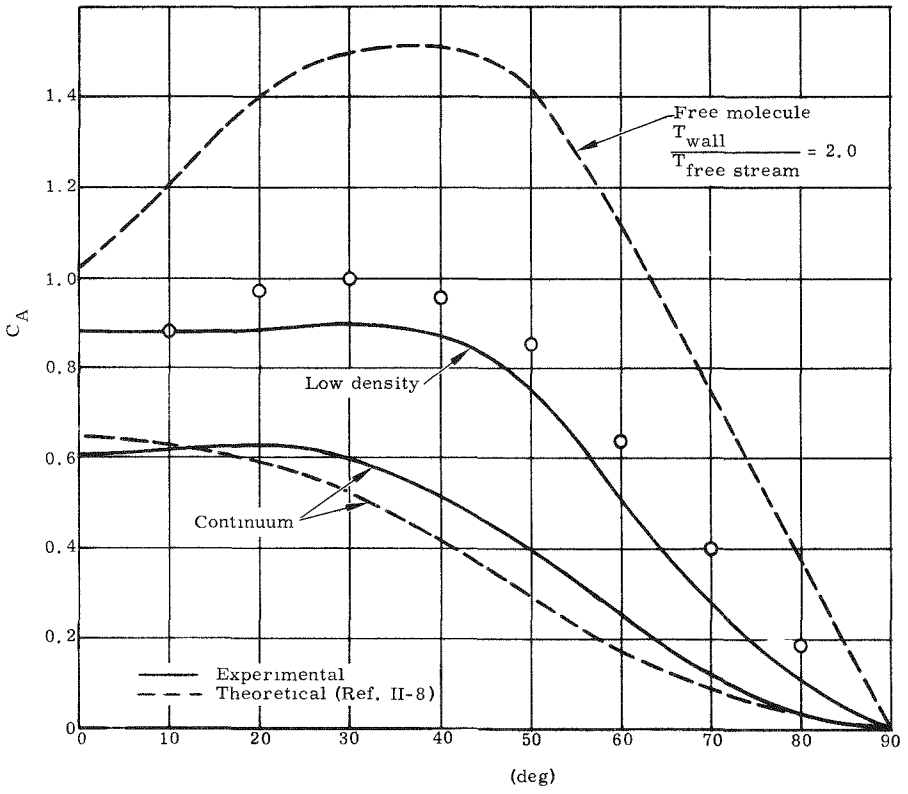

FIG. III-7. AXIAL FORCE AERODYNAMIC COEFFICIENTS FOR SNAP 19 FUEL CAPSULE

where:

$C_{x_{cont}}$ = continuum force coefficient

$C_{x_{FM}}$ = free molecular force coefficient

ρ = free stream density

R = reference length

E = adjustable constant

Using the measured normal force coefficients, C_N, and axial force coefficients, C_A, from the AEDC low density wind tunnel test of the fuel capsule (Ref. III-11) and the density corresponding to the test conditions, the constant E was evaluated for the 80° angle of attack case. Then the remainder of the curves were computed via the interpolation formula. The 80° angle of attack was chosen because it yielded the best fit of the data. Figures III-6 and III-7 show that the interpolation approximates the test data at all angles of attack.

The pitching moment coefficients, C_m, computed for free molecular flow and measured for transitional and continuum flow are shown in Fig. III-8. The free molecular values shown are based upon an assumed flat end on the capsule. The distinction between the flow regimes (Fig. III-8) is not as clear as for the C_N and C_A curves (Figs. III-6 and III-7). Therefore, a single curve was faired through the continuum and low density data for use throughout the altitude range of the trajectory. At zero angle of attack (Fig. III-8), the continuum and low density data exhibit stable and unstable trim points, respectively, whereas at a 90° angle of attack both sets of data indicate a relatively much stronger stable trim point. On the basis that the strong stable point would dominate the flight dynamics, a neutrally stable curve was used between a 0° and 24° angle of attack.

Shown for comparison with the continuum test data in Figs. III-6, III-7 and III-8 are semi-empirical curves based on the method described in Ref. III-12. The two sets of C_N and C_A curves are in good agreement but the C_m curves are not.

5. Aerodynamic Heating Characteristics

Although much work has been done on the re-entry burnup of cylindrical fuel capsules for various SNAP programs, the aerodynamic heating information has all been based on theoretical information and experimental data obtained on "long" cylinders (Refs. III-10 and III-11).

The method described in Ref. III-14 must be used with care because the averaging factors presented for the tumbling-spinning mode are not only spin- and tumble-averaged, but also represent the surface area average. For prediction of burnup, the heating at a given point on the tumbling and spinning capsule is of interest. The models used in both Refs. III-13 and III-14 are based on somewhat idealized situations, namely, a flat disk for the end-on flight mode and an infinite cylinder for the side-on or angle of attack case. The actual flow pattern on the SNAP 19 dispersion capsule differs from that of the analytical model because the capsule has a notched end which causes boundary layer separation on the face, and the low fineness ratio (2) may cause significant end effects

on the flow pattern and heating distributions at some angles of attack. Also, the location of the stagnation point shifts with angle of attack so that the boundary layer on the side of the capsule is different from that on an infinite cylinder. To determine the significance of these departures from the theoretical models, aerodynamic heating and pressure tests (Ref. III-15) were conducted at the Langley Continuous Flow Hypersonic Facility (M-10) on a full-scale capsule model. The experimental local-to-stagnation-point heating rate ratios in the windward and leeward planes, plotted versus distance from the stagnation point, are shown on Figs. III-9 and III-10 for two angles of attack. Theoretical heating rates calculated using the experimental pressure distributions are superimposed on Figs. III-9 and III-10, which show that at an angle of attack of 0° the correlation between theory and experiment is good on the capsule side. However, on the capsule face, the notches cause the flow to separate and the heating rates in the separated region cannot be predicted by the theory. At an angle of attack of 15°, the situation is similar, except that the region where the flow is separated is larger. Therefore, the use of the experimental heating rates was indicated for calculating the spin and tumble factors of the capsule. The experimental heating rates at each gage location were plotted against angle of attack and integrated numerically to find the tumble-averaged rates. All the gages on the capsule end-caps are about equally affected by tumbling, regardless of the spin angle, and the tumble-spin averaged values range between 0.43 and 0.5. On the side of the capsule, however, the heating rates are functions of both location and spin angle, so the tumble-spin averaged values represent a much wider range of values.

6. Design Limits

The minimum requirements for the fuel capsule to meet the system requirements of the SNAP 19 Nimbus B program are:

a. Thermal inventory

The thermal inventory of the loaded capsule assembly will be 570 watts. The total allowable tolerance for fuel inventory weighing and calorimetry error is $\pm$ 17 watts.

b. Leakage

The part must be rejected if the leak rate exceeds 5×10^{-7} cm^3/sec at STP) within a minimum period of 3 minutes.

c. Welding

Weld samples representative of the capsule shell and capsule cover (Martin Marietta drawings 452B1200005-001 and -011, respectively) closure joint welded with the same electron-beam weld procedures used for the fuel capsules must have a tensile strength of not less than 120,000 psi and an elongation of not less than 25% in 2 inches when tested at room temperature.

The series of subassemblies or fuel capsules must be rejected if the weld penetration is less than 75% of the nominal wall thickness for liners or less than 0.150 inch for shells.

d. Dimension checks

The completed capsule will dimensionally pass the go-not go gages (MRC Part No. M-66-4151-A3).

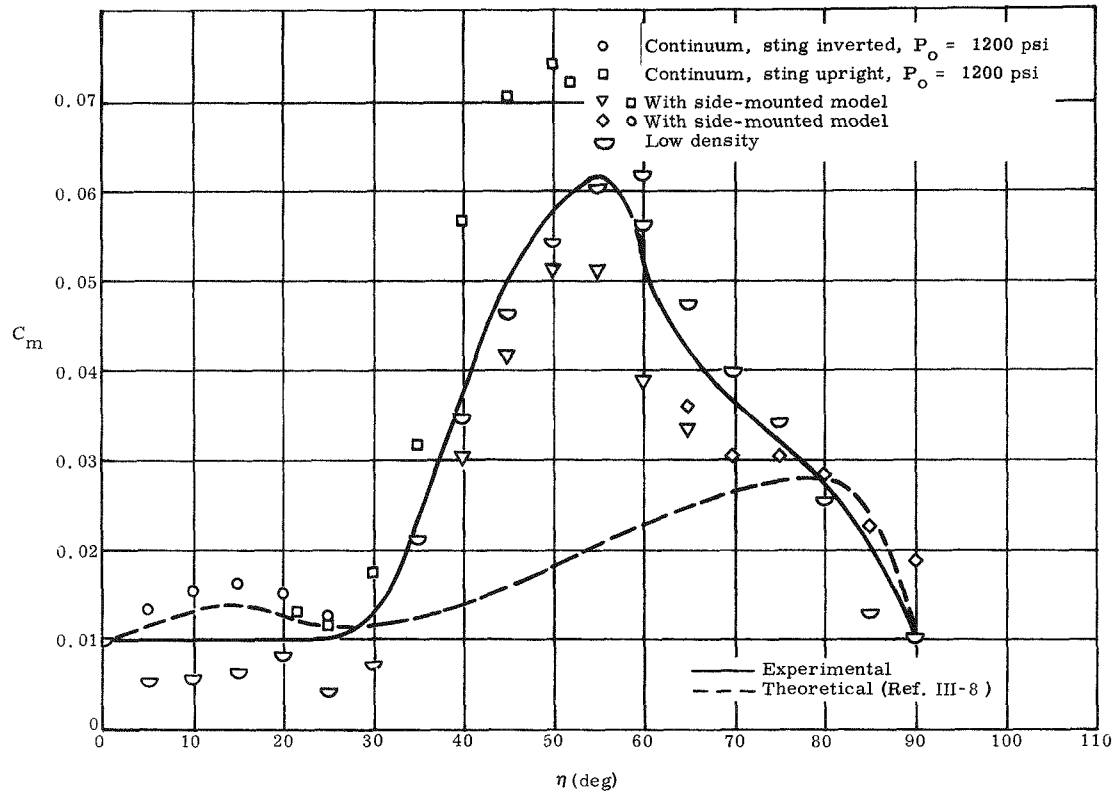

FIG. III-8. PITCHING MOMENT AERODYNAMIC COEFFICIENTS FOR SNAP 19 FUEL CAPSULE

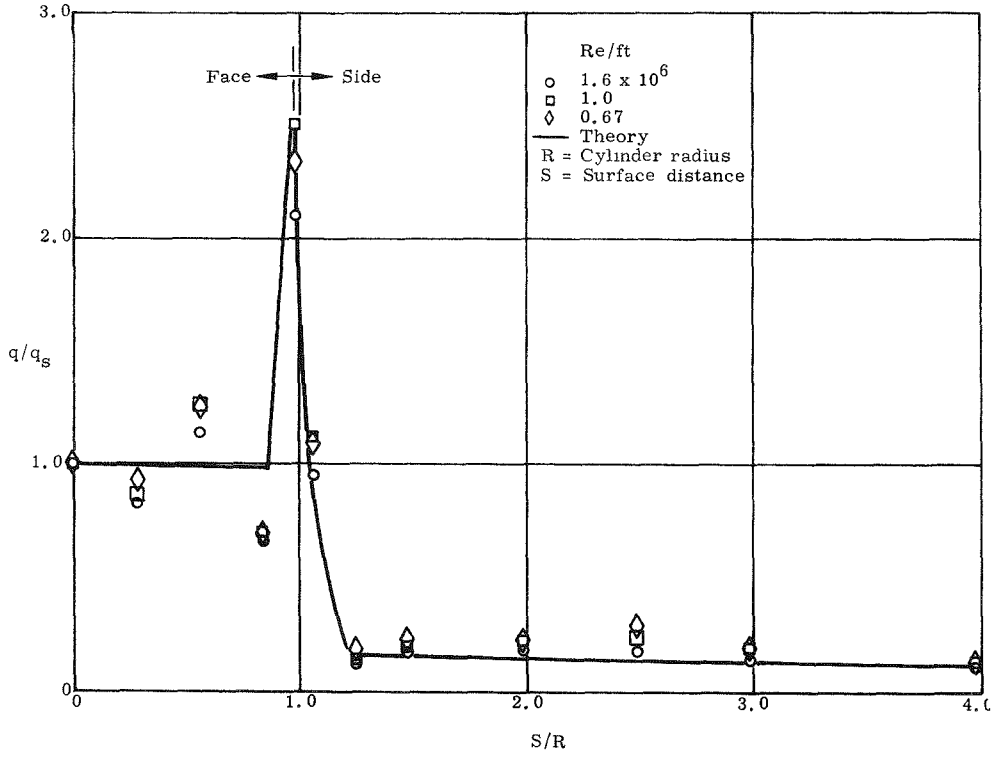

FIG. III-9. HEAT TRANSFER RATIO DISTRIBUTION, α = 0°

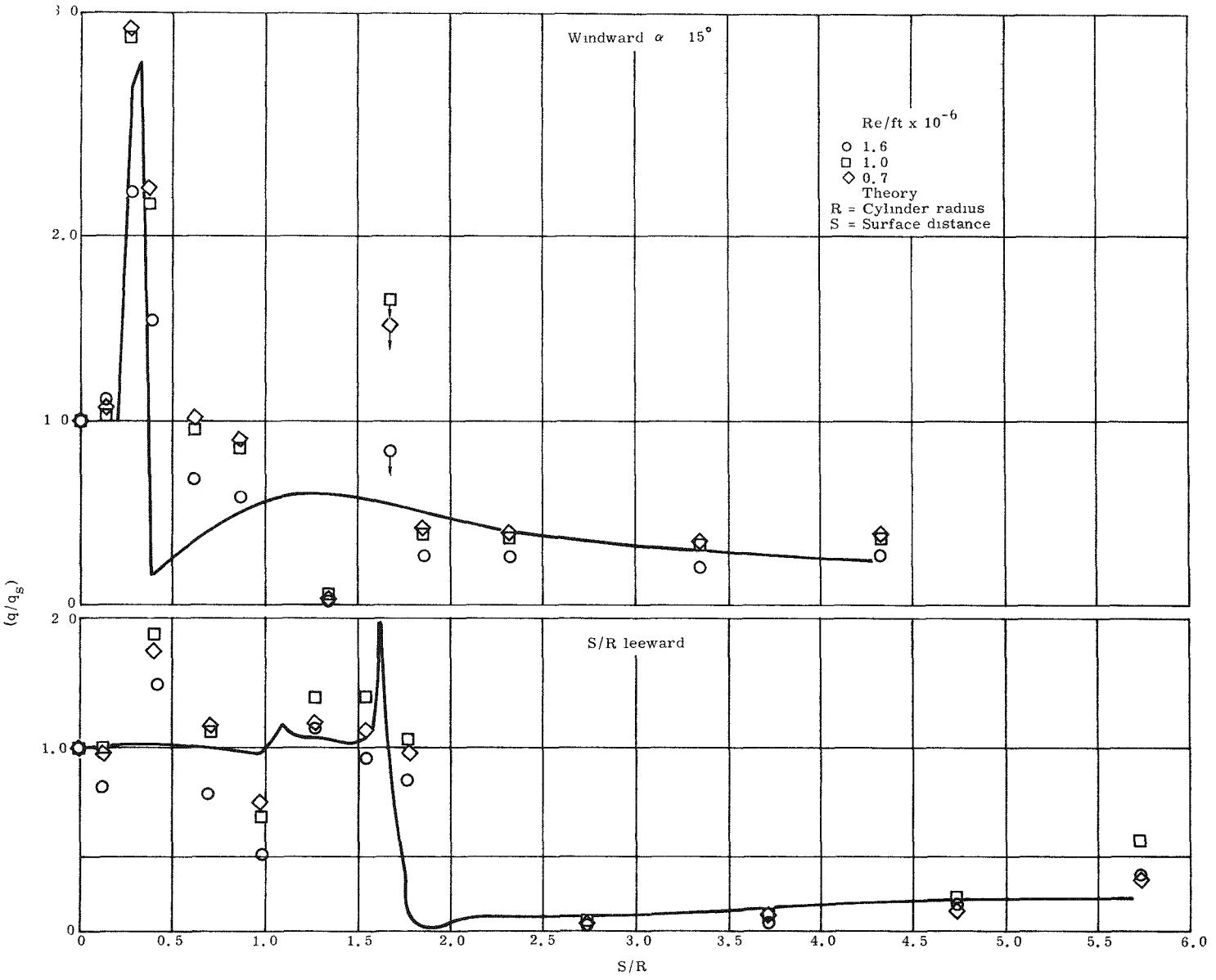

FIG. III-10. HEAT TRANSFER RATIO DISTRIBUTION, $\alpha = 15^{\circ}$

e. Radioactive contamination

The radioactive contamination of the exterior surfaces of the completed capsule shall be less than 20 dpm/100 cm^2.

f. Dose rate

Under any conditions, the radiation dose rate from the fuel capsule shall not exceed the following levels at one meter from the capsule centerline:

5.0 mrem/hr-gamma

45.0 mrem/hr-neutron

The total allowable tolerance for each reading is +10%.

C. FABRICATION AND ASSEMBLY OPERATIONS

The capsule shell was bored from 3-1/4-inch rod and the capsule caps were machined from 3/4-inch-thick disks of 3-1/4-inch rod. The liners were fabricated by seam welding 0.020-inch sheet.

The porous plugs are made of Haynes-25 felt metal with a pore size range between 4 and 26 microns. They were shrink-fitted into their supports employing a temperature differential of 900° F and the supports were electron beam welded to the liners.

The following description of the assembly fabrication was excerpted from the Monsanto Research Corporation Technical Manual (Ref. III-16).

"Upon receipt, the parts of the liner and shell assemblies are dimensionally checked and visually inspected. Each part is subjected to a dye-penetrant check to detect cracks, pin holes and other defects. Samples are selected, with the cognizance of the Quality Control Engineer, and submitted for chemical verification of the material certification.

Fabrication begins by spot-welding the inner tube of the liner to the liner end-cap. This assembly is fitted inside the outer tube of the liner and tungsten inert gas (TIG) welded in place, forming the liner subassembly. The bottom end-cap is electron beam welded to the shell, forming the shell subassembly. As examples of the welds on the fueled assembly, sets of components for both the liner and the shell are selected and welded following the same procedures. These examples are then inspected metallographically. After the metallographic inspection of the example weld and a dye-penetrant check of each subassembly, the liner subassembly is ready for fueling.

Microspheres of plutonium dioxide are received and a quantity sufficient to provide 570 $\pm$ 17 watts of thermal power is weighed and loaded into the liner subassembly. During loading, the liner subassembly is in a cooling block which is vibrated to assure good packing of the microspheres. The liner end-cap is TIG welded in place. The weld is visually inspected and the liner assembly is decontaminated. Each liner assembly is leak tested and the outside dimensions are checked.

Acceptable liner assemblies are inserted into the shell assembly and the top end-cap is welded in place with an electron beam welder. The capsule is evacuated and filled with helium twice. A pin of Haynes-25 is placed into the hole of the top end-cap

and TIG welded in place. Each welded shell assembly is visually inspected and tested for leakage in a helium leak tester. Before and after welding, examples are selected and welded, using the same procedure as for welding the fueled capsules. The example welds are metallographically inspected.

The completed fuel capsule is calorimetered to determine its power output, gaged to determine its outer dimensions, radiographed to determine the integrity of the welds, surveyed for radiation and packaged. Both the capsule and the package are certified to be at a safe level of contamination and external radiation by Health Physics."

D. HANDLING AND SHIPPING

The SNAP 19 shipping containers satisfy all government regulations relating to the shipment of the SNAP 19 fueled capsules. Furthermore, a Bureau of Explosives (BOE) permit was obtained for the transportation container, which provides shielding to comply with the ICC radiation criteria. All hypothetical accident conditions included in Title 10, Code of Federal Regulations, Part 71 have been investigated and shown to lead to no significant hazard.

Special Nuclear Material License No. 849, issued by the AEC to the Martin Marietta Corporation, authorizes the possession of the fuel and the assembly and performance testing of SNAP 19 generators at the Martin Marietta facilities in Middle River, Maryland.

During testing of the SNAP 19 generators, Health Physics personnel monitored the complete test program, imposing safeguards where required. For a complete description of safety controls, see Refs. III-17 and III-18.

Special nuclear material, including Pu-238, may cause a nuclear excursion under proper conditions of configuration and quantity. Unless used in proximity to other special nuclear material, the Pu-238 contained in a SNAP 19 generator presents no possibility of a nuclear incident. However, because of the possibility of proximity with other special nuclear material during transportation in commercial channels, AEC approval of the shipping methods and procedures was required prior to actual shipment. AEC concurrence was obtained in exclusive use of a courier van for transport of the SNAP 19 fuel capsules.

The Interstate Commerce Commission is also concerned with the safety of the public in connection with the transport of hazardous material including radioactive material, explosives and toxic chemicals. The ICC regulations for hazardous material, published in Tariff 15, define permissible radiation levels and shipping container specifications. Compliance with the permissible radiation levels was met in the design and construction of the shipping container. Approval of the container for use in interstate traffic was granted by the Bureau of Explosives.

The shipping container for dispersal capsules was designed to the above requirements and is described below.

1. Capsule Container

The fuel capsule shipping container (Fig. III-11) is made entirely of 6061T6 aluminum alloy. There are 80 fins soldered to the outer surface to provide heat rejection. The thickness of the aluminum housing was dictated by shielding requirements and physical protection of the fuel capsule. The container with capsule weighs about 325 pounds.

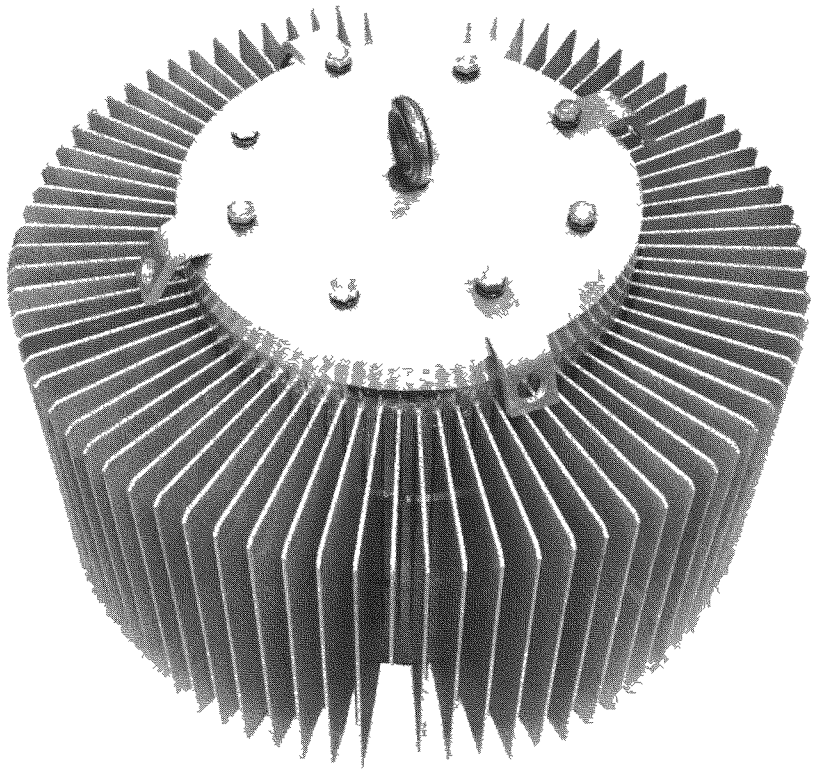

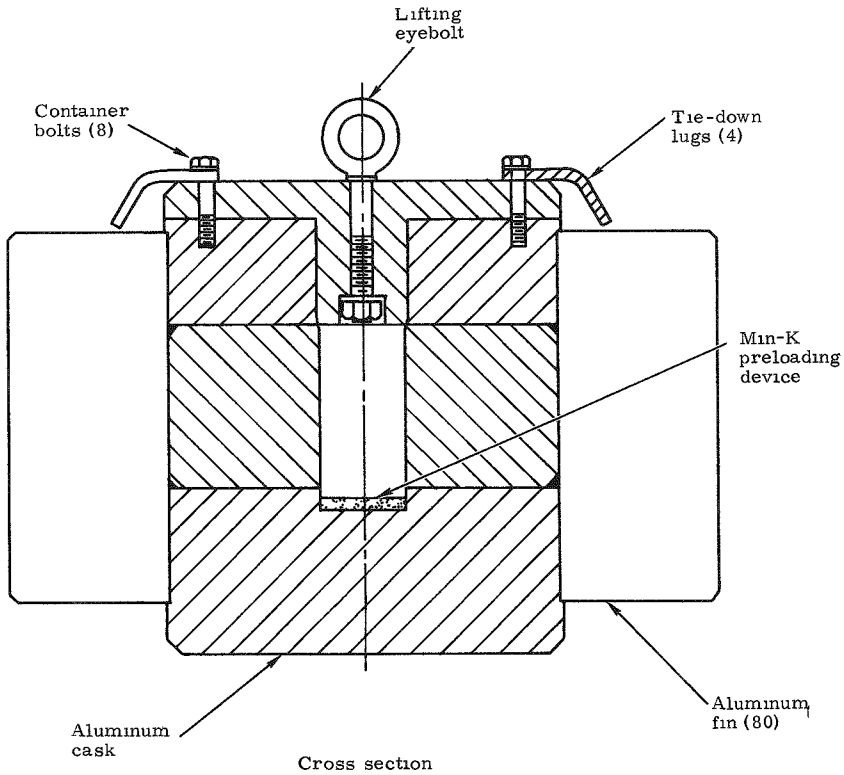

FIG. III-11. FUEL CAPSULE SHIPPING CASK

2. Hypothetical Accident Conditions

Analysis of the various accidental conditions which could occur during transportation or handling would involve numerous cases, of which only a few could be considered credible. Therefore, standard accidents were used to represent the credible accident conditions which could occur for the generator and fuel capsule during transportation, handling and testing. Enumeration and/or analysis of each shipment or test was not made; instead, standard accidents, such as drop, puncture, fire and water immersion, were evaluated.

a. Free drop and puncture

All mechanical accidents considered credible for the SNAP 19 capsule during handling and transportation are represented by the 30-foot drop test. The standard puncture test requires that a six-inch bar be used. Since the SNAP 19 dispersion capsule dimensions are 2.98 inches in outer diameter and 6.125 inches in length, a six-inch diameter bar would constitute an impact, not a puncture test. The energy available to cause rupture by dropping the capsule a distance of 40 inches for the puncture test is far less than that which would be available from the free drop test (30 feet). Therefore, the mechanical requirements imposed by the drop test were considered to encompass the puncture test requirements for this capsule design.

A comprehensive program of impact testing of fuel capsules was conducted before the first shipment of fueled generators was made. These tests determined the velocity of impact on granite required to destroy the containment integrity of the capsule. Failure velocities varied from 310 ft/sec at impact angles of 90° to 110 ft/sec at the critical impact angle of 33°. These failure velocities are greatly in excess of the maximum 44 ft/sec impact velocity associated with a 30-foot drop test.

b. Thermal

An analysis was performed to show conclusively that the conditions of Paragraph 71.37, Title 10, Code of Federal Regulations, Part 71 in regard to a standard fire will not result in a fuel release. The results of this analysis are summarized for these three limiting cases:

(1) A temperature of 1200° F at the inner surface (around the capsule) of the shipping cask

(2) The bare capsule exposed to 1475° F fire

(3) Maximum heat input to container from fire and fuel.

Case 1: Inner surface temperature of 1200° F. With the assumption that the gap between the fuel capsule and shipping container was filled with air and was 38 mils wide, the surface temperature of the fuel capsule necessary to reject the heat from the fuel by radiation and conduction across the air gap to a sink of 1200° F (the melting point of aluminum) was 1525° F. This is far below the melting point of the Haynes-25 capsule. In the analysis, the thermal conductivity of the air in the gap was taken to be 0.039 Btu/ft-hr-°F, and the emissivities of the fuel capsule and aluminum shipping container were assumed to be 0.30 and 0.15, respectively. The fuel inventory was taken as 625 watts in all three cases. The gap width was doubled to allow for differential expansion of the aluminum.

Case 2: Bare capsule in 1475° F fire. For this case, only radiation was considered, and any heat rejected by the ends of the fuel capsule was neglected. The emissivities used for the capsule and the flame were 0.3 and 0.9, respectively. This case assumed

that all of the aluminum shipping container has melted and fallen away, leaving the bare capsule. The calculated surface temperature of the capsule for this condition was 1775° F. The capsule temperature was below its melting point.

Case 3: Average temperature of shipping cask for maximum heat input. An analysis was performed to determine what would actually happen to the shipping cask during the 30-minute fire. To examine this case, it was conservatively assumed that the surface of the shipping cask was at a temperature of 120° F for the full 30 minutes in the determination of the heat input from the fire. Therefore, a maximum value for the heat input was used. With the heat input from the fire and from the capsule fuel, the average temperature rise of the aluminum was determined by using a value of 0.213 Btu/lb-°F for the heat capacity. As a result, it was found that the average temperature of the shipping container would be 970° F after the 30-minute fire. Even for this conservative analysis, the average temperature of the container is below the 1100 to 1205° F aluminum melting point.

Thus, the thermal requirements for shipping of the fuel capsule have been met in compliance with Title 10, Code of Federal Regulations, Part 71.

c. Water immersion

Failure of the capsule shipping cask in an accident is unlikely, but if the cask should fail, exposure of the capsule to thermal shock by immersion is possible. However, the capsule will not experience detrimental effects from the thermal shock, as proven by shock tests with the capsule at 1100° F(and 305 fps impact velocity). Capsules in the cask have an equilibrium temperature of only 550° F during transportation.

Release of fuel because of corrosive action does not represent a serious problem. Immersed in seawater, a bare capsule will not release fuel by corrosion for approximately 100 years, and the time-to-release in fresh water is even greater.

E. FUEL CAPSULE DEVELOPMENT AND EVALUATION TESTING

The SNAP 19 dispersion capsule assembly was subjected to a series of tests to evaluate the structural integrity under various conditions. A portion of the testing was designed to determine the mode of failure of the capsule and to evaluate the consequences of such failure. The scope of this effort included the investigation of environments related to (1) launch pad aborts, e.g., thermal shock related to water immersion, fireball and residual fire tests, and high velocity impact tests; (2) ascent trajectory aborts, e.g., capsule disintegration, aerodynamic force and moment tests, and pressure and heat distribution tests; and (3) the post-mission history, e.g., capsule-in-generator burst tests.

1. Thermal Shock Test

The objective of the thermal shock test was to determine the ability of the fuel capsule assembly to retain its structural integrity after being plunged into lake or ocean water at its re-entry temperature.

The capsule assembly was furnace-heated to 1800° F, air cooled to 1150° F and catapulted by rocket sled into a tank of water at 300 ft per second. The specimen was allowed to cool down while submerged. Visual, dye penetrant and radiographic examinations were made of each specimen.

No observable defects were found on the exterior of the test specimens. Gammagraphic examination of one specimen (2B-2) indicated that the inner liner column was slightly buckled and that one porous plug was dislodged from the retainer. There was no evidence of internal cracking or of migration of the fuel simulant into the central void.

Thus, it was concluded that the SNAP 19 fuel capsule assembly will retain its structural integrity when plunged into ocean or lake waters at expected re-entry temperatures.

2. Internal Pressure Test

The objective of this test was the determination of the rupture characteristics of an unrestrained fuel capsule assembly under two different conditions:

(1) The beginning-of-life temperature (1100° F)

(2) The 23-month internal pressure (272 psia).

Five capsule assemblies were tested in this series. Each was suspended, unrestrained, within a radiant heater assembly. Three capsules were held at a stable temperature of 1100° F ± 25° while the internal pressure was raised at a constant rate until failure occurred.

Two capsule assemblies were heated to a stable temperature of 1100° F ± 25° and then pressurized to 286 psig. The capsule pressurization system was sealed off and the temperature raised until failure occurred.

The difference in initial conditions of these tests resulted in two distinctly different failure modes.

a. Case 1, increasing pressure

Post-test examination indicates that the capsule circumference increases approximately 32% and is accompanied by thinning of the wall from 0.100-inch to approximately 0.072-inch thickness at the point of maximum circumference. Initial failure occurs at the maximum circumference point, followed by longitudinal propagation of the fracture to and around both end-caps. Heater destruction and capsule component separation were complete and the fuel simulant was completely dispersed. See Table III-3 for failure pressures.

b. Case 2, increasing temperature

Recorded data and post-test examination indicate that very little yielding of the sidewalls takes place at high temperature (Fig. III-12). End-cap yielding causes bending at the cap-wall weld zone, resulting in circumferential cracking at the weld area and subsequent loss of pressure. On one specimen (2B-5) the end cap completely separated and the liner assembly was ejected. No damage was done to the ceramic heater assembly used in these tests. See Table III-3 for failure data.

c. Conclusions

The failure mode of an unrestrained fuel capsule under short-term high pressure test may be described as catastrophic (Fig. III-13 and III-14). This test did not allow for or permit material creep to be a factor of consideration. The failure pressures realized agree favorably with the short-term calculated failure pressure of 7190 psig.

TABLE III-3

Fuel Capsule Test Summary

Test Name and Conditions	Test No.	Specimen Serial No.	Temperature at Failure (°F)	Pressure at Failure (psig)	Time to Failure	Remarks
Thermal Shock:						
Preheat to 1800° F; Air-cool to 1150° F;	301	2B-1	--	--	--	Dye penetrant and gamma-graph inspection revealed no failures.
Plunge into 65° water at 300 ft/sec	302	2B-2	--	--	--	
Internal Pressure Test--Capsule Unrestrained:						
Constant temperature of 1100° F ± 25° F;	1	348	1100 ± 25	6350	47 min	Violent sidewall rupture.
Increase pressure to failure	2	2B-3	1100 ± 25	5800*	31 min	Violent sidewall rupture.
	3	2B-4	1100 ± 25	6400	42 min	Violent sidewall rupture.
Initial lockup pressure 286 psig	4	2B-6	2140	410	40 min	Crack, EB weld area.
± 2 psi at 1100° F; Increase temperature to failure	5	2B-5	2150	405	40 min	Wall failure, EB weld area; end cap blown off.

*Heater failure at 4800 psig caused test abort and cooldown. Test resumed after temperature stabilized.

CONFIDENTIAL

TABLE III-3 (continued)

Test Name and Conditions	Test No.	Specimen Serial No.	Temperature at Failure (°F)	Pressure at Failure (psig)	Time to Failure	Remarks
Capsule-in-generator burst test: Constant temperature of 1360° F + 25°; initial pressure buildup ~50 psi/min/ Step pressure periodically to induce creep rupture	Capsule assembly No. 1	2B-1	1370	2300	23 hr	Pressure tube weld failure--no test.
	Capsule assembly No. 2	2B-2	1375	2650	99.85 hr	Former thermal shock capsule heated to 1800°F; crack in EB weld area.
	Capsule assembly No. 3	2B-14	1390	2300	9.9 hr	Crack in EB weld area
	Generator assembly No. 1	2B-11	1340	2300	1.8 hr	EB weld area failure--end cap blown off; generator housing pressure 230 psig decayed to 90 psig and held.
	Generator assembly No. 2	2B-9	1360	1965	3.4 hr	EB weld area cracks; generator housing pressure 192 psig decayed to 75 psig and held.
	Generator assembly	2B-1	1368	2300	0.6 hr (23.6 hr) (cumulative)	EB weld area cracks; capsule former thermal shock capsule and capsule assembly test No. 1. Generator housing pressure 230 psig slowly decayed.
	Generator assembly No. 4	2B-10	1350	2300	0.86 hr	EB weld area failure--end cap blown off; generator housing pressure 240 psi decayed to ambient in 13 hrs. Pressure tube-to-housing weld broken.

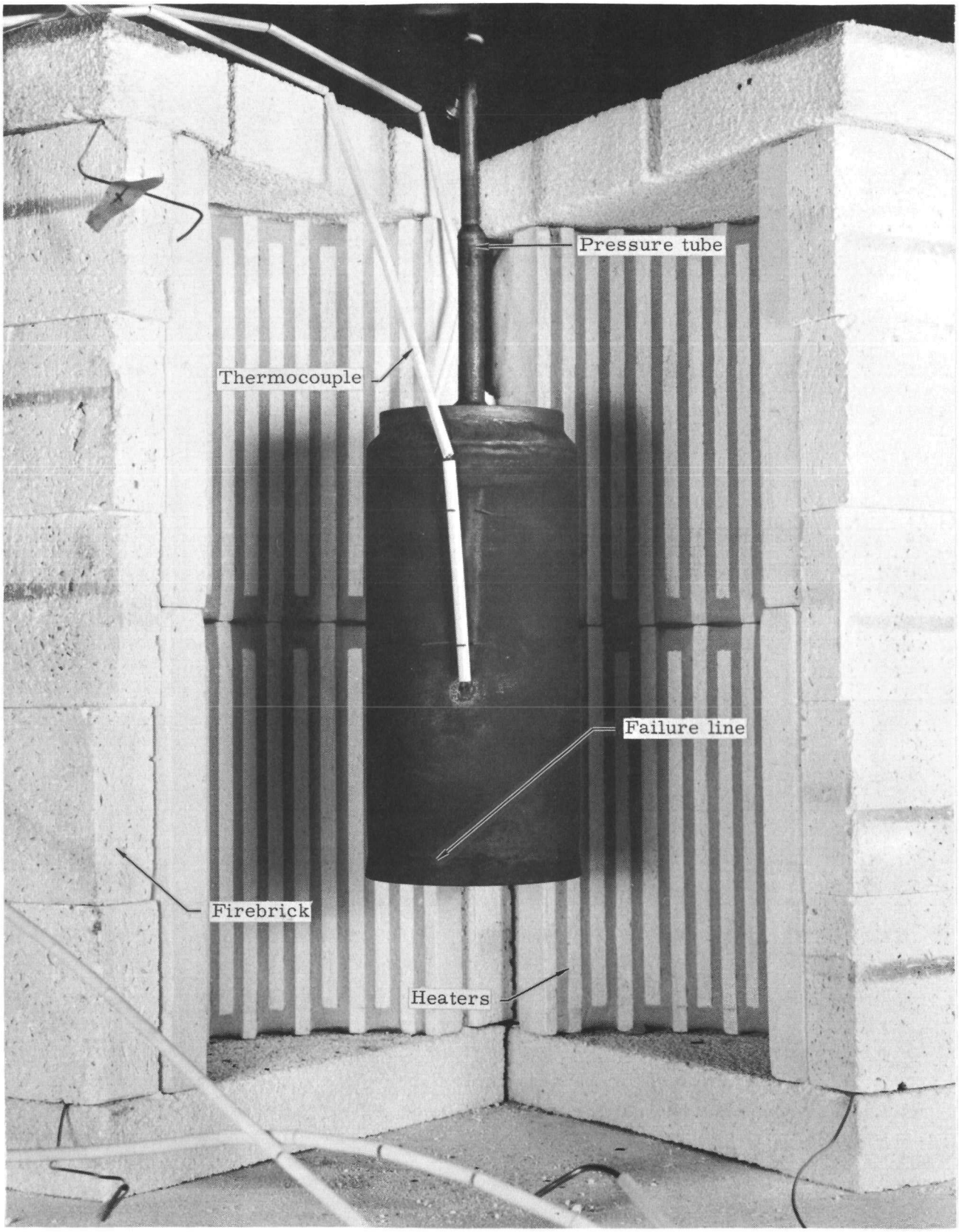

FIG. III-12. INTERNAL PRESSURE TEST NO. 4, CAPSULE 2B-6--POST-TEST CONDITION

FIG. III-13. POST-TEST RUPTURE AT 5800 PSIG

FIG. III-14. POST-TEST RUPTURE AT 6400 PSIG

The failure mode of the unrestrained fuel capsule under short-term, high temperature exposure is completely nonviolent, with all components remaining in the immediate area. This type of failure would compare favorably with that expected in a fire environment resulting from a transportation incident.

3. Capsule-in-Generator Burst Test

The objective of this series of tests was to ascertain:

(1) The failure mode of a restrained fuel capsule under pressurization

(2) The capability of the SNAP 19 generator housing to contain the radioisotope fuel particles after rupture of the fuel capsule

(3) A preliminary evaluation of the Larson-Miller parameter used to determine the creep rupture capability of the capsule.

Each capsule tested was installed in a generator housing (or simulated housing) and maintained at a temperature of 1360° F ± 25° by electric heater elements embedded in the surrounding graphite block. Pressurization of the capsules was accomplished with argon gas and a regulator in accordance with a pressure-versus-time schedule to induce creep rupture. Three capsules were tested in simulated housings (hereafter called capsule assemblies) and the remainder were tested in generator assemblies from SNAP 19 system No. 1. Each capsule assembly and generator assembly was instrumented for capsule pressure, capsule temperature and housing temperature. Each generator assembly was also instrumented for housing internal pressure.

Initial pressurization to 2300 psig was accomplished over a period of one hour and the system was isolated from the pressure source. Each 24 hours thereafter, the pressure was raised 100 psi until 2600 psig was achieved. At that point, pressure adjustment was in 50 psi increments at 12-hour intervals. In one case, initial pressure was set at 2000 psig.

The first capsule assembly test was aborted after 23 hours due to a leak at the pressurization tube weld. All other tests ran to capsule failure. In every instance, failure occurred in the EB weld area at the point where the sidewall bends and the end cap rotates as a result of yielding. In one instance (generator assembly No. 1), the end cap completely separated (Fig. III-15), the liner ballooned out 3/4 inch and the pressurization tube between the capsule and generator cover buckled in column loading.

The generator housing pressure in each case rose to a value of approximately 10% of capsule pressure at failure. The housing pressure initial decay rate of approximately 120 psi/hr decreased with time after the first hour. The generator housings maintained 50 to 90 psig in the systems for a minimum of twenty-four hours and until manually released. There was no evidence of housing or cover failure in any of the generator assembly tests. Upon disassembly of the generator housings, it was noted that the graphite block assembly in generator assemblies No. 1 and No. 3 was cracked longitudinally in the heater channels. In generator test No. 1, the end cap separation forces crushed the Min-K insulation approximately 1/2 inch and cracked it through in several places. Cracking of the Min-K blocks in the top of the generators was concentrated about the penetrations made for the pressurization tube, heater and thermocouple wiring. See Table III-3 for summary of results.

The primary and secondary objectives of the capsule-in-generator burst tests were realized.

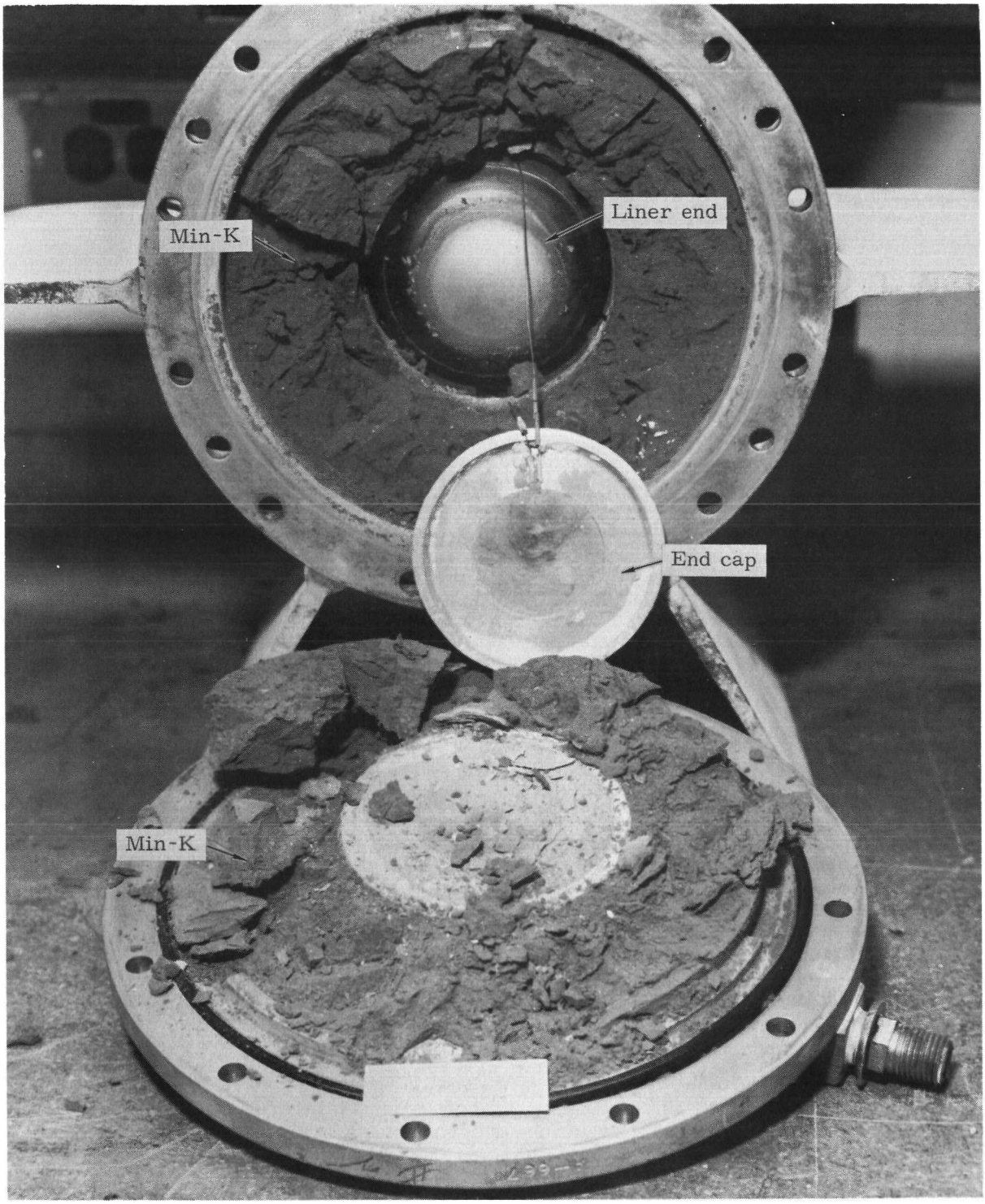

FIG. III-15. MODULE ASSEMBLY AFTER TEST, SHOWING CRACKING OF GRAPHITE-BLOCK AND MIN-K INSULATION

The mode of capsule failure when restrained in a generator is characterized by failure of the EB weld area in bending produced by yielding of the end caps. Separation of the end cap permits ballooning of the liner assembly until failure occurs, releasing gas pressure into the housing. The tests indicate that the housing design is capable of enduring a capsule rupture with containment of the capsule components.

Any evaluation of the Larson-Miller parameter used to determine creep rupture capability of the fuel capsule must consider the effect of capsule geometry change during yielding and also the material property changes created by the EB weld. It is significant that capsule No. 2B-2, which failed at 99 hours and 2650 psi (versus theoretical failure at 135 hours and 2800 psi), was previously exposed to 1800° F heat-up and quench, which materially increased the ductility of the weld areas.

4. Capsule Vibration Test

The objective of this development test was to investigate the structural characteristics of the capsule design prior to vibration testing of fueled SNAP 19 generators. A sinusoidal vibration test was performed on one fuel capsule (simulated fuel), S/N 99, and on one porous plug assembly, S/N 55. The internal fuel containment features of the capsule and the ability of the basic fuel capsule and the porous plug assembly to withstand a high-level vibration environment were demonstrated.

a. Test methods

The design configuration of the SNAP 19 fuel capsule includes a welded inner liner assembly containing two porous plugs to prevent fuel infiltration into the helium expansion void volume. At the time of this test program, complete fuel capsules containing the porous plugs were not available. However, a number of capsules intended for impact testing were available which were complete in all respects, including simulated fuel, except for the porous plug modification. Since the structural integrity of the inner liner is probably not changed significantly by the presence of the porous plugs, it was considered valid to perform vibration tests with one of the capsules intended for impact tests. All of the basic fuel retention properties of the capsule design would thus be demonstrated under a vibration environment except for the installation and construction of the porous plug details. These were demonstrated in separate vibration tests of a welded inner liner assembly with porous plugs installed. This assembly was selected from normal production hardware.

Specific test sequences are described in Ref III-19, where the laboratory test procedure is reproduced.

b. Fuel capsule results

The specimen mounting arrangement is illustrated in Fig. III-16 for the radial plane vibration. X-rays of the specimen before test were made in two orientations 90° apart.

No damage was evident after the completion of testing at 20 g and 40 g levels. The X-rays indicated that the simulated fuel did not leak into the inner portion of the capsule. Similarly, no damage was apparent to the specimen after the 60 g run (Fig. III-17). Pre-test and post-test leakage measurements indicated no change in the specimen. Results of the leak tests indicated no detectable leak at a sensitivity of 10^{-9} std cm^3He/sec.

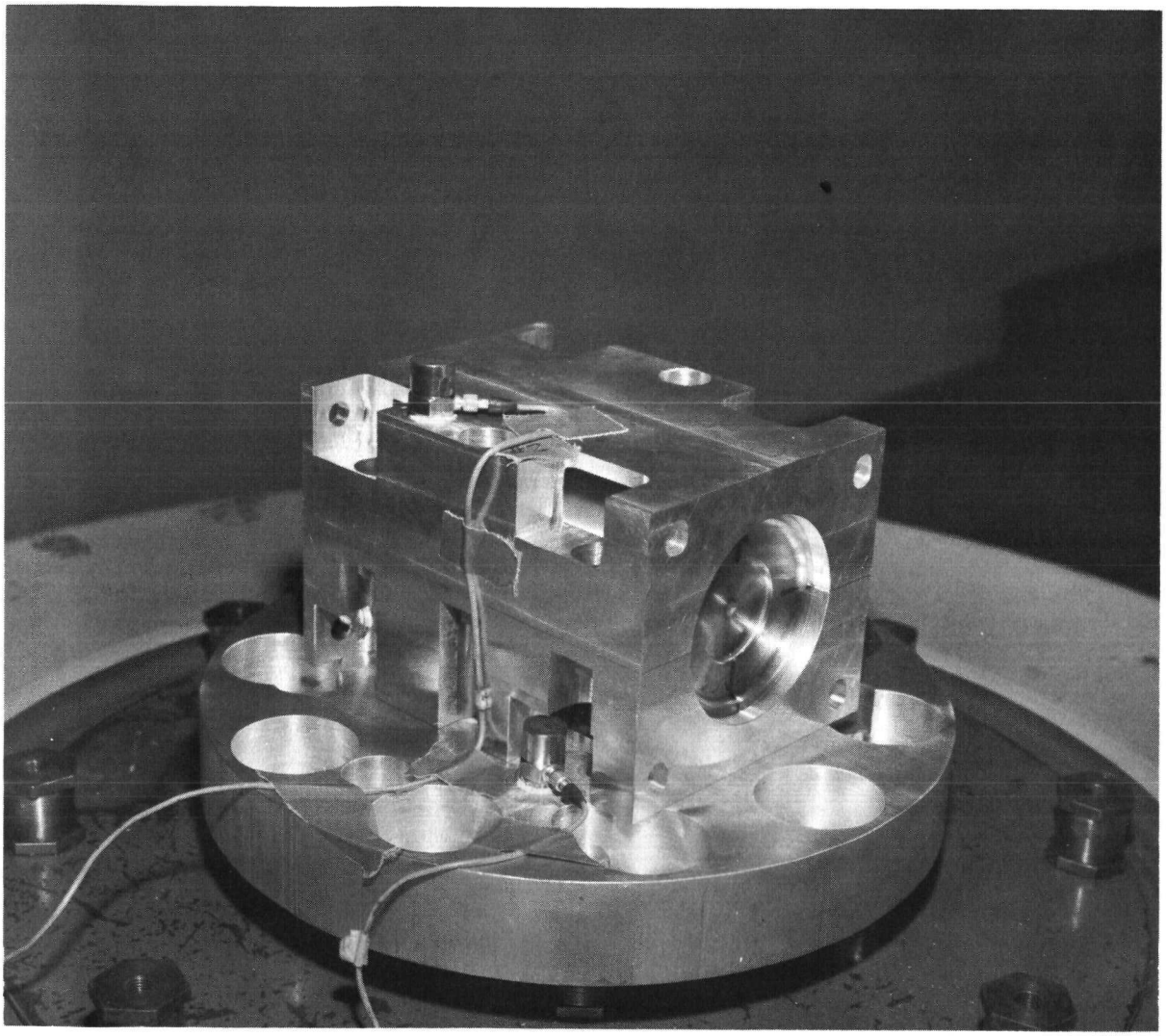

FIG. III-16. RADIAL PLANE VIBRATION

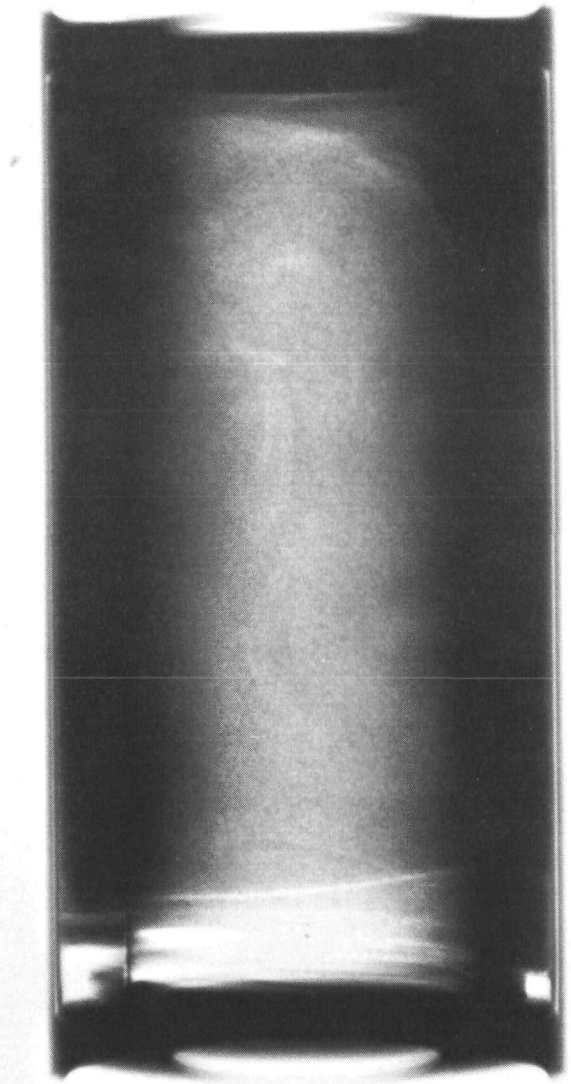

FIG. III-17. POST-LONGITUDINAL VIBRATION X-RAY NO. 1--60 G

c. Porous plug assembly results

The radial and longitudinal mounting configurations were similar to those of the fuel capsule.

No damage was visually evident after the completion of vibration tests at 20 g, 40 g and 60 g.

5. Impact Tests

Four series of impact tests were conducted during development of the dispersion capsule. The primary objective of Series 1 was to determine the critical angle of impact; that is, the angle at which the lowest failure velocity occurred. A secondary objective was to define the mode of capsule failure. The results of the Series 1 tests (test Nos. 101 to 129) are shown in Fig. III-18 and Table III-4. The tests consisted of 29 capsule impacts at angles of 0° through 86° and at velocities from 190 to 361 fps. All Series 1 tests were conducted using a granite target. Each test specimen was preheated to a temperature above the 1100° F $\pm$ 50° impact temperature, and calibration cool-down curves were used to establish actual impact temperature.

The failure/success data plot (Fig. III-18) indicates that the critical angle was at 33° $\pm$ 7° as measured between the capsule longitudinal axis and the line of flight. The actual impact angle was obtained from high speed motion picture film. Specimen velocity was derived from chronograph readings and analysis of high speed motion picture film.

Visual and radiographic examination of each test specimen indicated that failures may be classified into three general modes. The first, and most obvious, failure (Fig. III-19) is that in which the capsule wall buckles, rolls over the end cap and is torn away as the capsule rolls or slides after the initial impact. The second failure mode (Fig. III-20) is evident in the electron beam weld area, where hidden weld failure permits movement and/or bending at the cap-wall interface, often extruding the visible EB weld outward. The third type of failure (Fig. III-21) appears as a crack in the capsule side wall adjacent to the EB weld area and occurs when the wall deformation exceeds the end cap deformation.

The objective of Series 1R-1 tests was to further define the critical angle found from the Series 1 results. Six tests (test Nos. 130 to 135) were conducted, and the results are shown in Fig. III-22).

The objective of Series IIA tests (six capsules, test Nos. 201 to 206) was to explore the difference in impact characteristics between the Series 1 capsule design and the final SNAP 19 dispersion capsule design (Section III-B). The design changes included the addition of the porous plugs and an increase in the number and type of EB welds from four focused beam to five diffused beam passes. The results are shown in Fig. III-23 and indicate no significant positive effect of the design changes on capability to withstand impact.

The objective of Series IIB tests (five capsules, test Nos. 207 to 211) was to establish the minimum failure velocity at the critical angle. The results, presented in Fig. III-24, show a minimum failure velocity of approximately 110 fps. Capsule failure was defined as any leak greater than $10^{-3} cm^3/sec$.

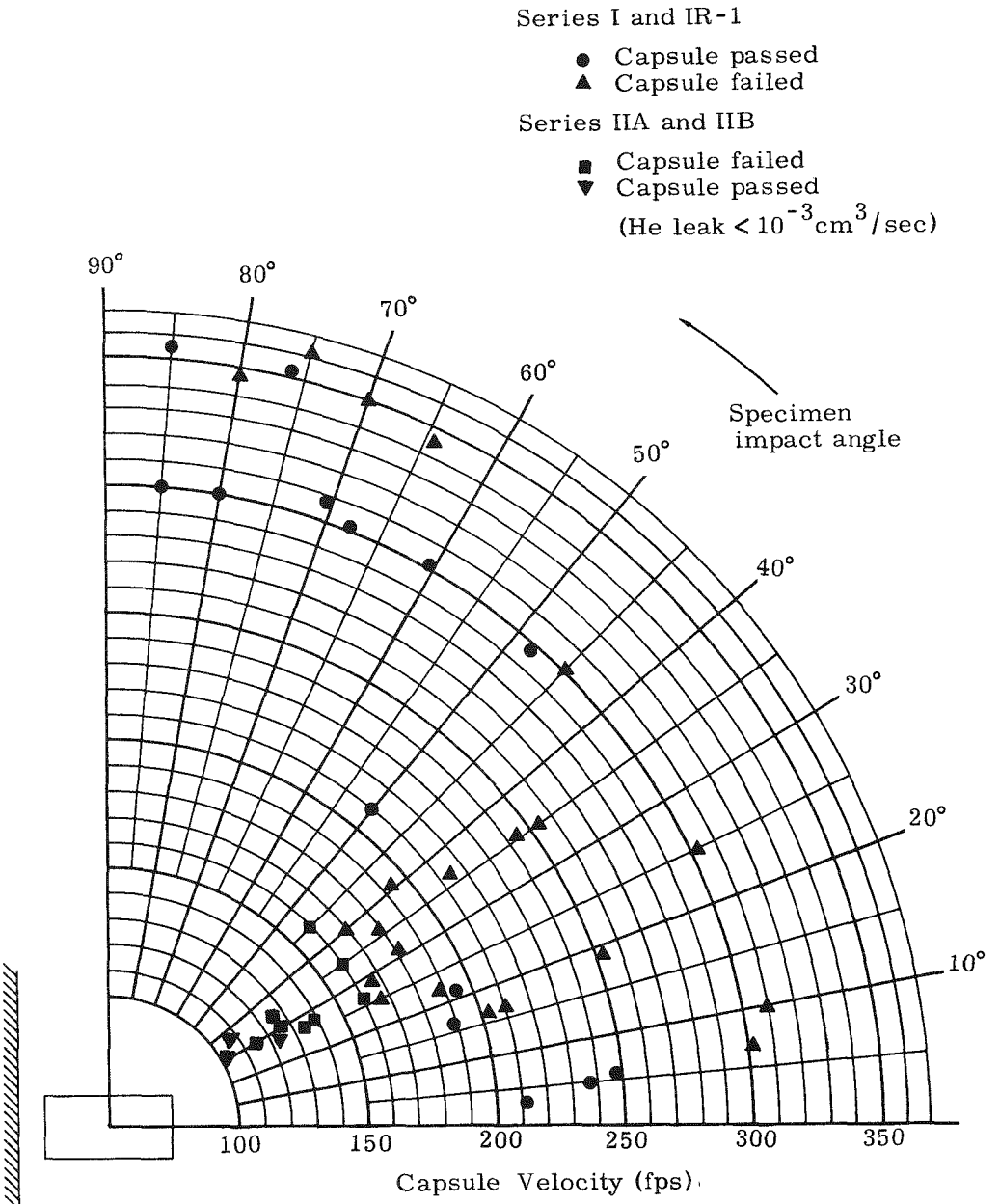

FIG. III-18. IMPACT TEST RESULTS

TABLE III-4

Capsule Impact Test Summary

Test No.	Specimen No.	Angle (deg)	Velocity (fps)	Result
101	3	7	300.1	F-PS
102	18	5	239.1	S
103	58	10	309.5	F
104	71	6	248.0*	S
105	10	25	301.8	F-W
106	37	19	252.1	F
107	64	17	209.7	F
108	72	17	205.5	F
109	4	45	302.1	F
110	39	35	255.3	F-PS-W
111	65	50	211.1	S
112	73	35	245.5	F-W
113	12	70	307.1	S
114	38	64	346.3	F
115	66	60	301.0*	S
116	74	70	350.3	F
117	9	68	301.9	S
118	40	75	361.0	F
119	67	80	301.0*	S
120	79	76	353.3	S
121	5	48	297.4	S
122	43	80	348.9	F-W
123	68	86	299.0*	S
124	80	85	356.0*	S
125	81	3	211.7	S
126	84	21	193.9	S
127	85	36	216.5	F-PS
128	87	40	195.0*	F-PS
129	90	16	190.0*	S
130	97	32	180.3	F
131	92	36	180.3	F
132	102	22	190.0	F
133	104	28	168.7	F
134	105	40	170.6	F
135	103	25	167.4	F-PS
201	312	35	162.7	F
202	313	45	159.9	F
203	314	27	159.2	F
204	317	28	137.3	F
205	318	27	121.6	S_H(F)
206	322	28	135.1	F
207	345	30	102.2	S
208	347	35	107.4	S
209	349	30	124.9	F
210	350	33	124.5	F-PS
211	351	30	116.4	F

*Velocity from film analysis
) = rotating at impact
S = success
F = failed weld area
W = torn wall
PS = powder spill at impact
S_H = success based on helium leak rate $< (10^{-3}$ cm^3/sec)

FIG. III-19 FAILURE DUE TO SIDE WALL BUCKLING

FIG. III-20. FAILURE IN THE WELD AREA

FIG. III-21. FAILURE OF THE CAPSULE SIDE WALL

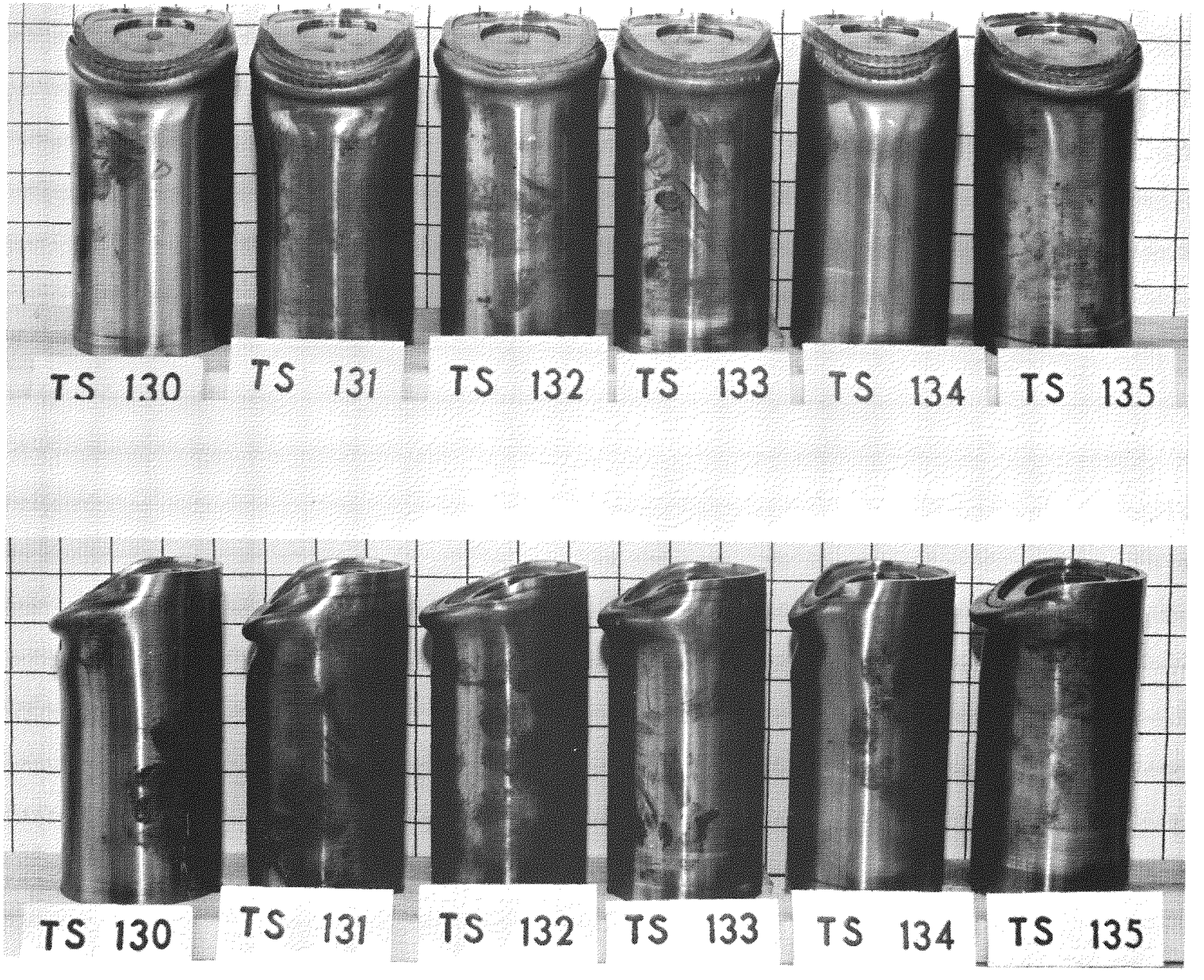

FIG. III-22. SERIES IR-1 IMPACT TEST CAPSULES

CONFIDENTIAL

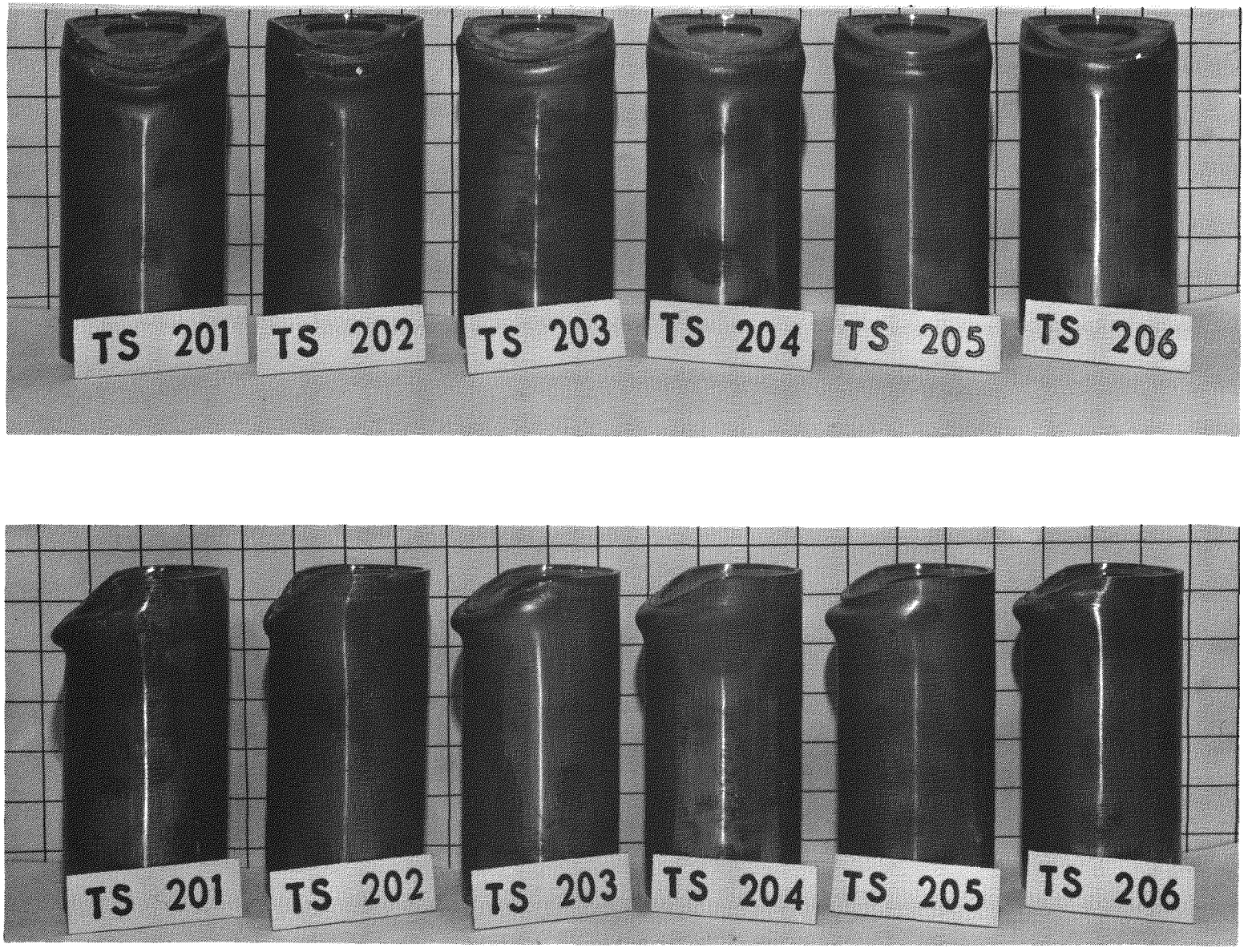

FIG. III-23. SERIES IIA IMPACT TEST CAPSULES

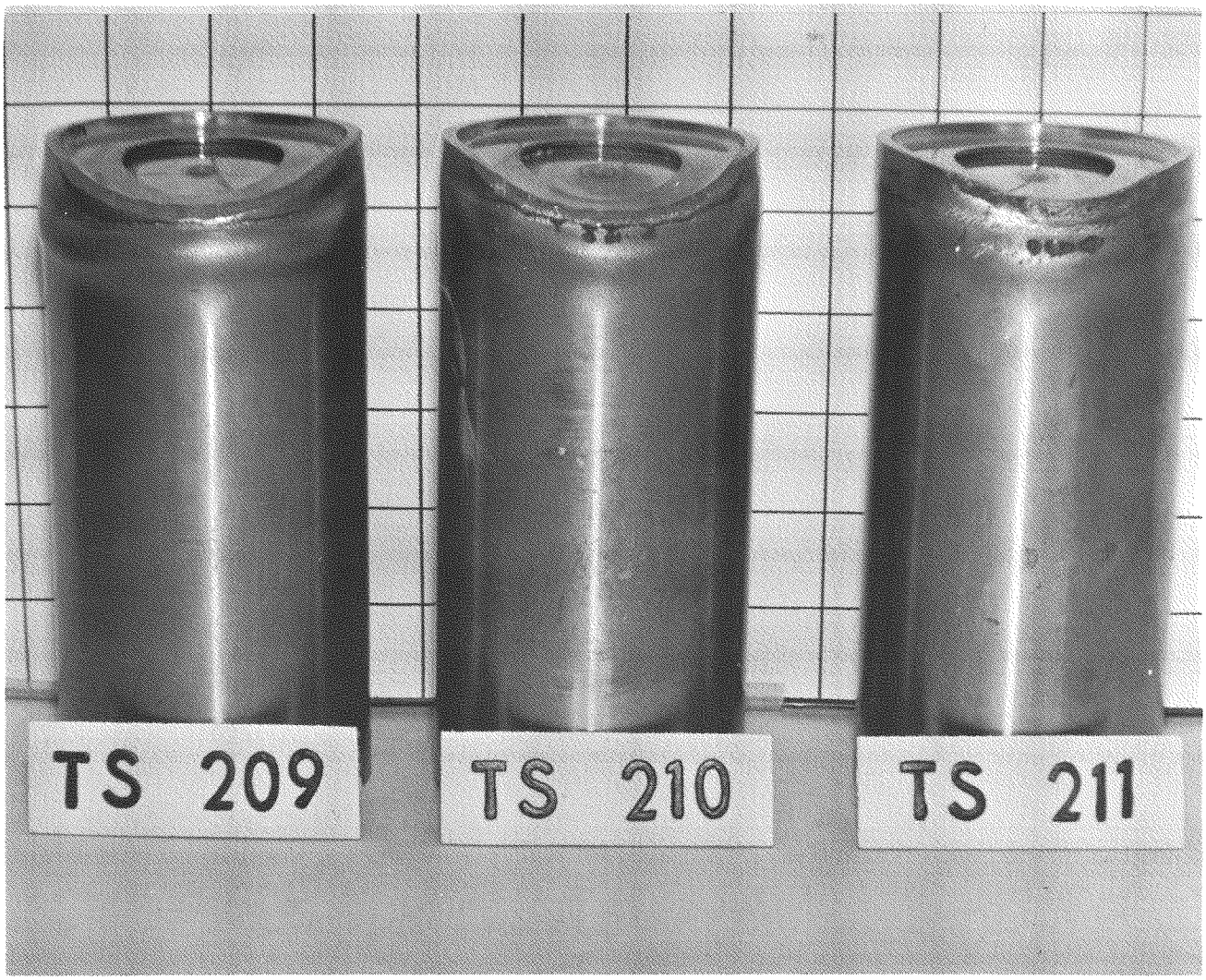

FIG. III-24. SERIES IIB TYPICAL TEST CAPSULES

6. Capsule Disintegration Test

The objective of this test was to determine the mode of failure of the capsule during re-entry. Twelve capsules, containing zirconium dioxide as a fuel simulant, and two graphite block specimens were tested. The capsules were tested at 0°, 30°, 60° and 90° angles of attack in both a static and a rotating condition. Each was preheated in a furnace to simulate normal operating temperature and then subjected to a programmed heating cycle that matched both the time and heat transfer rate levels of a nominal orbital decay re-entry where capsule release occurs at an altitude of 280,000 feet.

The tests were conducted in the planetary gas facility at the NASA-Ames Research Center, Moffett Field, California. The planetary gas facility is an arc-heated wind tunnel that generates a high enthalpy, supersonic plasma stream using air as a working gas.

Because no ground-based facility is able to simulate simultaneously all aspects of re-entry flight, it was decided to give primary emphasis to the correct heating environment. Although other parameters (such as free stream and dynamic pressure, enthalpy and molecular species) were not simulated exactly, the objective of the test was not compromised by this approach.

The test results showed that, for all re-entry attitudes (angles of attack, static, rotating), the capsules disintegrated. When the attitude was such that an end of the capsule received the greatest heating, a violent failure occurred in which the end-cap was blown off or shattered. Within about 6.9 seconds after loss of an end-cap, a large release of fuel occurred. When the side of the capsule received the greatest heating, a mild rupture of the sidewall occurred, followed by a gradual release of fuel.

In the two graphite block tests, which were designed to demonstrate intact re-entry, partial melting of the enclosed capsules occurred, but the graphite remained intact and no loss of fuel was experienced.

A summary of the test program and the test results is presented in Table III-5. Fig. III-25 gives a pictorial summary of a few typical disintegration tests.

Capsules were tested both nondestructively and destructively. The nondestructive tests were made at constant, low-level heating rates in order to measure internal temperatures in an invariant environment that was more amenable to analytical correlation. Before all capsule tests, both nondestructive and destructive, the capsules were preheated to a nominal operating temperature of approximately 1050° F. Each disintegration test was conducted for 4-1/2 minutes, which simulated the complete orbital decay re-entry of a capsule from the time of release from a SNAP 19 generator at 280,000 feet altitude to the time of negligible aerodynamic heating. Figure III-26 shows the nominal and actual heating rate-versus-time curves used for the disintegration test runs. The angle of attack and rate of (or lack of) rotation were held constant for a given run; therefore, these tests did not duplicate changes in flight motions that would begin to occur upon center-of-gravity changes from fuel loss, and upon change of external geometry (and, consequently, aerodynamic forces and moments) from melting. For all runs, at least until the time of the fuel release, the attitude and motion of the capsule was valid.

a. Temperature histories

Figures III-27 and III-28 show the temperature response of the capsule to constant heating at 14.75 and 32.4 Btu/ft^2-sec levels, with the capsule at $\alpha = 90°$ and spinning.

TABLE III-5

Summary of SNAP Capsule Disintegration Test
NASA-Ames Planetary Gas Facility

Run No.	Configuration	α (deg)	RPM	Internal Pressure	Capsule Instrumentation	Capsule Preheat Temperature (°F)	Serial No.	$\dot{q}$ (Btu/ft^2-sec)	Duration of Test (sec)	Pressure Lost (sec)	Test Results			
											Failure	Initial Rupture	Fuel Release	Comments
395	Hexagonal graphite	90	20*	Vented	1 T/C	70	--	18.6/1500 sec 215/100 sec	1600	--	None	None	None	Capsule, inside graphite, was partially melted
402	Round graphite	90	20	Vented	1 T/C	70	--	16.75/1513 sec 219/101 sec	1600	--	None	None	None	Capsule, inside graphite, was partially melted
419B	Capsule	90	20	Vented	4 T/C	1050	334	14.75	330	--	--	--	--	Nondestructive test
419C	Capsule	90	20	Vented	4 T/C	1050	334	32.4	120	--	--	--	--	Nondestructive test
420	Capsule	90	20	Vented	4 T/C	1050	334	Trajectory	270	--	Non-violent	Side	Slow	Sides melted; top fell off
422	Capsule	90	20	Pressure	None	1050	328	Trajectory	270	103	Non-violent	Side	Slow	Double longitudinal splits on side, sides melted; top fell off
438	Capsule	90	20	Pressure	None	1050	330	Trajectory	270	97	Non-violent	Side	Slow	Single longitudinal split on side; sides melted; top fell off. Repeat of Run 422
421	Capsule	90	0	Pressure	None	1050	326	Trajectory	270	46.5	Non-violent	Side	Slow	Minimum loss of fuel and metal
426	Capsule	60	20	Pressure	None	1050	323	Trajectory	270	80	Violent	End-cap	Fast	Fuel and internals ejected
425	Capsule	60	0	Pressure	None	1050	325	Trajectory	270	36	Non-violent	Side	Slow	Gradual erosion
427	Capsule	29	20	Pressure	None	1050	324	Trajectory	270	63	Violent	End-cap	Fast	End-cap and fuel ejected
441	Capsule	30	0	Pressure	None	1050	327	Trajectory	270	37	Non-violent	Corner	Slow	Gradual erosion
430	Capsule	0	20	Vented	5 T/C	1050	332	19.26	370	--	--	--	--	Nondestructive test
431	Capsule	0	20	Vented	5 T/C	1050	332	35.83	158.5	--	--	--	--	Nondestructive test
432	Capsule	0	20	Vented	5 T/C	1050	332	33.14	157	--	--	--	--	Nondestructive test. Repeat of Run 431
434	Capsule	0	20	Vented	5 T/C	1050	332	Trajectory	270	--	Non-violent	Side	Slow	Nearly completely melted
437	Capsule	0	20	Pressure	None	1050	333	Trajectory	270	114	Non-violent	Side	Slow	Nearly completely melted
440	Capsule	0	20	Pressure	None	1050	331	Trajectory	270	104	Non-violent	Side	Slow	Nearly completely melted. Repeat of Run 437
436	Capsule	0	0	Pressure	None	1050	329	Trajectory	270	71.5	Violent	End-cap	Fast	End-cap shattered; fuel and internals ejected

*Spin rate diminished and stopped at about 1400 seconds.

FIG. III-25. SUMMARY OF DISINTEGRATION TESTS--α = 90°, ROTATING AND STATIC

Run 434

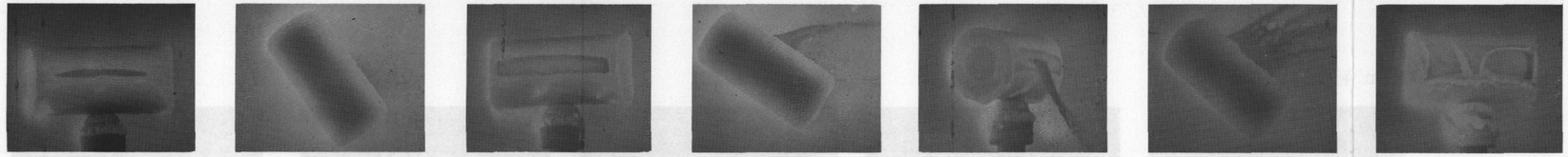

138 sec | 148 sec | 149.4 sec | 150 sec | 151.9 sec | 157 sec | 184 sec

Run 437

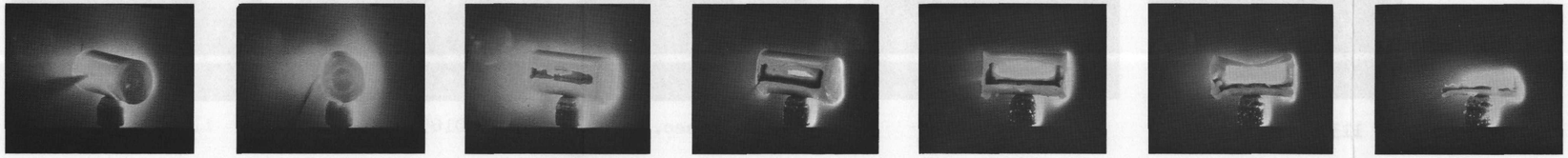

140 sec | 150.5 sec | 161.7 sec | 170.5 sec | 175 sec | 185.5 sec | 195 sec

Run 440

114 sec | 116.5 sec | 159 sec | 166 sec | 167 sec | 171 sec | 178 sec | 185.5 sec | 193 sec

Run 436

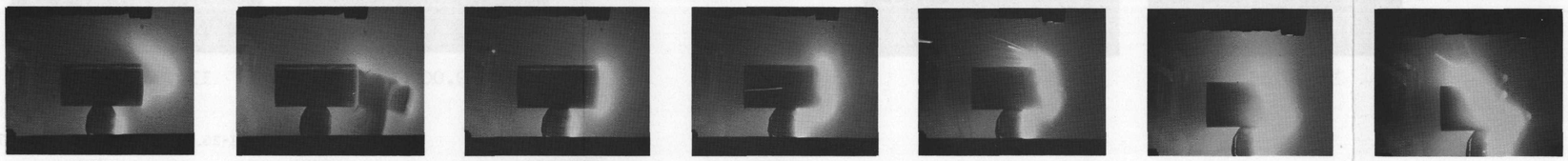

114 sec | 120 sec | 136 sec | 123 sec | 163 sec | 198 sec | 228 sec

FIG. III-25. (continued)--α = 0°, ROTATING AND STATIC

Run 436

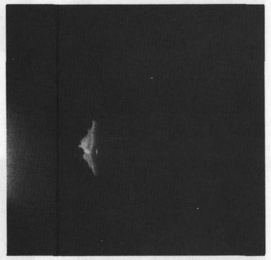

113.000 sec

113.005 sec

113.0095 sec.

113.0165 sec

113.0225 sec

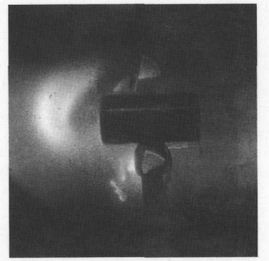

113.0425 sec

Run 436 (Cont'd)

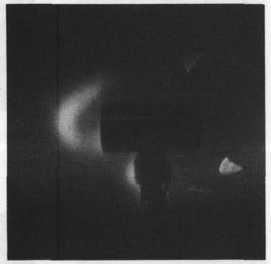

113.0735 sec

113.108 sec

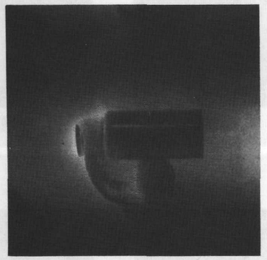

119.007 sec

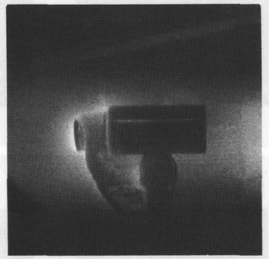

119.036 sec

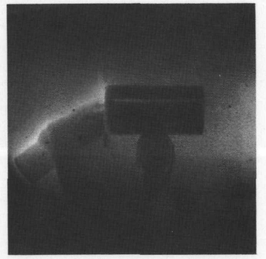

119.209 sec

FIG. III-25. (continued)--α = 0°, STATIC, HIGH SPEED PICTURES

Run 395 Run 402

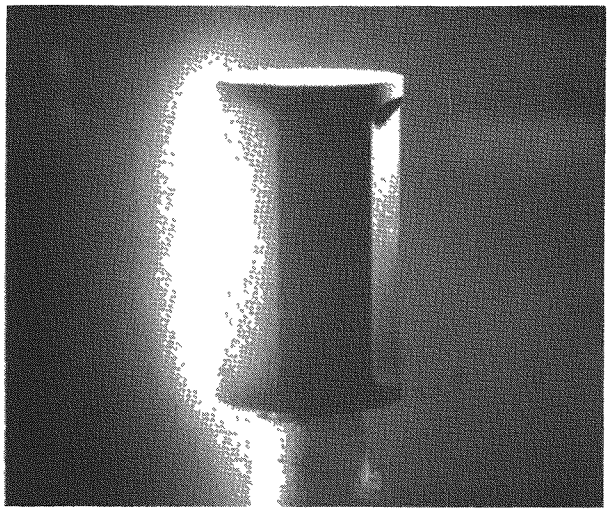

300 sec

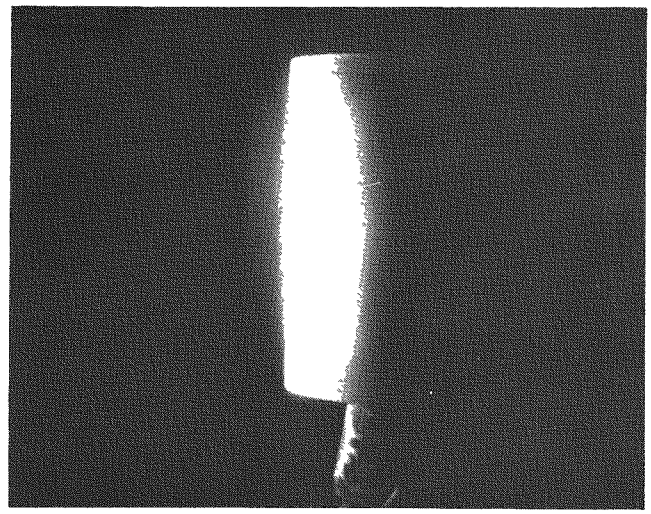

300 sec

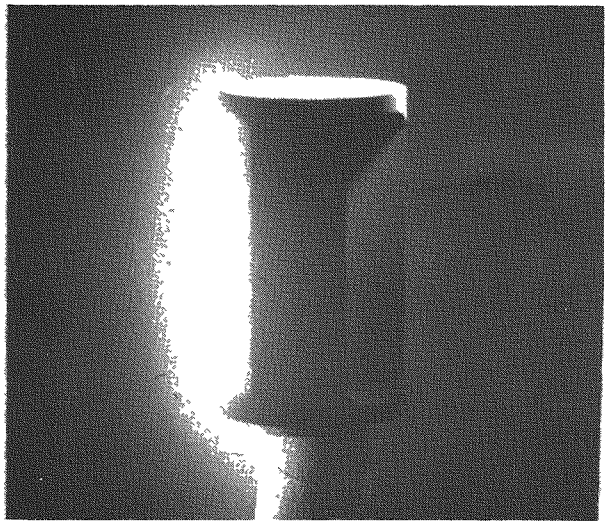

1500 sec

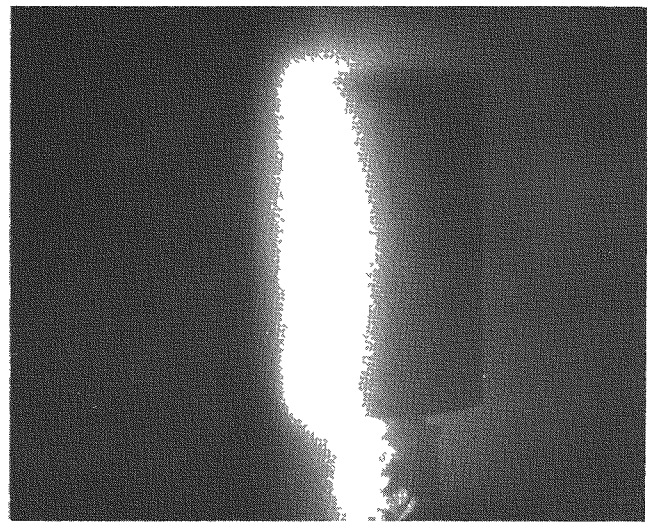

1500 sec

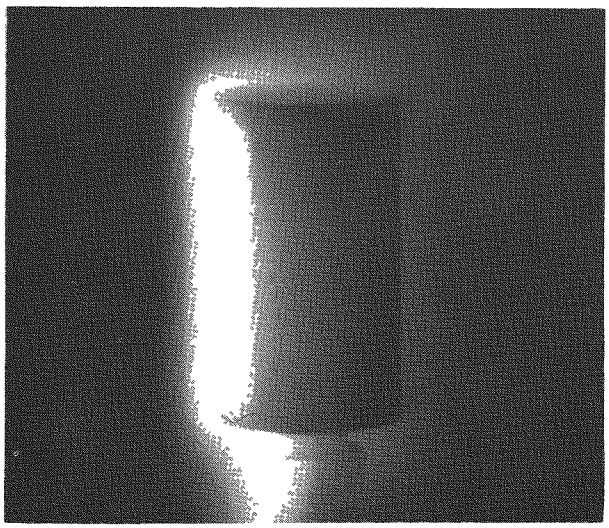

1600 sec

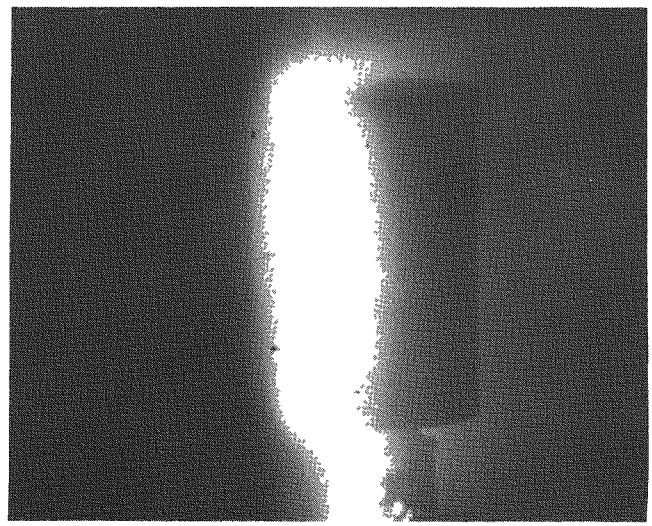

1600 sec

FIG. III-25. (continued)--α = 0°, STATIC, HIGH SPEED PICTURES

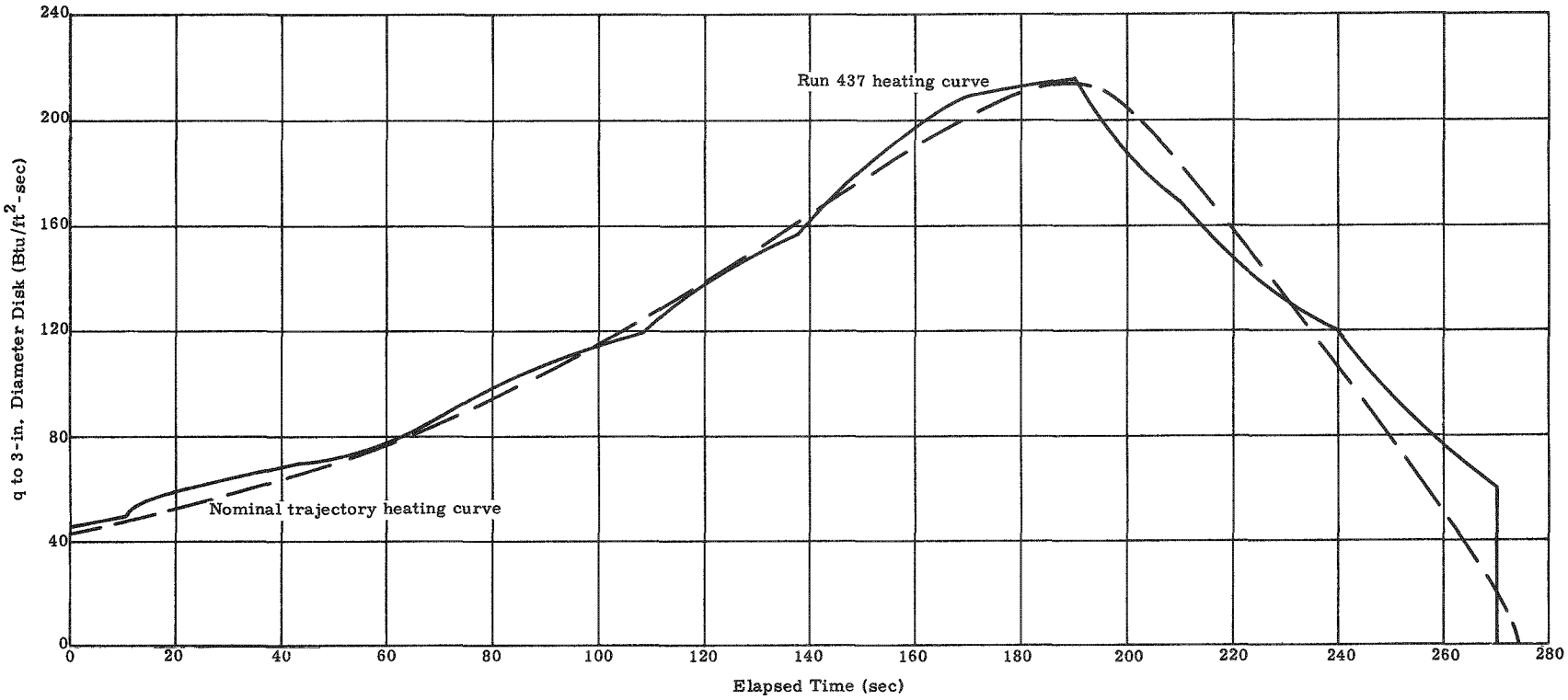

FIG. III-26. TYPICAL EXPERIMENTAL HEATING CYCLE

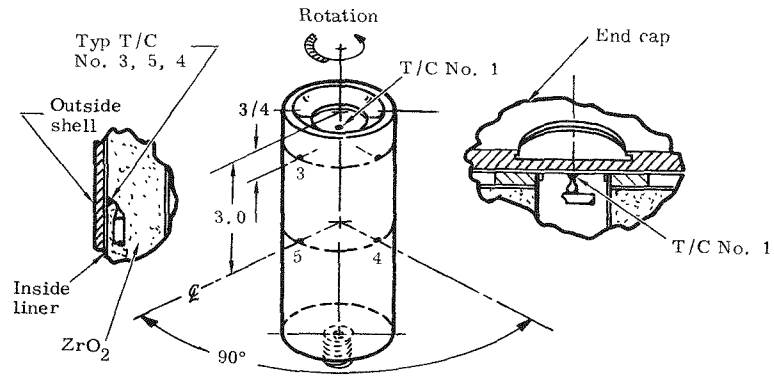

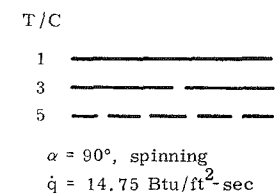

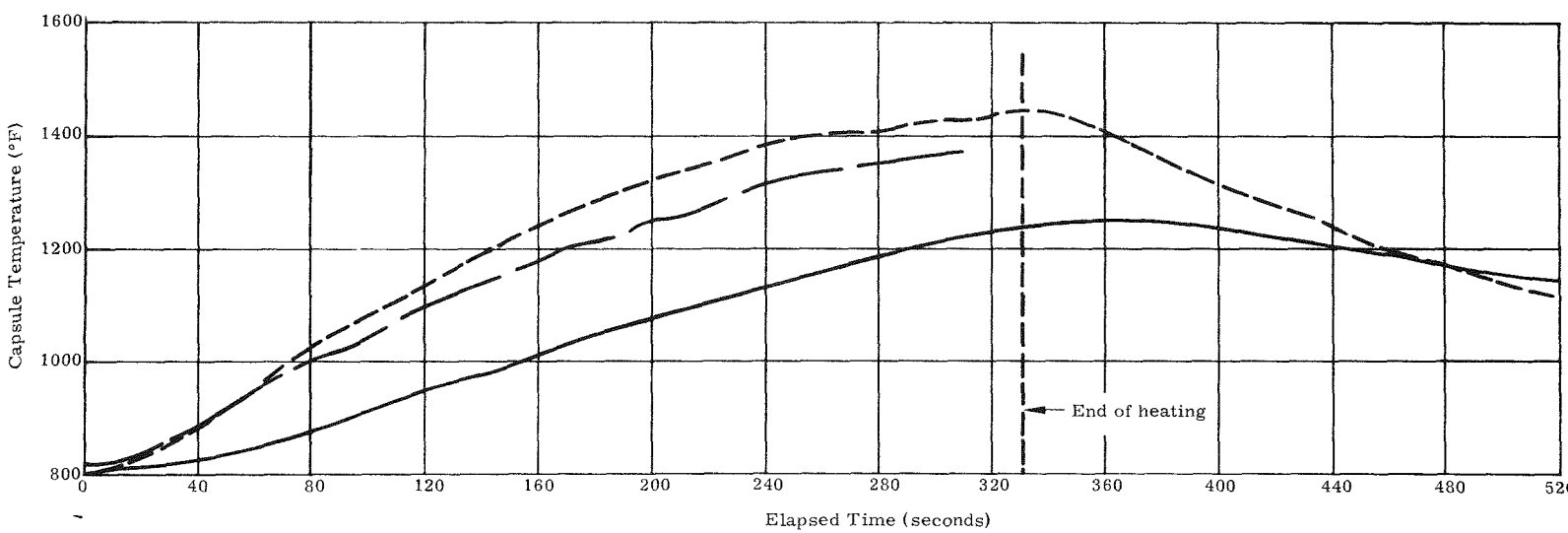

FIG. III-27. TEMPERATURE HISTORY OF SNAP 19 CAPSULES--RUN 419B NONDESTRUCTIVE TEST

CONFIDENTIAL

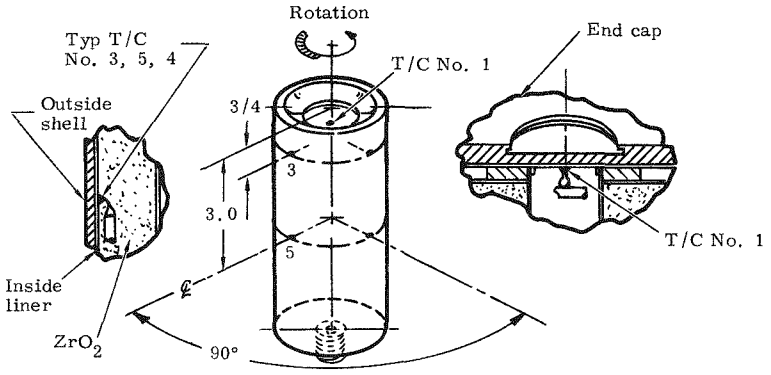

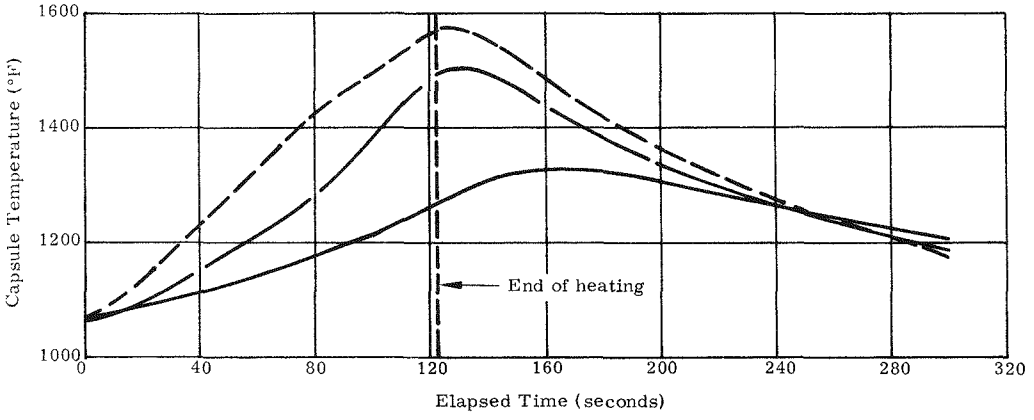

FIG. III-28. TEMPERATURE HISTORY OF SNAP 19 CAPSULES--RUN 419C, NONDESTRUCTIVE TEST

This capsule was unpressurized. The duration of each test was controlled so that no melting of the capsule occurred. The data show that the thermocouple at the center of the side of the capsule experienced the most rapid temperature rise and reached the highest temperature. The end-cap, a relatively large mass of metal, heated least rapidly and attained the lowest temperature. The thermocouple on the side, but near the end-cap, measured temperatures between the other two. As expected, the rate of temperature rise decreased as the capsule became hotter. Only a few seconds of temperature rise continued beyond the end of heating for the thermocouples on the side of the capsule, but the end-cap continued to absorb heat from the hotter portions of the capsule for 40 to 50 seconds.

Figure III-29 shows the temperature history of the same capsule at the same attitude, but during the disintegration test where the trajectory heating distribution was used. The rates of temperature rise are much steeper than before, but the same relationship between thermocouples (coolest at the end-cap, hottest in the middle of the sidewall) holds as in the nondestructive tests. The thermocouples ceased to give reliable indications after about two minutes (about the time that melting began).

b. Effect of rotation

The pressurized capsules were tested both statically and rotating at all angles of attack (90°, 60°, 30° and 0°). At 90°, the mode of failure was the same, a nonviolent failure of the sidewall. At α = 60° and 30°, rotation of the capsule changed the mode of failure from nonviolent (sidewall) to violent (end-cap). At α = 0°, there was a violent failure when static and a nonviolent failure when rotating.

All cases of violent failure resulted in the end-cap being blown from the capsule; the test conditions leading to this mode of failure were those which uniformly heated the end of the capsule.

All cases of nonviolent failure resulted in a rupture of the sidewall; the test conditions leading to this mode of failure were any conditions that did not uniformly heat the end-cap region. Most frequently, these were conditions that concentrated heat on the sides of the capsule.

c. Effect of angle of attack

When tested statically, the pressurized capsules failed nonviolently at α = 90°, 60° and 30°, but failed violently at α = 0°. When tested dynamically at α = 90° and 0°, a nonviolent (sidewall) failure occurred and at α = 60° and 30° a violent (end-cap) failure occurred. As noted earlier, end-cap failure occurred only when uniform heating of the end-cap was present.

d. Release of internal pressure and fuel simulant

Table III-5 contains a tabulation of the times-to-release of outer shell pressure, release of liner pressure and release of fuel. The table shows that, when the capsule shell failed violently, the loss of pressure from the liner followed within 6.9 seconds. Such liner failures always resulted in a large amount of simulated fuel (estimated at 50% to 80% of the total) being ejected from the capsule almost simultaneously. When, however, the failure was nonviolent, the loss of liner pressure came later (frequently half a minute later) than in the violent cases. In addition, there was never an eruptive gush of fuel in a nonviolent failure.

The data show that although, as would be expected, a pressurized capsule releases fuel earlier than an unpressurized one, the amount of time that it is earlier depends

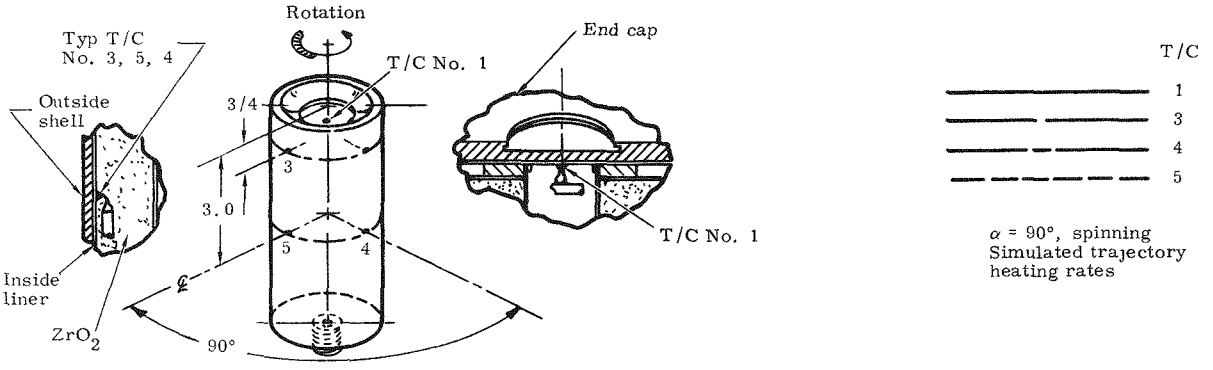

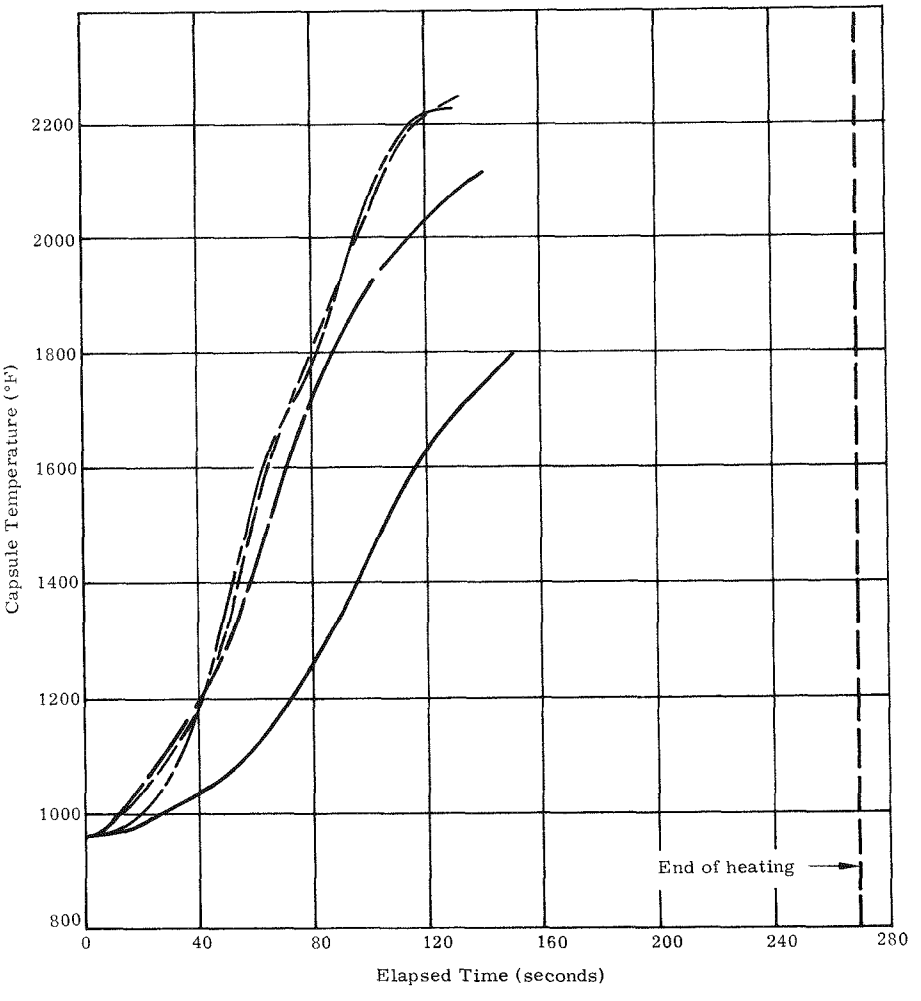

FIG. III-29. TEMPERATURE HISTORY OF SNAP 19 CAPSULES--RUN 420B, DISINTEGRATION TEST

on the attitude of the capsule. For example, at $\alpha = 0°$ and tumbling, the fuel release came about 23 seconds earlier (on the average) for the pressurized capsules, whereas at $\alpha = 90°$ and spinning, the release was only about 2 seconds earlier (on the average).

In comparing failure times of pressurized static and rotating capsules, it is apparent that the rupture of a static capsule happens much more quickly than its rotating counterpart. This was true at all angles of attack. Taken as a group, the static capsules lost pressure in from 35.0 to 70.0 seconds and lost fuel in from 41.9 to 76.9 seconds. In comparison, the rotating capsules lost pressure in from 62.0 to 113.0 seconds and lost fuel in from 62.0 to 140.8 seconds. Only a rotating capsule ($\alpha = 29°$) that failed violently even fell within the group of times for failure of static capsules.

It was difficult to determine the rate at which fuel was leaving the capsule because the quantity of fuel had to be judged from motion pictures or deduced by observing the "waterline" below which fuel was held. Nevertheless, for two runs at $\alpha = 0°$ and two at $\alpha = 90°$, such a determination was made. These results are shown in Fig. III-30. At both angles of attack and for those cases which were nonviolent failures, more than 50% of the fuel was dispersed within 30 seconds.

It is noteworthy that capsule failure, regardless of the re-entry attitude, is well assured. This can be seen from the fuel release times, which range from 41.9 seconds to 140.8 seconds. The peak of re-entry heating occurs at 190 seconds at ($\dot{q} = 164$ Btu^2-sec) and the highest heating rates occur during a 50-second period.

7. Project Pyro Test

A SNAP 19 test specimen (generator) was placed in a Project Pyro test, with an RP-1/LO_2-loaded simulated launch vehicle. The launch vehicle contained 25,000 pounds of propellants in stainless steel tanks (Fig. III-31) with a typical oxidizer-fuel ratio of approximately 1.5 to 1.0 and was dropped about 10 feet to simulate a launch pad fallback after liftoff.

The SNAP 19 test specimen was bolted to the drop test fixture at the top of the test vehicle (Fig. III-32), only partially simulating the location of a generator in a launch vehicle/spacecraft configuration. The test specimen was much closer to the oxidizer tank dome, and was without the shielding that would exist in a launch attempt. Consequently, it appears that the generator was exposed to greater overpressure and fragmentation hazards than would normally be expected.

Test procedures required that a diaphragm between the propellant tanks be ruptured just prior to the moment of impact. The LO_2 thus drops into the fuel tank and creates a higher degree of mixing with a resulting higher explosive yield.

Data on this test indicate that a yield of at least 35% equivalence was obtained. Mixing occurred in such a manner as to create a sizeable shaped charge effect, with the most severe effect of the blast being directed upward and outward from a point approximately 15 feet above the pad.

After the blast and fireball, there was residual burning on the pad for approximately eight minutes. In a sump approximately 40 feet from the point of impact, fuel burned for about 25 minutes. There was no attempt at fire extinguishment. When the area was in a condition to permit personnel entry, a preliminary search was made for remains of test articles. Those components and fragments found are identified in Fig. III-33. Splotches of magnesium oxide indicated, too, that fragments of the generator had been burning as they flew out from the center of the blast.

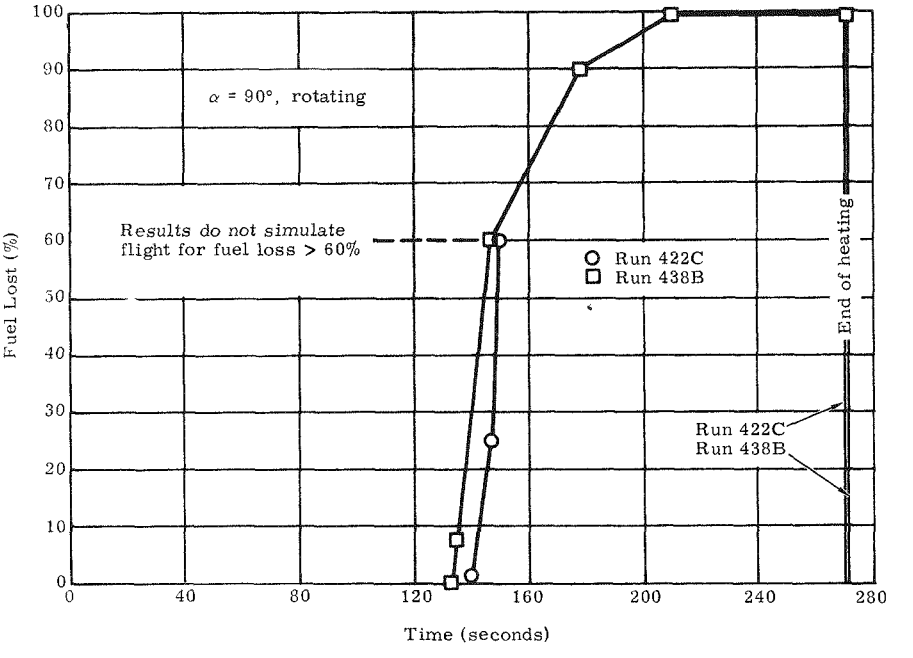

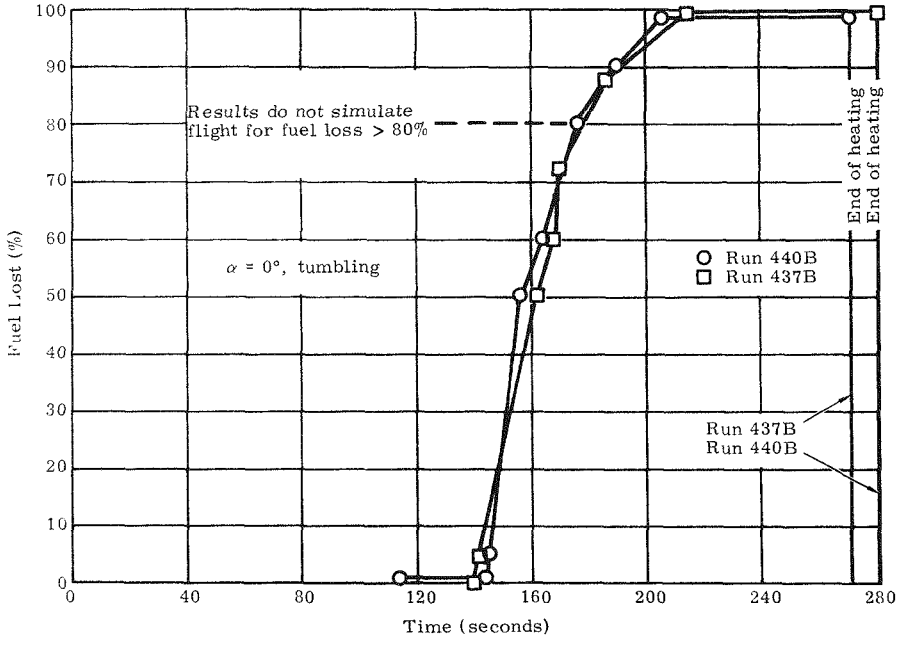

FIG. III-30. ESTIMATED LOSS OF FUEL VERSUS TIME

FIG. III-31. PROJECT PYRO/SNAP 19 TEST SETUP

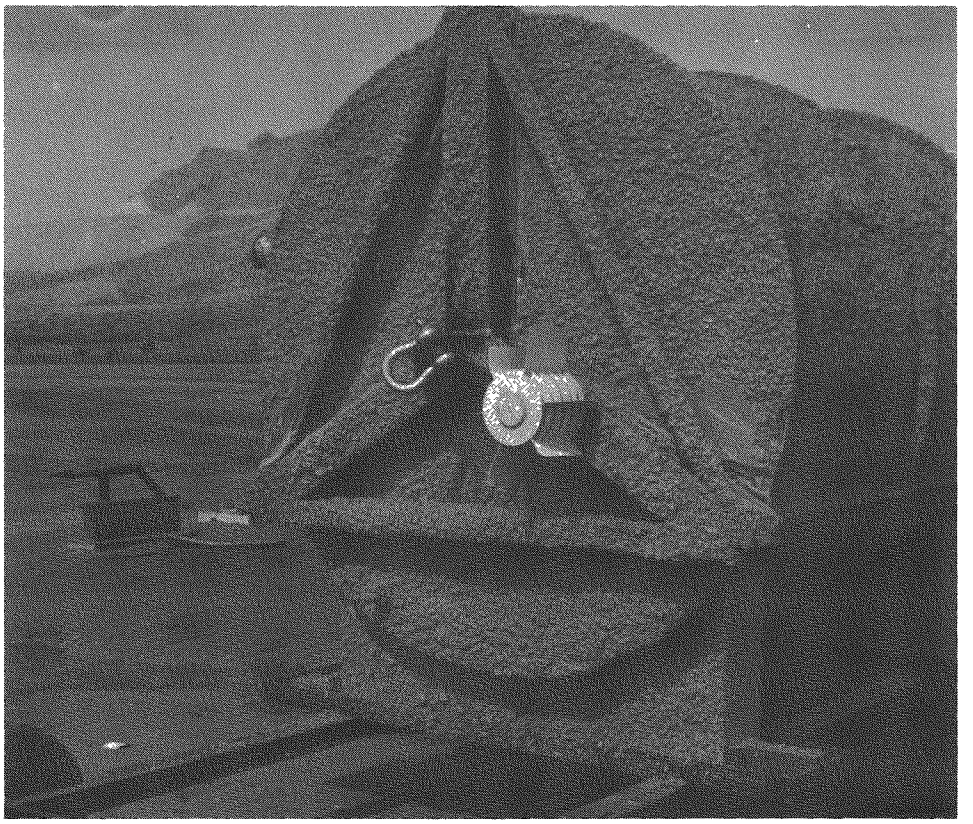

FIG. III-32. PROJECT PYRO/SNAP 19 TEST VEHICLE

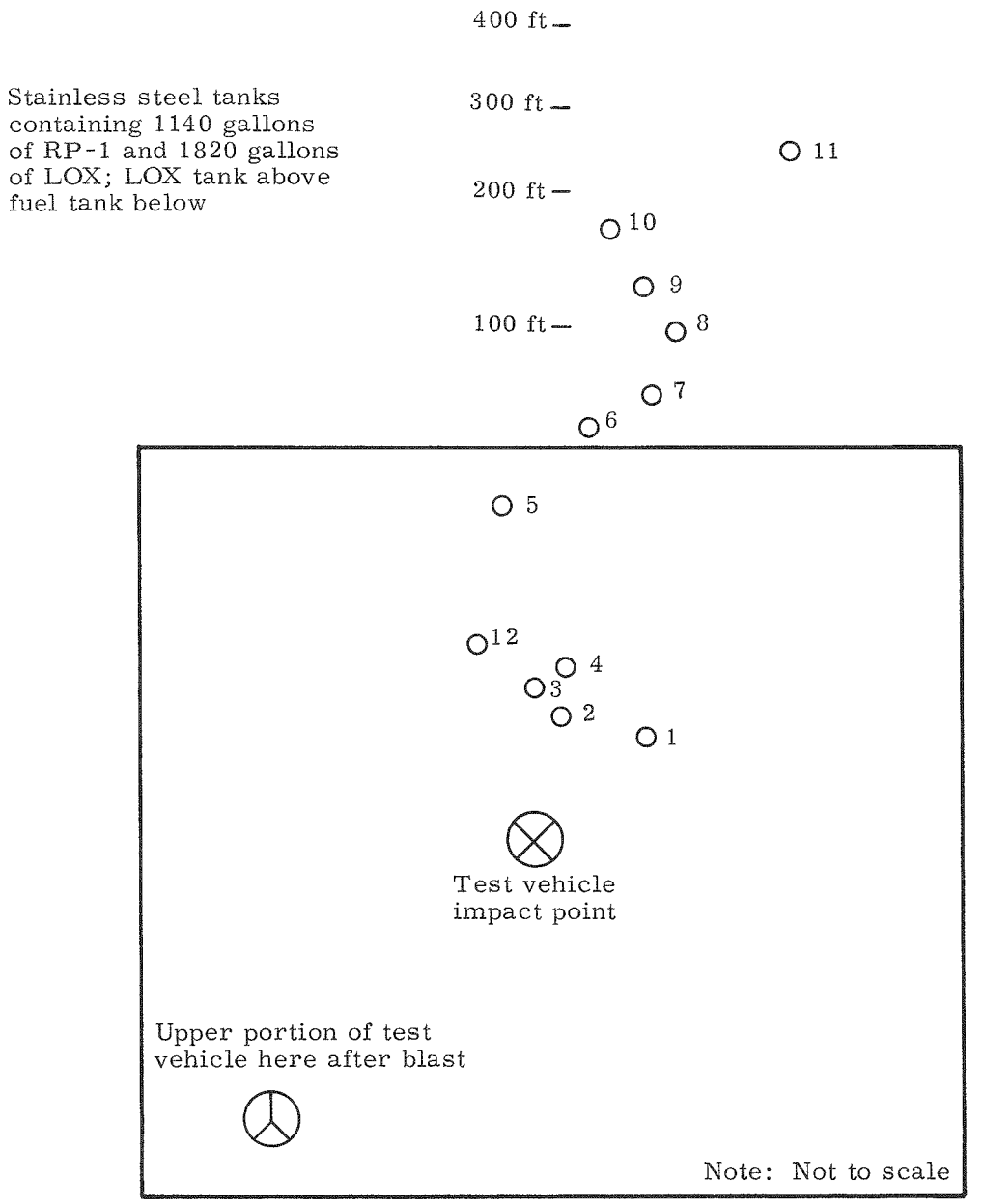

1. SNAP 19 capsule
2. Min-K
3. Graphite segment
4. Graphite segment
5. Graphite segment

6 to 10. Magnesium oxide

11. Bottom plate
12. Portion of fin

FIG. III-33. PROFILE OF TEST DEBRIS RESULTING FROM PROJECT PYRO/ SNAP 19 TEST

The base plate of the generator assembly was found 238 feet from the center of the explosion, with the capsule located approximately 18 feet from the center and showing very little evidence of having been exposed to high temperatures. The position of the capsule (Fig. III-34) and the pieces of the graphite which had surrounded it, indicate that the capsule was not exposed to the environment until it impacted on the pad, causing the graphite to break away. The only visible damage to the capsule was a slight flattening at the edge of one end.

8. Sandia Residual Fire Test

Two tests, which simulated the launch pad fire, were conducted at the Sandia Corporation during the program. In both tests, JP-4 was selected as the fuel, since it closely resembles hydrocarbon rocket fuels in rate of burning and temperatures produced.

For the first test, it was estimated that the 3500 gallons of fuel would burn for 30 $\pm$ 2 minutes. The fuel was ignited by remotely actuating electric squibs. The test generator was instrumented with 12 thermocouples located as follows:

(1) Three thermocouples (T/C Nos. 1, 2, 3) on capsule (top, bottom, center)

(2) Two thermocouples (T/C Nos. 4, 5) between Min-K and graphite

(3) Two thermocouples on (T/C Nos. 6, 7) cold shoes (1 each)

(4) Three thermocouples (T/C Nos. 8, 9, 10) root of fin (top, center, bottom)

(5) Two thermocouples (T/C Nos. 11, 12) measuring fire temperature.

Film coverage was provided by two 24-fps cameras. Thermocouple data indicated that the generator housing was probably 20 to 30% consumed by 150 seconds. Movies taken by one (the east) camera verified the start of magnesium burning. No magnesium fire indications were visible on the film from the other (south) camera or to observers at the south observation point.

Post-test inspection of the test stand area revealed that the test specimen toppled from the stand prior to being totally consumed by the fire. A later look at recorded data indicated that the toppling probably occurred just prior to 0 + 300 seconds. All of the magnesium fins and 20% of the magnesium housing were burned away as shown in Fig. III-35. A mass of melted-down magnesium was found on the bottom of the test tank when all water had been drained. The burning magnesium had fallen through the hydrocarbon fuel, which quenched the burning, and then had rested in the water in a comparatively cool environment during most of the fuel fire.

The end of the capsule nearest the point of most severe damage to the assembly was blackened, and the bands of temperature-sensitive paint were nearly obliterated on the side marked "B". This damage to the paint bands was determined to have been caused by corrosive action rather than by elevated temperatures.

All remaining components of the test specimen were recovered and packaged for a second test.

The most significant information gleaned from this test is the heat transfer data obtained for generator components. For instance, thermocouples Nos. 1, 2 and 3 on the capsule recorded temperatures of 65° to 70° F when the flame temperature was 1600° F and the fin root thermocouples were indicating 100° F.

The test setup for the second exposure of the SNAP 19 generator to a simulated residual fire is shown in Fig. III-36 (also shown is the IRHS generator mounted on a magnesium support stand). Figure III-36 also shows the dispersal generator system fuel capsule that survived the Project Pyro test. In this fire, the 2000 gallons of JP-4 fuel burned for approximately 26 minutes. The magnesium ignited in about two minutes and burned intermittently throughout the fire. At the end of the JP-4 fire (20 minutes after ignition), a pronounced magnesium fire was observed which burned for an additional 30 to 35 minutes. Figure III-37 shows the test setup after the fire was out. Note that the generator did not disassemble and the dispersion capsule appears undamaged after exposure to the edge of the magnesium fire. A closeup of the generator is shown in Fig. III-38.

Between 6 minutes and 26 minutes after ignition, temperature of the gases surrounding the generator ranged between 1670° and 1920° F. During this time period, the fuel capsule temperature, without isotope heating, increased from 200° to 1050° F, with a subsequent maximum temperature of 1250° F being encountered between 31 and 36 minutes after ignition. If the normal steady-state temperature gradient (600° F) is assumed to apply to this transient case, the actual fuel capsule would reach 2520° F, i.e., it would exceed the capsule failure temperature (2150° F) and approximate the melting temperature (2425° to 2570° F).

The peak temperatures for the bare, unheated dispersion capsule, which was located on the edge of the magnesium fire, ranged from 1670° F on the side to 1800° F on the top. Analyses indicate that the bare fuel capsule will not exceed its failure temperature.

9. Aerodynamic Tests

The various aerodynamic tests conducted, the facilities and their significant similarity parameters are shown in Table III-6. This table lists tests conducted with the spacecraft, generator and fuel capsule. A summary description of the tests conducted with the fuel capsule is presented below.

a. Capsule low Reynolds number force test

The objectives of this test program were to determine the aerodynamic force and stability characteristics of the capsule at low Reynolds number.

Low Reynolds number hypersonic force tests were conducted on 12.27% scaled models of a SNAP 19 fuel capsule as shown in Fig. III-39.

The capsule was tested through an angle of attack range of 0° to 90° under the following test conditions:

M_∞ = 9.37 free stream Mach number

T_o = 1660° K stagnation temperature

q_∞ = 8.24 lb/ft^2 free stream dynamic pressure

Re = 1200 Reynolds number based on model length (capsule)

The simulated altitudes were:

277,000 ft based on Reynolds No.

247,000 ft based on viscous interaction parameter, $M\sqrt{C_\infty}/\sqrt{R_\ell}$

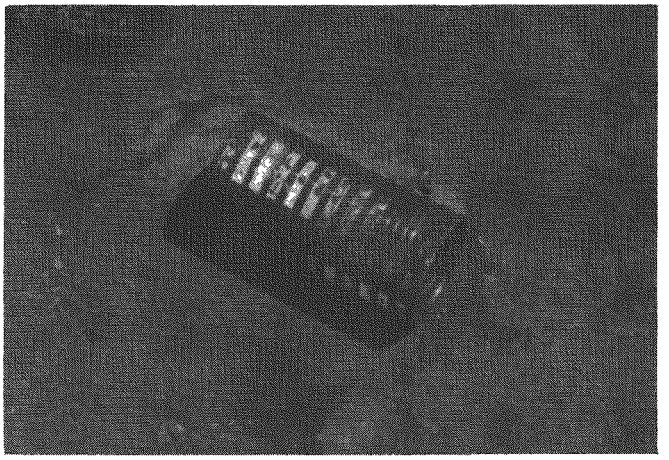

FIG. III-34. SNAP 19 FUEL CAPSULE AFTER PROJECT PYRO TEST

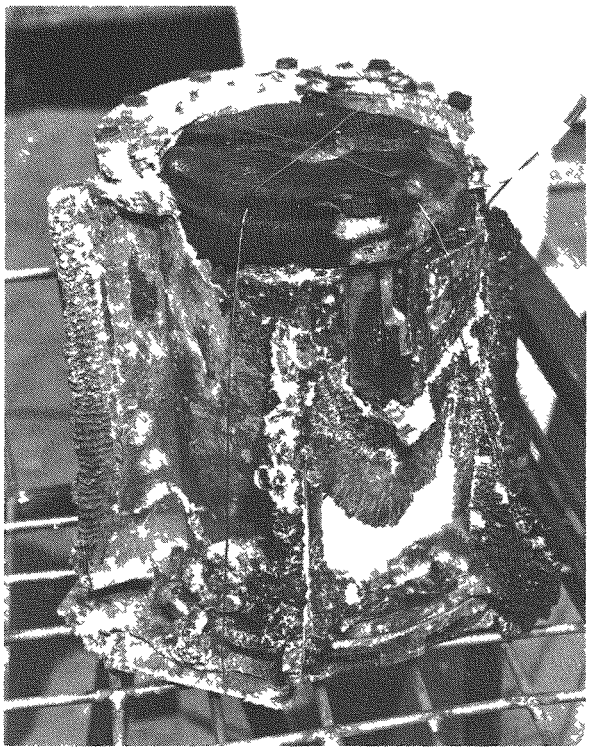

FIG III-35. SNAP 19 GENERATOR AFTER FIRST SANDIA RESIDUAL FIRE TEST

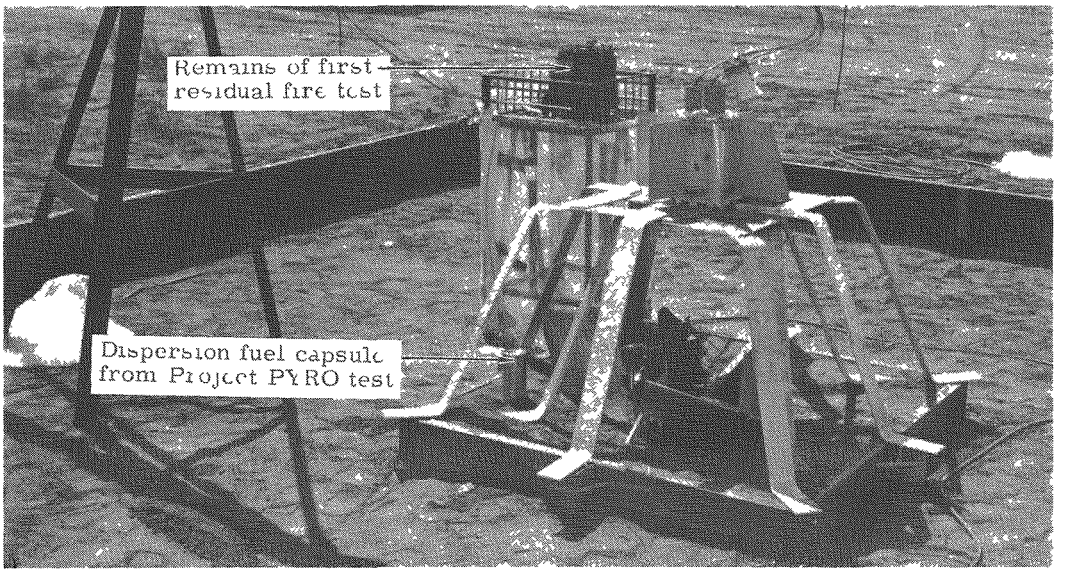

FIG III-36. TEST SETUP FOR SECOND SANDIA RESIDUAL FIRE TEST

TABLE III-6

Wind Tunnel Tests, Facilities and Similarity Parameters

Test	Facility	Mach No.	Reynolds No.	M/ Re	Model Scale* (%)
Fuel Capsule					
Continuum aerodynamics	Langley 31-inch	10	754,000	0.0120	100
Low density aerodynamics	ARDC LDH	9.37	1,200	0.2705	12.27
Continuum pressure and heating	Langley 31-inch	10.46 10.39 10.33	758,000 490,000 348,000	0.120 0.0148 0.0175	100
SNAP 19					
Continuum aerodynamics	Martin Hot Shot	20.53	31,537	0.1153	18
Continuum aerodynamics	AEDC Tunnel B	8	62,000	0.0321	30
Heating	AEDC Tunnel B	8	230,000	0.0167	30
Nimbus B					
Continuum aerodynamics	AEDC Tunnel B	8	184,000	0.0186	10
Heating	Ames 3.5 ft	10.36	187,500	0.0239	10

*Based on model reference length
Full-scale lengths are: Fuel capsule = 6.11 inches
SNAP 19 = 10.75 inches
Nimbus B = 57.12 inches

CONFIDENTIAL

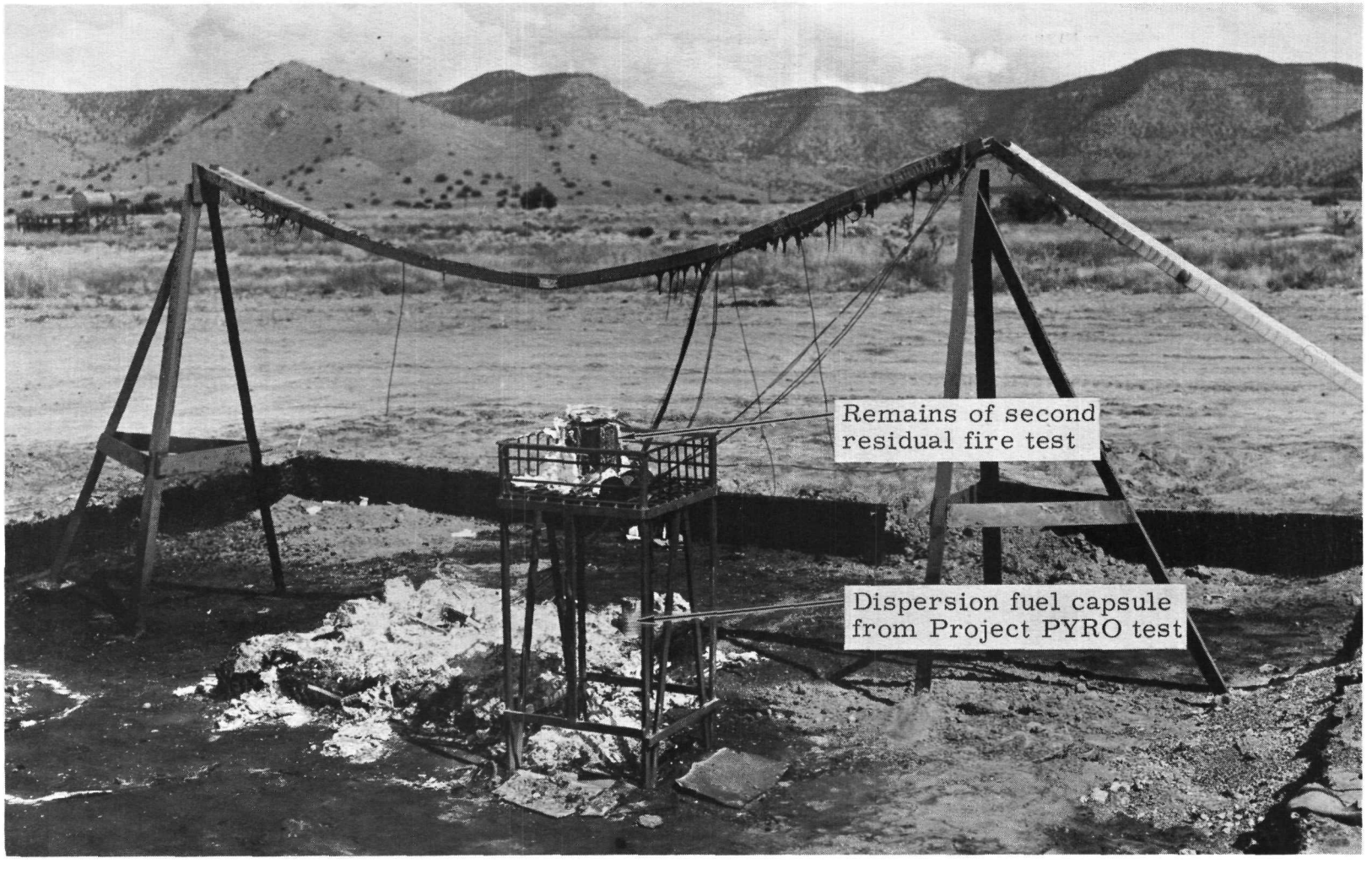

FIG. III-37. TEST SETUP AFTER SECOND SANDIA RESIDUAL FIRE TEST

CONFIDENTIAL

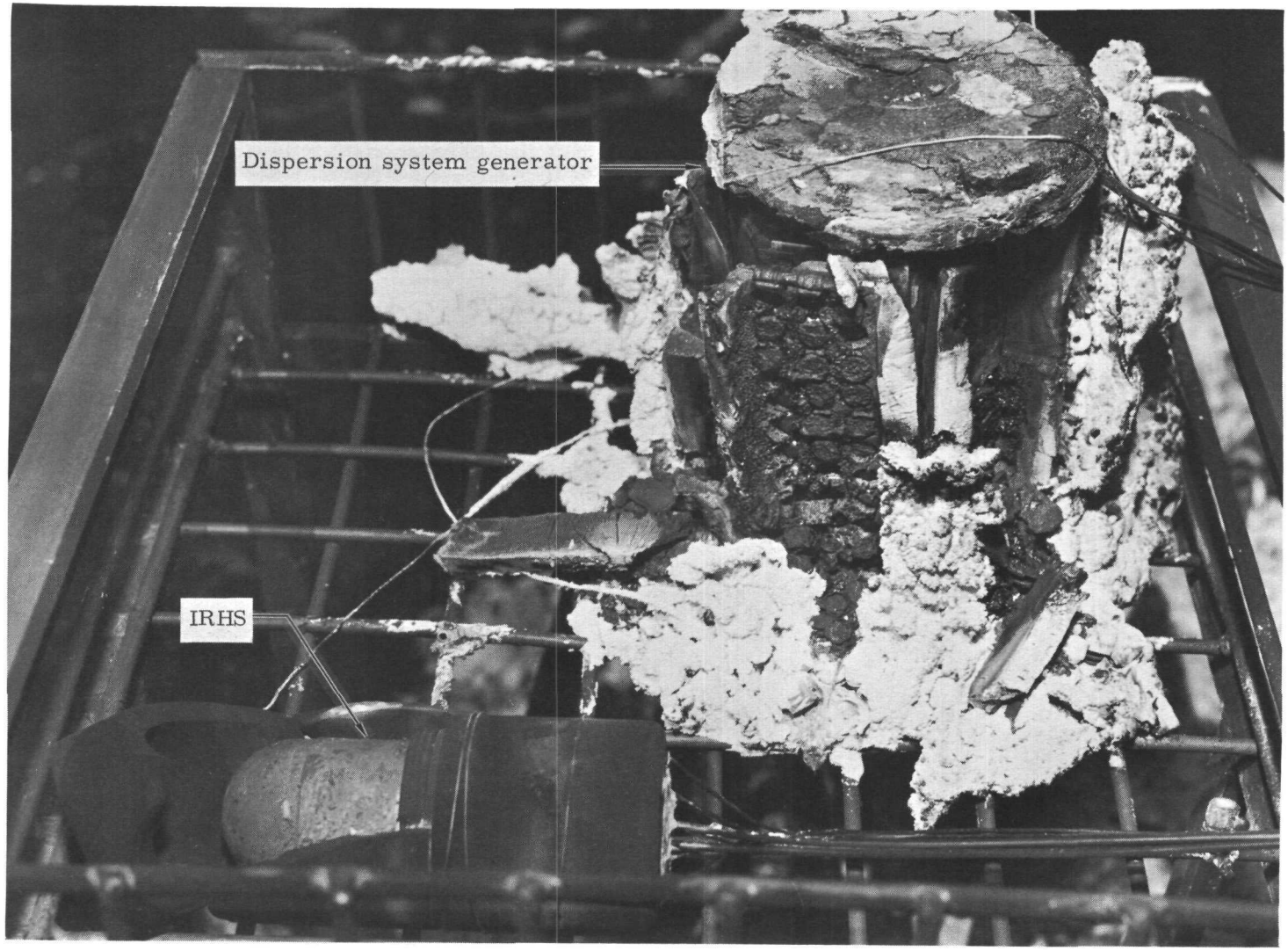

FIG. III-38. SNAP 19 DISPERSION SYSTEM GENERATOR AFTER SECOND SANDIA RESIDUAL FIRE TEST

CONFIDENTIAL

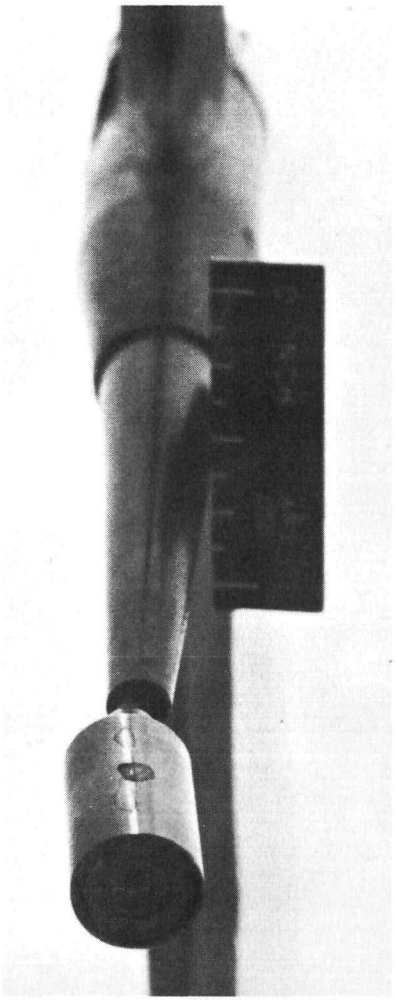

SNAP 19 Capsule Model,
Base Mount

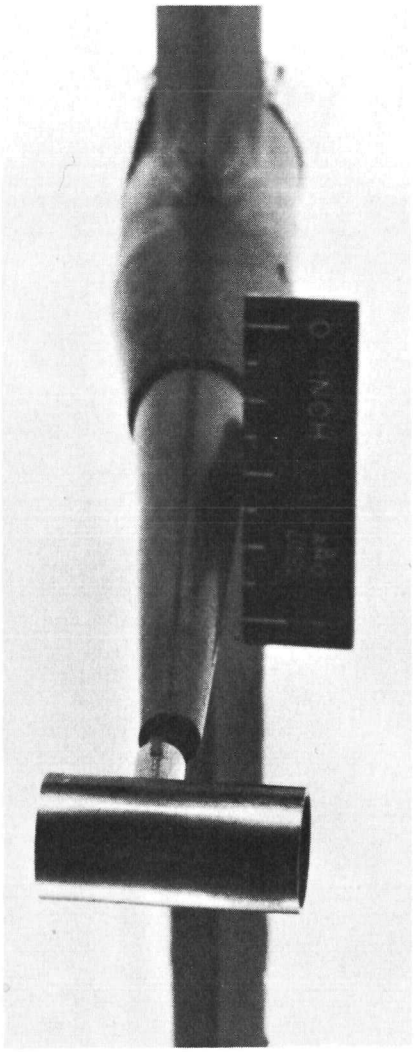

SNAP 19 Model, Side Mount

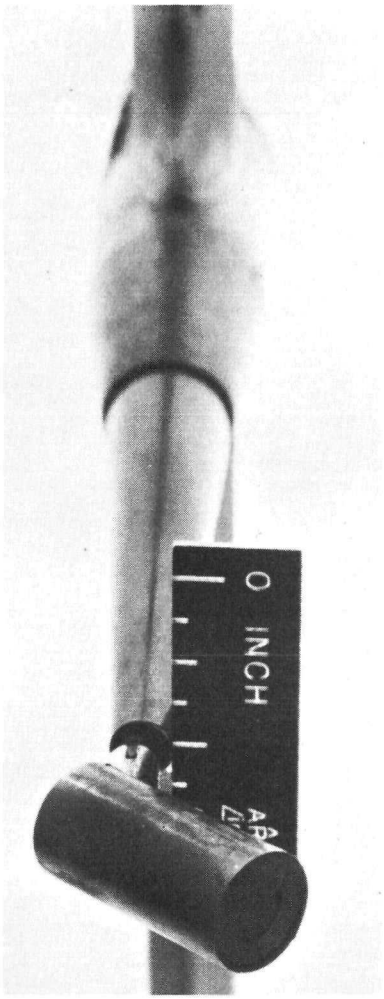

SNAP 19 Capsule Showing
40-Degree Mount

FIG. III-39. HYPERSONIC FORCE TEST SCALED MODELS

245,000 ft based on Knudsen No.

where C_∞ is constant in the linear viscosity-temperature relationship.

Lift and drag were measured for each angle of attack. The moment was calculated, using the two lift components and corresponding moment arm. Results are presented in Ref. III-20.

b. Capsule force and stability test, Mach 10

The objective of this test was to obtain aerodynamic force and moment data for the continuum regime of re-entry flight. These data were used in determining, by use of an analog computer program, the flight motions of the capsule.

The tests were conducted at the NASA-Langley Research Center 31-inch continuous flow hypersonic tunnel. The configuration was tested through an angle of attack range from 0° to 90°, using two full-scale models: one end-mounted model ($0° \leq \alpha \leq 53°$) and one side-mounted model ($37° \leq \alpha \leq 90°$). (See Fig. III-40.) The program included testing at four Reynolds numbers at Mach 10. The total pressures and approximate Reynolds numbers tested were:

P_o (psia)	Re x 10^{-6} (per ft)	R x 10_ℓ^{-6} (model)
1200	1.495	0.762
750	0.985	0.501
500	0.663	0.337
250	0.36	0.183

The normal force, axial force and pitching moment coefficients versus angle of attack are presented in Ref. III-20. In the range investigated there is no evidence of Reynolds number effect.

In an effort to determine the effect of the notches in the face of the capsule, tests were also conducted on a smooth-faced capsule (i.e., a configuration similar to the IRHS design--Chapter IV). The nominal and axial force coefficient were nearly the same as those measured on the notched-face dispersion capsule. However, the pitching moment for the smooth cylinder differed significantly from the dispersion capsule.

c. Capsule pressure and heat distribution tests, Mach 10.

These tests were formulated with the dual objectives of providing experimental hypersonic pressure data to support theoretical methods of predicting re-entry behavior of the capsule, and determining heat transfer rates for thermal analysis of capsule penetration. Two full-scale models were used; each was specifically suited for measuring one of the desired quantities. The models were individually tested in the NASA-Langley continuous flow hypersonic tunnel, using an injection mechanism which permitted short exposures of the models to the high energy airstream. Data measurements were collected from pressure and temperature transducers, recorded on magnetic tape and later processed through standard data reduction computer programs at the test facility.

All tests were performed at a nominal Mach number of 10. Initial plans called for test runs at four Reynolds numbers, corresponding to total pressures of 250,

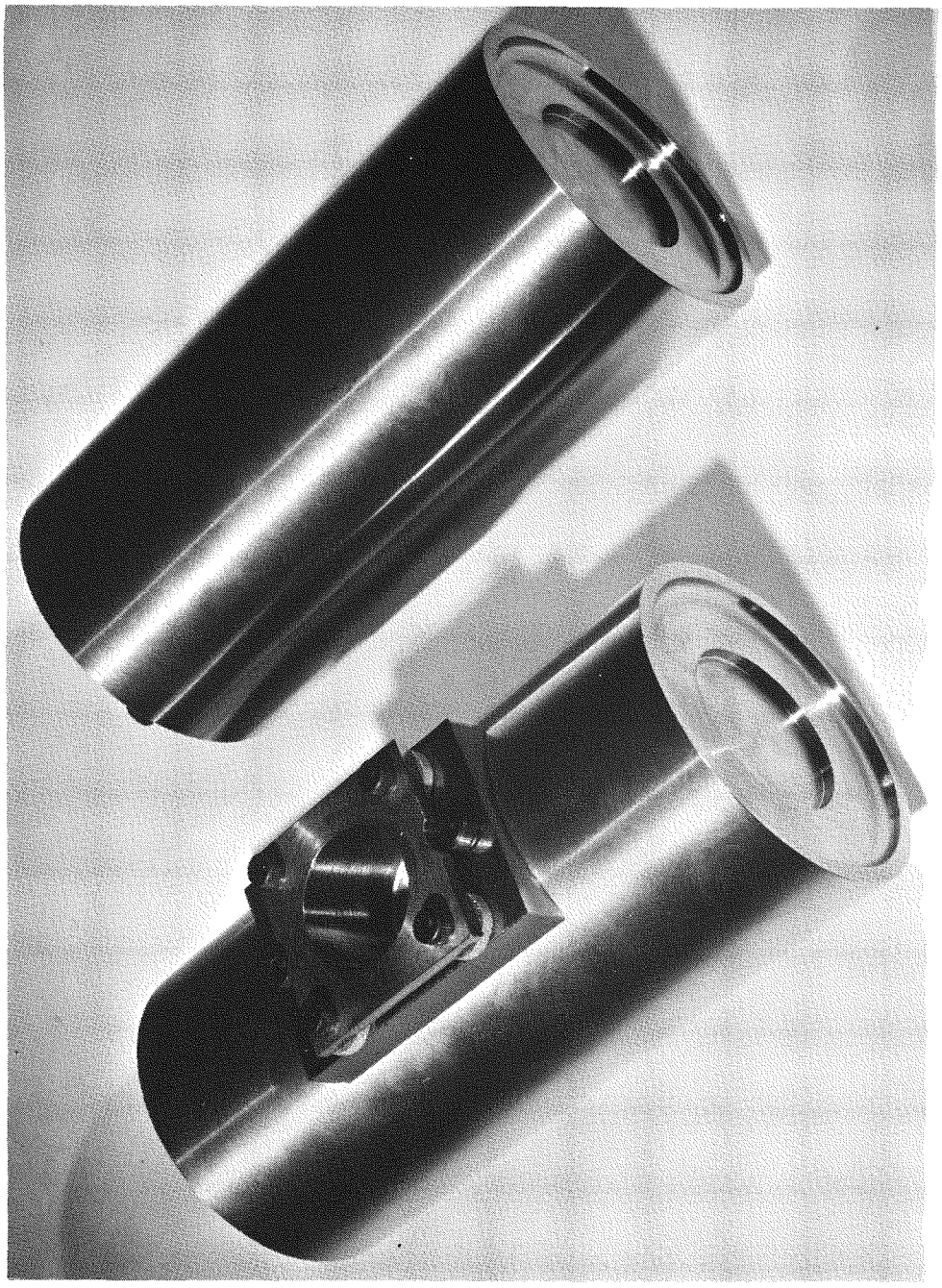

FIG. III-40. FULL-SCALE WIND TUNNEL MODELS OF SNAP 19 CAPSULE

500, 750 and 1200 psia. However, at the lowest pressure, 250 psia, the Mach 10 flow conditions could be maintained only marginally with an open test section. When the model was injected at this pressure, the additional airstream blockage and disturbance of the tunnel wall boundary layer caused the tunnel to "break flow" and hypersonic conditions could not be maintained. Therefore, tests were conducted only at the three higher pressures, which correspond to nominal Reynolds numbers of 0.81, 1.08 and 1.52 x 10^6 per foot, respectively.

The results of this test are presented in Ref. III-21.

IV. IRHS DESIGN AND DEVELOPMENT

The intact re-entry heat source (IRHS) that was developed and qualified for SNAP 19 is described in this chapter. A summary of the operating characteristics and manufacturing, fueling and assembly data is also presented. Detailed development and qualification test results are not included; however, a complete listing of all the various types of tests, objectives and significant results is presented. Separate reports (Refs. IV-1, IV-2 and IV-3) have been issued which present the heat source design and development history, detail analyses and results of safety tests.

A. DESCRIPTION AND OPERATING CHARACTERISTICS

1. Heat Source Description

The basic functional components of the IRHS (Figs. IV-1 and IV-2) are the PuO_2 fuel, a metallic fuel capsule for containing the fuel during normal operation and early abort situations, a graphite heat shield or outer shell for containing the internal parts during all modes of re-entry, and a barrier system to prevent chemical reaction between the graphite heat shield and the internal materials during the temperature extremes of re-entry. Design data are summarized in Table IV-1.

TABLE IV-1

IRHS Design Data Summary

1. Overall Assembly Data

Configuration	Right circular cylinder
Length (in.)	6.56
Diameter (in.)	3.0
Weight (lb)	5.65
Thermal power output (watts) (beginning of life)	570

2. Operating Radial Temperature Distribution (one atmosphere argon in generator; nominal orbit condition)

	Temperature (°F)
Heat shield	1040
Canister	1240
Capsule	1430
Volume averaged fuel temperature*	1600
Fuel center line**	2930

*Assumes one atmosphere helium in fuel void space
**Assumes argon fill gas only (essentially the case initially, after generator fueling)

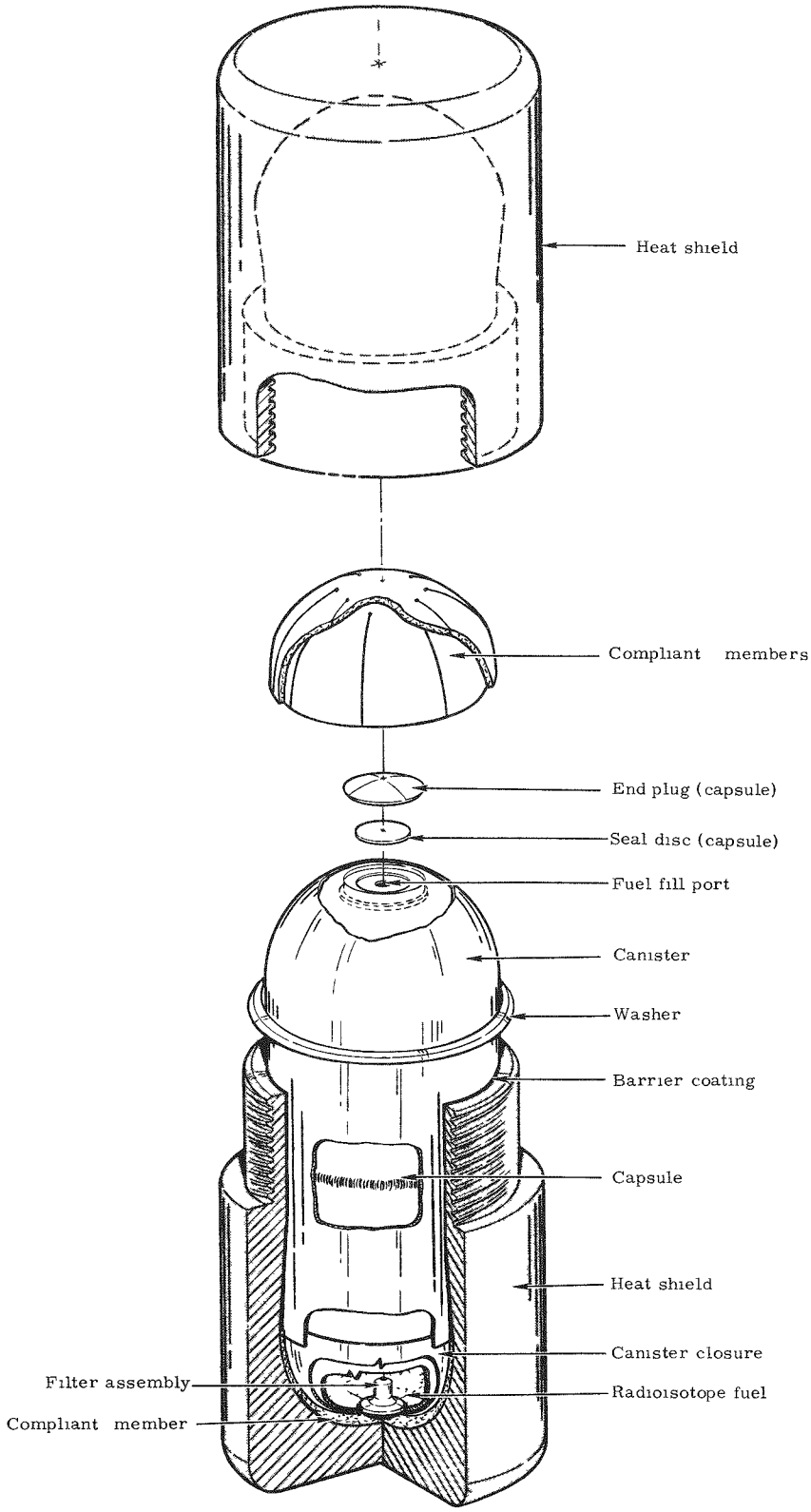

FIG. IV-1. IRHS OVERALL VIEW

FIG. IV-2. IRHS COMPONENTS

TABLE IV-1 (continued)

3. IRHS Component Design Data

Component	Material	Geometry and Characteristic Dimensions (in.)	Weight (lb)
Heat shield	High density fine grain graphite, coated inside with sprayed composite ceramic-metal barrier.	Right circular cylinder, 6.56 long x 3.0 diameter x 0.40 wall.	1.64
Canister	Tantalum, coated inside with flame-sprayed ZrO_2.	Cylinder with hemispherical ends, 5.48 overall x 2.14 outer diameter x 0.010 wall.	0.25
Capsule	Haynes-25	Cylinder with hemisperical ends, 5.39 overall x 2.12 diameter x 0.05 wall.	0.5
Filter element	ZrO_2, pressed and sintered	Cylinder, 0.040 diameter x 0.090 long, 40% porosity.	--
Compliant pads	Tantalum	Felted fiber, 6% of solid density, 0.12 thick.	0.11 (total)
Washer	Tantalum	Formed washer, 2.49 diameter x 2.20 diameter x 0.01 thick.	0.01
Fuel	PuO_2 microspheres	Approximately 75% bulk packing fraction.	3.14
		Total Weight	5.65

a. Plutonium dioxide fuel

The Pu-238 oxide fuel produces a nominal thermal power of 570 watts. The fuel particles are plasma-fired microspheres with a specified size range of 50 to 150 microns. Any void remaining within the metallic capsule was filled with plasma-fired ZrO_2 microspheres with a size range of 300 to 590 microns. Zirconium oxide is a high temperature material (melting point 4500° F) which has been shown by test to be compatible with PuO_2 and even plutonium metal at temperatures exceeding 1800° F. Though the ZrO_2 microspheres are initially placed on top of the fuel, normal handling causes them to disperse among the PuO_2 particles.

b. Fuel capsule

The fuel capsule is a single-containment, Haynes-25 structure made from two deep drawn cups with hemispherical ends and 0.050-inch nominal wall thickness. Two equal length cups are joined with a full penetration weld to form a 2.1-inch outside diameter by 5.4-inch-long fuel container. The single-containment envelope was made possible by development of a double-seal fueling port at one end. This feature, in conjunction with a special fueling fixture which protected the external surface of the capsule from contamination, enabled radioactive decontamination of the fueling port area after seal disk welding (before end plug welding).

The opposite hemispherical end of the Haynes-25 capsule contains a helium venting filter assembly (Figs. IV-1 and IV-3).

The filter assembly consists of a nail-head shaped receptacle into which a 0.040-inch diameter by 0.090-inch-long platinum-plated ZrO_2 filter element (Ref. IV 2) is installed. A 0.010-inch-thick seal disk is welded into the end of the receptacle as a temporary seal for fueling purposes. Following seal welding of the fueling port and decontamination, the filter assembly seal disk was punctured to make the filter operational. Helium generated from the decay of the radioisotope is vented from the capsule to prevent a buildup of pressure.

The configuration of the filter assembly was selected primarily to prevent impact damage to the filter element. Impact distortion energy tends to flow from the capsule wall through the larger diameter section without distorting the barrel around the filter element.

The fuel capsule will contain the PuO_2 fuel in normal operation or in early abort situations wherein no sensible aerodynamic heat is encountered. It is anticipated, however, that the Haynes-25 capsule will melt under orbital decay conditions and certain launch abort situations.

c. Heat shield

The outer shell of the IRHS is a heat shield made of fine grain graphite, produced by POCO Graphite, Incorporated, and is designated grade AXM-5Q. The heat shield is a right circular cylinder 3 inches in diameter and 6.56 inches long. The internal surface is roughly the shape of the capsule; however, the hemispherical ends have a diameter of 2.35 inches, which blends with the smaller 2.22-inch diameter cylindrical bore. This bulbous, hemispherical end accommodates the capsule compliant support pad.

The heat shield halves are threaded together at the mid-section with Acme stub threads to form a container for the internal materials. The flat on the end of the male threaded piece bottoms on a land in the female half of the heat shield.

d. Barrier system

A barrier system within the heat source precludes reaction between the molten Haynes-25 and the graphite during the re-entry heat pulse. This reaction would compromise the integrity of the heat shield if not retarded. The barrier also keeps the fuel microspheres from contacting the graphite if the capsule melts (there is some reaction between PuO_2 and carbon at higher temperatures).

Investigations showed that zirconium ozide does not react with the molten Haynes-25 or the PuO_2 at the predicted temperature extremes of re-entry. A coating of flame-sprayed ZrO_2 was therefore selected for the inside of the graphite heat shield as the primary barrier against reaction. Development led to a nominal 0.015-inch thick composite sprayed coating consisting of tantalum, molybdenum and ZrO_2.

A secondary, or redundant, barrier to reaction was provided by a 0.010-inch-thick tantalum canister with a 0.005-inch ZrO_2 sprayed coating on the inside. The canister was made from a cylinder and a welded hemispherical closure at one end. The other end of the cylinder was closed with a hemispherical end cap having a mechanical slip fit. The coated tantalum canister will retard the flow of molten

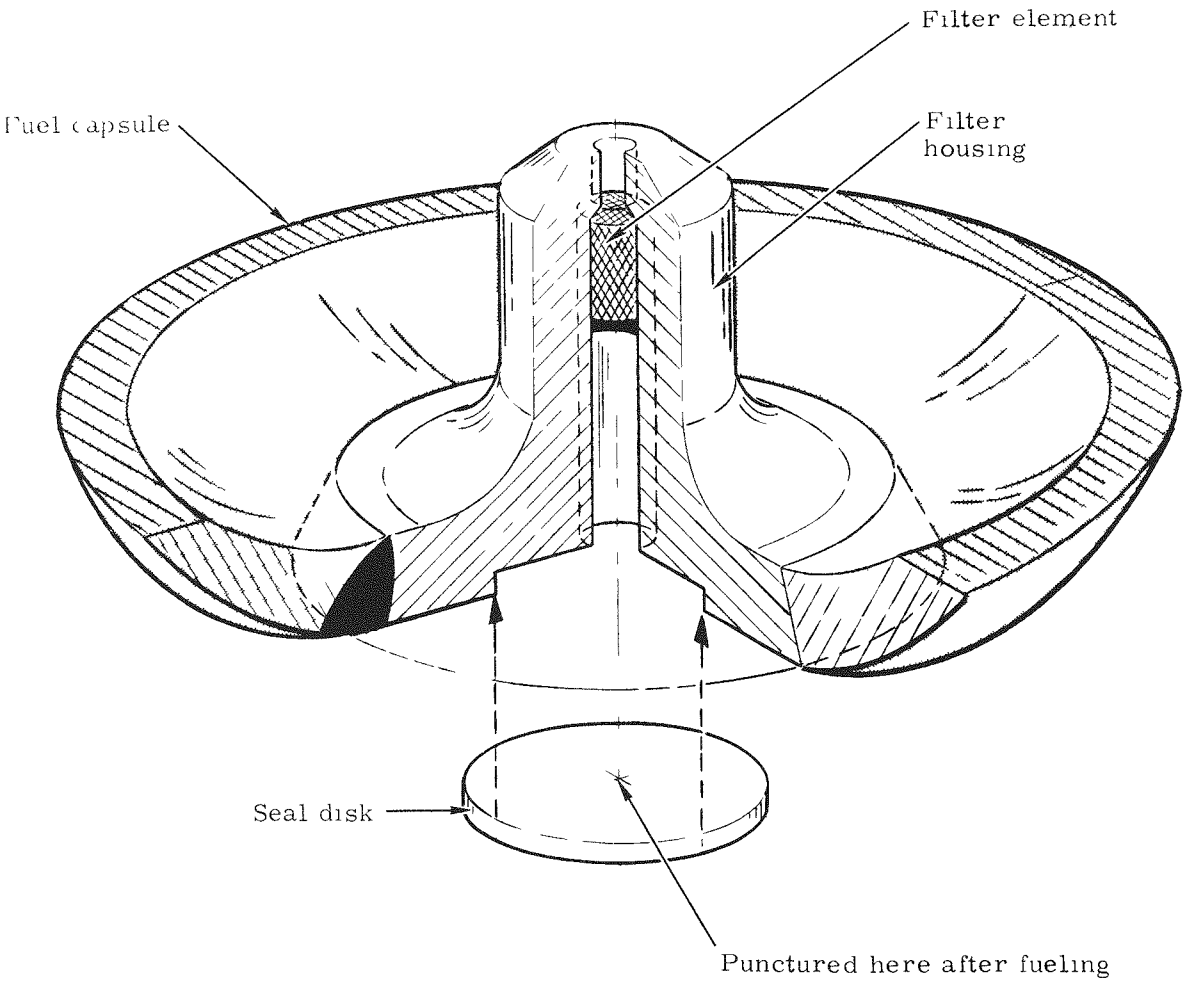

FIG. IV-3. FILTER ASSEMBLY

material to the coated graphite, thereby providing further assurance of heat source intact re-entry.

e. Capsule compliant support members

Unsintered tantalum felt pads at each end of the canistered capsule provide:

(1) Flexibility for take-up of manufacturing tolerances

(2) A compliant member for absorption of differential thermal expansion between the Haynes-25 and the graphite under normal operation and re-entry conditions

(3) A cushioning member to attenuate the dynamic loads between the capsule and the graphite heat shield.

Dynamic development testing of dummy IRHS assemblies resulted in a bulbous internal contour for the graphite heat shield (Ref. IV-3). This shape was necessary to provide room for the felt over the entire hemispherical end of the canistered capsule to provide lateral support.

The felt was made from 25-micron, hardened tantalum fibers oriented in a planar direction (rather than random orientation), needle punched to establish the desired density and thickness, and then calendered to close the needle holes. The 1/8-inch-thick (nominal) 6% density stock material was cut in a modified rosette pattern to form pads which could be fitted into the hemispherical heat shield configuration.

2. Re-entry Considerations

a. Environment

The re-entry conditions affecting IRHS design were derived from two basic types of ballistic trajectory: the return from an established orbit, and all other trajectories resulting from launch system malfunction during the ascent to planned orbit. To design the IRHS to withstand all such re-entry conditions and meet established intact re-entry objectives requires a detailed knowledge of the worst-case mechanical loads and component temperatures. Analyses and tests were performed to define representative trajectories, to evaluate heat transport mechanisms and calculate temperature distributions, and to calculate the extent of heat shield surface recession. Flight dynamics analysis, free-flight tests and wind tunnel tests were conducted to evaluate the body forces that could be developed in IRHS components during re-entry.

Trajectory data for this study were taken from the SNAP 19 dispersal system study (Ref. IV-4) and modified to account for the slightly different ballistic coefficient of the IRHS. This was possible because of the nearly identical shape and size of the dispersal heat source and the IRHS.

The SNAP 19/Nimbus B system will be launched from Vandenburg Air Force Base, California on a generally southward flight path. An abort trajectory beginning later than 8 to 12 seconds after lift-off will return the system to a Pacific Ocean impact. Earth impact velocity of an IRHS from an 8-second ascent would be about 260 feet/second. This velocity was used in impact tests against granite because it is the most probable maximum earth impact velocity from an abort trajectory.

Typical sets of trajectory parameters (altitude, velocity and averaged heating rate, all as a function of time) are presented in Figs. IV-4 and IV-5. Figure IV-4

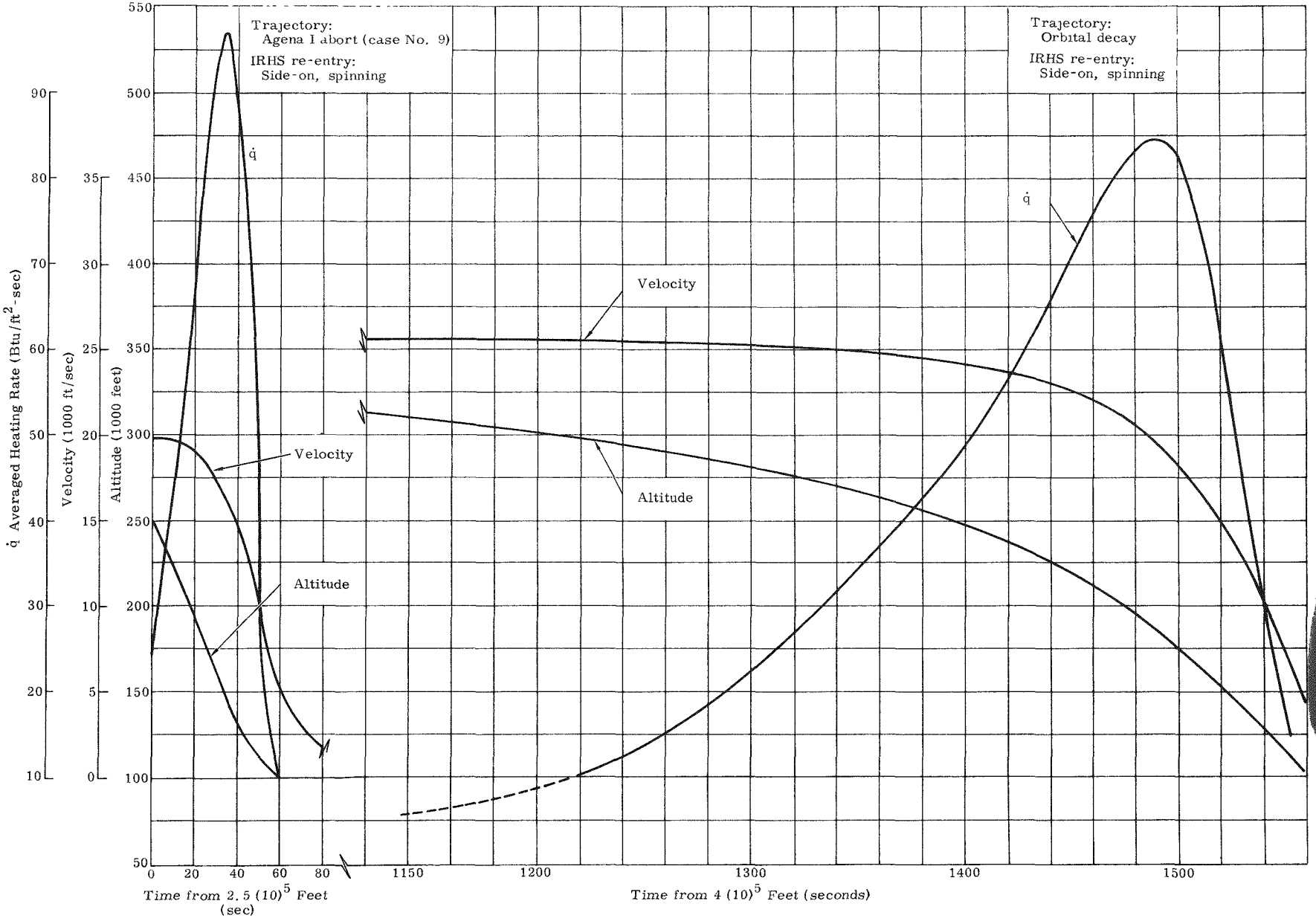

FIG. IV-4. IRHS TRAJECTORY DATA FOR SIDE-ON-SPINNING RE-ENTRY

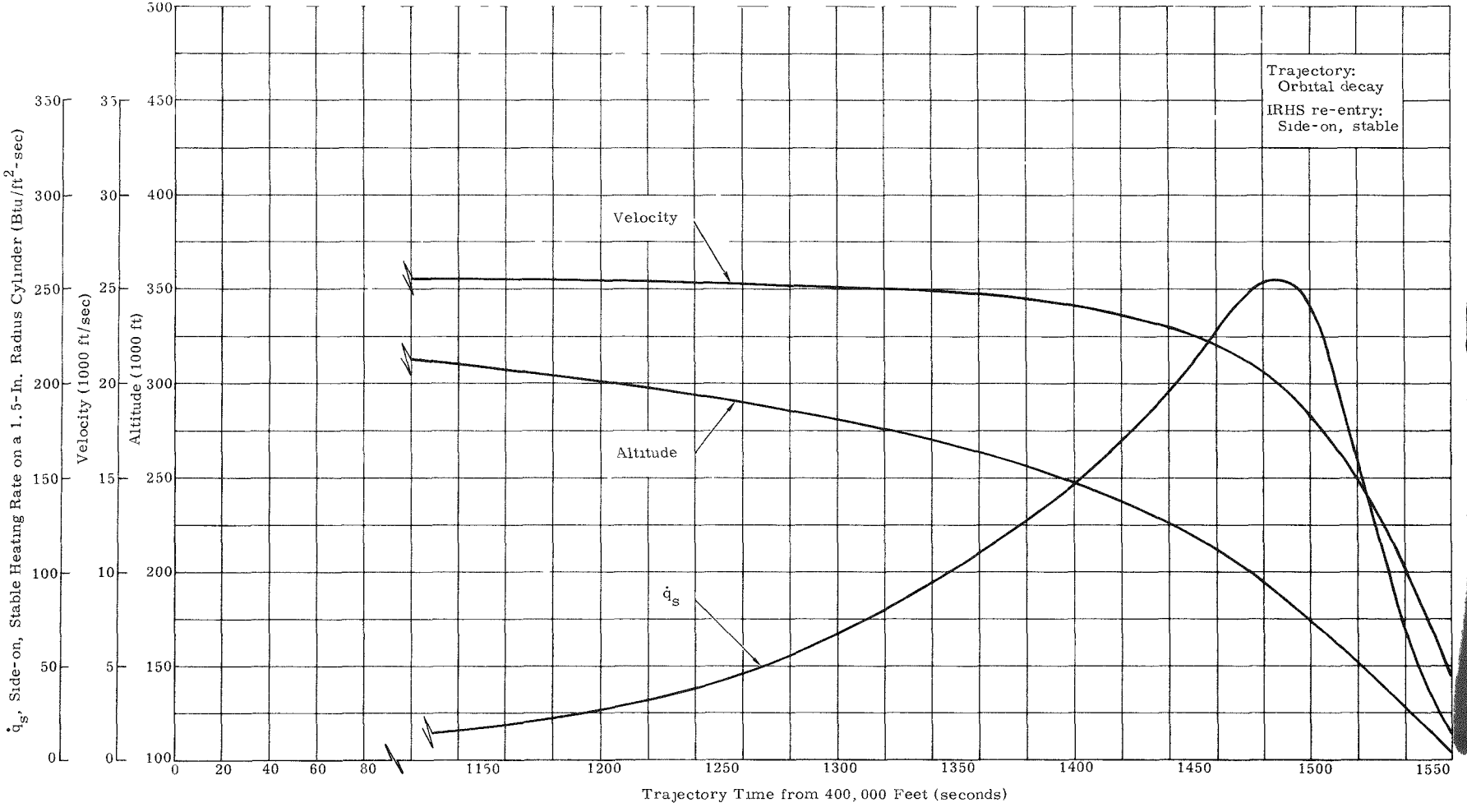

FIG IV-5. IRHS TRAJECTORY DATA FOR SIDE-ON, STABLE RE-ENTRY

shows parameters for an Agena abort trajectory from 250,000 feet and an orbital decay trajectory from 400,000 feet. The heating rate curves, $\dot{q}$, are typical of the side-on spinning IRHS re-entry mode. The relative magnitude of the two heating rate curves and their duration are easily compared. Figure IV-5 shows similar curves for a side-on stable IRHS re-entry from orbit. Note that the heating rates are considerably higher than for side-on spin orbital decay. All trajectories shown assume complete IRHS exposure at the maximum altitude shown on the trajectory curves. For example, the Agena I abort case starts at 406 seconds after liftoff (approximately 529,000 feet altitude), at which point the Nimbus B separates from the flight vehicle. The generator burns away and the IRHS is fully exposed at 250,000 feet, where the curves in Fig. IV-4 begin to trace the IRHS trajectory.

Aerothermal analyses and plasma arc tests were based on the trajectories and heating rates developed by the aerophysics analysis. Side-on, end-on and tumbling orientations of the heat source were considered for the Agena abort cases; a side-on flight mode was assumed for the cases of IRHS re-entry from orbit. The latter cases are conservative in that the heat source is assumed to re-enter unprotected by any other system components and must therefore sustain the total aeroheating. Several analytical models were used with two heat transfer computer programs. The design case established was more severe than the most probable re-entry case, and accounts for uncertainties in the prediction of thermal properties, heat fluxes, aerodynamic coefficients, etc., by increasing the heat flux by 30%.

A summary of cases analyzed for the IRHS is presented in Tables IV-2 and IV-3. Table IV-2 shows the trajectory case (orbital decay or abort), initial and final re-entry body configuration and flight motion, peak heat source temperatures, and the predicted recession of the graphite heat shield. Reference IV-4, Volume II gives a complete definition of the sequence of events occurring in the cases listed under "Vehicle Orientation at 400,000-foot Re-entry Point." In Table IV-3 different uncertainty factors are applied to the predicted nominal heat flux; Figs. IV-6 and IV-7 show typical component temperature histories for two cases (an Agena abort and a re-entry from orbit).

b. Design considerations

The important conditions affecting IRHS design for re-entry are temperature, temperature gradients, aerodynamic pressure forces and body forces generated by rotation about an axis through the IRHS. Initially, the IRHS heat shield configuration included two diametrically opposite 45° chamfers on the cylinder ends to induce tumbling during re-entry, thus reducing the local incident heat flux by averaging over the whole body surface. During preliminary aerothermal studies, it appeared possible that peak capsule temperatures could be held below the Haynes-25 melting point if tumbling modes could be guaranteed. Later analysis showed that temperatures were not reduced to the levels thought possible. Further, free flight tests suggested that the IRHS with chamfers would autorotate to high angular velocities. A modified three-degree-of-freedom digital trajectory code gave further indication that the IRHS would autorotate when given an initial negative (nose down) pitch rate. The autorotation would cause a buildup in the pitch rate during re-entry and the resulting axial stresses in the heat shield due to centrifugal force could exceed the graphite thread strength, permitting an atmospheric release of the fuel. Further analytical work with the three-of-degree-of-freedom program showed that reducing the graphite chamfer size reduced the pitch rate but damping coefficients, which significantly affect the maximum value, were questionable.

Without 45° chamfers, the most probable re-entry mode is side-on with some oscillation. The highest incident heat flux in the side-on configuration is encountered

TABLE IV-2

Summary--IRHS Re-entry Aerothermal Analyses

IRHS Re-entry Case	Vehicle Orientation at 400,000-foot Re-entry Point***	Flight Motion and Re-entry Configuration: Initial Configuration and Condition	Flight Motion and Re-entry Configuration: Assumed IRHS Re-entry Mode	IRHS Atmospheric Exposure Altitude ($ft \times 10^3$)	Assumed Heating Rate Uncertainty Factor	Peak Heat Shield Temperature (°F)	Peak Capsule Temperature (°F)	Peak Fuel Temperature (°F)	Heat Shield Maximum Surface Recession (in.)
Orbital decay*	Case 8***, orbital decay	IRHS, side-on	Side-on, spinning	400	1.3	3210	3160	3060	0.052
Orbital decay	Case 8, orbital decay	IRHS, side-on	Side-on, spinning	400	1.0	2970	2910	2880	0.039
Orbital decay	Case 8, orbital decay	IRHS, side-on	Side-on, spinning	400	0.7	2708	2608	2673	--
Orbital decay	Case 8, orbital decay	IRHS, side-on	Side-on, no-spin	400	1.0	3960	3420	3040	0.132
Orbital decay	Case 8, orbital decay	IRHS, tumbling and spinning	Tumbling and spinning	400	1.0	2660	2630	2680	0.047
Orbital decay	Case 8, orbital decay	IRHS, end-on	End-on	400	1.0	3100	2960	2850	0.180
Abort cases**									
1-A	Case 7, Agena II abort	IRHS, side-on	Side-on, spinning	400	1.3	3760	3280	2460	0.027
1-B	Case 7, Agena II abort	IRHS, side-on	Side-on, no-spin	400	1.3	5360	3920	2440	0.097
2	Case 4, Agena II abort	IRHS, side-on	Side-on, spinning	400	1.3	3390	3260	3060	0.05
3-A	Case 4, Agena II abort	IRHS, side-on	Side-on, spinning	400	1.3	3435	3395	3050	0.0049
3-B	Case 5, Agena II abort	IRHS, side-on	Side-on, no-spin	400	1.3	4575	3750	3025	0.138
4	Case 5, Agena II abort	IRHS, side-on	Side-on, spinning	400	1.3	3350	3170	2980	0.075
5	Case 7, Agena II abort	IRHS, tumbling	Tumbling and spinning	400	1.3	3780	3210	2420	0.044
6	Case 5, Agena II abort	IRHS, end-on	End-on	400	1.3	4200	3975	3300	0.190
7	Case 7, Agena II abort	IRHS, end-on	End-on	400	1.3	5060	4180	2600	0.15
8	Case 1, Agena I abort	Agena/Nimbus/S19 $\eta = 90°$ (coning angle)	Side-on, spinning	228	1.0	1940	1880	2050	--
9	Case 2, Agena I abort	Agena/Nimbus/S19 $\eta = 90°$	Side-on, spinning	252	1.0	2390	2265	2075	--
10	Case 3, Agena I abort	Agena/Nimbus/S19 $\eta = 80°$	Side-on, spinning	318	1.0	3080	2960	2740	--
11	Case 3, Agena I abort	IRHS, side-on	Side-on, spinning	400	1.0	3220	3060	2820	--
12	Case 8, orbital decay	Agena/Nimbus/S19 $\eta = 90°$	Side-on, spinning	320	1.0	2980	2820	2790	--
13	Case 8, orbital decay	SNAP 19 side-on, stable	Side-on, spinning	295	1.0	2980	2890	2775	--
14	Case 8, orbital decay	SNAP 19 tumbling and spinning	Side-on, spinning	260	1.0	2940	2800	2590	--
15	Case 8, orbital decay	Agena/Nimbus/S19 tumbling-spinning	Side-on, spinning	322	1.0	2980	2800	2880	--
16	Case 8, orbital decay	Agena/Nimbus/S19 end-on $\eta = 180°$ upper RTG	Side-on, spinning	255	1.0	2920	2840	2740	--
17	Case 8, orbital decay	Agena/Nimbus/S19 end-on $\eta = 180°$ lower RTG	Side-on, spinning	195	1.0	2920	2690	2450	--
18	Case 8, orbital decay	SNAP 19 tumbling and spinning	Side-on, spinning	290	1.0	2950	2880	2730	--
19	Case 8, orbital decay	SNAP 19 side-on, stable	Side-on, spinning	320	1.0	3000	2920	2830	--
20	Case 4, Agena II abort	Agena/Nimbus/S19 $\eta = 90°$	Side-on, spinning	320	1.0	3110	3020	2820	--
21	Case 6, Agena II abort	Agena/Nimbus/S19 $\eta = 90°$	Side-on, spinning	293	1.0	3390	3100	2570	--
22	Case 7, Agena II abort	Agena/Nimbus/S19 $\eta = 90°$	Side-on, spinning	275	1.0	3320	2920	2370	--

*Design case.

**Abort cases as defined herein include cases in which the IRHS is released from the generator during an orbital decay trajectory.

***See Table IV-3 for location and orientation.

TABLE IV-3

Vehicle Orientation at 400,000 Foot Re-entry Altitude used in Trajectory Computations

Case Number*	Ascent Trajectory Deviation (σ)	Ascent Trajectory Abort Time (sec)	Inertial Velocity (ft)	Inertial Flight Path Angle (fps)	Longitude (deg)	Latitude (deg)	Inertial Heading Angle + N to E (deg)
			Re-entry Condition for Release During Agena First Burn				
1	Nominal	355.27	16,576	-7.55	124.32 W	21.56 N	-170.86
2	Nominal	406.03	19,298	-5.55	125.04 W	18.96 N	-170.44
3	-3σ down	487.23	25,429	-1.07	135.44 W	23.13 S	-169.20
			Re-entry Condition for Release During Agena Second Burn				
4	Nominal	3233 to 3240*	26,600	-1.95	125.36 W	69.42 N	-152.32
5	Nominal	3233 to 3240*	26,600	-2.06	139.08 W	54.46 N	-163.68
6	Nominal	3233 to 3240*	26,500	-4.06	83.16 W	78.60 N	-112.28
7	Nominal	3233 to 3240*	26,000	-7.74	19.60 E	55.20 N	-17.64
			Re-entry Condition for Nominal Deorbit				
8	--	--	25,690	0.10	--	0	-90

*Use in conjunction with Table IV-2.

**At the apogee of the nominal trajectory (transfer ellipse) second burn ΔV's of 835 and 417.5 fps were applied in pulses at a number of angular orientations relative to the inertial velocity vector so as to cover all retrograde angles. These abort times and angles result in a hyperellipsoid pattern at the 400,000-foot re-entry point.

CONFIDENTIAL

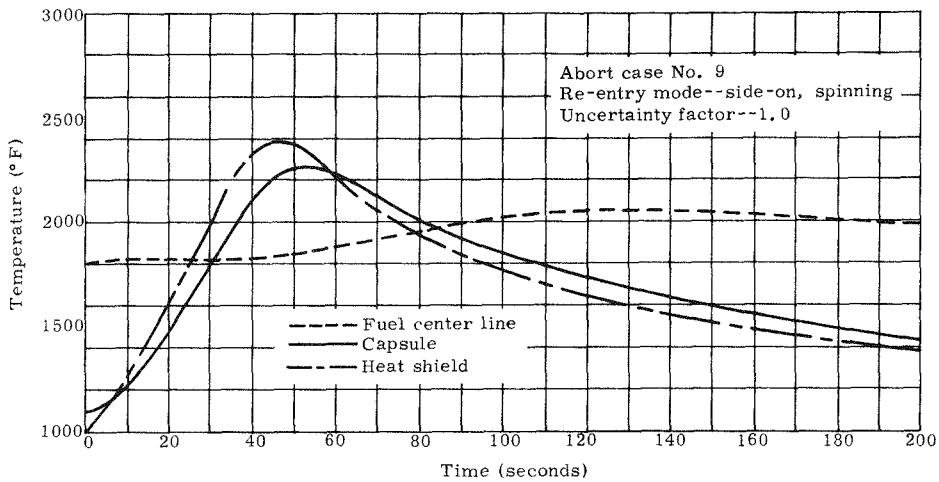

FIG. IV-6. RE-ENTRY TEMPERATURE AS A FUNCTION OF TIME--AGENA ABORT

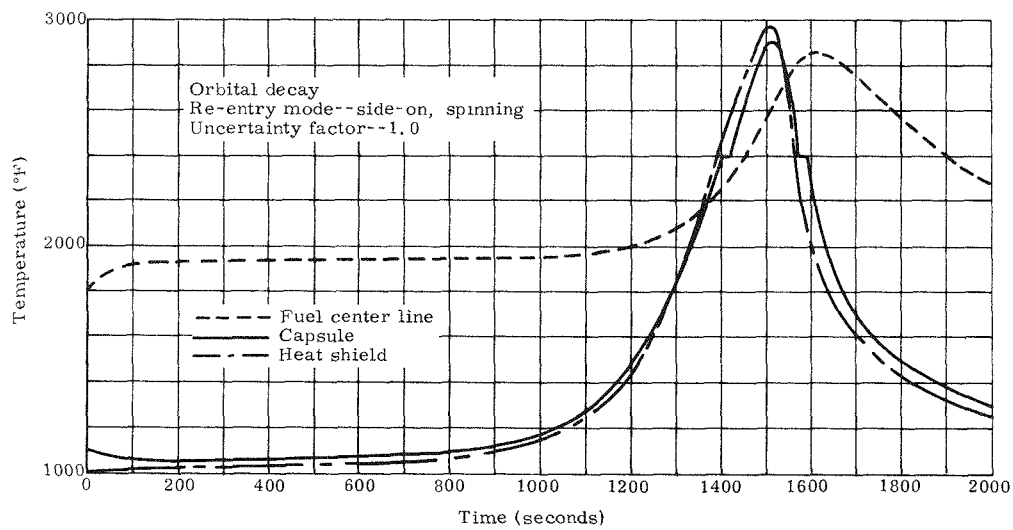

FIG. IV-7. RE-ENTRY TEMPERATURE AS A FUNCTION OF TIME--ORBITAL DECAY

in the side-on stable case (a highly improbable one, due to its ideal nature) for which no rotation about the IRHS longitudinal axis is assumed. The IRHS capability to withstand this side-on stable mode without breaching the graphite was subsequently demonstrated in three plasma-arc tests. Accordingly, the chamfers were eliminated from the graphite heat shield. (Four other side-on stable design verification plasma models provided further confirmation. See Section D-4 of this chapter.)

Another design area affected by the re-entry environment is that concerned with component materials compatibility. At peak re-entry temperatures (in excess of 3000° F), molten Haynes-25, PuO_2 fuel and graphite interact chemically. The PuO_2 fuel will react with graphite at elevated temperatures, producing lower melting plutonium carbides and mixtures of CO and CO_2. Also, liquid Haynes-25 in contact with PuO_2 microspheres is capable of dissolving small amounts of plutonium and will rapidly dissolve graphite. These chemical reactions could lead to gas production inside the heat shield, lower melting carbide compounds could be formed, and the graphite heat shield could be destructively attacked from the inside, leaving insufficient thickness for surface recession during the re-entry heat pulse.

This serious potential problem was solved by development and subsequent proof-testing of a barrier coating system that prevents contact between molten capsule materials and the graphite heat shield or the PuO_2 and the graphite. This coating system is comprised of a composite ceramic coating on the graphite inside surface and a ZrO_2 coating on the inner surface of a tantalum canister surrounding the fuel capsule. Plasma arc testing of completely simulated heat sources (Section D-4) has verified that the coating system developed will withstand all anticipated re-entry environments.

Graphite surface recession during re-entry was taken into consideration for the calculation of heat shield stresses caused by aerodynamic pressure loads. These stresses were negligible because aerodynamic pressures were low (Section A-4). Surface recession was, at most, 46% of the nominal wall thickness, and this was for the ideal side-on stable cases of severe but local recession along the stagnation heating line. Circumferentially uniform recession encountered in the side-on spinning cases was about 0.050 inch, or only about 25% of the nominal heat shield wall thickness.

The re-entry environment is a critical phase in the function of the compliant pads. Throughout launch and RTG operation at design temperatures, the compliant pads maintain an axial tension load in the graphite. This load is reacted by the axial compression of the canistered capsule. As capsule and graphite heat shield grow hotter during re-entry, differential expansion increases the load on the graphite. However, the Haynes-25 capsule rapidly loses strength (eventually melting), yields in compression and relieves the increasing graphite tensile stress. The design has been proven acceptable by several worst case plasma arc heating tests.

3. Thermal Analysis Summary for Operation in the RTG

The IRHS is rather complicated from a thermal design viewpoint. The complication arises from the several materials used, uncertainty in prediction of the radial gaps that exist between the component materials and the fact that the gas constituent mixture is changing throughout life. The gas constituent change results because the Haynes-25 fuel capsule is seal welded in pure helium, but, after piercing the filter diaphragm (so the helium vent will become operational), the following operations occur in pure argon:

(1) Assembly of the capsule into the IRHS

(2) Shipping and storage of the IRHS within the shipping cask

(3) Installation of the IRHS into the thermoelectric generator.

During and after the above operations, interdiffusion of the helium and argon will take place through the ZrO_2 filter. Consequently, the capsule will contain a helium/argon mixture at the beginning of the generator operating life. Conversely, the original 100% argon gas fill within the generator will be slowly diluted with helium due to the helium release from the Pu-238 fuel.

After the IRHS is placed in the SNAP 19 RTG, the generator gas fill will slowly change from approximately one atmosphere of argon to a mixture of helium and argon as the helium is released from the fuel. Both gases will diffuse through the generator Viton O-rings, but the helium gas will be replenished, and the argon partial pressure will continue to decrease. Based on tests and analyses, the helium and argon total pressure would reach values between 2.2 and 14 psia* after six months of generator storage and one year in orbit.

Table IV-4 summarizes IRHS component temperatures for different internal environments and operating conditions. Two temperatures are listed in Table IV-4 for fuel centerline with an argon gas fill in the generator. The higher value is computed with the assumption that the void space within the fueled capsule contains 100% argon gas. It is recognized that a 100% argon gas fill will not occur within the fuel due to the helium generation, but the value brackets the centerline temperature for the helium-argon mixtures. Except in the unlikely event of catastrophic leak resulting in generator evacuation, the increasing helium-to-argon ratio will lead to a change in IRHS component temperatures toward the lower values with helium gas fill.

The fuel centerline temperature for a vacuum condition is not presented in Table IV-4 because the effective conductivity data for packed PuO_2 microspheres in vacuum is not available. While this calculation would yield an interesting upper limit prediction of fuel centerline temperature, the filter restriction and finite helium generation rate will prevent a hard vacuum in the capsule.

One-dimensional (radial) heat transfer calculations were used for all IRHS temperature distribution analysis, ignoring axial heat flow into the Min-K 1301 insulation end support system within the thermoelectric generator. Heat transfer calculations were based on radiation and gas conduction across a gap from one component to the other; i.e., no solid conduction was assumed. These modes of transfer result in the gap width having a significant effect on the operating temperature of IRHS inner components. Table IV-5 shows the predicted component dimensions and gaps for a 100% argon gas fill and a generator fin root temperature of 337° F (nominal orbit condition). Figure IV-8 shows the thermal effect of varying the Haynes-25/tantalum gap, and the tantalum/POCO gap to 0.001 inch each and holding other parameters constant. As the Haynes-25 capsule outer surface approaches the tantalum canister inner diameter, the capsule temperature drops to approximately 1280° F. As the Haynes-25 and tantalum diameter are continued outward toward the POCO heat shield inner diameter, the Haynes-25 temperature drops to 1115° F and the tantalum temperature is reduced to 1080° F.

*Based on argon leak rates of 1×10^{-4} and 2×10^{-5} scc/sec, respectivley. See Section VII, Volume III.

TABLE IV-4

SNAP 19 IRHS/Generator Temperature Distributions

	RTG on Nominal Electrical Load			RTG in Open-Circuit Condition		
Q_{in} (thermal watts)	570	570	570	570	570	570
Generator gas fill	Argon (14.7 psia)	Helium (14.7 psia)	Vacuum	Argon (14.7 psia)	Helium (14.7 psia)	Vacuum
Thermoelectric cold junction temperature (°F)	400	370	460	400	370	460
Thermoelectric hot junction temperature (°F)	920	830	990	1160	1070	1230
Heat distribution block temperature (°F)	970	870	1090	1210	1110	1330
Heat shield temperature (°F)	1040	880	1280	1270	1120	1460
Tantalum temperature (°F)	1240	920	1730	1450	1170	1840
Capsule temperature (°F)	1430	960	1950	1620	1210	2030
Fuel centerline temperature (°F)	2930* 1960**	1640**	--	2960* 2100**	1800**	--

*Argon within fuel bed
**Helium within fuel bed

TABLE IV-5

SNAP 19 IRHS Dimensions and Gaps for Normal Operation*

Component	Material	Room Temperature Radius (in.)	Approximate** Operating Temperature (°F)	Thermal Expansion Coefficient, α (in./in.-°F) x 10^6	Operating Temperature Radius (in.)	Gap (in.)
Heat accumulator block	ATJ graphite (inside radius)	1.508	950	1.8	1.511	0.006
Heat shield	POCO graphite (outside radius)	1.500	1000	3.9	1.505	
Heat shield	POCO graphite (inside radius)	1.098	1000	3.9	1.102	0.009
Canister	Tantalum (outside radius)	1.088	1300	3.6	1.093	
Canister	Tantalum (inside radius)	1.074	1300	3.6	1.084	0.012
Capsule	Haynes-25 (outside radius)	1.059	1425	9.4	1.072	
Capsule	Haynes-25 (inside radius)	1.000	1425	9.4	1.010	

*One atmosphere of pure argon

**Approximate values used in computing radial gaps

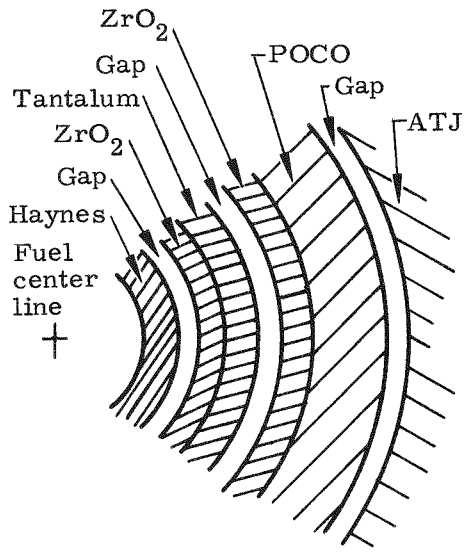

Cross-section of IRHS (not to scale)

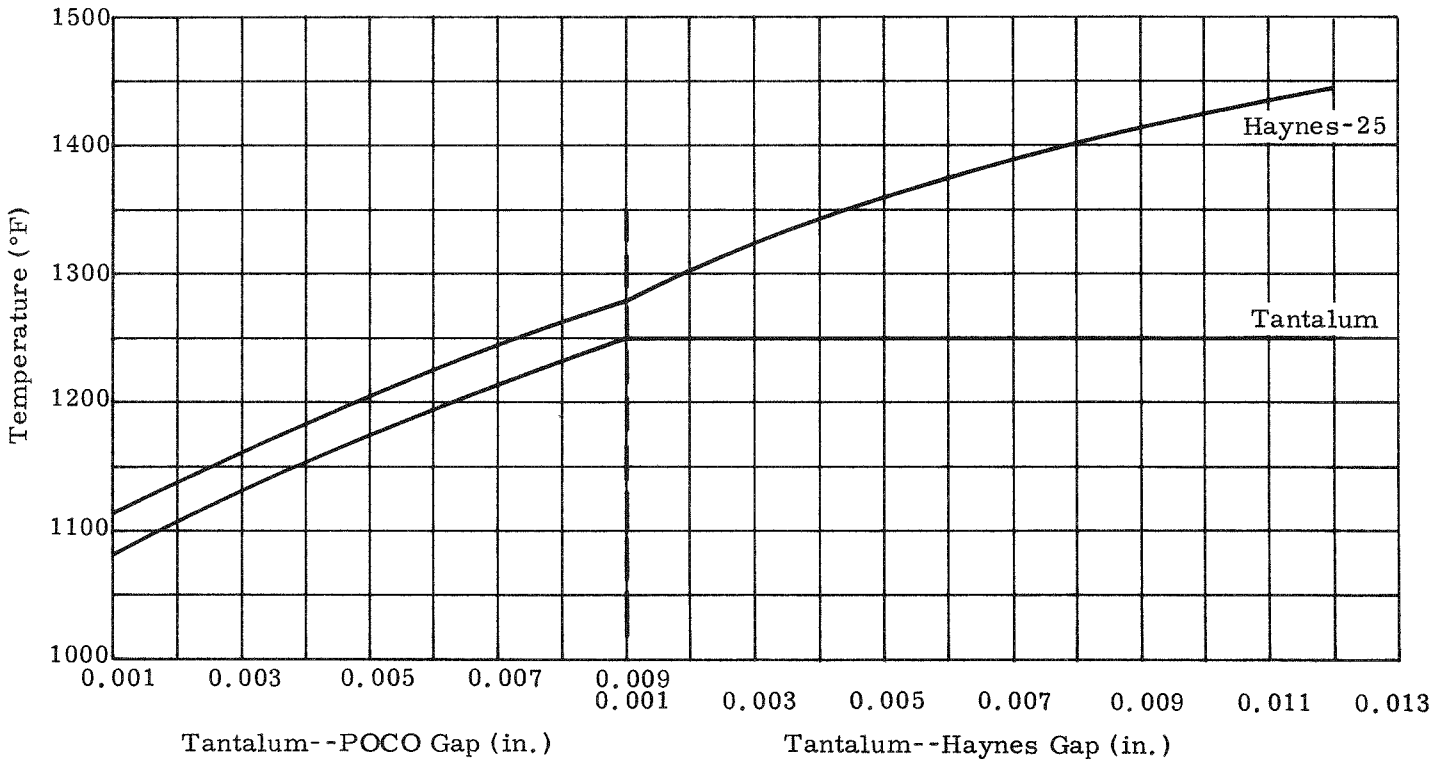

FIG. IV-8. IRHS CAPSULE AND CANISTER TEMPERATURES AS A FUNCTION OF INTER-COMPONENT SPACING

4. Structural Analyses Summary IRHS Assembly

The heat source components are exposed to loads that result in minimal stress levels during normal operation. This results from the fact that the Haynes-25 capsule is vented to minimize helium pressure buildup, and the assembly is operating in a static system in earth orbit. Since the normal operating conditions do not present a problem, a major portion of the structural analyses was directed toward the POCO heat shield to assure that atmospheric fuel dispersal will not be experienced under re-entry conditions. In addition, loads experienced during the heat source assembly operation, launch dynamic loads and loads resulting from a blocked filter assembly were analyzed. A summary of results follow; detailed analyses and results are in Ref. IV-3.

To provide high assurance that the POCO heat shield will not rupture under conditions that would allow an atmospheric release of the PuO_2 fuel, it was necessary to establish reasonable design stress limits for the graphite. Allowable stress levels were determined from a study of test data supplied by the graphite producer and the Southwest Research Institute. A summary graph of the test data and design allowable stress as a function of temperature is shown in Fig. IV-9. The test data are banded by the cross-hatched area, and the design allowable is shown under this band.

a. POCO graphite preorbit axial load

The axial load capability of the graphite heat shield is limited by the thread relief area of the joint and the associated stress concentration factor. (Tests were conducted to establish the approximate factor.) Based on the stress concentration factor and the ultimate tensile stress, nominal axial load capabilities of 2075 pounds and 2350 pounds were calculated for room temperature and 3000° F, respectively. Based on these predicted axial failure loads, maximum design loads of 1450 and 1900 pounds were selected.

The axial load required to compress the tantalum felt pads at the time of heat source assembly was computed to be approximately 640 pounds. This results in a graphite material tensile stress of approximately 425 psi at the female thread relief area and 670 psi at the male thread relief. The 640-pound load experienced at assembly is well below the recommended design load of 1450 pounds; also, the 640-pound assembly load soon reduces as the tantalum felt pads relax as a function of time and temperature.

The POCO graphite will experience dynamic loads as a result of relative motion between the capsule and the heat shield during system launch. Room temperature tests were conducted with dummy heat sources mounted directly to the vibration table as a means of screening candidate compliant pad members; but the tests were not directly applicable to actual launch loads, since the dynamic response characteristics of the relaxed tantalum felt pads at elevated temperature were unknown. This assurance of adequacy was provided through a generator subsystem prototype qualification test with fueled IRHS assemblies. Following prototype qualification testing, one generator with a fueled IRHS was subjected to flight acceptance level vibration testing and then both heat source assemblies were diagnostically disassembled. Though the actual loads imposed on the IRHS heat shield are not known under launch conditions, the degree of dynamic over-test provided high confidence that the heat shield integrity will not be compromised as a result of launch loads.

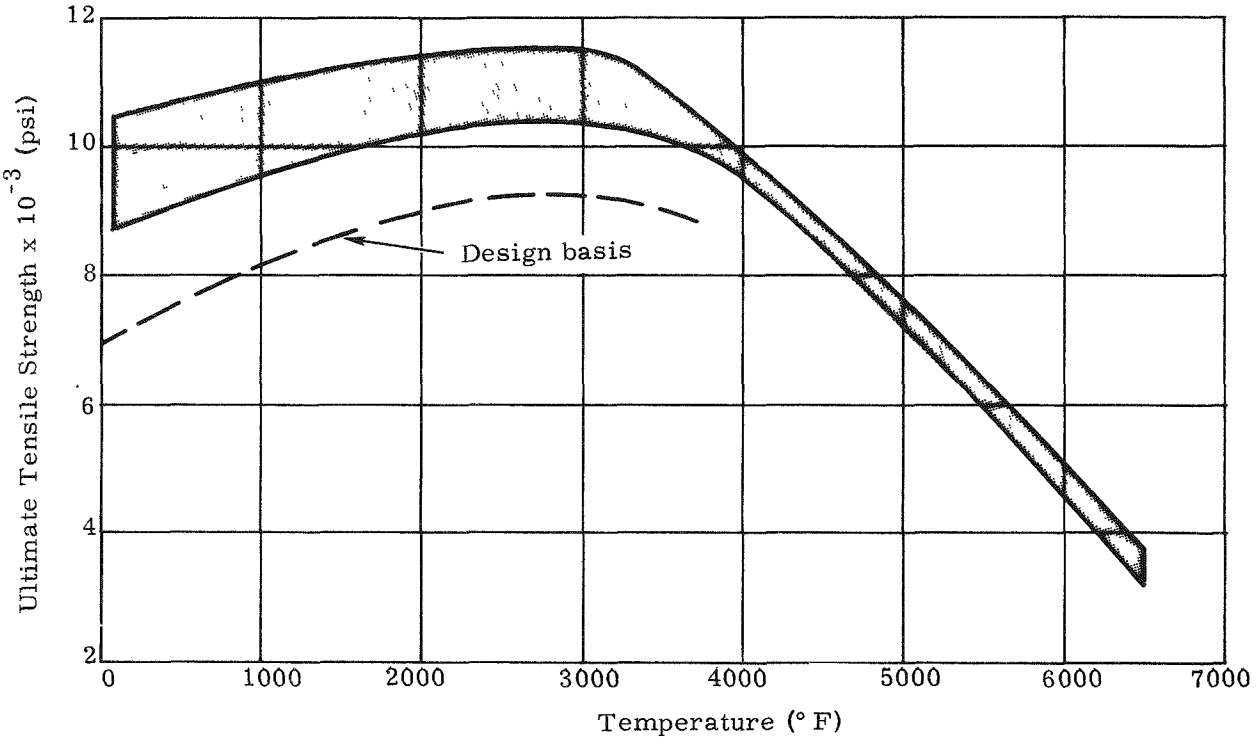

FIG. IV-9. ULTIMATE TENSILE AND DESIGN ALLOWABLE STRESSES AS A FUNCTION OF TEMPERATURE, FOR POCO AXM-5Q

b. Heat source re-entry stresses

The considered heat shield orbital re-entry stresses consisted of aerodynamic pressure stresses, thermal stresses under side-on spinning and side-on stable re-entry, and axial stresses resulting from a heat source tumbling mode of re-entry.

Aerodynamic pressure acting on the heat shield during re-entry was shown to result in negligible stresses. A uniform pressure equal to the peak stagnation point pressure was assumed to act over the entire cylindrical circumference. The resultant maximum stress (at the inner radius of the graphite) was only 47.5 psi. This maximum pressure point occurred at approximately 1576 seconds after the 400,000-foot re-entry altitude is reached, and since the resultant stress was so low it eliminated the need for more detailed examination.

The thermal stresses resulting from a heat source re-entry in a side-on spinning mode will result in temperatures being higher at the outer radius than at the inner radius of the graphite heat shield. For the orbital decay case, the peak stress occurs at about 1450 seconds after 400,000 feet re-entry altitude with a magnitude of approximately 2500 psi in tension. This peak stress area is located on the hemispherical inner surface at the location of maximum wall thickness.

Another factor studied was thermal stress resulting from the severe temperature gradient in the heat shield encountered during a side-on stable re-entry (a low probability, worst-case condition). The computer program used for this case has the capability of determining a circumferential stress distribution in a body of revolution. The temperature distribution used was circumferential only, from 3000° F along the stagnation line to 500° F on the opposite side. The maximum stress determined in this program was less than 1500 psi and occurred at the stagnation line. The heat shield thermal stresses analyzed for side-on spinning and side-on stable cases are well within the allowable design stress. Confirmation of heat shield adequacy under re-entry conditions was provided through plasma-arc tests under various side-on spinning and side-on stable re-entry conditions. Test conditions included abort situations and orbital decay.

Though tumbling of the right circular cylinder IRHS assembly is unlikely without tumble-inducing bevels, the results are still of interest to indicate the margin of safety, should the assembly develop some type of tumbling mode. The analyzed case assumes that the capsule has melted and (conservatively) the centroid of mass is approximately two inches from the yaw axis. With these assumptions, the heat shield can withstand a tumble rate of approximately 300 radians per second.

c. Results of blocked helium vent

The effect of capsule filter blockage on the integrity of the graphite heat shield was investigated. Blockage is highly unlikely because the element is extruded ZrO_2 material. For the case where the filter has become blocked, elapsed time for the capsule to creep to the point where load is being transferred to the graphite heat shield was computed. Further, the maximum fluid pressure that the heat shield can withstand was analyzed for cases where there is a rapid release of internal pressure.

The normal operating temperature of the Haynes-25 capsule in an argon environment with the generator in orbit is 1425° F. Should the filter element (helium vent) become blocked, the Haynes-25 capsule will expand and reduce the gap between capsule and tantalum canister, causing the capsule temperature to decrease. Continuing pressure increase will force the capsule/canister diameter to increase until the heat shield has been contacted (approximately 2% creep of the capsule). This limit will

result in a predicted Haynes-25 capsule temperature of 1115° F. With a capsule void volume of 79 cm^3 and a helium generation rate of 2.4×10^{-5} scc/sec, the time to 2% capsule creep was predicted to be 1.5 and 4.3 years, respectively, for the 1425 and 1115° F capsule temperatures. It was conservatively assumed that all helium generated was instantaneously released by the fuel particles.

The POCO graphite heat shield was analyzed to determine the maximum allowable internal fluid pressure (assumed no notch factor circumferentially) to simulate a sudden release of pressure from the Haynes-25 capsule. Based on an allowable 9000 psi material stress, a fluid pressure of 2630 psi would be contained. This fluid pressure is well above the creep-to-rupture pressure for the capsule.

Independent analyses conducted by the Oak Ridge National Laboratory indicated that the Haynes-25 capsule would age-harden and would probably rupture prior to 2% creep strain being achieved should the helium vent become blocked. Previous tests at Martin Marietta and Oak Ridge suggested that failure would occur as a small microfissure, allowing the pressure to slowly escape from the capsule. Limited testing to failure of pressurized Haynes-25 capsules, under normal operating temperatures and re-entry temperatures caused no damage to the surrounding graphite heat shield assembly. This indicates that the integrity of the heat shield could be assured even with a completely blocked filter element.

d. Heat source impact

Results of previous impact tests were examined from the viewpoint of gaining good design judgment which could be factored into the IRHS design. The adequacy of the selected IRHS design to withstand impact was then demonstrated through impact testing against granite at a nominal 260 ft/sec and 1000° F. Features of the IRHS design that inherently increase impact resistance are:

(1) Elimination of sharp corners in the capsule (hemispherical ends)

(2) Elimination of void within the capsule (use of ZrO_2 microspheres) to reduce sharp bends in the metal wall during impact

(3) Avoidance of sudden change in material thickness

(4) Minimization of welds

(5) Inclusion of the tantalum compliant member and the POCO heat shield which absorb a portion of the impact energy.

B. HEAT SOURCE ASSEMBLY OPERATIONS--MOUND LABORATORY

Fueling of the capsules and assembly of the intact re-entry heat sources were conducted at the Mound Laboratory of Monsanto Research Corporation. Close liaison was maintained throughout the program to assure:

(1) Development of mutually acceptable fueling procedures

(2) Integration of the evolved heat source design with the fueling facility capabilities, and design of fueling fixtures and tooling

(3) Exchange of developmental test results which might influence the design of the heat source or the fueling procedures and tooling.

During the SNAP 19 IRHS program span, a total of six heat sources were fueled and delivered to the Martin Marietta Corporation. Two of the heat sources were subsequently delivered to the Atomic Energy Commissionas a part of the flight generator subsystem for the Nimbus B application. The remaining four sources were returned to the Mound Laboratory for disassembly. Information provided in this section of the report summarizes activities with Mound Laboratory in the areas of prefueling liaison, Haynes-25 capsule fueling, heat source assembly, and heat source diagnostic disassembly.

1. Prefueling Activities

Initial liaison effort with Mound Laboratory was devoted to integration of the heat source design with the design of fueling tools and fixtures, and to establishment of mutually acceptable fueling procedures. As a result of the integrated design efforts, a single Haynes-25 capsule fuel container was made possible. Heretofore, plutonium microsphere fuel was first seal welded in a thin liner and the majority of liner surface radioactive contamination then removed. The liner was seal welded into a structural capsule, in a nonradioactive area, thereby assuring an outer surface that was free of radioactive contamination.

Figure IV-10 shows the Haynes-25 capsule welding fixture assembly (designed by Mound Laboratory) that resulted from the integrated design effort. Instead of double containment for the fuel as in the dispersal capsule, a redundant weld enabled radioactive decontamination to be performed between the welding operations. Prior to the fueling operation, the outer surface of the welding fixture (with the contained Haynes-25 capsule) was covered with a strippable coating and bagged for protection from surface contamination. Following installation of the PuO_2 microspheres and closure of the seal disk (in a glove box), the assembly was moved from the contaminated glove box to a lower activity level area. Removal of the bags and strippable coatings and washing of the exposed surfaces resulted in a clean capsule welding fixture assembly. This assembly was then moved to a clean box where the structural (or redundant) weld is accomplished.

A parallel effort was conducted at Martin Marietta and Mound Laboratory in the development of weld parameters for the fueling port seal closures. (All other capsule welds conducted at Martin Marietta Corporation.) This was necessary because schedule constraints precluded Mound from conducting the various closure welds on capsules for developmental tests (impact, plasma, vibration, burst tests, etc.). Two weld development capsules were returned to Martin Marietta from Mound Laboratory for impact tests to demonstrate that closure welds were comparable.

2. Capsule Fueling

The Haynes-25 capsules were fueled with approximately 570 thermal watts of plasma-fired PuO_2 microspheres (50- to 250-micron nominal size spectrum) prepared in accordance with Mound Laboratory Specification 1-11391. Loading of the fuel into the capsule was conducted in a helium-filled glove box with the capsule enclosed in the fixture shown in Fig. IV-10. Any void remaining in the capsule was filled with 300- to 590-micron plasma-fired ZrO_2 microspheres, also prepared in accordance with Mound Laboratory Specification 1-11391. The seal disk was welded in place and inspected; and the whole fueling fixture was then moved to an area of lower activity level for radioactive decontamination. Following decontamination, the welding fixture (with contained capsule) was moved to a noncontaminated, helium-filled glove box and the structural weld closure made using the TIG process. This procedure trapped helium between the seal disk and the structural end-cap, so that a helium leak check could be conducted on the structural weld closure.

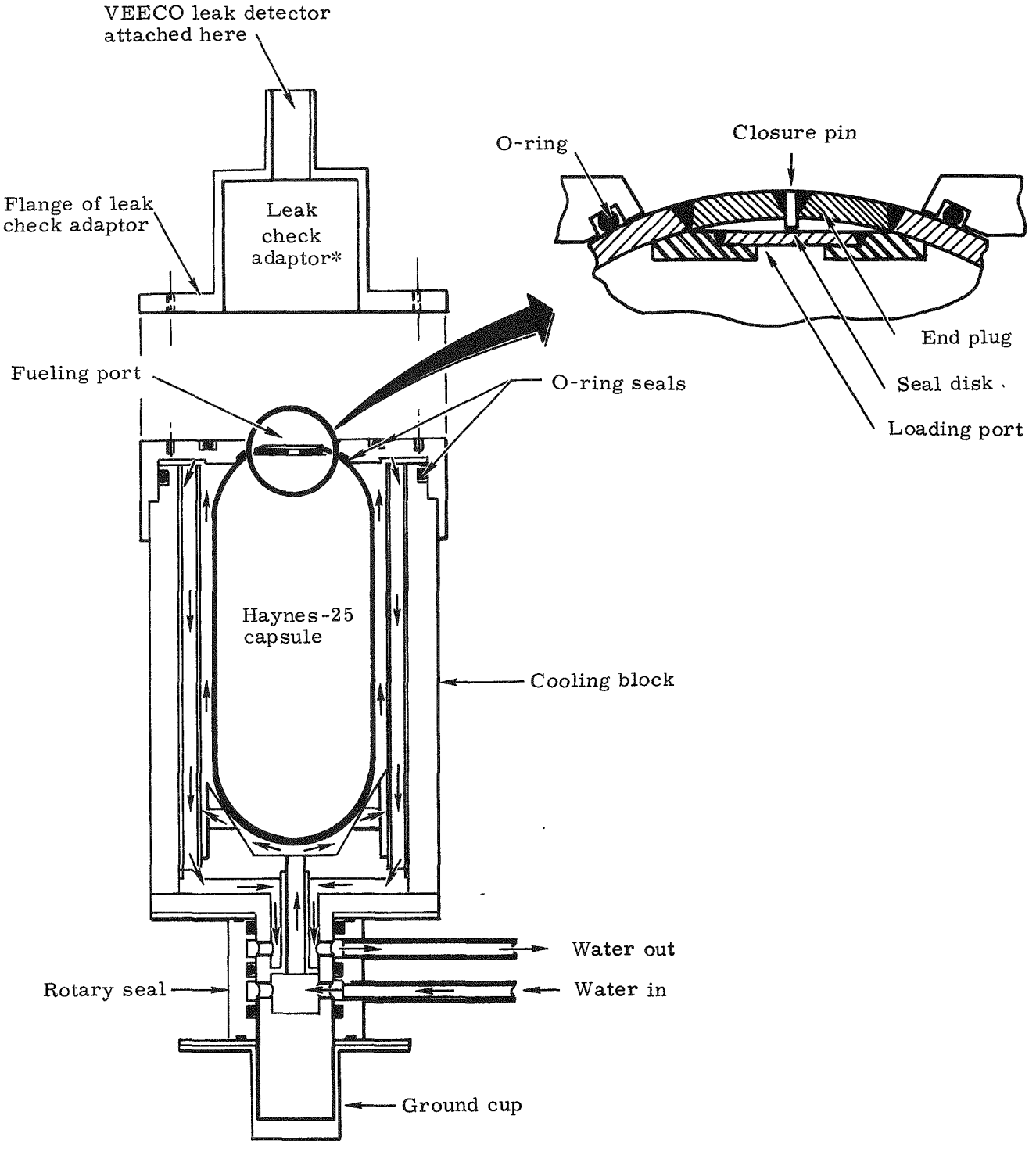

*Bolted to plate of cooling block during leak checking operation

FIG. IV-10. MOUND LABORATORY FUELING FACILITY WELDING AND COOLING FIXTURE, SHOWING HAYNES-25 CAPSULE IN POSITION FOR WELDING

To provide further assurance of a high-quality fueling port closure weld, complete Haynes-25 capsules were assembled into the welding fixture and welded for destructive control samples. A weld control sample was welded before and after the fueled capsule. The weld control samples were then subjected to the following quality assurance checks:

(1) Helium leak check

(2) Dye penetrant inspection for surface cracks

(3) Radiography for cracks or inclusions

(4) Metallographic examination for evidence of cracks and weld penetration.

A typical metallographic section through the weld zone of the capsule fueling port is shown in Fig. IV-11. The section shown is from one of the weld control samples used during the fueling operation for the two flight capsules. Note the weld area for the 0.010-inch seal disk and the full penetration weld for the structural end-cap in the one photomicrograph. The other photomicrograph is a view through the pin weld (the final seal point in the structural end cap).

Following the final welding and leak check operation on the capsules, which were fueled with the plutonium microspheres, the capsule was removed from the welding fixture. The capsules were then subjected to calorimetry measurements to assure that the thermal inventory met the 570 ± 17 watt requirement. Following neutron and gamma dose rate measurements, the fueled Haynes-25 capsule was ready for assembly into the intact re-entry heat source.

3. Heat Source Assembly

The capsules were assembled into the IRHS configuration at Mound Laboratory. All of the heat source components were vacuum outgassed and triple-sealed in bags in an argon atmosphere for storage and shipment from Martin Marietta Corporation to the fueling facility. The two inner bags were heat-sealed polyethylene. The outer bag was also heat sealed but was metalized to provide a vapor barrier. All components were kept in the protective atmosphere until they were passed into the inert atmosphere assembly glove box. The major steps in the heat source assembly operation were:

(1) The assembly glove box was conditioned with an inert atmosphere, and components were then moved in through a pass port.

(2) The Haynes-25 fueled capsule was placed in the ZrO_2-coated tantalum canister with the helium vent in the top position.

(3) The 0.010-inch diaphragm was pierced to allow the helium vent to become operable.

(4) The ZrO_2-coated tantalum end cap was pressed into position.

(5) The Haynes-25/tantalum canister assembly was then pressed into the male piece of the heat shield.

(6) The two halves of the ZrO_2-coated POCO heat shield were threaded together until the halves contacted the tantalum washer.

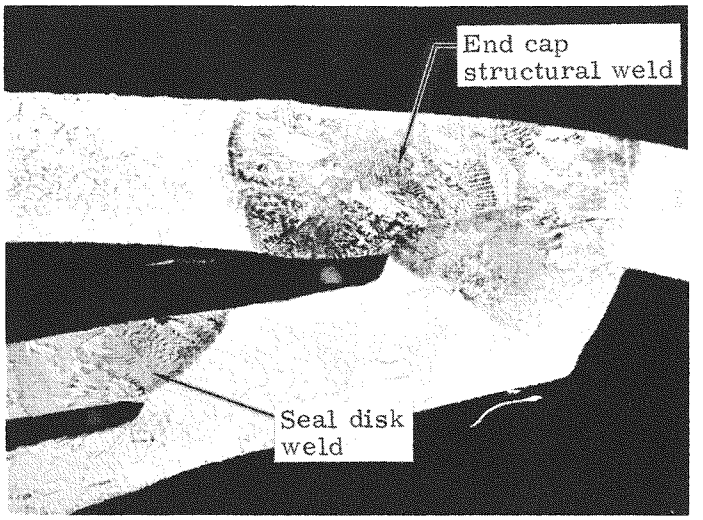

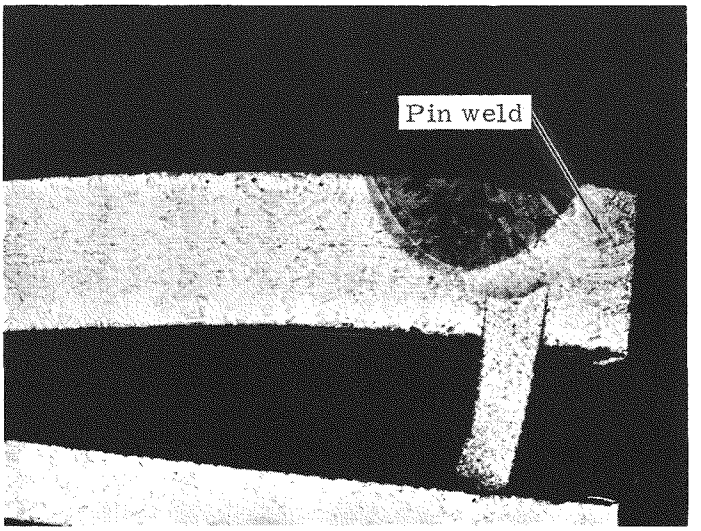

FIG. IV-11. TYPICAL METALLOGRAPHIC SECTIONS THROUGH WELD ZONE OF CAPSULE FUELING PORT (16X MAGN)

(7) The completed heat source was installed in the primary container of the shipping cask, removed from the controlled environment glove box and then installed in the body of the cask.

Some of the early fueled heat sources were assembled in a helium environment, but all of the later sources were assembled in argon so that a Veeco helium probe could be used to assure that the helium vent (filter assembly) was functioning properly. Table IV-6 presents the predicted stabilized component temperatures for the two assembly environments. Observations during the fueling operation indicate that the predictions are reasonable.

4. Compilation of Data for Fueled SNAP 19 IRHS Sources

Six Haynes-25 capsules were fueled with Pu-238 microspheres during the IRHS program. Of these, five were assembled into IRHS heat sources and delivered to the Martin Marietta Corporation for testing in thermoelectric generators. One capsule was reassembled into a new heat source configuration (no tumble-inducing chamfers on the heat shield) and delivered to Martin Marietta Corporation a second time for further testing in a generator subsystem. Table IV-7 is a compilation of data for the different fueled capsules and heat sources assembled during the program.

The original intent was that IRHS S/N 360/342 and S/N 370/376 would be tested in RTG subsystem S/N 8 and the subsystem prepared for flight. These plans proceeded to the point that flight acceptance testing was completed. Other program testing and analyses demonstrated that the Haynes-25 helium vents were becoming inoperable due to oxidation in the pores of the filter and, further, that it would be highly desirable to remove the chamfers from the heat shields.

At the conclusion of testing on the heat sources in RTG subsystem S/N 8, solution of outstanding heat source problems appeared practicable and the decision was made to specify the intact re-entry heat sources in place of the dispersal fuel capsules for SNAP 19. This decision made RTG subsystem S/N 6 available; its generators were converted to the IRHS configuration and the subsystem was designated S/N 6A. (See Volume I of this report for a description of the RTG's and the operating history.) This subsystem was used in prototype qualification testing with IRHS S/N 341/358 and S/N 370/376A.

The last two heat sources listed in Table IV-7 (S/N 361/368 and S/N 369/375) were used in flight RTG subsystem S/N 8A. The heat sources in subsystem S/N 8A contained the newly qualified platinum-plated ZrO_2 helium vent. Further, these units did not have the heat shield chamfers.

5. Diagnostic Disassembly of Prototype Qualification Heat Sources from RTG Subsystem S/N 6A

All of the fueled heat sources were disassembled, with the exception of IRHS S/N 361/368 and S/N 369/375. Only IRHS S/N 341/358 and S/N 370/376A were subjected to a diagnostic disassembly, however. Diagnostic requirements for disassembly to the component level were established by Martin Marietta Corporation, and Mound Laboratory conducted the disassembly in accordance with Mound Procedure 1-12047.

The IRHS S/N 341/358 and S/N 370/376A were prototype qualification tested as a part of SNAP 19 RTG subsystem S/N 6A. Generally, the test consisted of generator subsystem parametric tests, vibration, acceleration and thermal vacuum tests. Following the subsystem prototype qualification test, IRHS S/N 341/358 was temporarily removed from generator S/N 11A for inspection and reinstallation in the

TABLE IV-6

IRHS Component Temperatures During Assembly Operation

	Haynes-25 Surface Temperature (°F)		Surface Temperatures, Canister Assembled Over Capsule (°F)		Surface Temperatures, IRHS Assembly (°F)	
	Helium	Argon	Helium	Argon	Helium	Argon
Haynes-25 capsule temperature	990	1175	1154	1455	711	1159
Tantalum canister temperature with Haynes-25 encapsulated			1110	1260	668	918
POCO outer surface temperature with tantalum and Hanyes-25 encapsulated					620	700

Note:

All temperatures are based on assumption that the component is freely suspended in the gas environment at 70° F.

CONFIDENTIAL

TABLE IV-7

Complilation of Data for Fueled SNAP 19 IRHS Assemblies

Item	IRHS Assembly Serial Number*	POCO Graphite Heat Shield Number	Tantalum Canister Serial Number	Haynes-25 Capsule Serial Number	Measured Thermal Inventory of PuO_2 (watts)	IRHS Assembly Date	Associated RTG Subsystem Serial Number**	Associated SNAP 19 Generator Serial Number**	List of Applicable Footnotes	Disposition
1	360/342	35	11	360/342	575.8	9/2/67	8	22	1, 2, 4, 6, 8, 11	PuO_2 fuel removed from capsule and returned to Government stores.
2	370/376	40	12	370/376	591.9	9/1/67	8	23	1, 2, 4, 6, 8, 11	Capsule removed and assembled into IRHS S/N 370/376A.
3	NA	NA	NA	373/380	572.5	NA	NA	NA	1, 2, 4, 7	Fuel removed and reinstalled in capsule S/N 361/368.
4	341/358	65	35	341/358	572.7	11/20/67	6A	11A	1, 2, 4, 7, 9, 10, 11	PuO_2 fuel removed from capsule and returned to Government stores.
5	370/376A	70	44	370/376	571.9	11/30/67	6A	12A	1, 2, 4, 9, 11	PuO_2 fuel removed from capsule and returned to Government stores.
6	361/368	75	46	361/368	572.3	12/6/67	8A	22A	1, 2, 5, 8	Available for flight on Nimbus B.
7	369/375	74	40	369/375	574.6	12/5/67	8A	23A	1, 3, 5, 8	Available for flight on Nimbus B.

*The "A" designates that the fueled capsule was previously used in a different IRHS serial number.
**The "A" designates that the generator and subsystem previously existed with a different model heat source.

Footnotes

1. ZrO_2 microspheres (300 to 590 microns) used as inert filler material.
2. PuO_2 from available Government bonded inventory.
3. PuO_2 from SNAP 19 dispersal capsule No. 309.
4. Sintered Haynes-25 powder for helium vent in capsule.
5. Platinum plated ZrO_2 helium vent in the Haynes-25 capsule.
6. POCO heat shield with tumble-inducing bevels.
7. Capsule subjected to a special test at Mound Laboratory to determine if helium was flowing from the Haynes-25 helium vent.
8. Heat source subjected to flight acceptance level tests within an RTG subsystem.
9. Heat source subjected to prototype qualification tests within an RTG subsystem.
10. Heat source subjected to flight acceptance level vibration test in RTG following prototype qualification tests of the subsystem.
11. POCO heat shields returned to Martin Marietta for use in plasma arc test following IRHS disassembly.

generator; then it was subjected to flight acceptance level vibration in the three orthogonal axes. This special vibration test was conducted to demonstrate that the IRHS will survive launch loads after exposure for an extended period of time at operating temperature and to prototype qualification level testing.

Following the above tests, the two generators and the heat sources were diagnostically disassembled. The detailed results of this diagnostic disassembly are reported in Ref. IV-5.

Both heat sources were found to be in good condition. The detailed disassembly inspection indicated that the IRHS will perform the mission for which it was designed. Figure IV-12 shows three views of IRHS S/N 341/358 with the heat shield removed. A small piece of tantalum felt was diffusion-bonded to the bottom hemispherical end of the tantalum canister and pulled out from the compliant pad during disassembly. A small crack is visible in the tantalum canister located next to the tantalum felt. The one small crack in the tantalum canister is considered inconsequential, based on earlier IRHS plasma arc tests with badly cracked canisters. The tantalum canister from IRHS S/N 370/376A was completely free of cracks.

C. IRHS SHIPPING AND COMPONENT TEMPERATURES

The IRHS assembly, handling, shipping and storage requirements include all those of the dispersal system plus the necessity for:

(1) Maintaining an inert environment around the IRHS at all times to protect the hot refractory metal and graphite components.

(2) Providing the capability of sampling this nominally inert environment after shipment or long-term storage to determine whether mechanical damage or chemical reaction has resulted in an unacceptable contamination level within the shipping container.

The implications of the above requirements led to several changes in the SNAP 19 dispersal capsule shipping container. The original SNAP 19 shipping cask was an unsealed solid aluminum cask with a central cavity in which the dispersal capsule was positioned for shipment. The IRHS required a sealed shipping container which could be placed inside a controlled-environment working area (such as a drybox) for installation or removal of the heat source. The existing SNAP 19 aluminum cask was too large and heavy for practical handling in confined spaces, but did provide adequate structural protection and cooling. The approach taken was to provide a relatively small, lightweight, sealed inner container and carry it within the larger aluminum cask. During shipping or storage, this inner primary container is in the aluminum cask; fins on the cask provide for effective convective cooling and the heat source capsule temperature is maintained at about 1100° F. During IRHS handling operations at either the fueling facility or Martin Marietta Corporation, the source can be handled (or stored) in the primary container. Calculated equilibrium Haynes-25 temperature for the configuration is 1600° F, based on a stainless steel (primary container outer surface) emissivity of 0.2.

1. Shipping Container Design

The IRHS shipping cask (Fig. IV-13) is the basic SNAP 19 system cask modified by enlarging the central cavity and providing the Viton O-ring seal in the cask closure head. A segment of tube welded to the underside of the cask cover takes up the clearance between the installed primary container and the cash cover. A stainless steel-jacketed asbestos shim assembly is compressed between the tube segment and the upper surface of the primary container, providing a positive clamping force to hold the primary container relative to the aluminum cask.

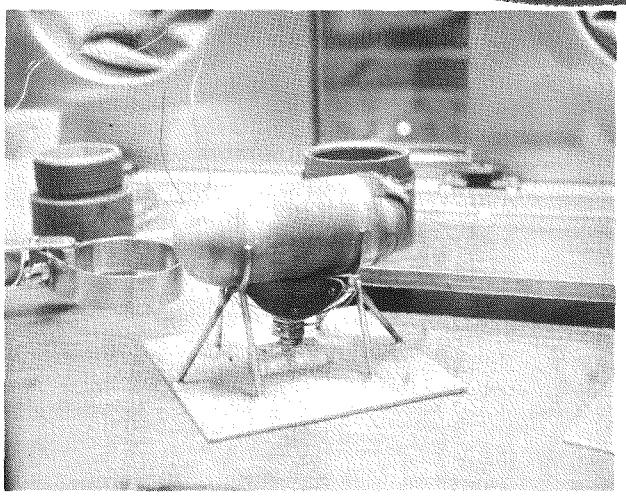

Side

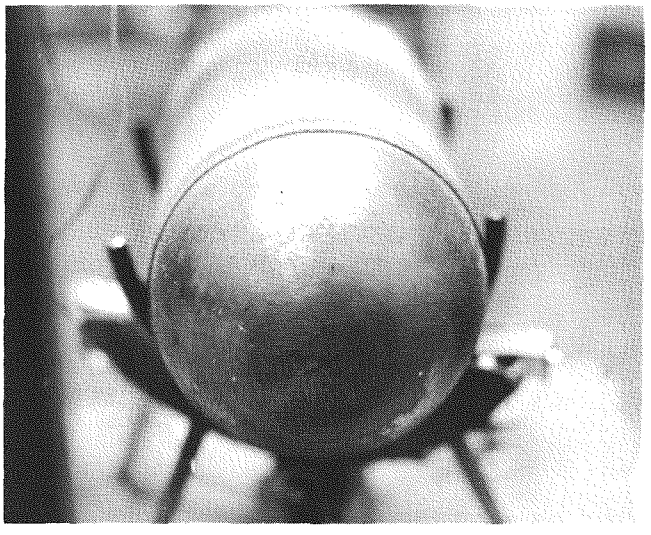

Vent End

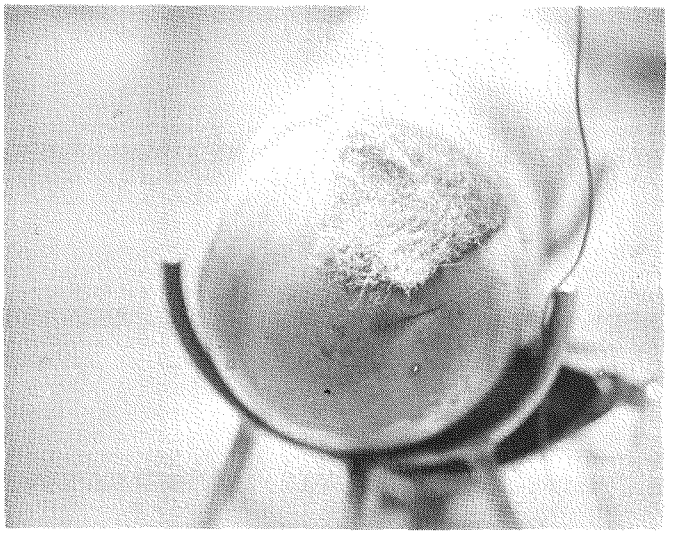

Bottom End

FIG. IV-12. UNSHIELDED HEAT SOURCE S/N 341/358, CONDITION AT DISASSEMBLY

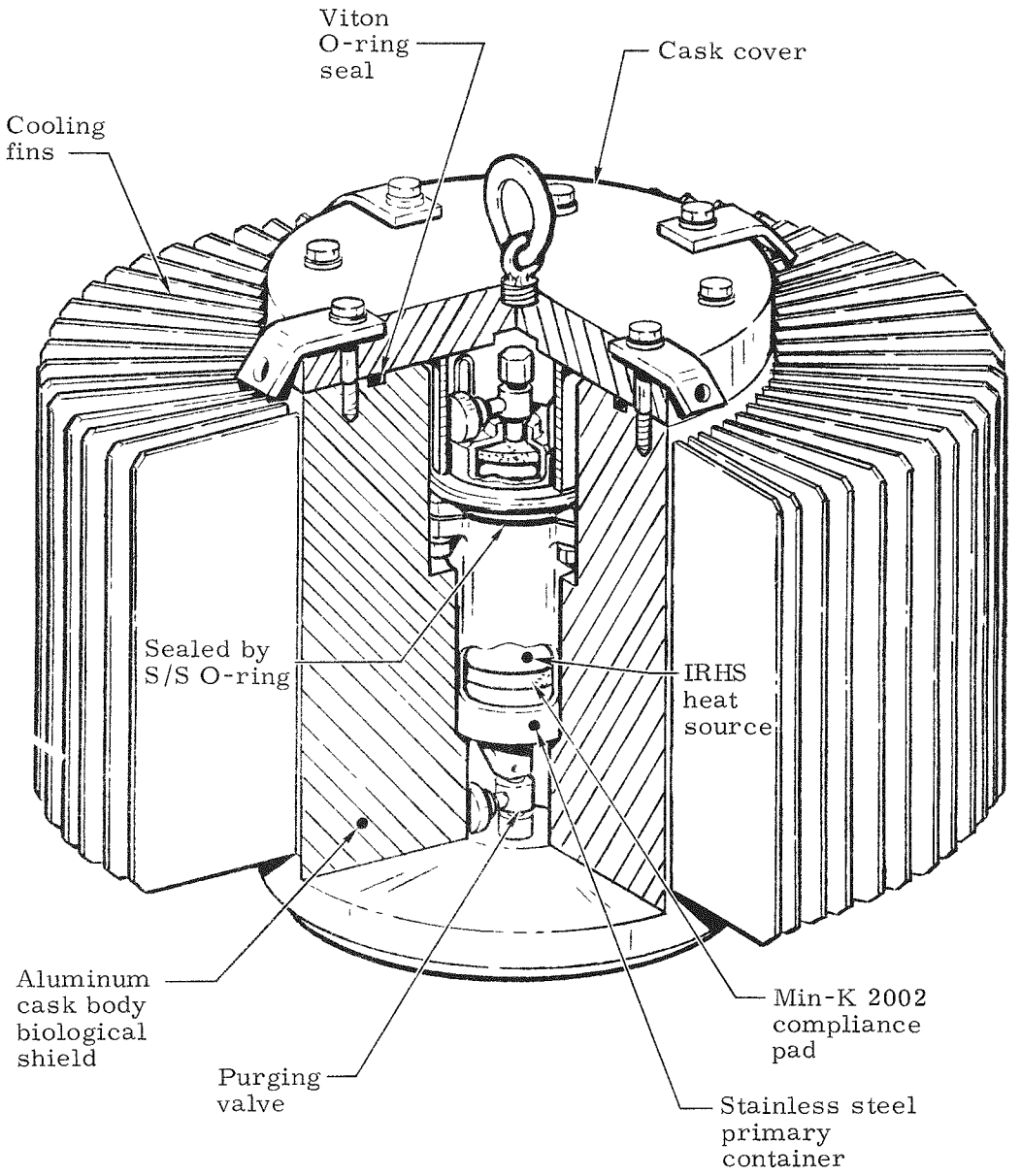

FIG. IV-13. IRHS SHIPPING CASK

The primary container is fabricated in two parts from 300 series stainless steel. The closure head is attached to the body with three bolts, and a silver-plated, metal O-ring seal is between the body and head. Valves welded into both the head and body of the primary container permit drawing a test sample of gas before opening the container at the generator fueling facility.

Min-K 2002 pads in the container ends support the IRHS during shipping and serve as shock absorbers.

2. IRHS Installation into Shipping Cask

Within an argon-filled drybox, the primary container closure head is positioned in a holding fixture and a Min-K pad is installed in the head. The IRHS assembly is lowered, filter end first (identified as a dimple in the graphite end surface), into the closure cap.

After cleaning the O-ring groove in the cap, if necessary, the metal O-ring is lowered into the groove in the cap, and the remaining Min-K pad is placed on the protruding end of the IRHS. The primary container body is lowered over the IRHS until it rests on the Min-K pad. The alloy steel bolts are inserted and tightened, compressing both the metal O-ring and the Min-K pads on the ends of the IRHS. Purging valves are checked to assure that they are closed, and the primary container is removed from the drybox in preparation for insertion into the aluminum shipping cask.

The cask body is purged with argon; then the primary container is lowered into the cask. The asbestos shim assembly is installed so that it rests on the primary container bolting lugs. With the argon purging line left in the cask, the cask cover is lowered into place. After several more minutes of purging, the argon line is removed and the cask cover bolts are tightened, completing the assembly.

3. Thermal Analysis

A thorough study of IRHS component and shipping container temperatures was completed to establish that the necessary heat rejection could be accomplished in all configurations of storage and handling. Selected results of this analysis are summarized here; Ref. IV-3 is a detailed report.

Table IV-8 presents the predicted component equilibrium temperatures associated with three storage situations.

---

* IRHS in primary shipping container, and container in air-cooled, finned cask. Both cask and container argon-filled.

** IRHS in helium-filled primary container, and container in large-volume helium atmosphere.

*** IRHS in argon-filled primary container, and container in air environment

TABLE IV-8

Equilibrium Storage Temperatures of the IRHS (70° F Ambient)

Component	Temperature (° F) Argon*	Helium**	Argon***
Cask fin root	90	--	--
Primary shipping container (outer wall)	194	782	1002
Heat shield	509	824	1252
Tantalum canister	795	873	1446
Haynes capsule	1110	917	1617

A significant difference in capsule temperatures exists between storage in the fully assembled cask configuration and storage of the primary container cooled directly by argon or helium.

4. Radioactive Gaseous Effluent Considerations

Inasmuch as the IRHS design employs a filtered venting provision to preclude a pressure buildup from helium, it must be presumed that radioactive gaseous effluents can also be released. Such radioactive effluents were, in fact, detected during incoming inspection of heat sources for generator subsystem S/N 8A. With the heat sources still in the primary shipping containers, a flow of argon gas through the containers swept out detectable quantities of radioactive gases. Quantitative experimental data regarding effluent release mechanisms and characteristics and amounts of effluent are not available. However, source terms were determined analytically for both isotopic decay products and fission products.

Source term calculations show that Rn-220 is the principal radioactive effluent for inventories accumulated in excess of six months. For inventories accumulated for less than six months, the fission products, particularly I-131, are the controlling effluents. Subsequently, the potential consequences of both a postulated continuous release or of an instantaneous release of accumulated products were evaluated for representative environments in terms of maximum concentrations. These maximum hypothetical concentrations were compared to maximum permissible concentrations (MPC) established by AEC regulations for each nuclide.

Concentration calculations of hypothetical releases of all accumulated radon and fission products (assuming a perfectly sealed generator housing) indicate that MPC levels can be achieved in the case of an instantaneous release into a stagnant volume. But, since the generator seals have a finite permeability, it can be concluded that a continuous leak will occur rather than an instantaneous release of large inventories. A continuous release of small quantities would be readily dissipated as a result of both the generally short half-lives of the effluents and the effect of natural or mechanical ventilation.

The operational safety evaluation indicated that no handling constraints in excess of the normal handling procedures already established would be necessary. A more complete discussion of this subject is in Ref.

D. DEVELOPMENT AND QUALIFICATION TESTS

The development and qualification of the IRHS were accomplished through the coordinated test effort of the AEC, Sandia Corporation, Mound Laboratory of Monsanto Research Corporation, Los Alamos Scientific Laboratories (LASL) and Martin Marietta Corporation. These tests were divided into the categories of materials test specimens, heat source components, full-scale dummy heat sources and fueled heat sources. A summary discussion of the tests leading to a qualified heat source follows.

1. IRHS Impact and Drop Tests

a. Impact

Impact testing of 15 intact re-entry heat source assemblies began with the testing of four developmental impact specimens at the Martin Marietta Corporation. The specimens (S/N 101, 102, 103 and 104) were heated and impacted against a granite target at a nominal velocity of 260 ft/sec. Pertinent data are presented in Table IV-9. Two of the capsules used in these units were fabricated from short-drawn cups welded to a cylindrical center section, and two were fabricated from half-capsule cups machined from bar stock and joined with a single weld. The dimensions of these specimens were representative of the final configuration. All specimens were enclosed in POCO-graphite heat shields of right circular cylinder form.

Following selection of the capsule design incorporating a mid-section weld (in addition to the filler cap and filter assembly), 11 additional specimens (S/N series 200 and 500) were enclosed in heat shields and impacted at various angles against granite targets. The heat shield geometry was varied on several tests to include chamfers on the ends (see Table IV-9).

Test specimens (S/N 501 and 502), loaded with fuel simulant and closures welded at Mound Laboratory) were impacted on the end containing the filling port to verify integrity of the closure. The flight configuration impact specimens (S/N 208 and 209, containing ZrO_2 filters) were impacted on the filter end. The filter was then subjected to helium flow and particle retention tests to assure acceptability.

Capsule deformation resulting from impact is illustrated in Figs. IV-14 and IV-15. The impact angle shown in the figures is measured between the longitudinal axis (filter end forward) and the line of flight. Thus, an angle of 152° is equal to an impact at a 28° angle on the end opposite the filter assembly. The holes in the wall are the result of post-impact rework to conduct leak checks.

Post-test examination of each specimen disclosed no leaks in the capsule walls or weld areas. Flow checks and particle retention tests on the filter assemblies following impact indicated that impact did not compromise functioning of the element. In every impact test, the heat shield assembly was completely shattered and separated from the capsule at impact. The relatively low-energy secondary impact of the bare capsules against ground, facility structure or concrete ramp did not cause significant damage to the capsule.

The data from the tests indicate that impact, under conditions as bad as the test conditions, will not compromise the capability of the capsule to contain the fuel particles.

TABLE IV-9

IRHS Assembly Impact Test Data

Impact Test Conditions

Date (1967)	Specimen Serial No.	Velocity (ft/sec)	Angle* (deg)	Temperature (°F)	Remarks
5-27	101 ▲	259	36	1070	(1) Surface crack ~0.020 inch deep
5-31	102	262	29	1038	(1)
6-1	103	261	27	1034	(1)
6-1	104	258	22	1043	(1)
6-7	201 ▲	258	25	1013	(1, 3)
7-13	202 ■	258	45	983	(1, 2) Microcrack in fill end weld
7-12	203	257	48	987	(1, 3) Microcrack in fill end weld
7-13	204	253	28	1003	(1, 2) Microcrack filter end weld
7-13	205	255	13	1005	(1, 3)
7-12	206 ■	257	47	963	(1, 2)
8-2	501 ▲	258	9	1004	(1, 2) Mound Laboratory welded fill port closures
8-3	502	259	24	980	(1, 2) Mound Laboratory welded fill port closures
8-28	207	261	2	1032	(1, 3) Aged 100 hr in argon at 1470° F
11-20	208	241	8	1010	(1, 3)
11-20	209 ▲	257	21	1015	(1, 3)

Notes:

*Angle measured between longitudinal axis of capsule and line of flight

▲ Right circular cylinder heat shield

■ Chamfered heat shield

(1) No detectable He leaks following impact
(2) Impacted on fill end
(3) Impacted on filter end

IRHS 202 145° | IRHS 203 48° | IRHS 204 152° | IRHS 205 13° | IRHS 206 143°

FIG IV 14 IRHS CAPSULE IMPACT SPECIMENS

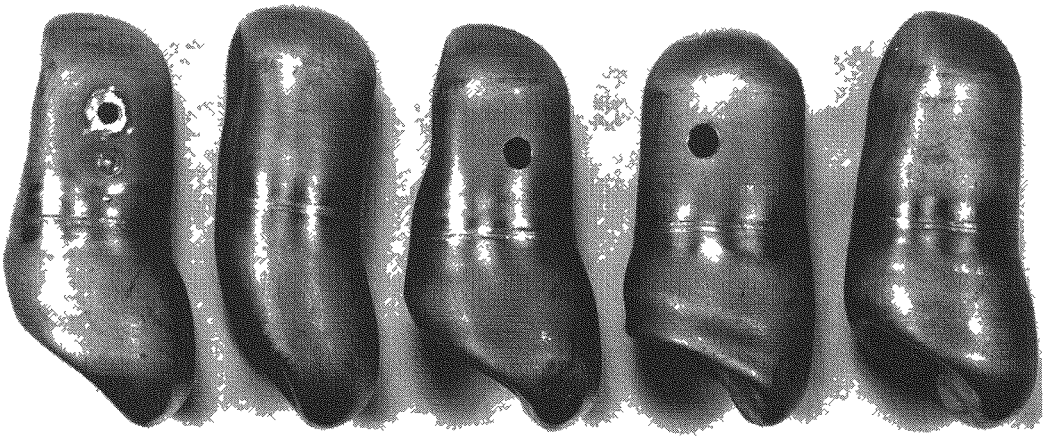

FIG IV-15 IRHS CAPSULE IMPACT SPECIMENS (ROTATED 90° FROM FIG IV-14)

b. Drop test

The objective of the four drop tests was to obtain data on the availability of fuel for resuspension after re-entry impact and to obtain correlation data or predicted impact velocities. All drops were made from a mile above the terrain at the Sandia Corporation Tonapah Test Range. One complete test specimen was subjected to the simulated orbital decay re-entry thermal environment in the Martin Marietta plasma arc facility prior to drop testing. The three other specimens consisted of a graphite heat shield housing, a tantalum canister and tungsten-molybdenum powder (fuel weight simulant).

Two units were impacted on a dry lake bed with no dispersion of the simulated fuel (Fig. IV-16). (One of these units had previously been tested in the plasma arc.) Two other heat sources were impacted (Fig. IV-17) on hard ground to determine the effect of a harder impact medium. The maximum visible dispersion of simulated fuel was approximately 10 feet from one capsule and approximately 7 feet from the other.

The two heat sources dropped on hard ground had a greater dispersion of the heat source components and fragments than the two that were dropped on the dry lake bed. Each of the two dummy intact re-entry heat sources formed a crater approximately 1 foot in diameter and 3 inches deep. The body of one of the tantalum canisters was located approximately 2 feet from the impact crater and the other was 12 feet from the crater. The distances of the two canister caps from the crater were more consistent, measuring 7 feet and 10 feet. Numerous pieces of POCO graphite were found around the impact area. The farthest piece was generally in the line of plane flight and was located approximately 33 feet from the impact point.

The third drop test (No. 343-22, plasma-arc sample 2A-14) was on a dry lake bed. There was no visible dispersion of the fuel simulant. The graphite heat shield cracked and dispersed but most of the graphite remained in the impact crater. The farthest piece of graphite was about one foot from the crater (see Fig. IV-16). The maximum depth of the crater was 3 inches after the capsule was removed from the cavity. The tantalum canister crumbled as it was being removed from the crater.

The last drop (Sandia test 343-23, capsule S/N 29) was on a dry lake bed. There was no dispersion of simulated fuel, as the tantalum canister was still intact. Even though somewhat flattened, the cap was still on the canister body. The capsule penetrated the lake bed about 3 inches. All heat source parts stayed in the crater with the exception of a few pieces of graphite.

The heat sources that were dropped were noted to tumble, roll and perform various gyrations following release. These motions were most likely caused by the chamfers originally incorporated in the heat shield design. One of the heat sources was tracked by radar during the free fall, and earth impact velocity was measured at 340 ft/sec. This value is a little less than the calculated impact velocity for these conditions as noted in Table IV-10.

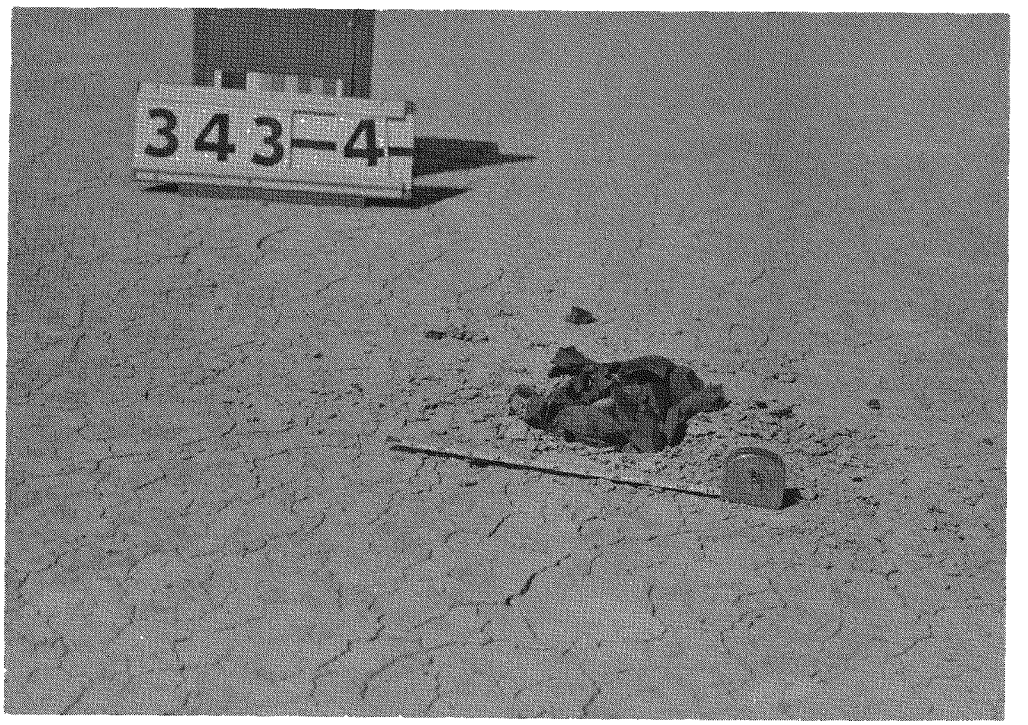

FIG. IV-16. RESULTS OF IRHS DROP TEST ON DRY LAKE BED--NO DISPERSION OF SIMULATED FUEL

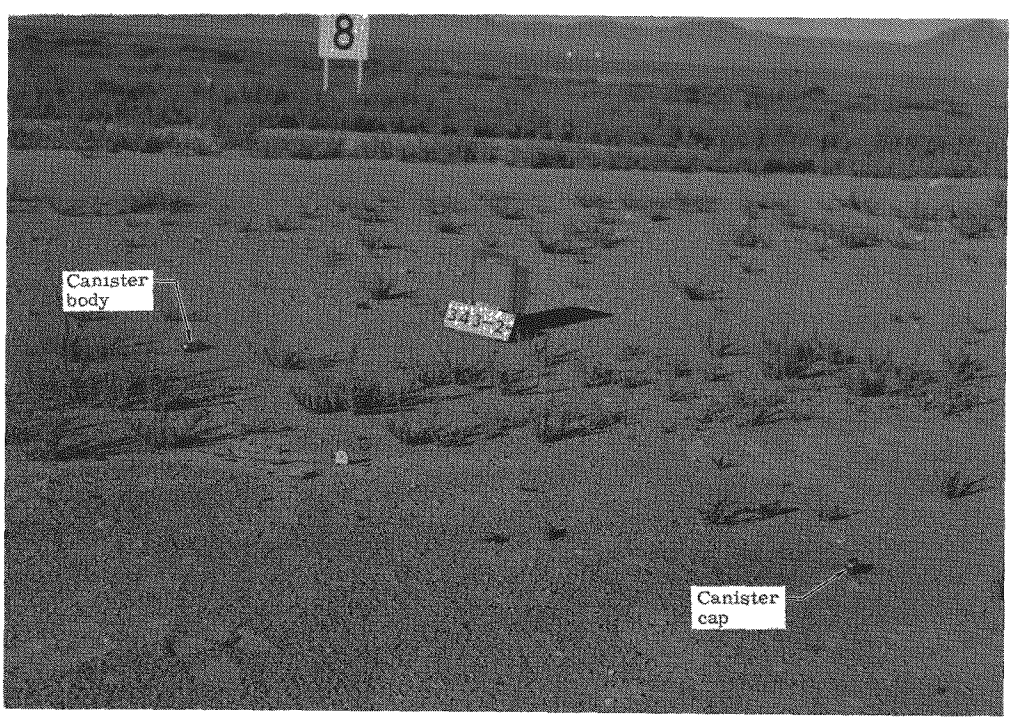

FIG. IV-17. COMPONENTS FROM IRHS DROP TEST ON HARD SOIL

TABLE IV-10

Calculated Impact, Terminal and Equilibrium Velocities of SNAP 19 IRHS

Impact Altitude (ft)	IRHS Orientation	Impact Velocity (H_o = 10,000 ft) (fps)	H_o to achieve Terminal Velocity (ft)	Terminal Velocity (fps)	Equilibrium Velocity (fps)
5300	Side-on,	360	30,000	490	470
	tumbling	390	25,000	465	445
Sea level	Side-on,	434	22,000	450	435
	tumbling	417	20,000	427	410

2. Chemical Reaction Barrier System Tests

Material compatibility tests for the IRHS were conducted at Martin Marietta and Mound Laboratory to evaluate the components of the heat source assembly and to demonstrate that these components do not preclude, from a chemical compatibility standpoint, the intact re-entry of the heat source.

Zirconium oxide (ZrO_2) was selected for the IRHS as a nonwetting barrier to prevent contact of the PuO_2 microspheres with the graphite heat shield during re-entry.

Significant characteristics of the IRHS with respect to the barrier configuration are as follows:

(1) PuO_2 microspheres are contained in a Haynes-25 capsule (nominal 50-mil wall).

(2) A 10-mil tantalum canister surrounds the Haynes-25 capsule. The canister is internally coated with a composite 5-mil layer of zirconium oxide and tantalum substrate to provide a nonwetting barrier to molten Haynes-25.

(3) A 0.4-inch-thick POCO-AXM-5Q graphite heat shield surrounds the tantalum canister and Haynes-25 capsule. The graphite is internally coated with a composite 12-mil layer of zirconium oxide on substrates of zirconium oxide/tantalum, molybdenum and tantalum.

Compatibility tests at Martin Marietta were conducted at temperature profiles (simulating re-entry) that resulted in the Haynes-25 being above the solidus temperature for more than 350 seconds. Peak Haynes-25 temperatures achieved during the tests were approximately 3400° F.

Compatibility test configurations (simulating the final design configuration) and the results of the tests performed at Martin Marietta are summarized in Table IV-11. Test configurations and results of the tests performed at Mound Laboratory are summarized in Table IV-12.

Following development of the barrier system with the crucibles, a total of 12 non-instrumented intact re-entry heat sources were subjected to plasma arc tests simulating various re-entry condition. (See listed models between serial numbers 35 and 60 in Table IV-13 for test conditions and configurations.) Five of the heat source specimens were tested in a side-on, spinning mode and six other models were tested in a side-on, no-spin mode. One model (S/N 54) was subjected to both modes of re-entry for the full duration of each. There was no evidence of molten Haynes-25 escaping from any of the models.

TABLE IV-11

Development Martin Marietta Chemical Barrier System
Test Configurations and Results

Capsule Test Number	POCO Graphite Crucible	Tantalum Cup	Haynes-25 Configuration	Other Metals Tested	Penetration into POCO Graphite
X	ZrO_2 coated	ZrO_2 coated	Sleeve	None	None*
R	ZrO_2 coated	Uncoated	Sleeve	None	None
G	ZrO_2 coated	Uncoated	Sleeve	None	None
A-1	ZrO_2 coated	None	Cup	Tantalum felt pad	None
B-1	ZrO_2 coated	None	Cup	Nickel alloy felt pad	None

*Tantalum canister remained intact. No reaction between Haynes-25 and tantalum canister. Slight reaction zone between exterior tantalum canister and zirconium oxide coating on POCO graphite crucible.

TABLE IV-12

Chemical Barrier System Test Configurations and Results
Conducted at Mound Laboratory

Capsule Test Number	POCO Graphite Crucible	Tantalum Cup	Haynes-25 Sleeve	Pu-238 O_2 Microspheres	Penetration or Reaction
1	ZrO_2 coated	ZrO_2 coated	Yes	None	None
2	ZrO_2 coated	ZrO_2 coated	Yes	8 grams production grade	None
3	ZrO_2 coated	ZrO_2 coated	Yes	8 grams production grade	None

TABLE IV-13

Summary of IRHS Plasma Arc Test Configurations

Phase I Test Models

Test Model Serial Number***	Trajectory Simulated	Flight Motion Simulated	Test rpm	Capsule Pressure and Type* (atm)	Remarks
1	Agena II abort case No. 17	Side-on, stable	0	Vented dummy	10 thermocouples
2	Orbital decay	Side-on, spinning	20	Vented dummy	10 thermocouples
3	Orbital decay	Side-on, spinning	20	Vented dummy	10 thermocouples
5	Orbital decay	Side-on, spinning	20	Vented dummy	10 thermocouples
6	Orbital decay	Side-on, spinning	20	Vented dummy	10 thermocouples
7	Orbital decay	Spinning and tumbling	20	Vented dummy	9 thermocouples
8	Orbital decay	Spinning and tub	20	Vented dummy	9 thermocouples
9A	Orbital decay	End-on	0	Vented dummy	9 thermocouples
10A	Orbital decay	End-on	0	Vented dummy	9 thermocouples
1A-15	Orbital decay	Side-on, spinning	20	1.0 (air) prototype	No thermocouples. All contained uncoated tantalum canisters. Model 2A-14 used in drop test at Sandia. Other two sectioned for study of Haynes containment.
2A-14	Orbital decay	Side-on, spinning	20	1.0 (air) prototype	
3A-17	Orbital decay	Side-on, spinning	20	1.0 (air) prototype	All filled with tungsten-molybdenum powder for weight simulant

*Dummy--Refers to a capsule which was not manufactured with a helium filter or a standard fueling port.

Prototype--Refers to capsules with the above mentioned parts. The helium filter, in all cases had been welded closed to allow pressurization.

All specimens contained ZrO_2 fuel simulant except 1A-15, 2A-14 and 3A-17.

TABLE IV-13 (continued)

Phase II Test Models

Test Model Serial Number	Trajectory Simulated	Flight Motion Simulated	Test rpm	Capsule Pressure and Type* (atm)	Remarks
53	Orbital decay	Side-on, stable	0	Vented dummy	No thermocouples
54	Orbital decay	Side-on, spinning	20	1.0 (air) prototype	No thermocouples
54R	Orbital decay	Side-on,** stable	0	1.0 (air) prototype	No thermocouples
55	Orbital decay	Side-on, stable	0	Vented dummy	No thermocouples
56	Orbital decay	Side-on, stable	20	1.0 (air) prototype	No thermocouples
57	Orbital decay	Side-on, spinning	20	8.5 (helium) prototype	No thermocouples. All capsules pressurized with 125 psi of helium to simulate block filter element.
58	Orbital decay	Side-on, spinning	20	8.5 (helium) prototype	
59	Orbital decay	Side-on, spinning	20	8.5 (helium) prototype	
60	Orbital decay	Side-on, spinning	20	8.5 (helium) prototype	
40	Orbital decay	Side-on, stable	0	1.0 (argon) prototype	No thermocouples. From RTG subsystem 8 design verification.
65	Orbital decay	Side-on, stable	0	1.0 (argon) prototype	No thermocouples. From RTG subsystem 6A design verification.
35	Agena I abort case No. 11	Side-on, stable	0	1.0 (argon) prototype	No thermocouples. From RTG subsystem 8 design verification.
70	Agena I abort case No. 11	Side-on, stable	0	1.0 (argon) prototype	No thermocouples. From RTG subsystem 6A design verification.

*** All models contained ZrO_2 coated tantalum canisters and tantalum felt compliance pads.

** Retested; previous test resulted in 0.043-inch recession of heat shield.

Three other models listed in the table (1A-15, 2A-14, and 3A-17) showed similar results. However, the tantalum canister was not coated with ZrO_2 and the fuel simulant was tungsten-molybdenum powder rather than ZrO_2 powder. The ZrO_2 powder is a thermal simulant for the fuel and the tungsten-molybdenum powder is a weight simulant.

In some cases, the ten instrumented plasma arc specimens listed in Table IV-13 did not release Haynes-25, but none are claimed as evidence of containment, since there were penetrations into the inner cavity.

3. Aerodynamic Tests

A series of static and dynamic aerodynamic tests were performed on the various chamfered and unchamfered SNAP 19 IRHS configurations. Initially, static hypersonic aerodynamic coefficients were measured for the 29%-180° * chamfered IRHS. Later in the SNAP 19 IRHS program, a series of free-flight tests were performed at Arnold Engineering Development Center (AEDC) VKF Tunnel B to determine pitch damping coefficients using the film data. In addition, the Sandia Corporation performed a series of one-degree-of-freedom hypersonic tests at their facility. The latter tests were used to investigate the autorotation capability of the various IRHS designs.

a. Hypersonic static coefficient test

For many configurations, Newtonian theory is reasonably accurate in predicting the aerodynamic force coefficients, but not as acceptable for predicting the aerodynamic moment coefficients. Because the original IRHS configuration with the 29%-180° chamfers is unique insofar as re-entry bodies are concerned, the validity of the Newtonian estimates could be determined only by conducting a wind tunnel test program to obtain static aerodynamic, force and moment coefficients and comparing these with the theoretical coefficients. An abbreviated test program of 46 data points provided a series of spot checks on the theoretical estimates.

The test was conducted in the Martin Marietta Hot Shot Tunnel. Three coefficients (normal and axial force and pitching moment) were obtained at roll angles of 0°, 30°, 60° and 90°. The test was conducted at a Mach number of 20 and a Reynolds number of 154,400.

The experimental results of this test have, in general, shown good agreement with the Newtonian predictions for the static forces. The normal force coefficient shows excellent agreement with the Newtonian predictions throughout the angle of attack range (0° to 180°).

b. Free-flight tests

A series of hypersonic free-flight tests were made in Tunnel B at Arnold Engineering Development Center (AEDC) by the Martin Marietta Corporation in cooperation with the Sandia Corporation. The purpose of the tests was to obtain motion histories so that pitch damping coefficients could be deduced. Tunnel B is a 50-inch hypersonic tunnel which operates continually over a range of pressure levels. For damping data, models are launched upstream with a pneumatic launcher. Aerodynamic data were obtained by analysis of high-speed films.

---

* 45° chamfers that consumed 29% of the projected diameter end area, and located at 180° from each other on opposite ends of the IRHS.

Thirteen free-flight models were launched and 10 of these flights yielded useful data. The models were constructed of styrofoam with a tantalum slug inside. They were painted white with black vertical and horizontal stripes to enable visual detection of rolling motion about the longitudinal axis. The models were 42% scale size; the mass and moments of inertia were not scaled. Care was taken to ensure that the mass-to-pitch moment of inertia ratio was large so that the maximum number of oscillations during flight could be obtained. The models weighed approximately 0.3 pound and their pitch moment of inertia was 0.042 lb/in^2. Three types of cylindrical models were tested: unchamfered, 29%-180° chamfered and 29%-90° chamfered. The chamfers on the 180° chamfered configuration were parallel and those on the 90° configuration were perpendicular to each other. These three configurations were launched with end-on, side-on and tumbling initial orientations.

The motions of these configurations were recorded by high-speed photography. Two cameras viewed the flight plane from the side, and a third viewed down from the top of the tunnel test section.

c. Hypersonic one-degree-of-freedom tests

The Sandia Corporation performed a series of hypersonic one-degree-of-freedom tests to investigate the autorotation of various SNAP 19 IRHS configurations.

The models were mounted in the yoke assembly. Shielded ball bearings within the models allowed the models to rotate about a diameter through their geometric centers. The models were not balanced before testing but, because of symmetrical construction and close-tolerance fabrication, they seemed to be in a good state of balance.

The models contained two small magnets and a Hall gage, which together produced an electrical signal that was recorded on 6-inch self-developing tape in a Visicorder. This record enabled the spin rate of the capsules to be measured as a function of time.

Four SNAP 19 configurations, a cylinder and cylinders with 15%, 30% and 45%-180° chamfers, were the principal models tested. The SNAP 19 models were approximately 50% geometric scale. Moments of inertia were not scaled.

It was apparent from these tests that:

(1) The rate of rotation increases as the percentage of chamfer increases.

(2) The tip speed ratio decreases between the subsonic and hypersonic regimes.

(3) The rate of rotation increases with increasing dynamic pressure.

Based on the AEDC free-flight tests and Sandia hypersonic one-degree-of-freedom tests, it was concluded that the 45° chamfer area on the heat shield should be reduced of, if possible, eliminated to reduce the heat shield tip speed which could be caused by autorotation during re-entry. The maximum rotational speed is highly dependent on damping, but the damping coefficients were not well known for the re-entry conditions. Following successful plasma arc tests in the side-on stable mode (see Section D.4) it was decided to remove the chamfers from the heat shield. These conservative plasma tests showed that the heat shield will survive re-entry even if there is no spin or tumbling motion to the heat shield.

For most re-entry trajectories, the unchamfered IRHS will probably re-enter side-on with some oscillations. As recession of the heat shield takes place along the stagnation line, some rotation about the axial centerline should be imparted. If the IRHS has an initial orientation of end-on with a finite roll rate (<5 radians/second), the end-on orientation could be retained throughout the re-entry trajectory.

4. IRHS Simulated Re-entry Tests

Development and qualification of the IRHS required extensive testing in a simulated re-entry environment to determine the thermal response of the heat source components, to correlate response levels with predictions, and to verify the integrity of the heat shield when subjected to the environmental extremes of re-entry. To this end, 24 full-scale IRHS models were manufactured and tested. Nine of the IRHS assemblies were instrumented with thermocouples to measure the thermal response of the heat source components and the remaining 15 were uninstrumented in order to be more representative of the flight heat sources.

a. Technical approach

The re-entry environment of the IRHS can be best simulated in the plasma arc facility, also known as the hyperthermal wind tunnel. Re-entry conditions are simulated by passing an electric arc through a gas flow of synthetic air and expanding the heated gas to hypersonic velocity by means of a contoured nozzle. The test models were placed in the flow, and their interaction with the flow produced the simulated re-entry environments.

The response of these test models to the plasma environment was measured by thermocouples to determine internal temperature distributions, pyrometers to determine peak surface temperatures and physical measurements of the models before and after test to determine surface recession.

To check the accuracy of the computer programs used for the response analysis, a mathematical computer simulation of the test model was devised. The temperature and surface recession response of the computer test models was then compared with that of the actual test models. A good correlation of the results meant that the computer program was accurate in predicting the thermal response of the test models and, by analogy, would accurately predict the response of an IRHS undergoing re-entry.

b. Apparatus

The Martin Marietta Corporation plasma arc facility was used to produce the thermal environments used in these tests. Equipped with an F-5000 plasma arc generator made by Thermal Dynamics Corporation, a 10-inch exit diameter supersonic nozzle, and employing the chemical equivalent of air as the test medium, the facility produced stagnation point heat fluxes on the cylindrical side of the IRHS calibration model ranging from 30 to approximately 385 Btu/ft^2-sec within a 7- to 10-inch flow diameter.

To hold and rotate the full-scale IRHS models during test, a spin rig was designed and manufactured by the Martin Marietta Corporation. It allowed for the single-axis rotation of the models about the support stud and the passage of instrumentation wiring from the models to the data acquisition equipment.

The plasma environment was calibrated with the aid of a water-cooled pitot pressure probe and a custom-designed, full-scale model water-cooled calorimeter equipped with Gardon steady-state heat flux gages. These gages were located to measure both the stagnation point heat fluxes and the heat flux distribution around the body.

One optical pyrometer and one total radiation pyrometer were employed to obtain model surface temperatures.

All output from the calibration probes, the model instrumentation, etc., was recorded redundantly on Bristol millivolt chart recorders and a SYSTRAC data acquisition system employing magnetic tape output which is suitable, with computer conversion, for use with automatic curve plotting devices.

c. Models

The 24 models used in this test series were full-scale simulations of the contemporary IRHS design. Table IV-13 presents a summary of the configurations subjected to plasma arc tests during the development and qualification program. The Phase I (Table IV-13) models include instrumented specimens which were used to determine component response and validate the computer code, and three noninstrumented early developmental specimens which are not fully representative of the final design in the area of compatibility barriers. Phase II models contained no instrumentation and consisted of heat shields, barrier systems and compliant pad supports that were representative of the designed flight system. Phase II test specimens are considered design verification models. The differences between the plasma test models and the fueled flight configuration are enumerated below:

(1) In all the aerothermal test models, the presence of the plutonium dioxide fuel was simulated by zirconium dioxide powder. Three other models (A-15, 2A-14 and 3A-17) were designed and fabricated for impacting at high velocity after experiencing a simulated re-entry in the plasma arc facility (plasma-impact models). The fuel simulant in these models was a mixture of molybdenum and tungsten powders for weight simulation.

(2) All test models were manufactured with, or reworked for the addition of, a stud for support during test. The design of this stud varied for different flight motion simulations (side-on, end-on, etc.) during the Phase I tests. The stud design was later improved to decrease the amount of heat loss from the model to the water-cooled spin rig. A specially designed stud adapter was necessary for testing of defueled flight assemblies (from RTG subsystems 6A and 8).

(3) All Phase I aerothermal test models (not including the plasma-impact models) were instrumented with tungsten-5% rhenium/tungsten-26% rhenium thermocouples. Some were located to determine the peak temperature histories of the heat shield, capsule and fuel simulant centerline. The other thermocouples were located so that axial and concentric temperature gradients in the model could be determined. One model configuration used during Phase I is shown in Fig. IV-18. (See Ref. IV-1 for other configurations used.)

(4) The Phase I aerothermal test models were manufactured before the tantalum canister was incorporated in the IRHS flight design. Therefore, these models did not contain tantalum canisters at the time of test; they also had penetrations through the ZrO_2 coating in the heat shield.

(5) Due to the passage of thermocouple lead wires, the mid-line joints of the Phase I aerothermal test models had to be converted from screw joints to graphite bonded lap joints. Compromise in ZrO_2 coating was necessary to allow assembly.

(6) Since the main emphasis in those tests following the 10 instrumented models was on the strength and thermal response of the heat shield, some of the models were assembled with dummy capsules which did not have the standard fueling port or helium filter assembly.

The three types of heat shield support studs employed in Phase II test models are shown in Fig. IV-19. The side-on spinning test models (Table IV-13) employed the solid support. When the side-on stable plasma tests were conducted to evaluate

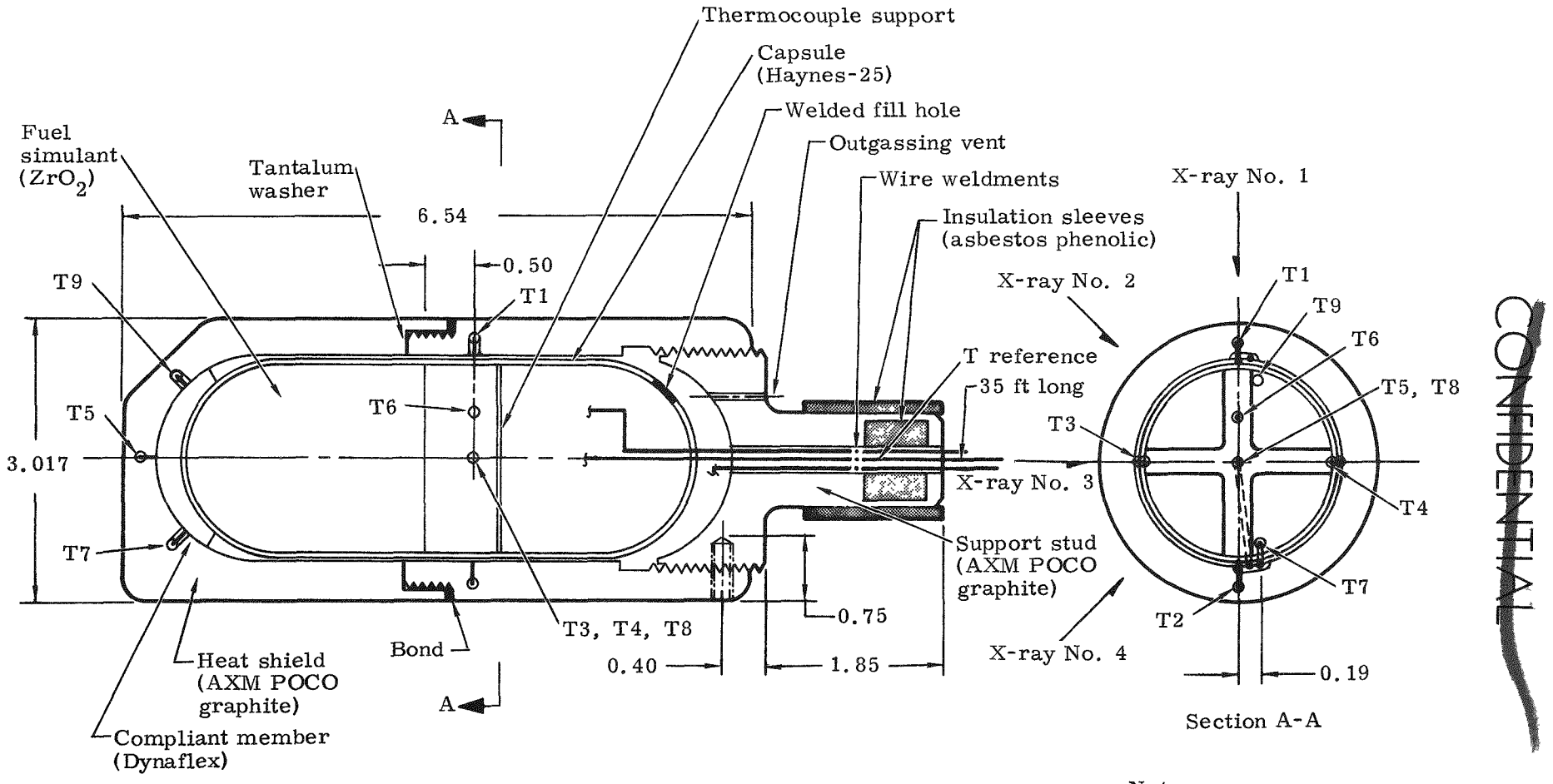

Note:

T1 denotes thermocouple No. 1, etc. All dimensions in inches.

FIG. IV-18. PLASMA-ARC SIDE-ON SPIN DESIGN ASSEMBLY

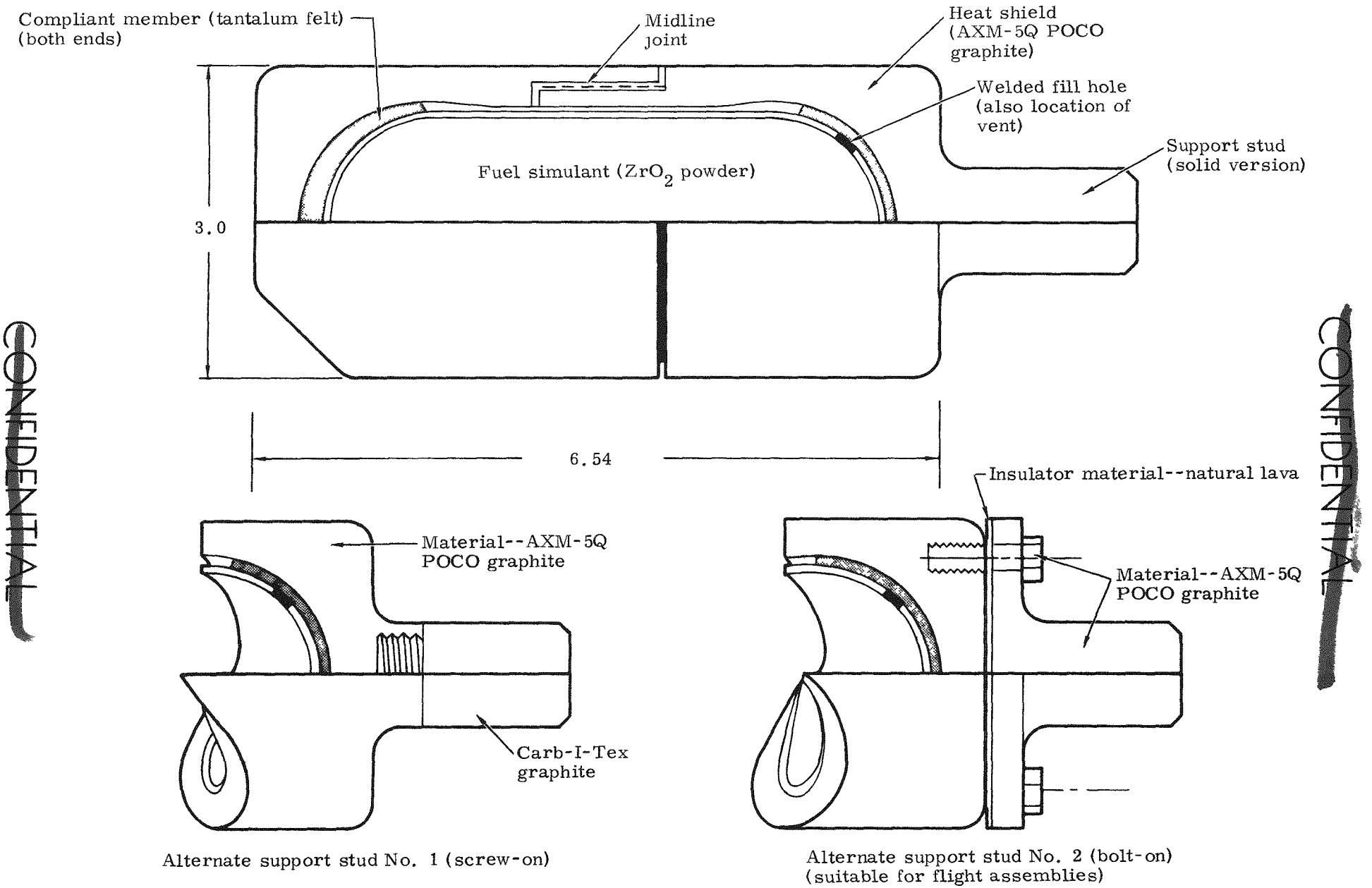

FIG. IV-19. PHASE II PLASMA-ARC TEST MODEL AND SUPPORT STUD DESIGNS

the feasibility of removing the chamfers from the heat shield (Models 53, 54R and 55), the solid support stud was modified with a piece of Carb-I-Tex graphite (Carborundum Graphite Products Division) to reduce the heat loss from the end of the specimen. The side-on stable design verification models (S/N 40, 65, 35 and 70) required a special adapter design (as noted in Fig. IV-19) since the heat shields and tantalum support pads had been previously used in Pu-238-fueled IRHS assemblies and subjected to thermal vacuum and dynamic tests in RTG subsystems 6A and 8.

d. Test conditions

The Martin Marietta plasma arc facility environmental conditions were changed in four discrete steps during each test. Before testing began, values of stagnation point heat flux, stream enthalpy, stagnation pressure and step timing were chosen to best simulate the re-entry environment being investigated. These chosen values were sometimes not within the performance envelope of the plasma arc facility. When this occurred, the following priority was followed:

(1) Stagnation point heat flux

(2) Stream enthalpy

(3) Stagnation point pressure.

Step timing could be continuously controlled.

A heat flux survey of the plasma stream is shown in Fig. IV-20 and comparison of the flight and nominal test environments is presented in Fig. IV-21. The actual environments for each of the models tested is presented in Table IV-14.

TABLE IV-14

Summary of Heat Flux Inputs to IRHS Plasma Test Models

	Phase I		
Model	$\dot{q}_{stag}$ (Btu/ft^2-sec)	Test Time (seconds)	Integrated Heat (Btu/ft^2)
1	203	0 to 100	20,300
2	35	0 to 1005	
	60	1005 to 1215	
	187	1215 to 1328	52,500
3	34	0 to 647	
	61	647 to 807	
	169	807 to 1017	
	34	1017 to 1217	59,000
4	Not tested		
5	38	0 to 930	
	60	930 to 1140	
	180	1140 to 1330	
	208	1330 to 1383	
	38	1383 to 1676	85,000

TABLE IV-14 (continued)

Model	$\dot{q}_{stag}$ (Btu/ft^2-sec)	Test Time (seconds)	Integrated Heat (Btu/ft^2)
6	33	0 to 920	
	67	920 to 1130	
	177	1130 to 1240	51,000
7	39	0 to 1005	
	73	1005 to 1170	
	212	1170 to 1260	
	39	1260 to 1580	63,000
8	36	0 to 1231	
	61	1231 to 1596	
	185	1596 to 1713	
	36	1713 to 2128	75,000
9A	36	0 to 300	
	185	300 to 824	
	36	824 to 1269	113,000
10A	36	0 to 300	
	182	380 to 904*	
	36	904 to 1349	113,000
1A-15	36	0 to 900	
	68	900 to 1110	
	176	1110 to 1300	
	222	1300 to 1353	
	36	1353 to 1643	81,700
2A-14	35	0 to 900	
	62	900 to 1110	
	156	1110 to 1300	
	169	1300 to 1353	
	35	1353 to 1643	77,600
3A-17	34	0 to 900	
	67	900 to 1110	
	194	1110 to 1300	
	204	1300 to 1353	
	34	1353 to 1643	85,000
		Phase II	
53	34	0 to 930	
	63	930 to 1140	
	187	1140 to 1330	
	246	1330 to 1383	
	34	1383 to 1673	84,000
54	32	0 to 647	
	59	647 to 807	
	183	807 to 1017	
	32	1017 to 1217	59,500
54R	35	0 to 930	
	70	930 to 1110	
	189	1110 to 1300	
	240	1300 to 1353	
	35	1353 to 1643	86,600

*For 80 seconds, the arc was unstable and the heat flux was very low.

TABLE IV-14 (continued)

Model	$\dot{q}_{stag}$ (Btu/ft^2-sec)	Test Time (seconds)	Integrated Heat (Btu/ft^2)
55	35	0 to 930	
	61	930 to 1140	
	188	1140 to 1330	
	246	1330 to 1353	
	35	1353 to 1673	85,000
56	38	0 to 930	
	63	930 to 1140	
	176	1140 to 1330	
	246	1330 to 1353	
	38	1353 to 1673	86,000
57	35	0 to 930	
	65	930 to 1140	
	176	1140 to 1330	
	246	1330 to 1353	
	35	1353 to 1673	84,000
58	35	0 to 647	
	64	647 to 807	
	188	807 to 1017	
	35	1017 to 1217	
59	35	0 to 930	
	63	930 to 1140	
	167	1140 to 1330	
	238	1330 to 1353	
	35	1353 to 1673	81,500
60	37	0 to 647	
	63	647 to 807	
	183	807 to 1017	
	37	1017 to 1217	63,000
40	32	0 to 930	
	67	930 to 1120	
	188	1120 to 1310	
	238	1310 to 1360	
	32	1360 to 1580	90,000
65	30	0 to 930	
	63	930 to 1140	
	183	1140 to 1330	
	220	1330 to 1390	
	30	1390 to 1742	93,000
35	30	0 to 225	
	30 to 385	225 to 250	
	385 const	250 to 300	
	385 - 30	300 to 338	13,000
70	32	0 to 225	
	127	225 to 245	
	352	245 to 268	
	127	268 to 280	
	32	280 to 306	13,000

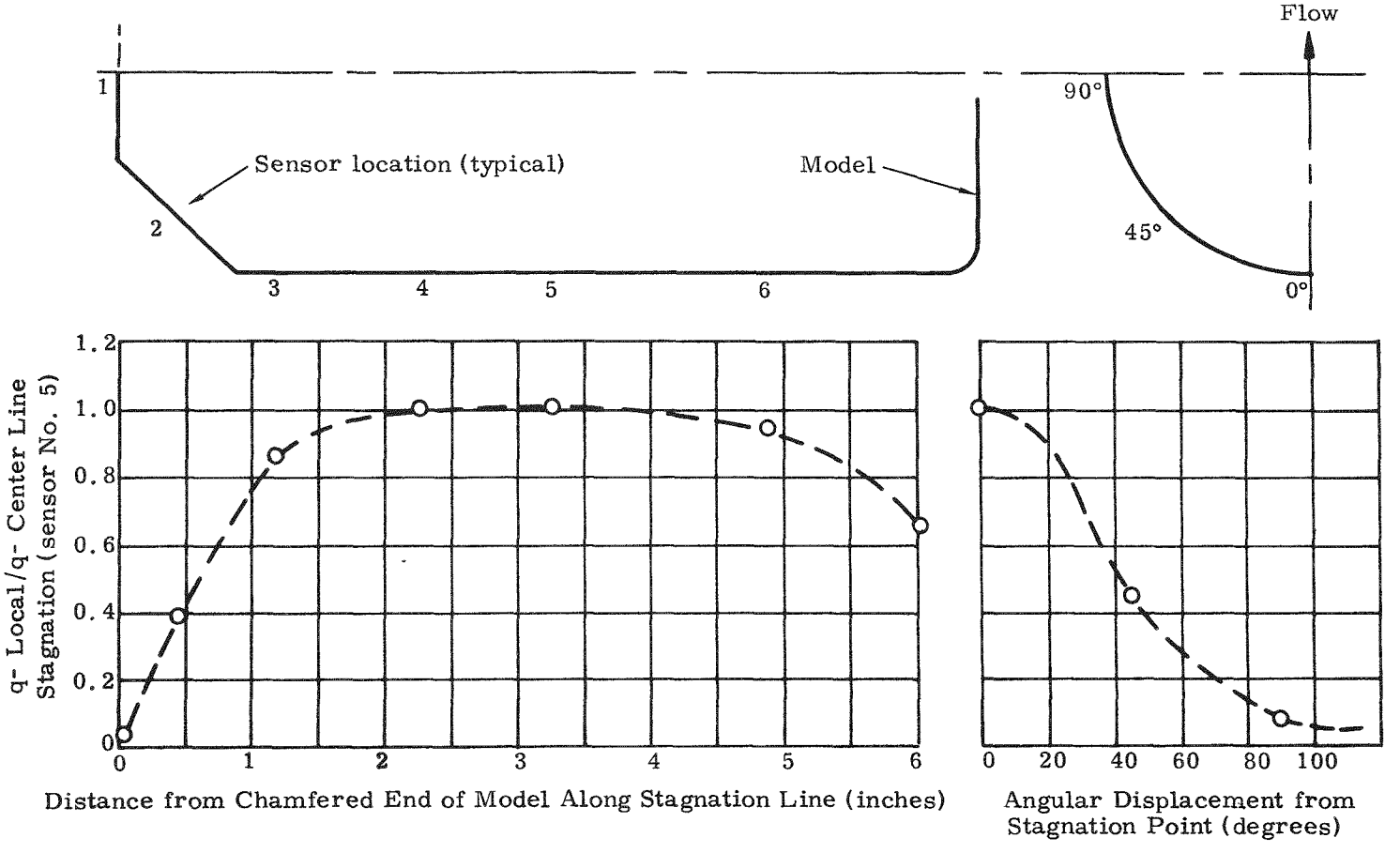

FIG. IV-20. SNAP 19 IRHS PHASE II TYPICAL HEATING RATE DISTRIBUTION OVER MODEL FOR SIDE-ON PLASMA-ARC RE-ENTRY TEST--STAGNATION POINT HEATING RATE, 220 Btu/ft-sec (nominal)

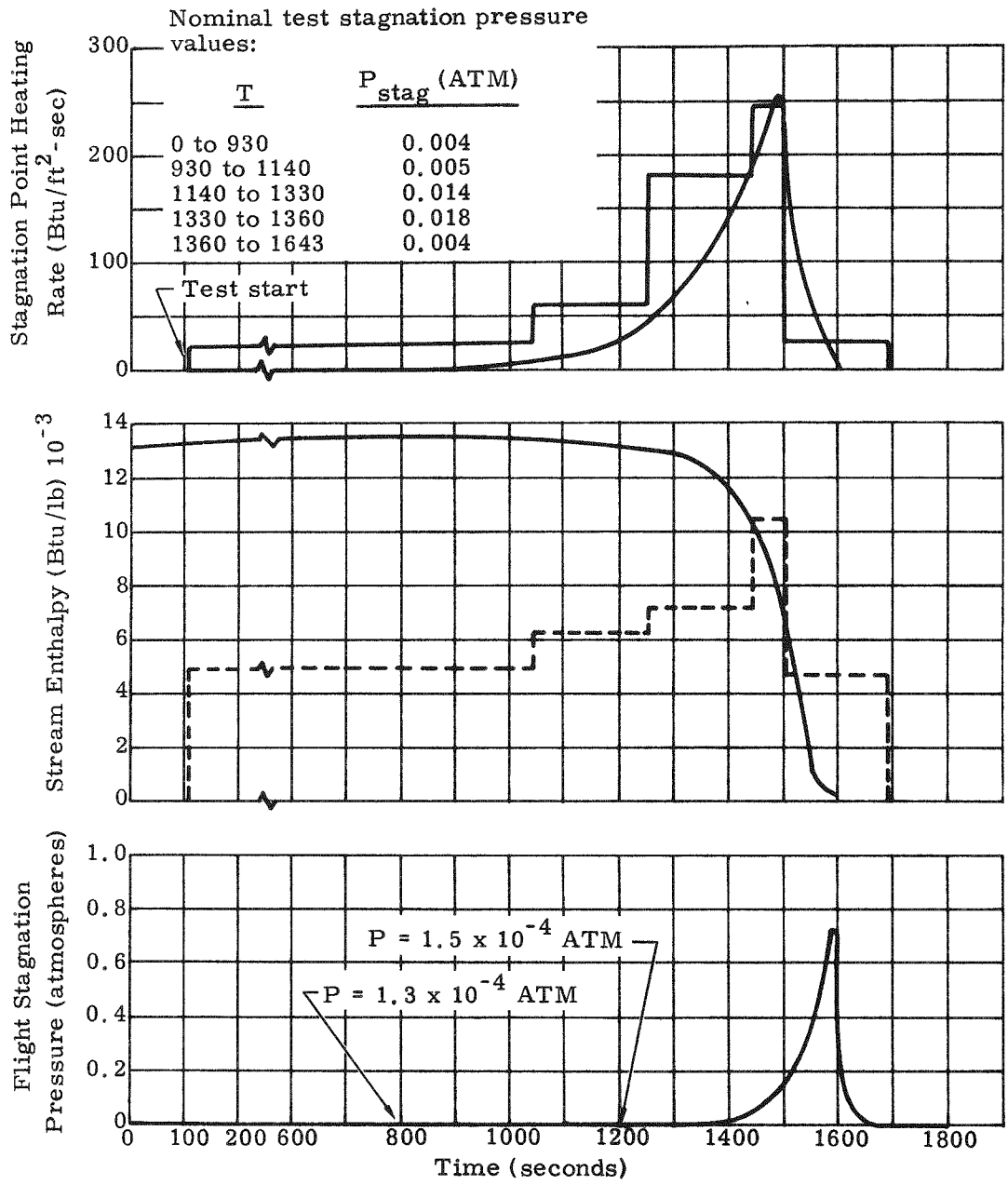

FIG. IV-21. COMPARISON OF TEST AND FLIGHT ENVIRONMENTS FOR THE IRHS SIDE-ON ORBITAL DECAY TRAJECTORY

e. Results

(1) Phase I

Peak heat shield temperature and total surface recession for the Phase I tests are compared in Table IV-15 with predicted nominal flight re-entry data for fueled heat sources.

Thermocouple output curves for model No. 6 are shown in Figs. IV-22 and IV-23. The pyrometer output curve for model No. 6 is shown in Fig. IV-24. These curves are typical of the output from the other Phase I aerothermal models. The pyrometer yields reasonable temperature correlation with thermocouples at the higher temperatures. Some thermocouples were erratic during the test.

During test, three of the Phase I models, Nos. 1, 2 and 6, exhibited loss of Haynes-25 alloy from the melting capsule through breaks in the heat shield. It was determined that the heat shield crack in No. 1 was due to thermal stress in the assembly resulting from improper clearance. The graphite cement used to bond the midline lap joint on the Phase I models tended to ooze into the thermal expansion gap between the heat shield and the capsule and fill it. Pretest gammagraphs of model No. 1 indicate that this had happened.

The plasma-impact models, which had a contemporary flight-type screwed joint instead of the bonded fit joint, were tested after the above mentioned models. None of the three exhibited any type of heat shield failure. Figure IV-25 is a photograph of a sectioned plasma-impact model which was not impact tested.

(2) Phase II

Due to the problems of molten Haynes-25 leakage which occurred in the Phase I models, the Phase II models were constructed to more closely simulate the flight design. There were no thermocouples placed in the models and they were assembled in a clean argon or helium atmosphere. As a result, none of the Phase II models exhibited the heat shield leaks found in some of the Phase I models.

A summary of the Phase II peak surface temperatures and total surface recession responses is presented in Table IV-16.

The post-test condition of the four side-on stable design verification models is shown in Fig. IV-26. Their condition is typical of the condition of all of the Phase II models; no Haynes-25 was released nor were there cracks in the heat shield.

A post-test section of one of the Phase II models (side-on stable test) is shown in Fig. IV-27. The molten Haynes-25 alloy dissolved some of the tantalum canister, even though the peak model temperature of approximately 4200° F was well below the melting point of tantalum (5600° F).

f. Correlation

The purpose of the correlation effort was to establish the accuracy of the computer programs used to calculate the flight thermal and thermochemical responses of the IRHS during different modes of re-entry. The five tests chosen for correlation represented the best data return from a cross section of the various flight motions simulated. (Instrumented plasma models S/N 1, 3, 6, 7 and 9A.)

TABLE IV-15

Comparison of Phase I Plasma Test Results with Predicted Flight Results

Test Model***	Peak Surface Temperature (°F)			Peak Surface Recession (in.)			Peak Heat Flux (Btu/ft -sec)			Integrated Heat Flux (Btu/ft^2)		
	Test	Flight**	$\frac{T_{test}}{T_{flight}}$	Test	Flight**	$\frac{X_{test}}{X_{flight}}$	Test	Flight**	$\frac{\dot{q}_{test}}{\dot{q}_{flight}}$	Test	Flight**	$\frac{Q_{test}}{Q_{flight}}$
1*	3620	3960	0.91	0.026	0.132	0.20	203	252	0.807	20,300	48,600	0.42
2	3040	2970	1.02	0.027	0.039	0.69	187	252	0.74	52,500	48,600	1.08
3	3240	2970	1.09	0.035	0.039	0.90	169	252	0.67	59,000	48,600	1.21
5	3380	2970	1.14	0.040	0.039	1.03	208	252	0.83	85,000	48,600	1.75
6	3330	2970	1.12	0.027	0.039	0.69	177	252	0.70	51,000	48,600	1.05
7	2920	2660	1.10	0.032	0.047	0.68	212	293	0.72	63,000	50,100	1.26
8	2830	2660	1.06	0.044	0.061	0.72	185	293	0.63	75,000	50,100	1.49
9A	3100	3100	1.0	0.165	0.180	0.91	185	234	0.79	113,000	55,800	2.03
10A	3100	3100	1.0	0.134	0.180	0.74	182	234	0.78	113,000	55,800	2.03
1A-15	3260	2970	1.10	0.043	0.039	1.10	222	252	0.88	82,000	48,600	1.69
2A-15	2970	2970	1.0	0.044	0.039	1.13	169	252	0.67	78,000	48,600	1.60
3A-17	3100	2970	1.04	0.046	0.039	1.18	204	252	0.809	85,000	48,600	1.75

*Aborted test
**Predicted nominal re-entry values for flight motion simulated
***See Table IV-13

CONFIDENTIAL

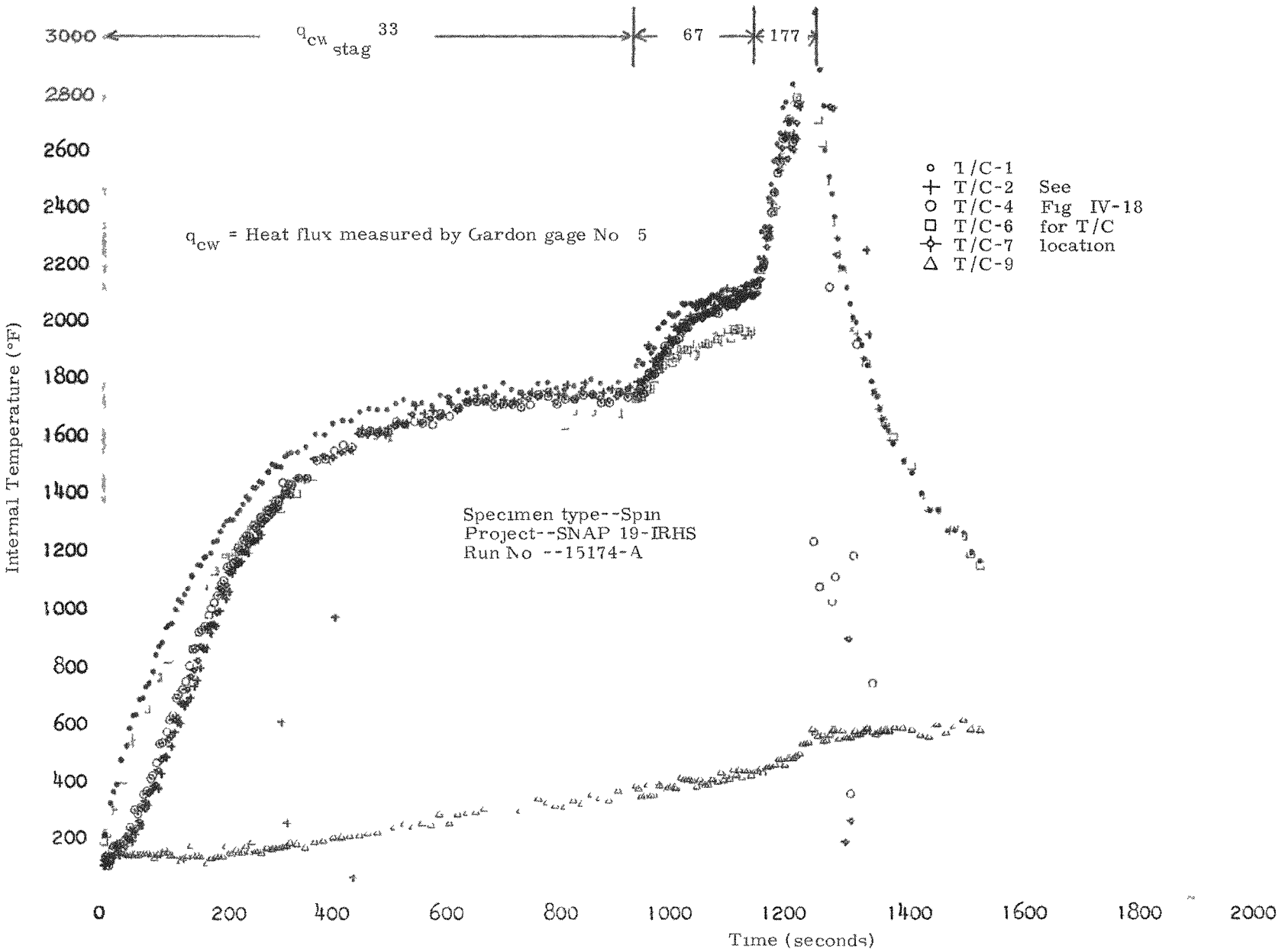

FIG. IV-22. PLASMA-ARC MODEL NO. 6 INTERNAL THERMOCOUPLE READINGS VERSUS TIME

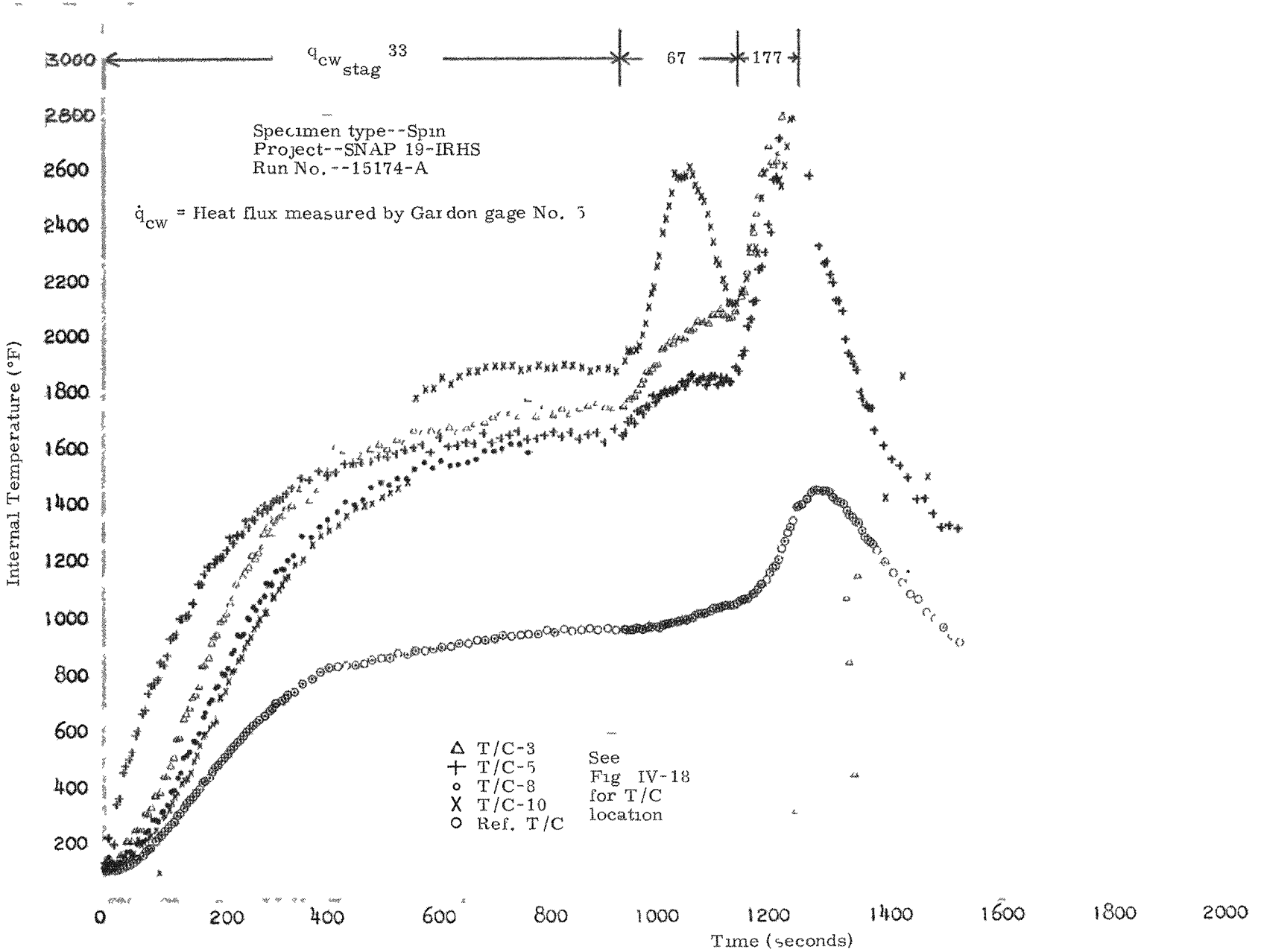

FIG. IV-23. PLASMA-ARC MODEL NO 6 INTERNAL THERMOCOUPLE READINGS VERSUS TIME

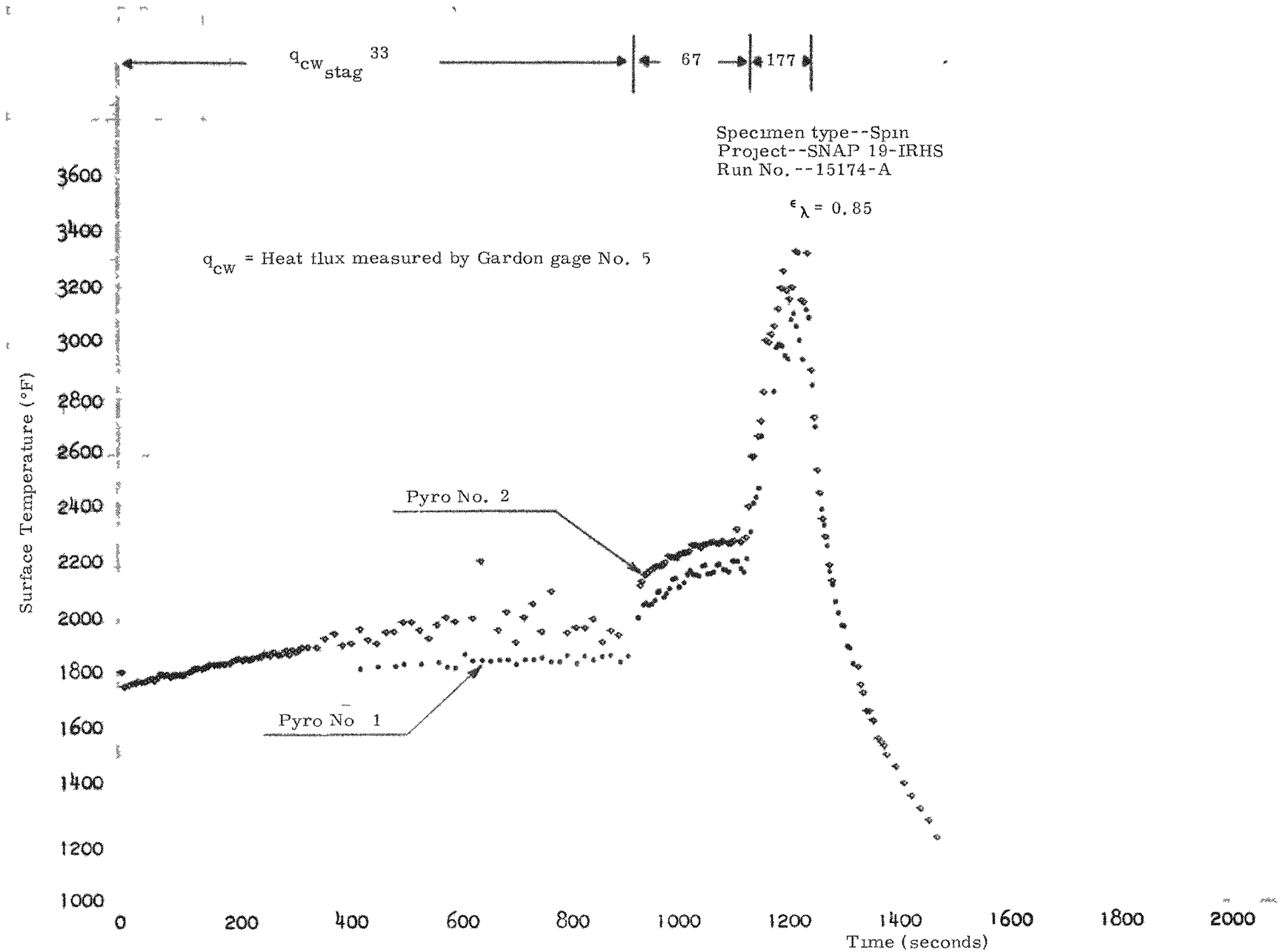

FIG. IV-24. PLASMA-ARC MODEL NO 6 PYROMETER MEASURED SURFACE TEMPERATURE VERSUS TIME

TABLE IV-16

Comparison of Phase II Plasma Test Results with Predicted Flight Results

Test Model†	Peak Surface Temperature (°F)			Peak Surface Recession (in.)			Peak Stagnation Point Heat Flux (Btu/ft^2-sec)			Integrated Heat Flux (Btu/ft^2)*		
	Test	Flight***	$\frac{T_{test}}{T_{flight}}$	Test	Flight***	$\frac{Rs_{test}}{Rs_{flight}}$	Test	Flight***	$\frac{\dot{q}_{test}}{\dot{q}_{flight}}$	Test	Flight***	$\frac{Q_{test}}{Q_{flight}}$
53	3820	4270	0.89	0.172	0.176**	0.98	246	255	0.96	84,000	49,000	1.71
54	2920	2970	0.98	0.031	0.039	0.79	183	255	0.72	59,500	49,000	1.21
54R	3780	4270	0.89	0.205	0.176**	1.16	240	255	0.94	86,600	49,000	1.77
55	3800	4270	0.89	0.171	0.176**	0.97	246	255	0.96	85,000	49,000	1.73
56	3250	3210	1.01	0.043	0.052	0.83	246	255	0.96	86,000	49,000	1.76
57	3200	3210	0.997	0.042	0.052	0.81	246	255	0.96	84,000	49,000	1.71
58	2930	2970	0.99	0.032	0.039	0.82	188	255	0.74	63,000	49,000	1.29
59	3230	3210	1.01	0.040	0.052	0.77	238	255	0.93	81,500	49,000	1.65
60	2900	2970	0.98	0.034	0.039	0.87	183	255	0.72	63,000	49,000	1.29
40	4100	3960	1.04	0.114	0.132	0.86	238	252	0.94	80,000	49,000	1.63
65	4160	3960	1.05	0.140	0.132	1.06	220	252	0.87	83,000	49,000	1.69
35	4200			0.017			385	290	1.3	13,000	10,000	1.3
70	4200			0.017			352	290	1.2	13,000	10,000	1.3

*Integrated with respect to time. Test values also corrected to account for axial variations in stagnation heat flux found from stream survey.

**Extrapolated from analytical data.

***Predicted nominal re-entry values for flight motion simulated.

†See Table IV-13.

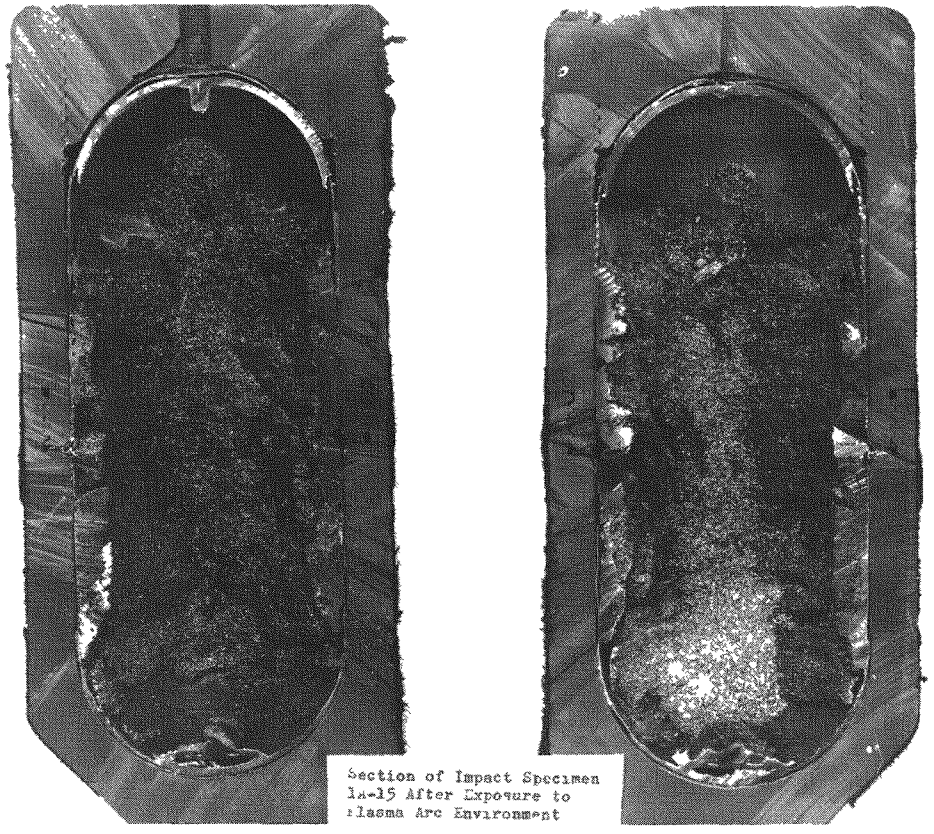

FIG IV-25. SECTION OF SPINNING MODEL 1A-15 AFTER EXPOSURE TO PLASMA-ARC ENVIRONMENT

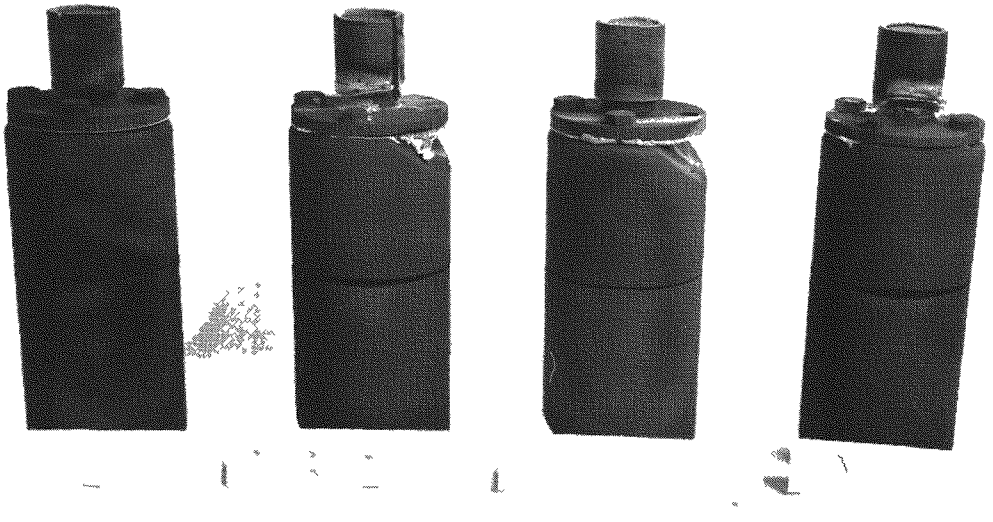

FIG. IV-26. PLASMA-ARC SIDE-ON, STABLE DESIGN VERIFICATION MODELS (NOS. 35, 40, 65 AND 70)

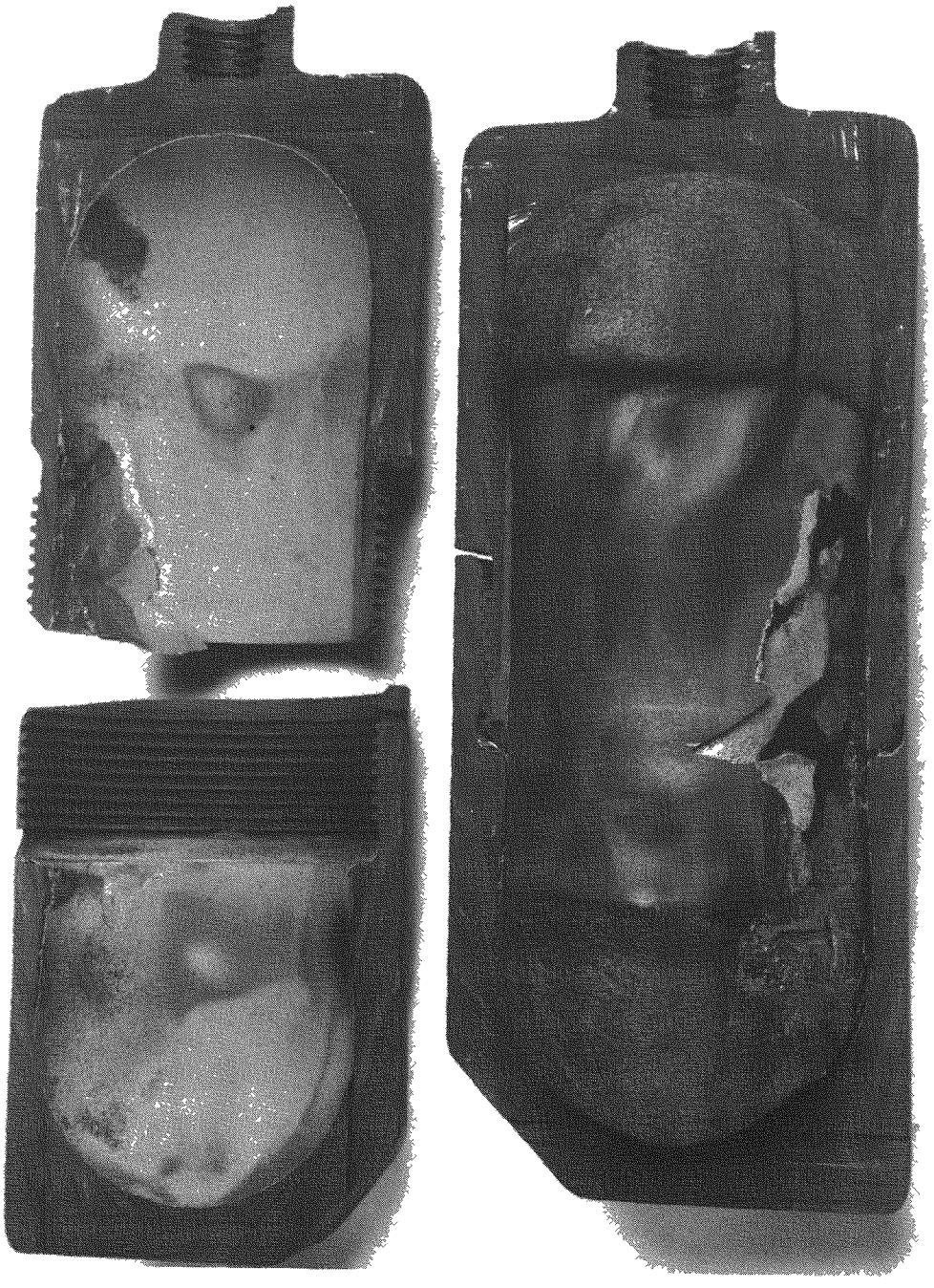

FIG. IV-27. POST-TEST SECTION SIDE-ON, STABLE PLASMA MODEL NO. 55

The computer models devised for this correlation study are geometrically similar to the 2-D models used in the aerothermal analysis. The following conditions were peculiar to the test computer model:

(1) Internal heat generation was not required since a fuel simulant was used in the models.

(2) No provision was made to account for heat losses to the support stud or the water-cooled spin rig.

(3) Heat losses through thermocouples lead wires and wire passages were not considered.

(4) Test environment data from the instrumented plasma arc test calibration runs were used where possible as boundary conditions for the test computer model. In the few instances where test data were unreliable or not available, such as some of the end-on heat flux distribution data, comparable theoretical data were used.

An internal temperature correlation was performed by forcing the temperature of the heat shield to follow thermocouple and pyrometer data from each test. The capsule and fuel simulant were then permitted to respond freely. The value of fuel simulant conductivity was then parametrically determined by matching the capsule and fuel simulant response with the test data. This value was close to the value predicted from packed bed theory for zirconium dioxide powder. Typical internal temperature correlation curves are presented in Fig. IV-28 and IV-29.

The calibrated heat flux and enthalpy environment from each test was then applied to the surface of the model and the entire model was permitted to respond freely. A comparison of surface test results with predicted test results is shown in Table IV-17.

The surface recession correlation was accomplished by applying a surface temperature and stagnation pressure profile to a one-dimensional graphite computer model. Since surface recession is purely a surface phenomenon and the effects of surface recession on surface temperature are small and always conservative, as shown in Fig. IV-30, the one-dimensional computer model is sufficient for this analysis. The results of the predicted surface recession histories are compared with the measured values from each of the respective tests in Table IV-17.

The results from the twenty-four IRHS plasma arc tests showed that the heat source will meet the requirement of intact atmospheric re-entry under launch abort or orbital decay conditions. Specific conclusions are:

(1) The nine instrumented IRHS models yielded thermal response data that correlates with predictions in a reasonable manner.

(2) The thirteen Phase II plasma tests conducted under side-on spinning or side-on stable re-entry modes at various orbital decay and abort situations demonstrated that the integrity of the heat shield will be maintained under all conceivable atmospheric re-entry conditions associated with the Nimbus-B mission. Seven of the models successfully passed the highly improbable side-on stable condition. It is expected that some aerodynamic motion would be imparted to the re-entering IRHS and absolute side-on stable conditions would not be maintained.

(3) Some melting of the Haynes-25 capsule is expected for all orbital re-entry conditions.

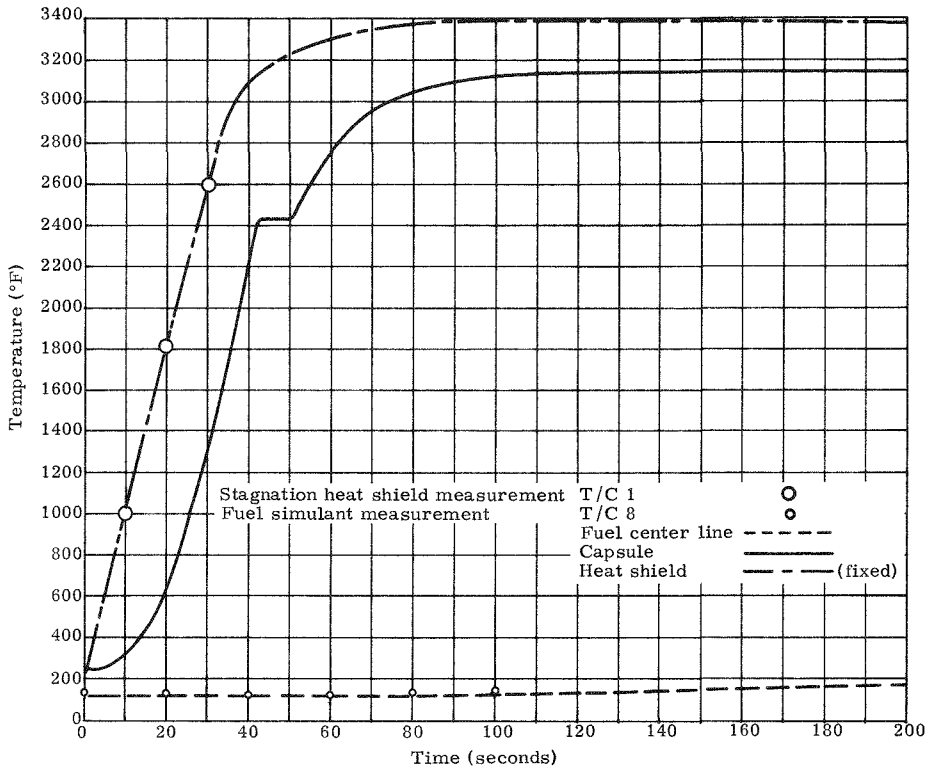

FIG. IV-28. IRHS INTERNAL TEMPERATURE CORRELATION, PLASMA UNIT NO. 1 SIDE-ON, STABLE--CONSTANT HEAT FLUX

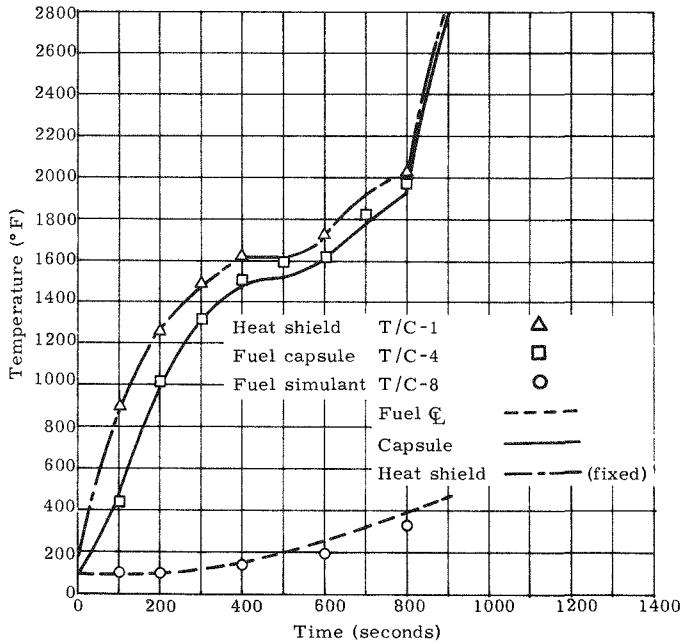

FIG. IV-29. IRHS INTERNAL TEMPERATURE CORRELATION, PLASMA UNIT NO. 3 SIDE-ON, SPINNING--VARIABLE HEAT INPUT

TABLE IV-17

IRHS Re-entry Modes--Correlation of Heat Shield Test Results with Predictions

Test Unit Serial Number	Assembly	Mode of Test Heat Flux Loading	Peak or Highest Recorded Surface Test Temperature (°F)	Predicted Temperature at Same Time (°F)	Error* (%)	Total Test Surface Recession (in.)	Total Predicted Surface Recession (in.)	Error* (%)
1	-009	Side-on stable 203 Btu/ ft^2-sec	2600	2675	+2.9	0.026	0.031	+19.2
3	-009	Side-on spinning 1.0 nom Q	2680	2600	-3.1	0.0350	0.0354	+1.1
6	-029	Side-on spinning 1.3 nom Q	2840	2720	-4.4	0.027	0.0205	-24
7	-019	Tumbling 1.0 nom Q	2750	2790	+1.5	0.032	0.032	0
9A	-039	End-on 1.0 nom Q	3000	2890	-3.7	0.165	0.194	+18

*+ Indicates conservative prediction.
- Indicates nonconservative prediction.

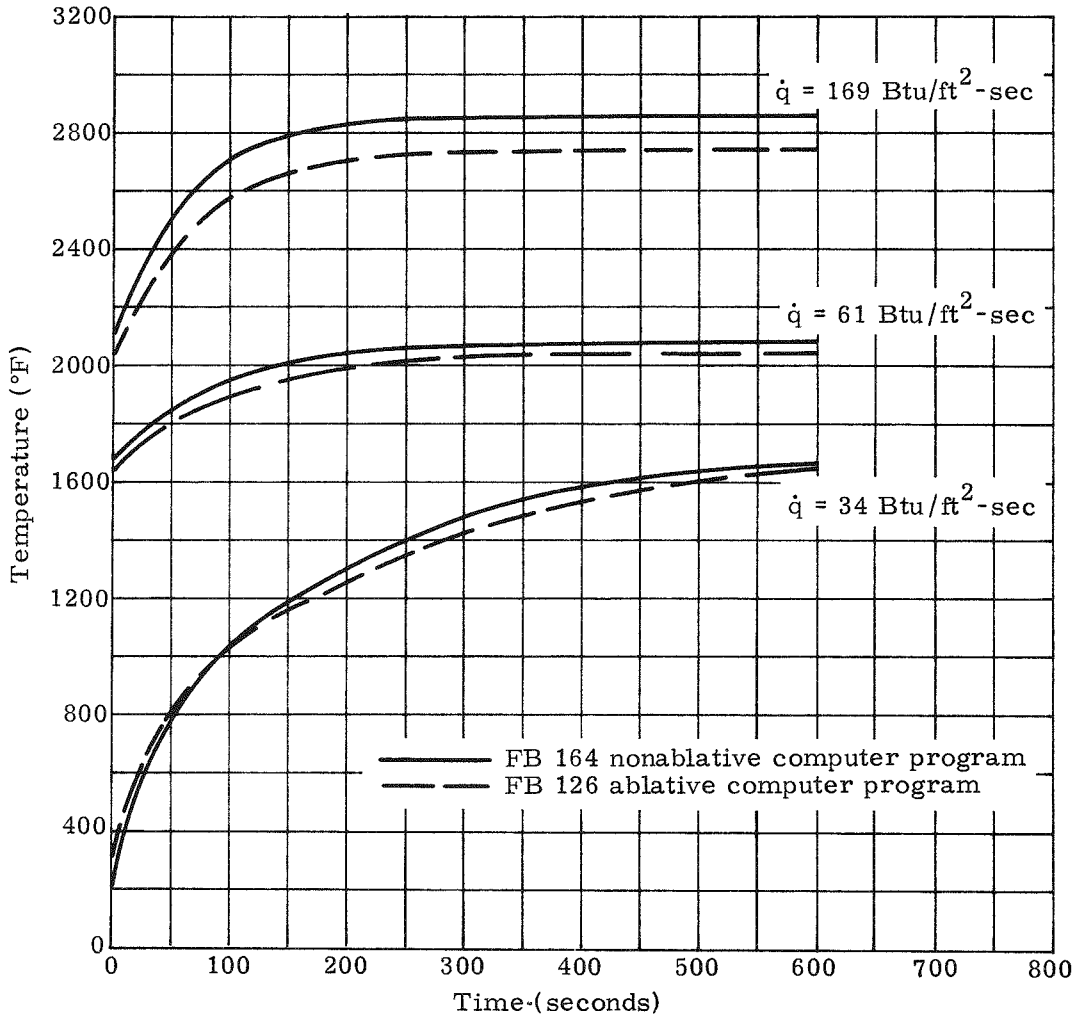

FIG. IV-30. COMPARISON OF ABLATIVE AND NONABLATIVE IRHS SURFACE TEMPERATURE RESPONSE DURING RE-ENTRY

(4) The duration of time above the Haynes-25 melting temperature (2430° F) for the side-on spinning deorbit case is approximately 190 seconds.

(5) Heat shield surface recession for all cases studied is small; i.e., 0.050 inch for the side-on spinning mode and 0.130 inch for the side-on stable re-entry mode.

5. Filter Development Program (Capsule Helium Vent)

The principal objective of the filter development task was to qualify a helium vent for use in the SNAP 19 intact re-entry heat source. The filter element allows the gases from the Pu-238 isotope to escape from the capsule without release of particulate matter.

The early candidate material for the vent was powdered Haynes-25 pressed and sintered into a filter element. Though this vent worked properly at the lower temperatures, it became apparent that the filter element was highly sensitive to only a few parts per million of oxygen at the normal operating temperature (1425° F), with the result that the element became impervious to helium flow. The clogging phenomenon was ultimately ascertained, through use of microprobe analysis, to be caused by buildup of oxides within the filter element pores.

When the powdered Haynes-25 element deficiency was identified, experimental effort was initiated to qualify an alternate filter element. Those elements investigated included sintered platinum powder elements, nickel-plated zirconium oxide, uncoated zirconium oxide and platinum-plated zirconium oxide.

Based on limited test data, the sintered platinum powder element becomes impervious to helium flow between the temperatures of approximately 1325° F and 1450° F. The unplated ZrO_2 and nickel-plated ZrO_2 elements did not exhibit any problems, based on limited test data, but further work on these was held in abeyance since the platinum-plated ZrO_2 filter element was qualified through environmental stability, chemical compatibility and particle retention tests. Tests were conducted at the component level as well as on the complete heat source.

Development and qualification testing of the platinum-plated ZrO_2 filter was one of the major efforts on the IRHS program. A definition of the program established to qualify the ZrO_2 filter and significant summary results follow; detailed results are in Ref. IV-2.

a. Description of filter development and qualification program

The program for developing the platinum-plated ZrO_2 filter was designed to yield chemical compatibility data and helium flow characteristics following exposure to thermal environments in helium, air and vacuum. Further, the program was designed to develop the manufacturing techniques and establish long-term stability data on the filter in different environmental extremes. The development, manufacturing and evaluation test program was divided into four different categories. The four categories were not programmed in series but were, in general, worked in parallel. The four categories are:

(1) Filter element in-process evaluation and manufacturing sequence

(2) Filter assembly environmental tests, metallography and physical property measurements

(3) Capsule environmental tests, particle retention tests and impact tests

(4) A parallel filter evaluation effort conducted by the Mound Laboratory of Monsanto Research Corporation. This effort included radioactive particle retention tests with PuO_2 microspheres.

Figure IV-31 shows the ZrO_2 filter in-process evaluation up to the point of insertion of the element into the receptacle. (Representative metallographic sections of the filter are shown in Figs. IV-32 and IV-33.) The completed filter assembly moved to a subsequent manufacturing step or was placed on a filter assembly test, as appropriate.

Figure IV-34 shows the sequence and types of tests conducted on filter assemblies with platinum-plated ZrO_2 elements. (A filter assembly consists of the Haynes-25 receptacle and the filter element.) Twenty-one filter assemblies were manufactured for tests, of which 15 were placed on thermal soak tests in environments of air, helium and vacuum, with soak times ranging from one week to approximately 1500 hours. Post-soak tests generally consisted of helium flow checks, element push-out checks, metallography, and percent voids and pore width spectrum measurements. One as-manufactured assembly was subjected to an element push-out test and one was subjected to metallographic examination.

Four filter assemblies were subjected to different types of rapid thermal cycling tests as defined in Fig. IV-35. Following the thermal cycling tests, the specimens were subjected to helium flow checks, metallography, and then element percent void and pore width measurements.

To assure that welding of the filter assembly into the Haynes-25 capsule would not have a detrimental effect, several half-capsule and full-capsule assemblies were manufactured for evaluation testing. Figure IV-35 shows the type and sequence of tests. Seven filter assemblies were welded into half-capsule test specimens for PuO_2 simulant particle retention tests, short-term helium flow stability tests and long-term helium flow stability tests. It was planned that the filter assemblies would be subjected to push-out or metallographic examination following the tests. In addition to the half-capsule tests, two full-scale intact re-entry heat sources with ZrO_2 filter elements were impact tested. Following impact, the filters were subjected to helium flow checks and particle retention tests.

To provide further assurance that the selected ZrO_2 filter assemblies would perform as designed, thirty filter test specimens of various configurations were manufactured and delivered to Mound Laboratory for their independent test and analysis. A listing of the Mound test plan, which describes test condition, specimen configuration and number tested is shown below. All results were positive.

(1) Thermal vacuum tests: Fourteen-day tests performed on half-capsule assemblies containing fuel and operating at 1425° F. Four half-capsules with installed filters and two separate filter assemblies were provided. Radioactive product retention was determined.

(2) Vacuum thermal environment tests: Fourteen-day test operated at 1425° F at vacuum of 10^{-6} torr or less. Six modified half-capsules with filter assemblies were provided. Periodic vacuum measurements were made. Upon termination of tests, post-test analysis of zirconia and filter element-filter assembly interfaces, using such techniques as microprobe, microhardness, and high magnification metallographs, were conducted.

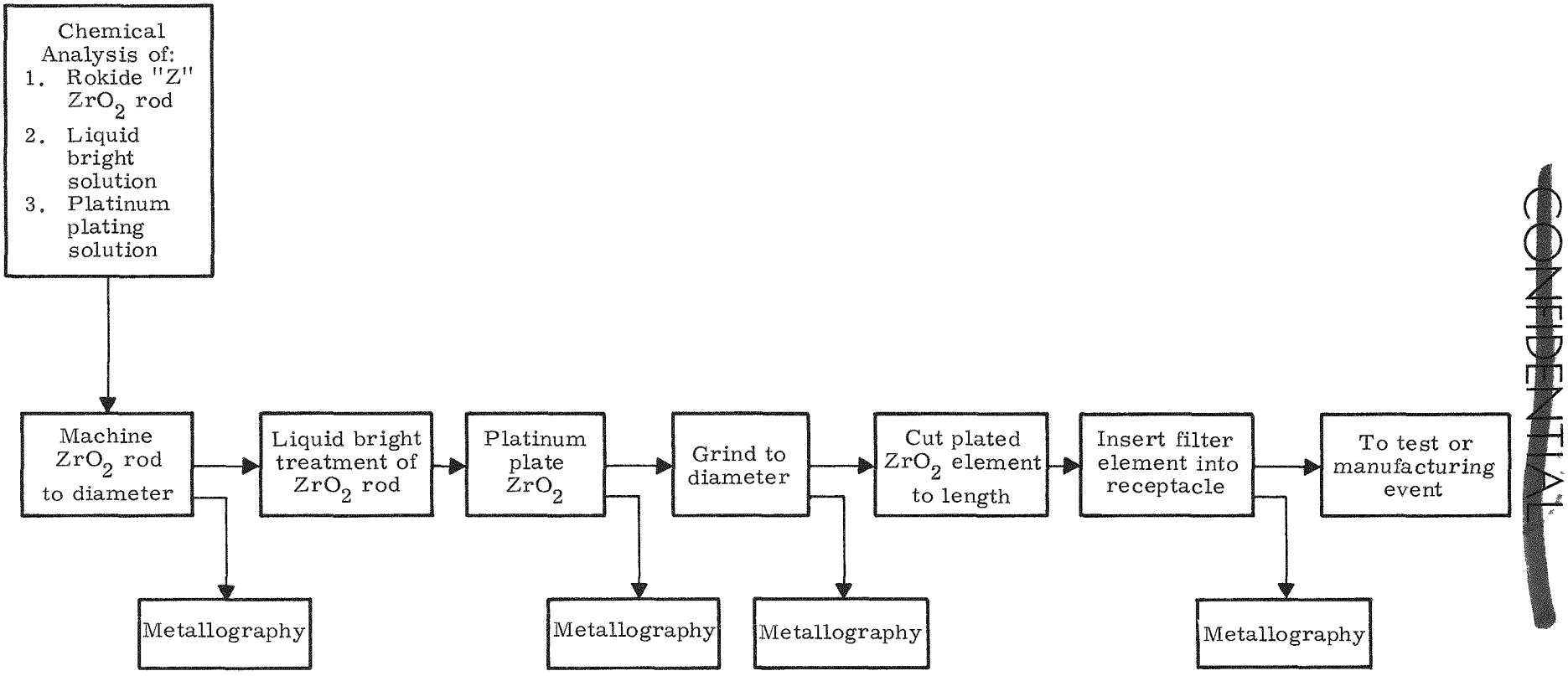

FIG. IV-31. FILTER ELEMENT EVALUATION AND MANUFACTURING FLOW CHART

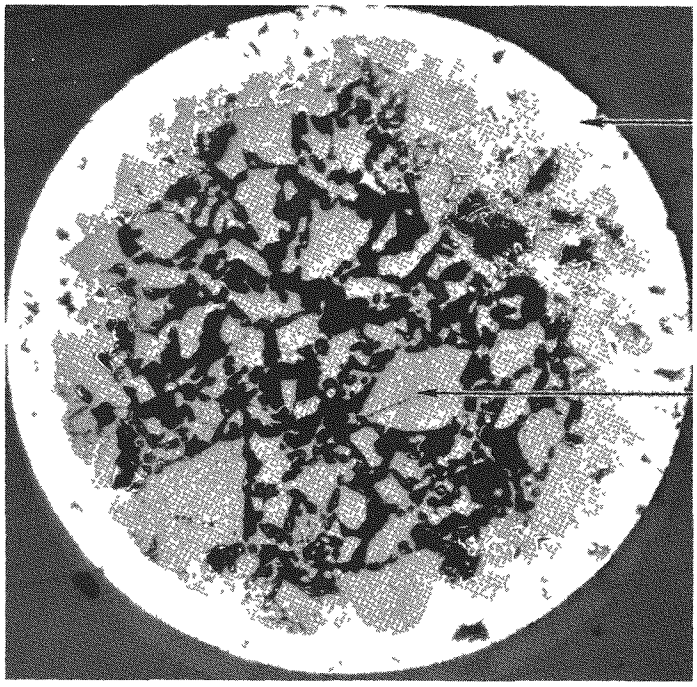

Magnification 100X, as polished

Transverse Section

Platinum plating

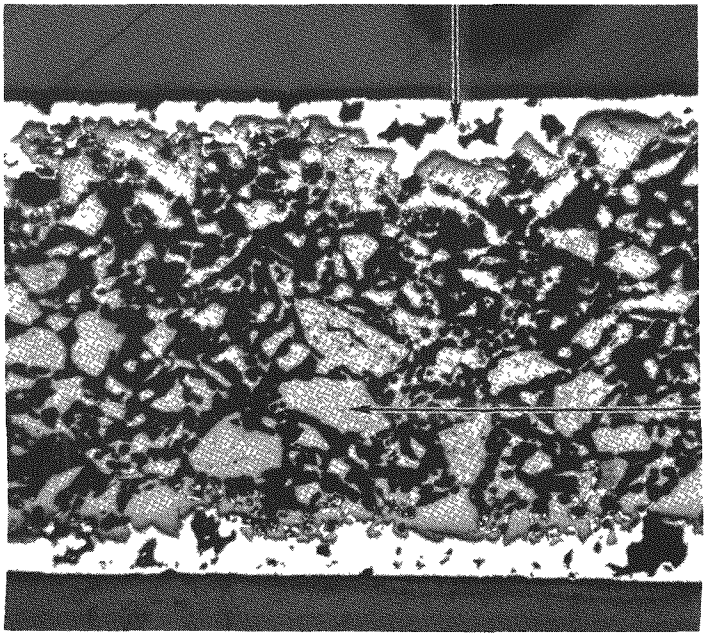

Magnification 75X, as polished

Longitudinal Section

FIG. IV-32. SECTIONS, PLATINUM-PLATED ZrO_2 FILTER ELEMENT AFTER MACHINING

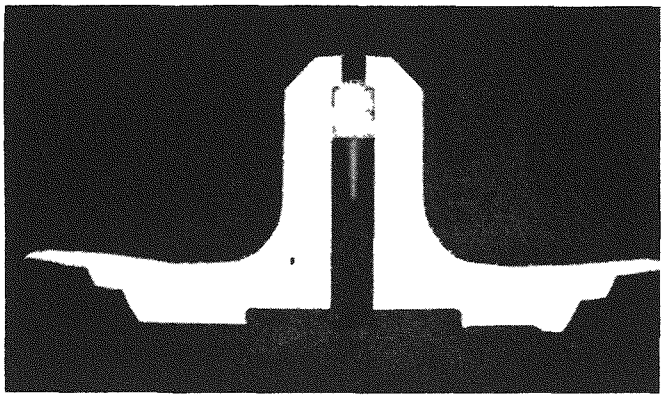

Haynes-25 element

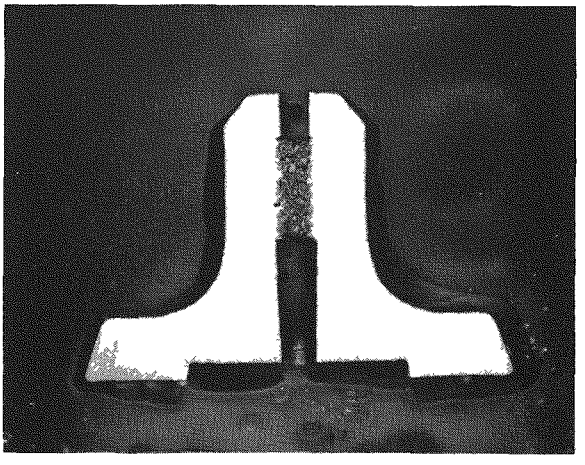

ZrO_2 element

FIG. IV-33. LONGITUDINAL SECTIONS, MACROPHOTO OF FILTER ASSEMBLIES, 7X

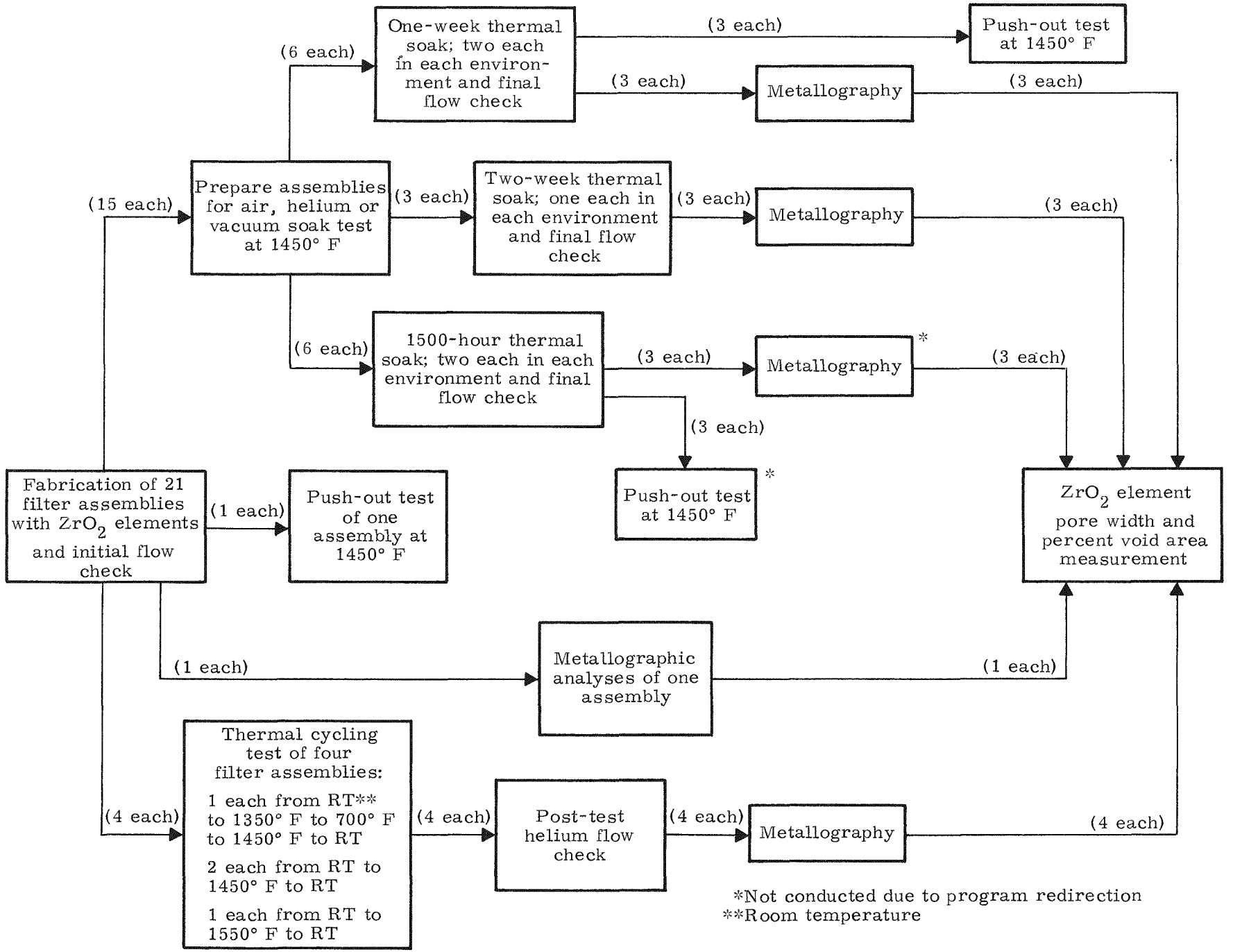

FIG. IV-34. FILTER ASSEMBLY DEVELOPMENT TEST PLAN FLOW CHART

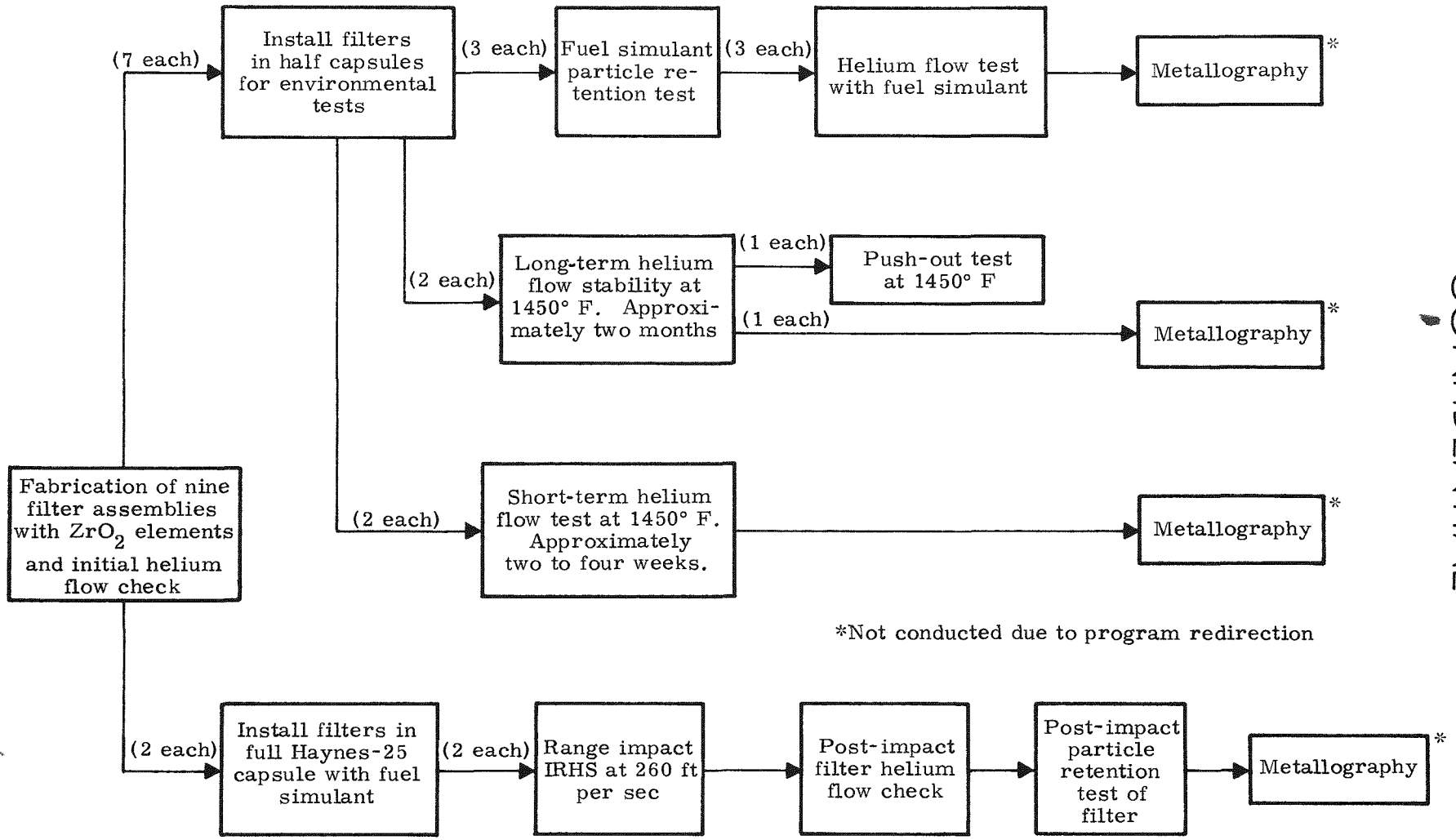

FIG. IV-35. FILTER/CAPSULE ASSEMBLY DEVELOPMENT TEST PLAN FLOW CHART

(3) Blow-out tests: Filter assemblies were pressurized to measure the pressure to break the filter element-filter housing joint interface at 1425° F. Six modified half-capsules were supplied. Post-test analysis of the joint and filter element structure was accomplished.

(4) Thermal cycling tests: This test consisted of fifteen cycles between 100° F and 1425° F during one week in a vacuum of 10^{-6} torr or less. Flow rate and pressure were recorded. Metallographs were made of the filter element-filter housing interface. Six half-capsules were provided.

(5) Accelerated vacuum thermal environment test: These were 100-hour tests at 1690° F and 10^{-6} torr vacuum or less. Post-test data were provided as required for Item (2) above. Six filter assemblies were provided.

(6) Chemistry studies: Composition of the filter material and electro-deposited materials was determined.

b. Filter evaluation tests

Figure IV-36 is a histogram of the initial room temperature helium diffusion rates through 74 different filter assemblies with applied upstream pressures of 1 and 5 psia (see Fig. IV-33 for a macrophotograph of a filter assembly). With an applied helium pressure of 5 psia, the majority of the initial rates ranged between 1 and 2×10^{-2} scc/second. This flow rate will prevent a significant pressure buildup in the Haynes-25 capsule, since the helium generation rate in the fuel is approximately 2.4×10^{-5} scc/second.

Filter assemblies were held at 1450° F for approximately 1500 hours in environments of air and vacuum. The helium diffusion rates were measured as a function of pressure before and after the soak tests. As shown in the representative results in Figs. IV-37 and IV-38, there was little or no change in flow resulting from the environmental extremes.

Figure IV-39 presents the result of flowing helium through a platinum-plated ZrO_2 filter element at 1450° F for approximately 1300 hours. Helium diffusion was occasionally measured at room temperature and 1450° F as a function of applied pressure. There is some scatter in the data but the flow rates compare favorably with those presented in Figs. IV-37 and IV-38, indicating stability of the materials.

Simulated fuel particles consisting of UO_2 spiked with strontium-90 in the form of $SrTiO_3$ were placed in contact with the filter elements in three half-capsule assemblies and subjected to a helium pressure of 40 psi. The half-capsules were manually vibrated periodically to prevent any localized fixing of the 0.1- to 0.5-micron size particles. These initial short-term tests resulted in a decontamination factor greater than 10^{-6} after each time period (24, 72 and 160 hours). The application of the decontamination factor to this study related the number of particles passing through the filter per unit quantity of particles present. Therefore, less than one particle per one million particles coming in contact with the filter passed through. The results from relatively long-term testing of two additional half-capsules verified these values of the decontamination factor. These two additional particle retention tests were run for 212 and 336 hours. The particle retention tests conducted by Martin Marietta are considered highly conservative because the nominal size range for plasma-fired PuO_2 is 50 to 250

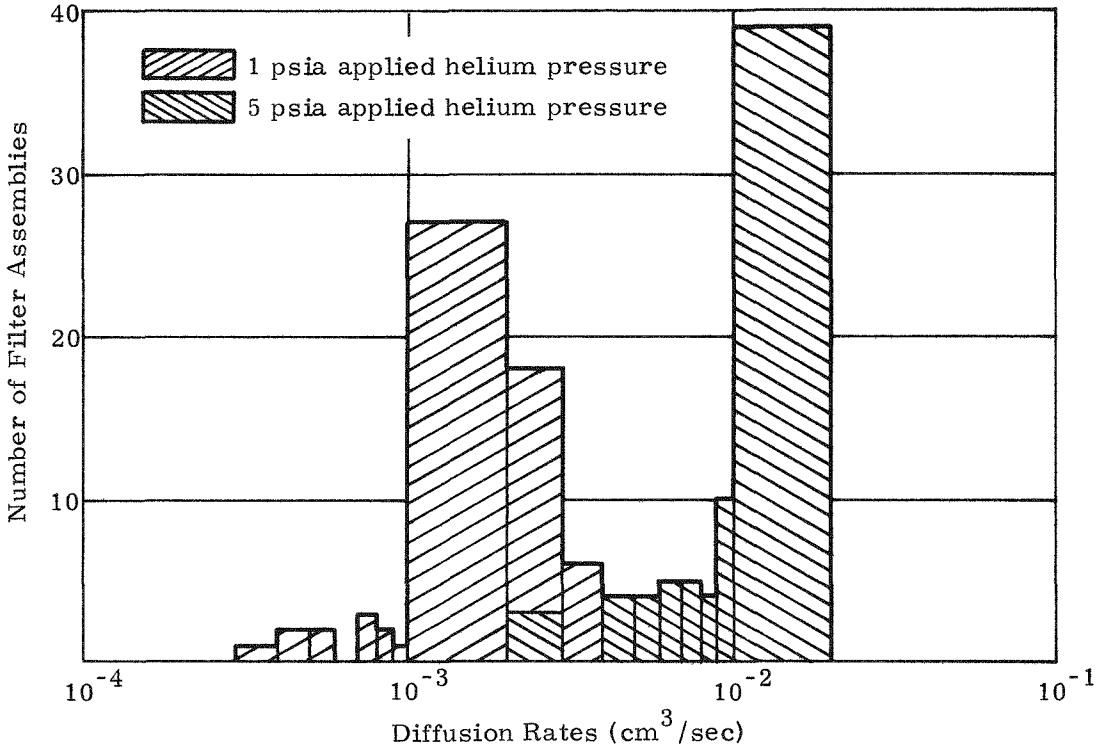

FIG. IV-36. INITIAL HELIUM DIFFUSION RATES THROUGH PLATINUM-PLATED ZrO_2 FILTER ASSEMBLIES

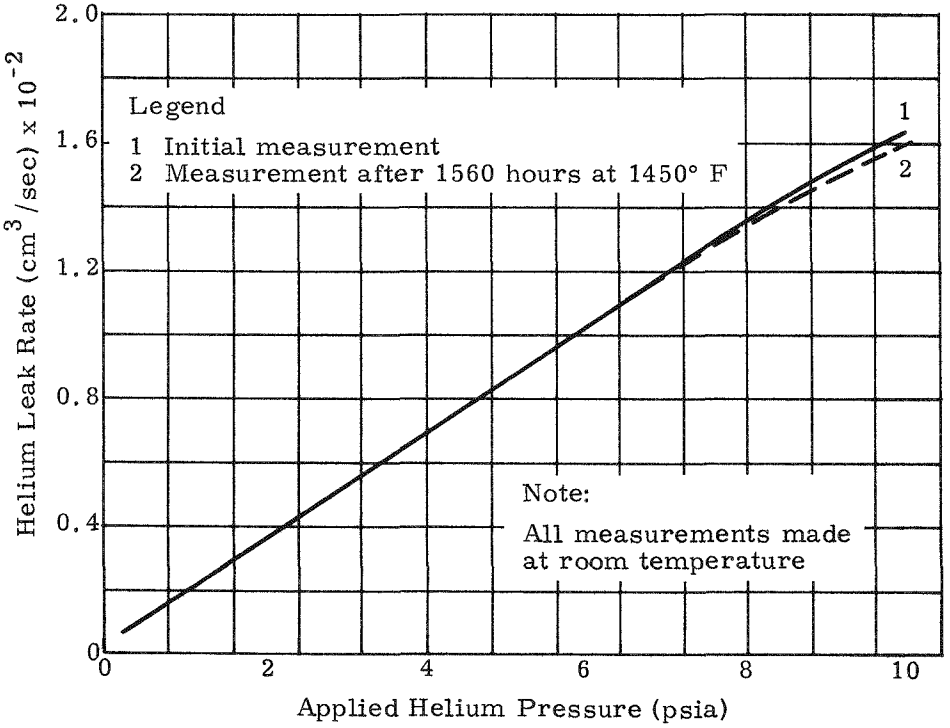

FIG. IV-37. HELIUM DIFFUSION RATES OF AN AIR SOAKED, PLATINUM-PLATED ZrO_2 FILTER ASSEMBLY

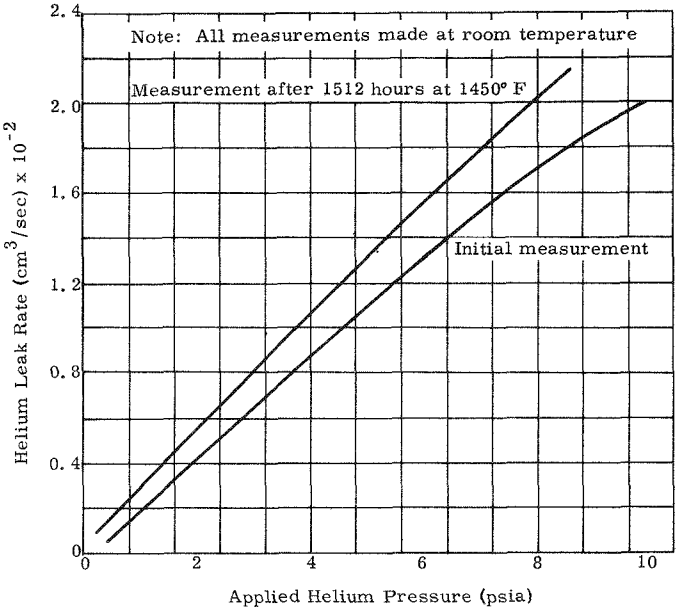

FIG. IV-38. HELIUM DIFFUSION RATES OF A VACUUM-SOAKED, PLATINUM-PLATED ZrO_2 FILTER ASSEMBLY

Legend:

1 Initial room temperature measurement of the filter assembly
2 Initial one-half capsule measurement at 1450° F
3 Measurement at 1450° F after 336 hours
4 Room temperature measurement after 336 hours
5 Measurement at 1450° F after 594 hours
6 Room temperature measurement after 594 hours
7 Measurement at 1450° F after 1314 hours
8 Room temperature measurement after 1314 hours

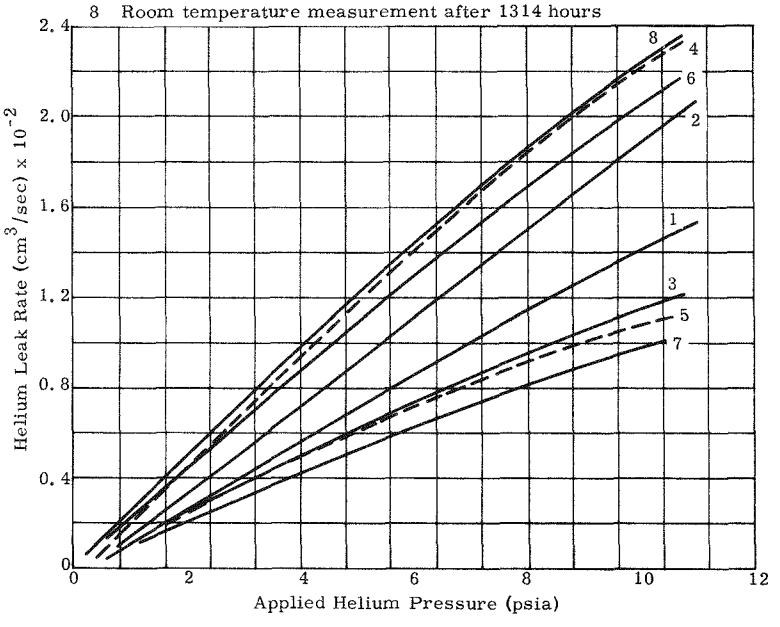

FIG. IV-39. HELIUM DIFFUSION RATES OF A HELIUM-FLOWED (AT 1450° F), PLATINUM-PLATED ZrO_2 FILTER IN HALF CAPSULE

microns. Mound Laboratory tests with production grade fuel confirmed that the filters do not pass the fuel particles.

c. Filter element push-out tests

Evaluation of the pressures required to push the filter element out of the assemblies (at operating temperature) was performed on an as-prepared assembly and three assemblies after exposure (one assembly to each environment) to air, helium and vacuum soak for 168 hours at 1450° F. No difference was noted in the pressures required before and after treatment as all tungsten push-out pins failed at the equivalent of 40,000 psi capsule gas pressure. This test indicated that the capsule will rupture before the platinum-plated ZrO_2 element can be pushed out.

Haynes-25 capsules Nos. 368/361 and 369/375 were fueled with Pu-238 oxide microspheres for the flight generator subsystem. Assembly of the capsule into the intact re-entry heat source (see Fig. IV-1) was conducted in an argon atmosphere. During the assembly sequence, the diaphragm over the ZrO_2 filter element was pierced to allow the helium to vent. Immediately after the diaphragm was pierced, a Veeco helium probe was placed over the vent opening to assure that helium was flowing. The Veeco signal indicator increased from zero to 100% of the 1000 scale in 25 to 30 seconds for both capsules.

Following shipment of the IRHS sources to Martin Marietta in argon-filled shipping casks, installation into argon-filled thermoelectric generators was accomplished. Thermal vacuum testing of generator subsystem S/N 8A (two generators) was required as a part of the flight acceptance test. During this subsystem test, the argon and helium leakage rate from the two generators was measured. Figure IV-40 presents the results of these measurements. The helium leakage rate was on the order of 10^{-5} cm^3/second and was varying as a function of generator fin root temperature. (This variation was expected because permeation rate of the gas through the Viton O-ring seals is temperature-dependent.) The detection of the strong helium signal from the generator subsystem during thermal vacuum testing is further confirmation that the ZrO_2 filter element was venting helium from the fuel as designed.

6. Helium Diffusion Rates Through ZrO_2 Spray-Coated POCO Graphite

During the experimental effort directed at development of the IRHS, helium diffusion rate measurements through ZrO_2-coated POCO AXM-5Q graphite were performed. The POCO graphite test samples were prepared by slip-fitting a graphite plug 0.400 inch thick by 0.750 inch in diameter inside a stainless steel tube. The graphite plug was at 2100° F at insertion into the tube to take advantage of the different thermal expansion of the two materials. After fitting, the temperature was decreased to 1800° F and the graphite was diffusion-bonded to the tube.

Metallographic examination of the samples showed that there was a good bond between the graphite and the stainless steel tube, so the diffusion path was through the plug and not along the graphite-stainless steel interface.

Figures IV-41 through IV-44 present trend curves from the different diffusion tests which were conducted at room temperature, 1000° F and 1300° F as a function of applied helium pressure. (The scale on the curves for helium leakage is not the same on all the figures.)

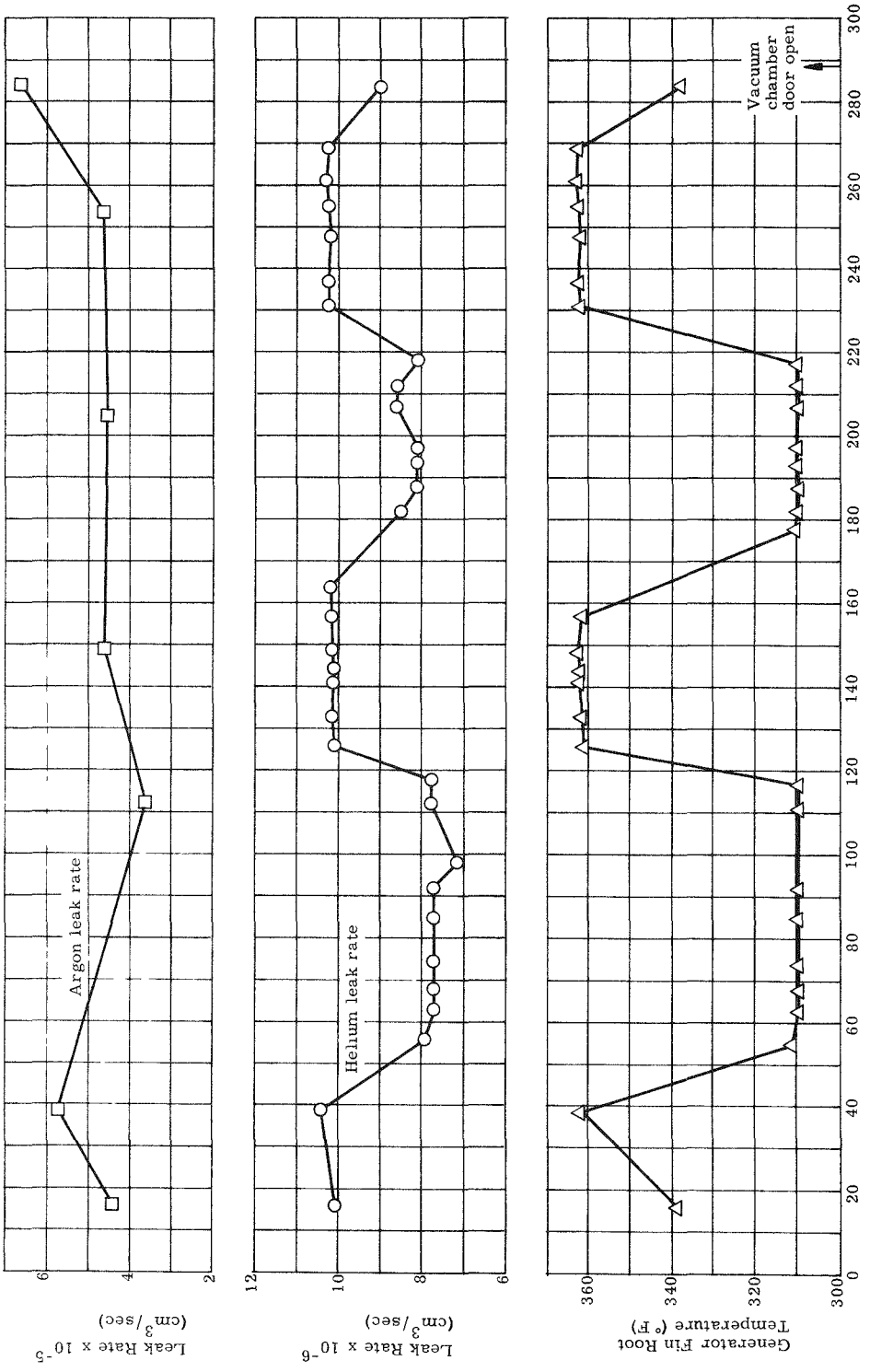

FIG. IV-40. HELIUM AND ARGON LEAKAGE RATE--SNAP 19 RTG SUBSYSTEM 8A IN THERMAL VACUUM CHAMBER

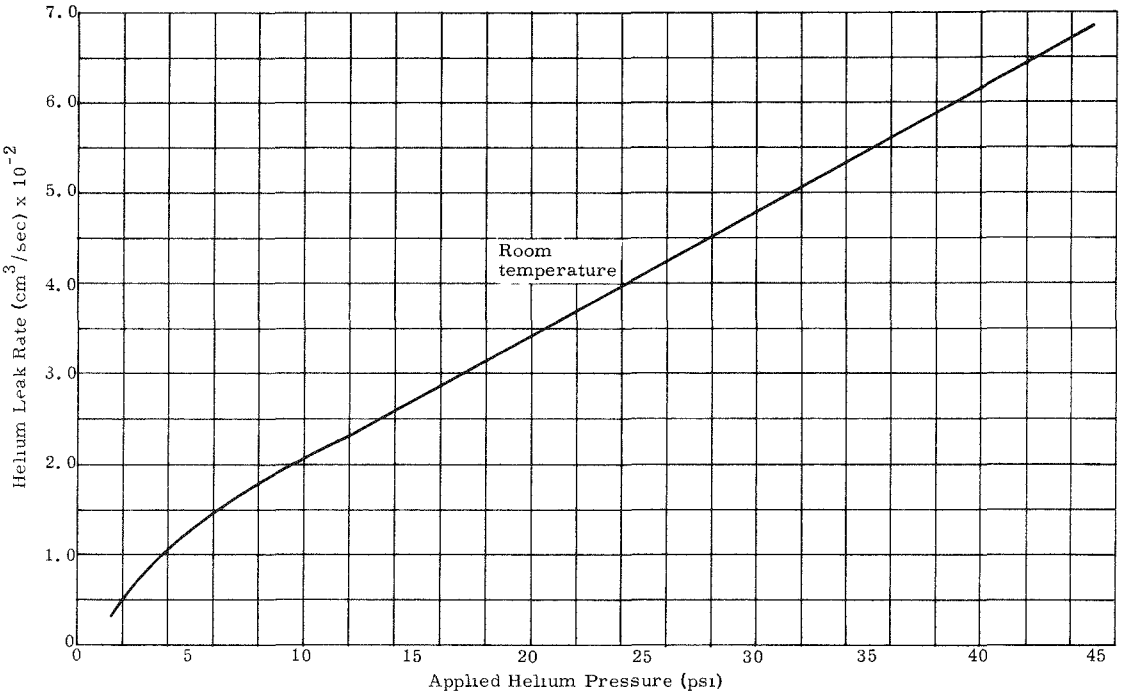

FIG. IV-41. HELIUM DIFFUSION RATE THROUGH ZrO_2-COATED POCO GRAPHITE--WITH THE GRAIN

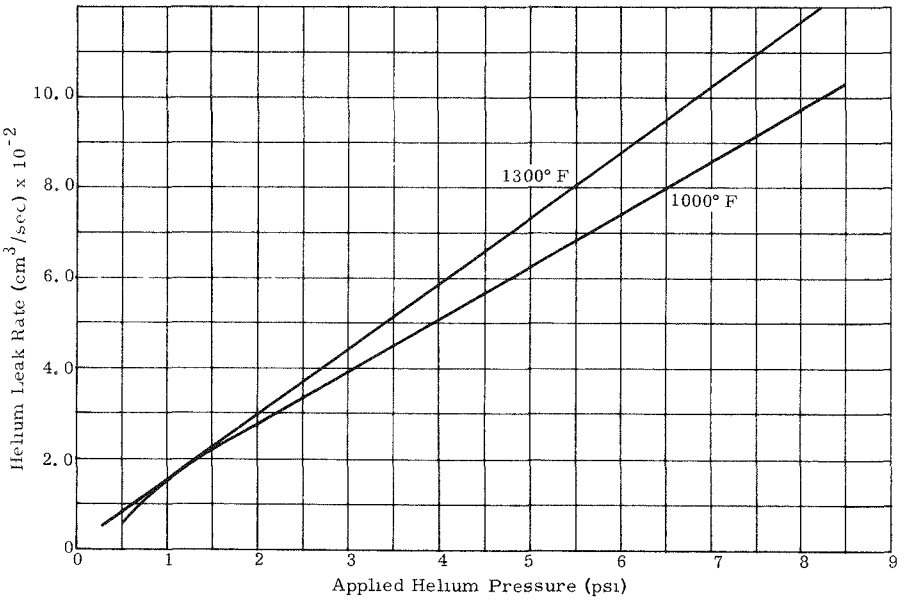

FIG. IV-42. HELIUM DIFFUSION RATE THROUGH ZrO_2 POCO GRAPHITE--WITH THE GRAIN

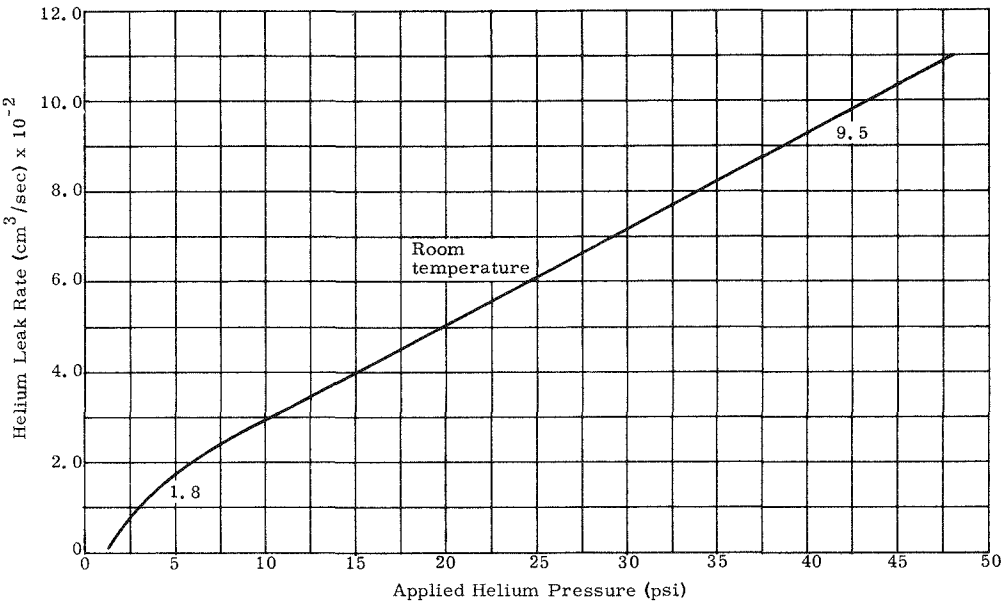

FIG. IV-43. HELIUM DIFFUSION RATE THROUGH ZrO_2-COATED POCO GRAPHITE--AGAINST THE GRAIN

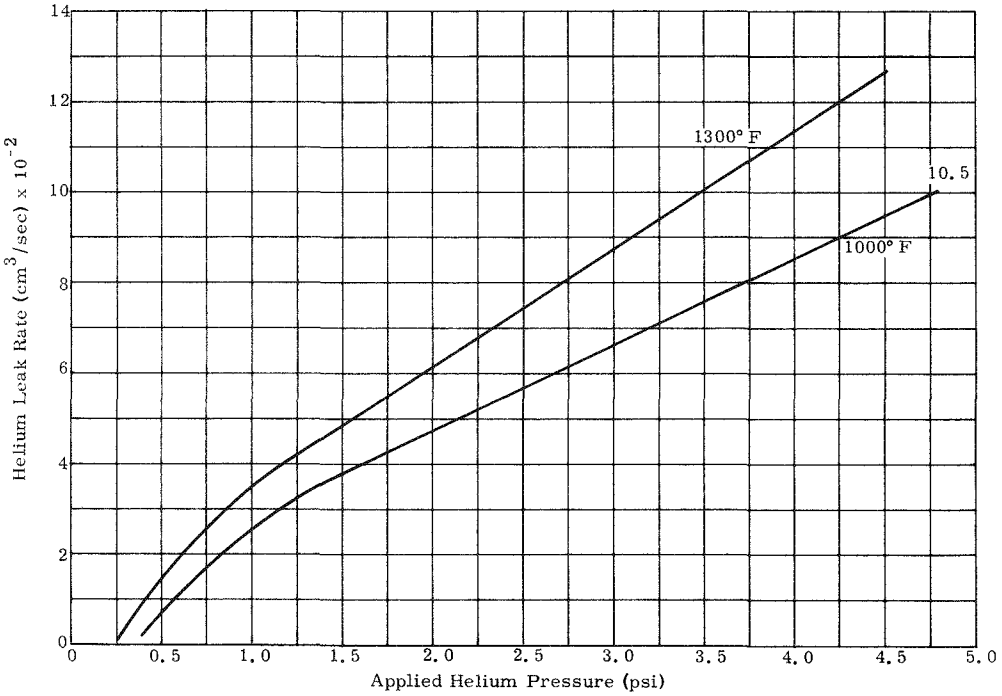

FIG. IV-44. HELIUM DIFFUSION RATE THROUGH ZrO_2-COATED POCO GRAPHITE--AGAINST THE GRAIN

The flow rates are roughly equivalent with the grain and against the grain for the ZrO_2-coated POCO. The flow increases rapidly at the higher temperatures. The theoretical helium generation rate is 2.4×10^{-5} scc/sec for a SNAP 19 fuel inventory. Because an IRHS heat shield presents a flow area approximately 70 times greater than these test specimens, there is little likelihood of any overpressure in the graphite container.

7. IRHS Tests with Pressurized Capsules

The filter element originally chosen for the IRHS was a pressed and sintered Haynes-25 alloy powder. This element exhibited severe reduction of the helium flow rate when exposed to oxygen-bearing environments at 1450° F. While filter element redesign was in progress, a series of burst tests investigated the results of a continuous pressure increase in an IRHS capsule. The primary objective of these tests was to determine the effect of capsule failure on heat shield integrity. Three specimens were tested, two as bare capsules and one as a complete heat source assembly. In each test, the capsule failed by development of a slow leak through longitudinal microcracks in an area of local yielding. No adverse effect on the heat shield due to capsule rupture was found, and the oxide coatings on both heat shield and canister were in excellent condition. Figure IV-45 shows the microfissure in the girth weld zone of a short-term test to failure. Figure IV-46 is a view of the failure point in the parent material of a thermally aged capsule.

Four plasma arc test IRHS assemblies were made and tested with helium-filled pressurized capsules to demonstrate that the rapid heating and sudden release of helium pressure would not rupture the heat shield. Capsule fill pressures were set to simulate the helium pressure due to radioisotope decay for seven months after a complete filter blockage. (As in other IRHS design analysis, all helium produced by plutonium decay was assumed to be instantaneously released by the fuel particles.) In two of the tests, the capsules melted, releasing helium at approximately 400 psi. No heat shield failure resulted from the rapid pressure release. The two other assemblies tested with lower total heat input did not result in capsule melting, but gammagraphs showed that the capsule did assume the general contour of the heat shield inner surface without causing heat shield damage.

Though it is highly unlikely that the capsule ZrO_2 filter element will become impervious to helium flow, these test data indicate that the capsule would fail in a manner to preclude damage to POCO heat shield. These tests, therefore, provide further assurance on intact re-entry.

8. Launch Pad Residual Fire Test

A fire test was conducted by the Sandia Corporation in support of the SNAP 19 program wherein specimens were exposed to burning JP-4/magnesium flame. The objective of the test was to demonstrate the capability of the intact re-entry heat source to contain the PuO_2 fuel during exposure to a fire representative of a launch pad abort situation. Due to the nature of the fire, the test was conducted at Sandia's Coyote Canyon Range. Specimens exposed to the fire consisted of an internally heated bare IRHS heat shield, and an IRHS assembly within an electrically heated thermoelectric generator (in addition to two dispersal fuel capsule specimens).

The bare intact heat source consisted of a solid stainless steel (shipping dummy) capsule housed in an uncoated POCO graphite heat shield. The stainless steel capsule was drilled and fitted with a 1000-watt electric heater. The purpose of the heater was to preheat the test specimen to the normal operating temperature of the

FIG. IV-45. METALLOGRAPHIC VIEW OF CRACK IN PRESSURE-TESTED IRHS CAPSULE--WELD ZONE CRACK

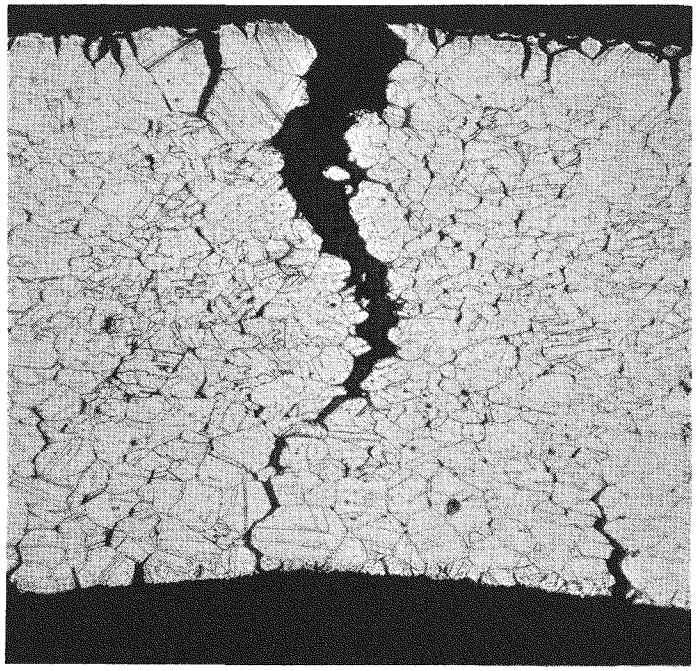

SNAP 19
IRHS Test

FIG. IV-46. METALLOGRAPHIC VIEW OF CRACK IN PRESSURE-TESTED CAPSULE--PARENT MATERIAL CRACK

bare IRHS and to simulate the isotopic heat input subsequent to the initiation of the fire. Testing of the bare IRHS, which was forced to remain in the residual JP-4 fire, was designed to yield information on the maximum oxidation effect of the residual fire independent of the contribution of the magnesium fire.

The thermoelectric generator test specimen consisted of the complete generator S/N 2 with an intact re-entry heat source installed. The assembly was heated with six 600-watt electric heaters installed in the ATJ graphite heat distribution block. The purpose of these heaters was to regulate the surface of the IRHS at 1240° F at the initiation of the fire and to simulate the isotopic heat input subsequent to the initiation of the fire. The objective of the generator test was to obtain information on the combined effect of the residual (propellant) fire and the associated magnesium fire on the integrity of the IRHS which is initially housed in the generator.

The residual propellant fire was simulated with 2000 gallons of JP-4 fuel contained in a 20-foot by 10-inch-deep earthen pit lined with polyethylene. A sandpile 4 feet by 4 feet by 5-5/8 inches high (Fig. IV-47) was constructed in the center of the pit. The SNAP 19 IRHS generator was mounted on a magnesium stand weighing about 30 pounds, thereby placing the generator in the fuel fire and later in the magnesium fire on top of the sandpile. Scattered on the sandpile under the generator were about ten pounds of scrap magnesium to simulate the material of the Nimbus and the Agena D.

The 2000 gallons of JP-4 fuel burned at high intensity for approximately 26 minutes, and were essentially consumed at 30 minutes. The magnesium ignited about two minutes after ignition of the JP-4 and burned intermittently during the first 26 minutes. Following the high intensity burning of the JP-4 fuel, a very pronounced magnesium fire was observed which burned for an additional 30 to 35 minutes.

The electrically heated bare IRHS heat shield assembly which had been placed on top of a stainless steel stand (forcing it to remain in the chemical fire) had ruptured. The rupture of the POCO occurred due to insufficient clearance between the internal stainless steel heater block and the graphite. However, the test showed evidence of only minor POCO graphite oxidation as a result of exposure to the chemical fire.

The magnesium stand supporting the generator with the IRHS assembly collapsed about 4 minutes after ignition of the JP-4 and dropped the generator into the scrap magnesium on top of the sandpile. At the conclusion of the chemical fire and magnesium fire it was determined that the generator housing was essentially completely consumed and the ATJ graphite heat accumulator block was about half consumed. The POCO graphite heat shield had sustained some oxidation as a result of the intense magnesium fire, but the heat shield was not breached. Figure IV-48 is a view showing generator debris resulting from the JP-4 and magnesium fire. Figure IV-49 shows the non-breached IRHS assembly that had been in the generator. The view also shows the debris from the ruptured bare IRHS heat shield test specimen and the internal stainless steel heater block.

The residual fire test was considered to be a successful demonstration of the reactions of the SNAP 19 hardware to a fire involving about 2000 gallons of JP-4 fuel and about 40 pounds of magnesium. It should be noted that there are many possible orientations of the SNAP 19 generator in relation to variable ratios and quantities of chemical fuel and magnesium that might result from an actual launch pad abort situation. The test, however, did give a reasonable simulation of a typical pad abort residual fire, and did subject the SNAP 19 to an intense fire environment. The results strongly indicate that the IRHS assembly will withstand a launch pad residual fire situation without release of the PuO_2 fuel inventory.

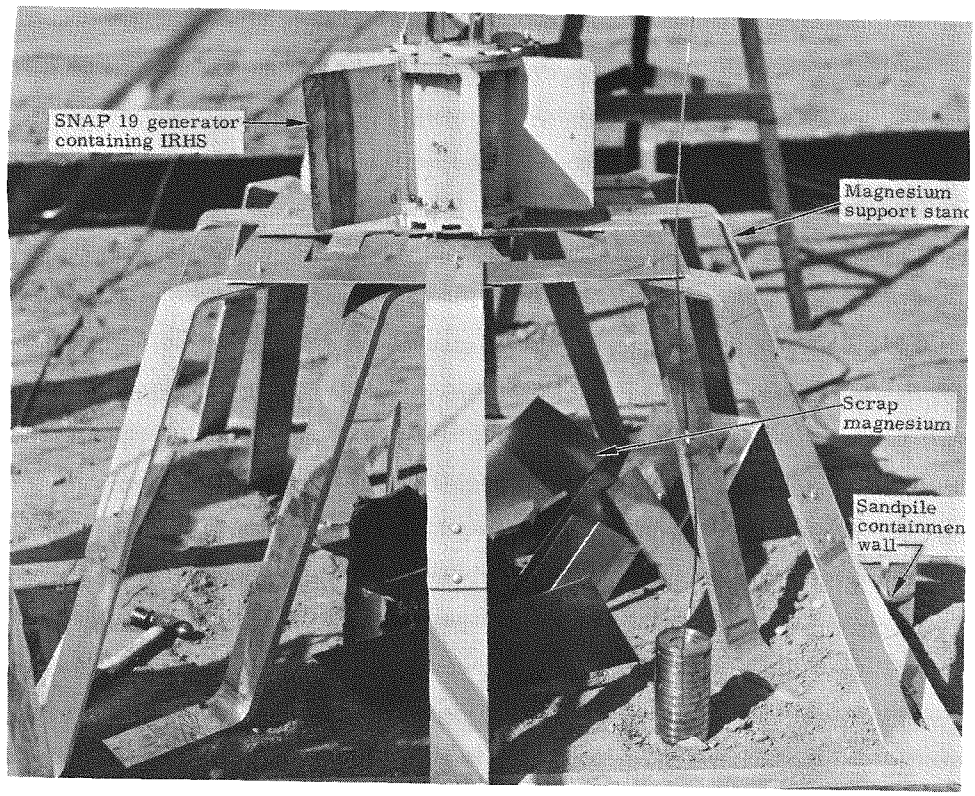

FIG. IV-47. SNAP 19 IRHS RESIDUAL FIRE TEST SETUP

FIG. IV-48. GENERATOR DEBRIS FOLLOWING JP-4 AND MAGNESIUM FIRE

9. Tantalum Compliant Pad Tests

Development of the IRHS compliant support member required extensive analytical and test evaluation. Several materials and support techniques were evaluated and reported in Ref. IV-3. Test results given in this report are primarily concerned with:

(1) Heat source dynamic test (room temperature)

(2) IRHS prototype qualification tests in an unheated RTG

(3) Load deflection test of aged compliant support assemblies.

The vibration response spectrum of an instrumented (accelerometer) dispersal heat source was modified slightly and used as the input spectrum for the IRHS compliant pad screening tests. IRHS assemblies containing compliant pad test samples were rigidly mounted to the vibration table and driven at room temperature over the established test input spectrum (see Table IV-18). Assemblies were examined after vibration to determine if pad breakdown or heat shield damage had resulted. The simulated capsule inside the test assembly was equipped with a three-axis accelerometer so that capsule response could be measured as a function of input to the IRHS assembly. While these tests could not verify the suitability of a particular pad material or configuration at design operating temperatures, the tests could and did eliminate some materials from further consideration. Failure in room temperature tests was interpreted to mean failure at higher temperatures, because of the reduced elastic modulus and compression set, or load relaxation.

Several materials were considered during the initial screening tests to determine what material and configuration best suited the high temperature, high spring rate requirements. The materials tested were Dynaflex, a Johns Mansville quartz fiber felt with organic binder, ZrO_2 felt, Min-K 2002, a high nickel content superalloy felt by Brunswick Corporation, and tantalum felt also by Brunswick. The nonmetallic fibrous compounds, chosen for their high temperature chemical inertness, could not absorb large elastic strains and broke up during either handling or test. The tantalum and nickel alloy felts were nearly identical and completely acceptable in room temperature performance, but the tantalum felt demonstrated an advantage in increased resistance to load relaxation at design operating temperature. The tantalum felt was selected as the reference design compliant member.

IRHS assemblies containing 6% dense tantalum felt pads were tested in POCO heat shields with the selected internal "shape" as described in Section IV-A. The assemblies were rigidly mounted to the vibration table and, at room temperature, successfully withstood the resonance search and high level vibration input spectra defined in Table IV-18. The dynamic response of the mass simulated capsule (containing a triaxial accelerometer) is shown in Table IV-19. The resonant input frequency in the three axes is in the 1100 to 1200 Hz range, which results in a maximum response load of about 100g. Inspection of the heat source and the compliant pads revealed no damage.

TABLE IV-18

IRHS Compliant Pad Development Vibration Criteria

1. X Axis (Yaw)

a. Resonant search

5 to 7 cps at 0.4-inch double amplitude displacement
7 to 2000 cps at 1.0-g peak
Frequency sweep rate: 1 octave/minute

b. High level exposure

5 to 20 cps at 0.4-inch double amplitude displacement
20 to 50 cps at 8.0-g peak
50 to 100 cps at 40.0-g peak
100 to 2000 cps at 5.0-g peak
Frequency sweep rate: 1 octave/minute

2. Y Axis (Pitch)

a. Resonant search

5 to 7 cps at 0.4-inch double amplitude displacement
7 to 2000 cps at 1.0-g peak
Frequency sweep rate: 1 octave/minute

b. High level exposure

5 to 38 cps at 0.4-inch double amplitude displacement
38 to 50 cps at 30.0-g peak
50 to 500 cps at 10.0-g peak
500 to 2000 cps at 5.0-g peak
Frequency sweep rate: 1 octave/minute

3. Z Axis (Roll)

a. Resonant search

5 to 7 cps at 0.4-inch double amplitude displacement
7 to 2000 cps at 1.0-g peak

b. High level exposure

5 to 38 cps at 0.4-inch double amplitude displacement
38 to 50 cps at 30.0-g peak
50 to 500 cps at 10.0-g peak
500 to 2000 cps at 5.0-g peak
Frequency sweep rate: 1 octave/minute

TABLE IV-19

Vibration Response Data for IRHS Capsule Supported on 6% Dense Tantalum Felt Pads at Room Temperature

Axis	Vibration Input Level	Resonant Frequency (Hz)	Maximum Response (g)
X	Low, 1 to 2 g	1250	44
Y	Low, 1 to 2 g	1150	31.8
Z	Low, 1 to 2 g	1130	34
X	High*	1190	102
Y	High*	1100	82
Z	High*	1080	93

*See Table IV-17

The test was successfully completed with non-aged tantalum felt (no thermal relaxation of load in the felt pad) at room temperature. The next vibration test was conducted on a noninstrumented dummy IRHS assembly in an unheated thermoelectric generator. The heat source was assembled and held at 1400° F for 24 hours to allow some load relaxation to take place in the tantalum pads. Following the thermal soak test, the dummy IRHS was installed in SNAP 19 generator S/N 8 and subjected to prototype qualification dynamic tests in the three axes. Post-test examination revealed no damage to the heat shield or compliant pad.

The tests that fully demonstrated the capability of the tantalum compliant pads to fulfill their design requirement were in the complete prototype testing of RTG subsystem 6A (generators S/N 11A and S/N 12A). Following prototype qualification testing of the RTG subsystem, generator S/N 11A was revibrated in the three axes at flight acceptance levels. Both heat sources were then returned to Mound Laboratory for diagnostic disassembly. (Prototype qualification of fueled generators and their diagnostic disassembly are discussed in more detail in Sections B 5 and D 10 of this chapter.)

Heat shields from generators S/N 11A and S/N 12A were returned to Martin Marietta from Mound Laboratory for inspection. The original tantalum felt pads were left in the heat shields.

Full-scale load deflection tests were performed on the aged felt pads by reseating one set from each heat shield and load-deflection testing them to 1000 pound maximum load between the platens of a tensile test machine, as shown in Fig. IV-50. One of the dummy heat shield shipping capsules was used as a loading head.

Compression test data from the female heat shield halves are plotted in Fig. IV-51 for the second load/unload cycle. Little difference exists between the characteristics of the felt pads from generator S/N 8, which were aged for 24 hours, and those from generator S/N 11A, which were aged for 1000 hours. Two new (unaged) felt pads installed in the female half of the generator S/N 8 heat shield were compression tested to 1000 pounds and the data were plotted in a similar manner.

Comparing the second cycle load/unload curves for the new pads and those aged for 24 and 1000 hours shows that most of the aging effects occur in the first 24 hours; extended storage prior to launch is therefore acceptable.

FIG. IV-49. IRHS AND DISPERSAL HEAT SOURCES AFTER RESIDUAL FIRE TEST

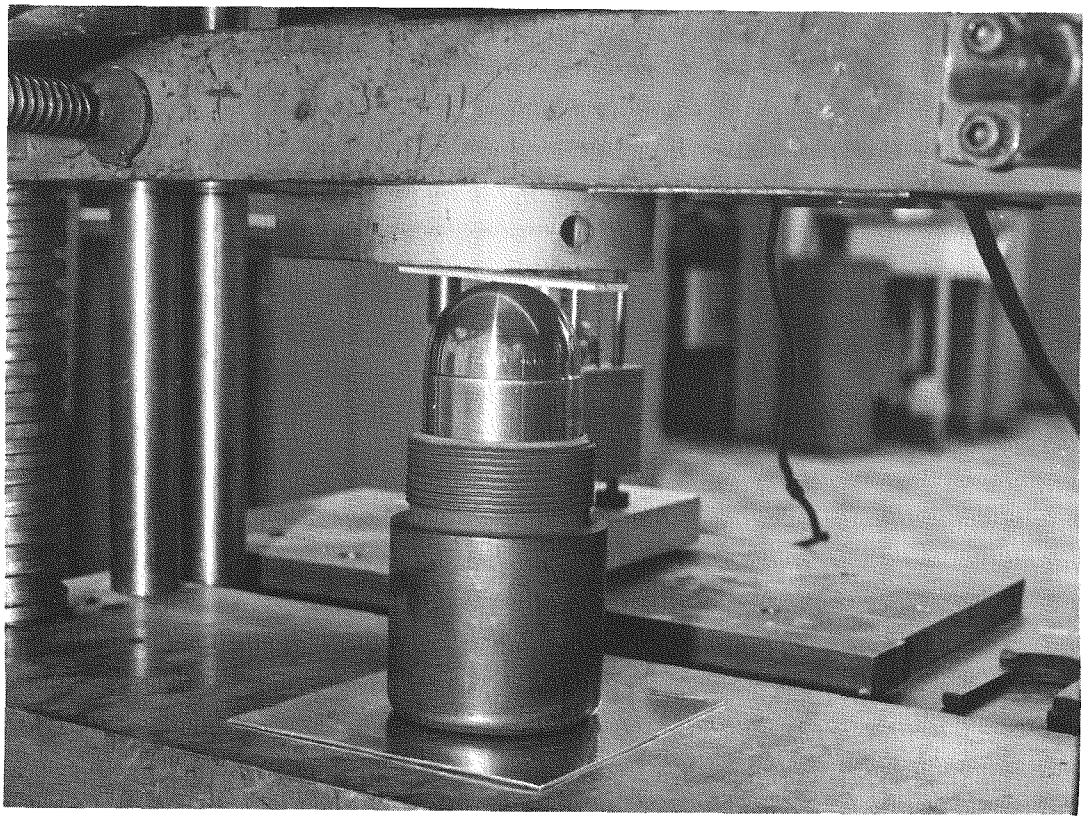

FIG. IV-50. TANTALUM COMPLIANT PAD LOAD DEFLECTION TEST SETUP

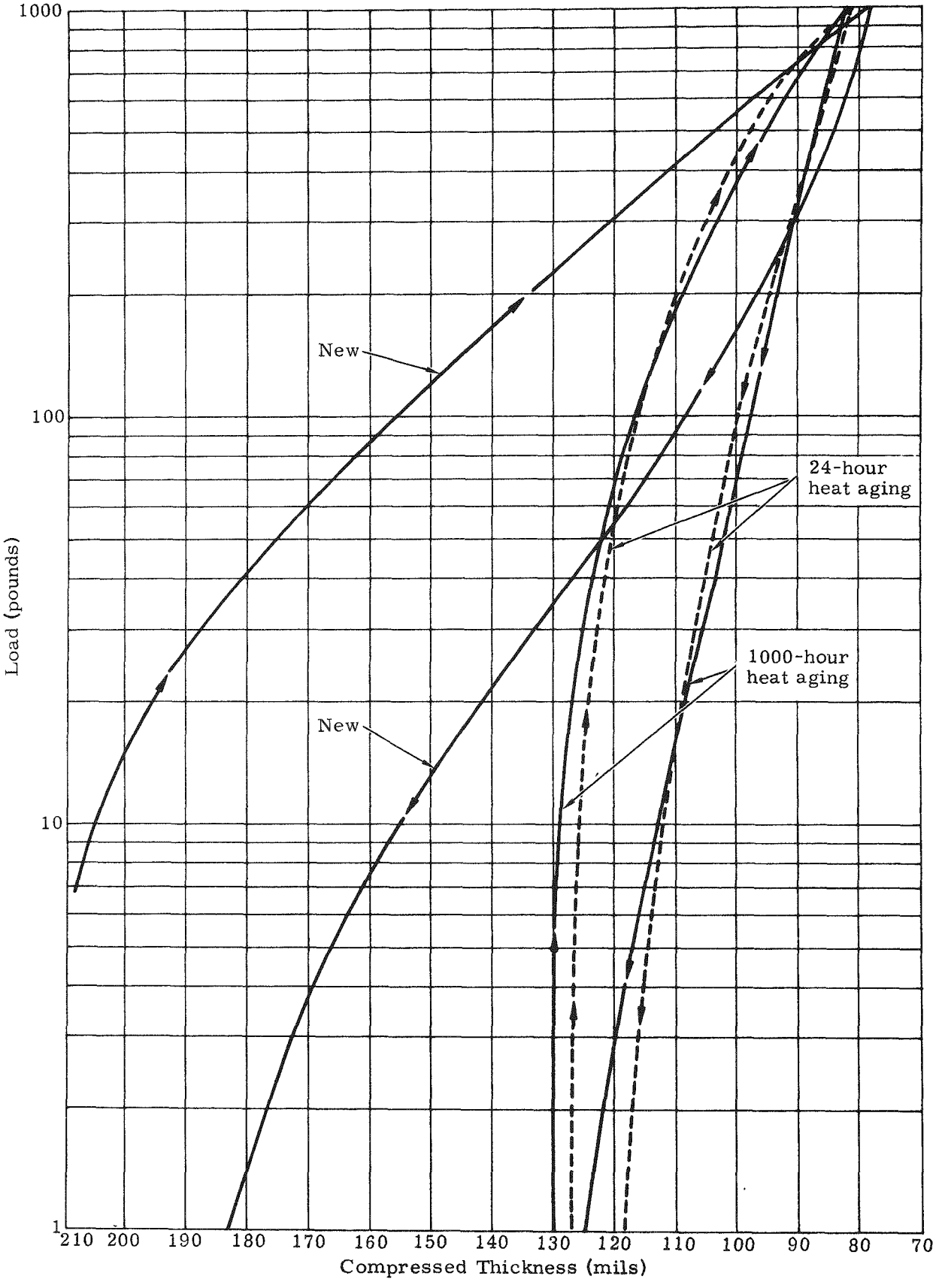

FIG. IV-51. LOAD DEFLECTION TESTS, AGED AND NEW TANTALUM FELT (TWO FELT PADS IN INTERNALLY THREADED HEAT SHIELD)

10. IRHS Prototype Qualification

Two fueled IRHS assemblies (S/N 341/358 and 370/376A) were subjected to prototype qualification testing as a part of RTG subsystem S/N 6A and then diagnostically disassembled. Prototype qualification testing of the subsystem consisted of vibration, acceleration and thermal vacuum testing. Prototype test requirements are presented in Vol. I, Section IV-C. Diagnostic disassembly results are summarized in Section B 5 of this chapter and detailed in Ref. IV-5.

Based on the results of the RTG subsystem prototype qualification test, and all the other heat source development and qualification tests, it is concluded that the IRHS will perform the mission for which it was designed.

V. FLIGHT HEAT SOURCE SELECTION

The nuclear safety assessments (Ref. V-1) of both the dispersion capsule and the IRHS designs were conducted by evaluating each sequential operation of the mission profile. These operations were grouped into the following phases: transportation, launch pad activities, ascent trajectory, low orbit aborts and post-mission history. A probabilistic combination of potential abort events, disposition of fuel and biological response of humans was used to establish the risk. This risk was compared to established safety criteria and used to compare the merits of the dispersal and intact re-entry safety philosophies (Chapter II). The hazards evaluated arise from inhalation, ingestion and exposure to direct radiation. The results of the biological response study were based on recommendations of the International Commission on Radiological Protection (ICRP) for nuclear energy programs.

The risk associated with the SNAP 19 dispersion capsule design is derived primarily from the probability of inhalation and ingestion of fuel released to the atmosphere subsequent to ascent trajectory abort. The phase of the flight sequence yielding the highest probability of adverse atmospheric release is the re-entry associated with Agena first burn abort (occurrence probability 1.3×10^{-2}). This release is characterized by low but tangible exposure of a large number of people. The risk associated with the dispersion system is subject to a number of uncertainties concerning the ultimate nature and disposition of the fuel form which could change the risk expectation two or three orders of magnitude. The technical factors accounting for much of this uncertainty are fuel form size degradation during atmospheric re-entry, particle fallout rates and fall velocities, inhalation probabilities, resuspension characteristics and rate of depletion of the number of particles available for resuspension.

The risk associated with the SNAP 19 IRHS design is derived primarily from the probability of inhalation and ingestion of fuel released subsequent to land impact. The phase of the flight sequence yielding the highest probability of land impact is the random re-entry associated with a short orbit abort (occurrence probability 2×10^{-2}). This release is characterized by a small exposure of a small number of people. The risk associated with the IRHS system is subject only to the uncertainties concerning the fuel form size spectrum upon impact, point source resuspension and rate of depletion of the number of particles available for resuspension.

A comprehensive review of the safety analyses for each system was conducted and the Atomic Energy Commission ultimately selected the intact re-entry heat source for the SNAP 19/Nimbus B mission. As discussed in Volume I of this report, generator subsystems S/N 8, S/N 6A and S/N 8A were assembled and tested with intact re-entry heat sources. Finally, subsystem S/N 8A was accepted for integration with and flight in Nimbus B.

BLANK

VI. REFERENCES

II-1. "SNAP 19 Fuel Form Selection and Capsule Configuration." MND-3169-77, Martin Marietta Corporation, December 1965.

III-1. "SNAP 19 Phase II Final Summary Report." MND-3169-83, Martin Marietta Corporation, August 1965.

III-2. Grove, G. R., et al., "Plutonium-238 Isotopic Power Sources: A Summary Report." MLM-1270, Monsanto Research Corporation, August 1965.

III-3. "SNAP 19 Fuel Form Selection and Capsule Configuration." MND-3607-77, Martin Marietta Corporation, December 1965.

III-4. "SNAP 19 Phase III, Quarterly Progress Report No. 1." MND-3607-50, Martin Marietta Corporation, February 1966.

III-5. "SNAP 19 Interim Safety Analysis Report, Volume 1, Reference Design Document." MND-3607-133, Martin Marietta Corporation, June 1967.

III-6. Larson, F. R. and Miller, James, "A Time-Temperature Relationship for Rupture and Creep Stresses." Transactions of the ASME, July 1952, pp 765 to 775.

III-7. McCoy, H. E., "Creep-Rupture Properties Under Conditions of Constant and Varying Stresses." Nuclear Applications, Volume 2, December 1966.

III-8. Sentman, L. A., "Free Molecule Flow Theory and Its Application to the Determination of Aerodynamic Forces." Lockheed Aircraft Corporation Report, LMSC-448514, October 1, 1961.

III-9. Stouffer, C., "SNAP 19 Capsule Force and Stability Test Conducted in the NASA-Langley 31-inch Continuous Flow Hypersonic Tunnel at Mach 10." MND-3607-90, Martin Marietta Corporation, December 1966.

III-10. Matting, F. W. and Chapman, D. R., Private Communique, NASA Ames, May 1966.

III-11. Stouffer, C., "SNAP 19 Capsule Low Reynolds Number Force Test." MND-3607-89, Martin Marietta Corporation, September 1966.

III-12. Culotta, A. J., "RFD-2 Flight Test Program Supplementary Analysis Report." MND-3283-3, Martin Marietta Corporation, January 1966.

III-13. Hagis, W., "SNAP Programs Upper Atmosphere Experimental Re-entry Study Final Summary Report." MND-P-2953, Martin Marietta Corporation, April 1963.

III-14. Klett, R. D., "Drag Coefficients and Heating Ratios for Right Circular Cylinders in Free-Molecular and Continuum Flow from Mach 10 to 30." SC-RR-64-2141, Sandia Corporation, December 1964.

III-15. Lambert, W. and Coughlin, T. L., "Distribution of Heat and Pressure on the SNAP 19 Fuel Capsule in Hypersonic Flow." MND-3607-93, Martin Marietta Corporation, March 1967.

III-16. Letter from Dr. F. D. Lonadier of Mound Laboratory to Mr. J. L. Powell of Martin Marietta Corporation, January 23, 1967. (Mound Laboratory, Ref MN3607-380)

III-17. "Technical Manual, Operation and Field Maintenance, SNAP 19 Radioisotope Power Supply." MND-3607-80, Martin Marietta Corporation, October 1967.

III-18. "SNAP 19 In-House Hazard Review." MND-3607-118, Martin Marietta Corporation.

III-19. "SNAP 19 Fuel Capsule Vibration Engineering Evaluation Report." MND-3607-121, Martin Marietta Corporation, November 1966.

III-20. "SNAP 19 Interim Safety Analyses Report, Accident Model Document." MND-3607-133-2, Volume II, Martin Marietta Corporation.

III-21. "Distribution of Heat and Pressure on the SNAP 19 Fuel Capsule in Hypersonic Flow." MND-3607-93, Martin Marietta Corporation, March 1967.

IV-1. "SNAP 19 Safety Analysis Report--IRHS Supplement." MND-3607-133-S, Martin Marietta Corporation.

IV-2. "Filter Development Program for SNAP 19 Intact Re-entry Heat Source." MND-3607-237, Martin Marietta Corporation.

IV-3. "SNAP 19 Program Intact Re-entry Heat Source Design Development Report." MND-3607-238, Martin Marietta Corporation.

IV-4. "SNAP 19 Safety Analysis Report--Volumes I, II, III and Addendum." MND-3607-133-1, -2, -3 and -A, Martin Marietta Corporation.

IV-5. Himes, J., et al., "Subsystem 6A (IRHS Prototype) Diagnostic Disassembly Report." MND-3607-235, Martin Marietta Corporation, February 1968.

IV-6. "SNAP 19 Operational Safety Review, IRHS Addendum." MND-3607-118A, Martin Marietta Corporation, January 1968.

V-1. "SNAP 19 Safety Analysis Report, Volumes I, II, III, Addendum and Supplement." MND-3607-133-1, -2, -3, -A and -S, Martin Marietta Corporation.